

## **NOTE TO USERS**

**This reproduction is the best copy available.**

UMI<sup>®</sup>



**Dynamic Modeling, Intelligent Control and Diagnostics  
of Hot Water Heating Systems**

**Lian Zhong Li**

**A Thesis**

**In the Department**

**of**

**Building, Civil and Environmental Engineering**

**Presented in Partial Fulfillment of the Requirements  
For the Degree of Doctor of Philosophy (Building Engineering) at  
Concordia University  
Montreal, Quebec, Canada**

**December 2008**

**© Lian Zhong Li, 2008**



Library and Archives  
Canada

Published Heritage  
Branch

395 Wellington Street  
Ottawa ON K1A 0N4  
Canada

Bibliothèque et  
Archives Canada

Direction du  
Patrimoine de l'édition

395, rue Wellington  
Ottawa ON K1A 0N4  
Canada

*Your file* *Votre référence*  
ISBN: 978-0-494-63447-9  
*Our file* *Notre référence*  
ISBN: 978-0-494-63447-9

#### NOTICE:

The author has granted a non-exclusive license allowing Library and Archives Canada to reproduce, publish, archive, preserve, conserve, communicate to the public by telecommunication or on the Internet, loan, distribute and sell theses worldwide, for commercial or non-commercial purposes, in microform, paper, electronic and/or any other formats.

The author retains copyright ownership and moral rights in this thesis. Neither the thesis nor substantial extracts from it may be printed or otherwise reproduced without the author's permission.

---

In compliance with the Canadian Privacy Act some supporting forms may have been removed from this thesis.

While these forms may be included in the document page count, their removal does not represent any loss of content from the thesis.

#### AVIS:

L'auteur a accordé une licence non exclusive permettant à la Bibliothèque et Archives Canada de reproduire, publier, archiver, sauvegarder, conserver, transmettre au public par télécommunication ou par l'Internet, prêter, distribuer et vendre des thèses partout dans le monde, à des fins commerciales ou autres, sur support microforme, papier, électronique et/ou autres formats.

L'auteur conserve la propriété du droit d'auteur et des droits moraux qui protègent cette thèse. Ni la thèse ni des extraits substantiels de celle-ci ne doivent être imprimés ou autrement reproduits sans son autorisation.

---

Conformément à la loi canadienne sur la protection de la vie privée, quelques formulaires secondaires ont été enlevés de cette thèse.

Bien que ces formulaires aient inclus dans la pagination, il n'y aura aucun contenu manquant.

■ ■ ■  
**Canada**

# ABSTRACT

Dynamic Modeling, Intelligent Control and Diagnostics of Hot Water Heating Systems

Lian Zhong Li, Ph.D.

Concordia University, 2008

Heating, ventilating and air-conditioning (HVAC) systems have been extensively used to provide desired indoor environment in buildings. It is well acknowledged that 25~35% of the total energy use is consumed by buildings, and space heating systems account for 50~60% of the building energy consumption. Furthermore, roughly half of the energy consumed goes to operation of heating systems. In the past few years the energy use has shown rapid growth. Therefore, it is necessary to design and operate HVAC systems to reduce energy consumption and improve occupant comfort. To improve energy efficiency, HVAC systems should be optimally controlled and operated.

This study focuses on developing advanced control strategies and fault tolerant control (FTC) using information from fault detection and diagnosis (FDD) for hot water heating (HWH) systems. To begin with, HWH system dynamic models are developed based on mass, momentum and energy balance principles. Then, embedded intelligent control strategies: fuzzy logic control and fuzzy logic adaptive control are designed for the overall system to achieve better performance and energy efficiency. Moreover, in designing the advanced control strategies, the parameter uncertainty and noise from measurement and process are taken into account. The extended Kalman filter (EKF) technique is utilized to handle system uncertainty and measurement noise, and to improve

system control performance. After that, a supervisory control strategy for the HWH system is designed and simulated to achieve optimal operation. Finally, model-based FDD methods were developed by using fuzzy logic to detect and isolate measurement and process faults occurring in HWH systems. The FDD information was employed to design model-based FTC systems for various faults and to extend the operating range under failure situations.

The contributions of this study include the development of a large scale dynamic model of a HWH system for a high-rise building; design of fuzzy logic adaptive control strategies to improve energy efficiency of heating systems and design of model-based FTC systems by using FDD information.

## ACKNOWLEDGEMENTS

I would like to express my sincere gratitude to Dr. M. Zaheeruddin for his constant guidance, advise, encouragement, help, sustained interest, and financial support throughout the whole span of this thesis.

My thanks are also to the staff in BCEE Department, as well as my colleagues, especially to Dr. Min NING.

The financial assistance from Concordia University and NSERC is also gratefully acknowledged.

I would like to dedicate and express my appreciation for this thesis to my wife, Tong ZHANG, and my lovely daughter, Jia Meng LI for their patience, understanding, encouragement and support during my whole studies.

# Table of Contents

<b>List of Figures</b> .....	<b>x</b>
<b>List of Tables</b> .....	<b>xv</b>
<b>Nomenclature</b> .....	<b>xvi</b>
Greek Letters.....	xx
Subscripts.....	xxi
Acronyms.....	xxiv
<b>Chapter 1 Introduction, Objectives and Contributions</b> .....	<b>1</b>
1.1 Introduction.....	1
1.2 Hot water heating systems .....	2
1.3 HWH System Control.....	4
1.4 The importance of this research.....	7
1.5 Scope & objectives .....	8
1.6 Contributions and summary.....	9
<b>Chapter 2 Literature Review</b> .....	<b>12</b>
2.1 Introduction.....	12
2.2 System design consideration and operation.....	12
2.3 Dynamic models and simulations .....	14
2.3.1 Component level models.....	15
2.3.2 System level models .....	22
2.3.3 Available simulation software packages.....	25
2.4 System control strategies .....	26
2.4.1 System control and optimal operation .....	26

2.4.2 PID tuning methods .....	30
2.4.3 Fuzzy control .....	31
2.5 The Kalman filtering techniques.....	35
2.6 Fault detection and diagnosis (FDD).....	37
2.7 Fault tolerant control (FTC).....	42
2.8 Summary .....	45
<b>Chapter 3 Dynamic Modeling of a One Room HWH System.....</b>	<b>47</b>
3.1 Dynamic modeling of a one room heating system.....	47
3.1.1 Baseboard heater model in a room.....	47
3.1.2 Dynamic model of heat transfer from the bare pipe with the cover to the room air .....	62
3.1.3 Room model.....	63
3.1.4 Outside wall model .....	64
3.2 Zonal model with full order baseboard heater model .....	65
3.3 Model reduction of the one room heating system.....	65
3.4 Simulation results of the one room heating system .....	68
3.4.1 Simulation results of the room heating system .....	68
3.4.2 Simulation results of the reduced-order one room model.....	78
<b>Chapter 4 Dynamic Modeling of Multi-Zone HWH Systems.....</b>	<b>80</b>
4.1 Dynamic modeling of a SFMZ HWH system.....	80
4.1.1 Physical model of the SFMZ system .....	80
4.1.2 Temperature dynamics.....	82
4.1.3 Water mass flow rate dynamics .....	83

4.2	Parameter aggregation for model reduction.....	87
4.2.1	Aggregation model of the SFMZ system.....	87
4.2.2	Aggregation model of the basement heating system .....	90
4.3	Dynamic model of a MFMZ HWH system .....	90
4.3.1	Physical model of the high-rise building HWH system.....	90
4.3.2	Dynamic modeling of the MFMZ system.....	92
4.4	Simulation results of the MFMZ HWH system.....	100
4.4.1	Results from the SFMZ heating system.....	101
4.4.2	Results from the aggregated heating system.....	108
4.4.3	Results from the MFMZ heating system .....	109
<b>Chapter 5 Design of Control Strategies for the HWH System .....</b>		<b>120</b>
5.1	Introduction.....	120
5.2	Control strategy design .....	124
5.2.1	Design of boiler control strategy based on average water temperature .....	124
5.2.2	Design of fuzzy logic adaptive PI control (FLAC) strategy .....	129
5.2.3	Design of hybrid control strategy with the EKF .....	137
5.3	Energy efficiency and set point accuracy evaluation.....	155
5.3.1	Energy efficiency evaluation .....	155
5.3.2	Set point accuracy evaluation .....	156
5.4	Design of supervisory control system.....	161
<b>Chapter 6 Model-Based Fault Detection Diagnosis and Fault Tolerant Control of</b>		
<b>HWH Systems.....</b>		<b>172</b>
6.1	Introduction.....	172

6.2 Methodologies for the FDD and FTC strategies.....	174
6.2.1 Fault detection and diagnosis of MFMZ HWH system .....	174
6.2.2 Fault tolerant control of MFMZ HWH system .....	176
6.3 Case studies.....	177
6.3.1 FTC system for measurement fault.....	179
6.3.2 FTC system for process fault .....	183
<b>Chapter 7 Conclusions, Contributions and Recommendations for Future Research</b>	
.....	<b>195</b>
7.1 Conclusions and contributions.....	195
7.1.1 Dynamic modeling of the overall HWH system.....	195
7.1.2 Design of intelligent control strategies .....	198
7.1.3 Model-based fault tolerant control strategies.....	200
7.2 Recommendations for future research .....	202
<b>References.....</b>	<b>204</b>
<b>Appendices.....</b>	<b>213</b>
Appendix A Zonal model with the full order baseboard heater model.....	213
A.1 Zonal model .....	213
A.2 Simulation results.....	217
Appendix B Pressure drops from pipe segments, fittings and equipment .....	220
Appendix C Aggregation model of a basement HWH system .....	223

## List of Figures

Figure 1.1 A typical HWH system for a high-rise building.....	3
Figure 1.2 HWH system control configuration.....	5
Figure 3.1 Schematic diagram of the room with the baseboard heater.....	49
Figure 3.2 Separation of the vertical channels for the baseboard heater and the connections .....	49
Figure 3.3 Schematic diagram of the vertical channel and the control volume.....	50
Figure 3.4 Nodes and friction coefficients in the finned-tube vertical channel.....	53
Figure 3.5 Layout of the one room heating system .....	67
Figure 3.6 Dynamic responses of the outputs in the finned-tube vertical channel .....	71
Figure 3.7 Output responses as a function of water supply temperature at control volume 2.....	72
Figure 3.8 Lines of constant outputs in zone air and supply water temperature plane.....	73
Figure 3.9 Heat outputs from the bare pipe vertical channel .....	74
Figure 3.10 Dynamic responses of the baseboard heater and the room at $T_s=90^\circ\text{C}$ and $\dot{m}_w=0.0358\text{Kg/s}$ .....	76
Figure 3.11 Comparison of heat output between the model and the manufacture data....	77
Figure 3.12 Comparison with dynamic responses of the room models.....	79
Figure 4.1 HWH system layout of the SFMZ system.....	81
Figure 4.2 Schematic drawing with nodes for the HWH system.....	82
Figure 4.3 Schematic diagram showing states of the aggregated SFMZ HWH system...	88
Figure 4.4 Hydraulic system of the ten-floor high-rise building HWH system.....	91
Figure 4.5 Details of mechanical room and differential pressure position .....	91

Figure 4.6 Schematic diagram of the entire HWH system .....	92
Figure 4.7 Diagram of the closest circulating water loops .....	94
Figure 4.8 Room temperature responses in the SFMZ heating system .....	102
Figure 4.9 Room temperature responses of the zones .....	103
Figure 4.10 Room air temperature responses in north zone .....	104
Figure 4.11 Water mass flow rates at differential pressures .....	105
Figure 4.12 Total, static and dynamic pressures in Loop n .....	107
Figure 4.13 Static pressure drops in all loops .....	108
Figure 4.14 Comparison of dynamic responses with two SFMZ models .....	109
Figure 4.15 Dynamic responses of the floor heating systems and the pump-motor unit	111
Figure 4.16 Dynamic responses of water mass flow rates .....	112
Figure 4.17 Zone air temperatures under decreased supply water temperature .....	113
Figure 4.18 Relationship between supply water temperature and outside temperature .	114
Figure 4.19 Dynamic responses of total pressure at different points .....	116
Figure 4.20 Pressure drops without gravity pressure in the hydraulic system .....	117
Figure 4.21 Dynamic responses of changing electrical voltage control signal .....	118
Figure 5.1 Configuration of control strategies used for the HWH system .....	121
Figure 5.2 Disturbances acting on the heating system .....	123
Figure 5.3 Control system configuration in the boiler control strategy .....	125
Figure 5.4 Average water temperature set points .....	126
Figure 5.5 Dynamic responses of water temperature and fuel control signal .....	127
Figure 5.6 Dynamic responses of the zone air temperatures (boiler control only) .....	128
Figure 5.7 Fuzzy logic adaptive control system configuration .....	130

Figure 5.8 Two types of fuzzy systems .....	131
Figure 5.9 Membership functions for $T_{ssp}$ .....	132
Figure 5.10 Dynamic responses of the major outputs.....	135
Figure 5.11 Dynamic responses of zone water temperatures and water flow control signals .....	136
Figure 5.12 Dynamic responses of the zone air temperatures (FLAC) .....	137
Figure 5.13 Control system configuration with the EKF.....	140
Figure 5.14 Memberships functions of the linguistic variables for $T_{ssp}$ .....	141
Figure 5.15 The <i>posteriori</i> estimate error covariance.....	144
Figure 5.16 Dynamic responses of the outputs in the control system with the EKF .....	145
Figure 5.17 Responses of return water temperatures and mass flow rate control signals .....	146
Figure 5.18 Temperature dynamic responses with and without the EKF .....	148
Figure 5.19 Comparisons of zone air temperature responses with and without noises ..	150
Figure 5.20 Dynamic responses of the system by changing noise levels .....	151
Figure 5.21 Temperature dynamic responses for different noise conditions.....	152
Figure 5.22 Dynamic responses of the system outputs considered uncertain parameters .....	154
Figure 5.23 Dynamic responses of the system control signals .....	154
Figure 5.24 Definition of set point accuracy for zone air temperature .....	157
Figure 5.25 Degree of membership functions for set point accuracy estimation .....	158
Figure 5.26 Set point accuracy estimation in the boiler control strategy.....	159
Figure 5.27 Set point accuracy estimation by using FLAC strategy .....	160

Figure 5.28 Set point accuracy estimation in the control strategy with the EKF .....	161
Figure 5.29 Configuration of the supervisory control system .....	162
Figure 5.30 Optimization process at $t=3000s$ .....	165
Figure 5.31 Dynamic responses of the optimal system outputs.....	167
Figure 5.32 Dynamic responses of the optimal signals in the optimal control system...	168
Figure 5.33 Comparison of dynamic responses between optimal and typical control ...	170
Figure 6.1 Model-based FDD configuration.....	175
Figure 6.2 Model-based FTC configuration .....	176
Figure 6.3 Membership functions of deviation of $T_s$ and fault level .....	179
Figure 6.4 FDD for the $T_s$ sensor fault .....	181
Figure 6.5 Responses of the FTC system for the $T_s$ measurement fault.....	183
Figure 6.6 FDD for the baseboard heater efficiency ( $H_e$ ) fault .....	185
Figure 6.7 Configuration of the FTC system for the heater fault .....	186
Figure 6.8 Dynamic responses of the FTC system for the heater fault.....	188
Figure 6.9 The FIS used to isolate the control valve fault .....	189
Figure 6.10 FDD for the multi-fault .....	192
Figure 6.11 Dynamic responses of the FTC system for the multi-fault.....	194
Figure A.1 Cells in the room with the hot water baseboard heater.....	214
Figure A.2 Dynamic responses of cell temperature and air mass flow rate .....	218
Figure A.3 Air temperature and air mass flow rate distribution .....	219
Figure B.1 Momentum balance in a pipe segment .....	220
Figure C.1 Layout of the basement heating system.....	223
Figure C.2 Schematic diagram of the basement heating system with nodes .....	224

Figure C.3 Dynamic responses of air temperature and water mass flow rate..... 226

## List of Tables

Table 3.1 Convection heat transfer correlations for air and water .....	61
Table 3.2 Correlations for computing friction coefficients for air and water .....	62
Table 3.3 Design parameters.....	69
Table 4.1 Water mass flow rates with variation of differential pressures .....	105
Table 4.2 Comparison of the pump-motor operation parameters with the power law ...	119
Table 5.1 Parameters of the HWH system.....	122
Table 5.2 Rule-base for the FIS.....	141
Table 5.3 Energy consumptions over one day .....	156
Table 5.4 Constrains of the optimal variables .....	164
Table 5.5 Energy consumptions over one day.....	171

## Nomenclature

$A$	Area ( $m^2$ )
$A_{eq}$	Equality matrix
$A_d$	Perimeter of pipe section (m)
$A_{fin}$	Surface area of fin per unit length ( $m^2/m$ )
$A_{ineq}$	Inequality matrix
$A_k$	Jacobian matrix at time step $k$
$A_o$	Total surface area of baseboard heater per unit length ( $m^2/m$ )
$A_p$	Outside surface area of bare pipe per unit length ( $m^2/m$ )
$A_t$	Surface area of finned-tube per unit length ( $m^2/m$ )
$A_w$	Inside surface area of tube per unit length ( $m^2/m$ )
$b$	Vector
$B$	Fraction factor ( $Kgm^2/s$ )
$c$	Specific heat ( $J/Kg\ ^\circ C$ )
$c_p$	Specific heat of air at constant pressure ( $J/Kg\ ^\circ C$ )
$c_v$	Specific heat of air at constant volume ( $J/Kg\ ^\circ C$ )
$C$	Thermal capacity ( $J/^\circ C$ )
$C_f$	Friction coefficient
$C_h$	Dimensionless pressure head coefficient
$dx, dx_p$	Length of finned-tube and bare pipe segments along the $x$ axis (m)
$dy$	Height of control volume along the $y$ axis (m)
$D$	Diameter (m)
$e$	Error signal

$E$	Total energy of air (J/Kg)
$f$	Frictional force (Pa)
$f_w$	Correction factor of water mass flow rate
$E_m$	Armature voltage (V)
$F_f$	Friction force acting on control volume (N)
$F_{vf}$	View factor
$g$	Acceleration due to gravity ( $m/s^2$ )
$G$	Mass (Kg)
$Gr$	Grashof Number
$h$	Heat transfer coefficient ( $W/m^2\text{ }^\circ C$ )
$H$	Height (m) or pressure head (Pa)
$H_e$	Heater efficiency
$H_k$	Jacobian matrix at time step $k$
$HV$	Heat value (J/kg)
$i$	Enthalpy of indoor air (J/Kg)
$I$	Unit matrix
$I_m$	Current (A)
$j$	Row of heater section
$J$	Moment of motor inertia ( $Kgm^2$ ) or objective function
$k$	Column of heater section or conductivity of fin material ( $W/m^\circ C$ )
$k_i$	Integral gain
$k_p$	Proportional gain
$\dot{k}_i$	Fuzzified integral gain

$\dot{k}_p$	Fuzzified proportional gain
$K_b$	Back emf constant (Vs/rev)
$K_i$	Toque constant (Nm/A)
$K_k$	Kalman gain at time step k
$l$	Number of hour
$L$	Length (m)
$L_m$	Armature inductance (H)
$\dot{m}$	Mass flow rate (Kg/s)
$m$	Mass per unit length (Kg/m)
$M$	Intermediate variable (1/m) or matrix
$n$	Integer
$N$	Motor speed (rev/s)
$Nu$	Nusselt Number
$P$	Pressure (Pa)
$P_k^-$	Priori estimate error covariance
$P_k$	Posteriori estimate error covariance at time step k
$Pr$	Prandtl Number
$q$	Rate of heat transfer (W)
$Q$	Rate of heat transfer per unit area ( $W/m^2$ )
$Q_k$	Process noise covariance at time step k
$r$	Inside radius of finned-tube (m)
$R$	Outside radius (m) or ratio

$Re$	Reynolds Number
$R_{ft}$	Ratio of face area of finned-tube to entire area of top cover
$R_k$	Measurement noise covariance at time step $k$
$R_m$	Armature resistance ( $\Omega$ )
$R_{tb}$	Ratio of face area of bare pipe to entire area of top cover
$R_{top}$	Ratio of non-hole width of top cover to whole width of top cover
$t$	Time (s)
$u$	Control variable
$T$	Temperature ( $^{\circ}C$ )
$T^*$	Fuzzified temperature ( $^{\circ}C$ )
$U$	Heat transfer rate ( $W/m^{2^{\circ}C}$ )
$V$	Velocity (m/s) or volume ( $m^3$ )
$V_k$	Jacobian matrix at time step $k$
$W$	Width of baseboard heater (m)
$W_k$	Jacobian matrix at time step $k$
$x$	Optimal variable
$\hat{x}_k^-$	Priori state variable
$\hat{x}_k$	Posteriori estimate state variable
$X$	State variable
$Y$	Measurement variable
$z, z_0$	Height and height of fictive plume origin
$z_k$	Measurement vector at time step $k$

## Greek Letters

$\alpha$	Fitting coefficient
$\alpha_{FI}$	Fault isolation factor
$\beta$	Factor
$\gamma$	Factor
$\gamma_{FI}$	Fault level
$\rho$	Density (Kg/m <sup>3</sup> )
$\varepsilon$	Emissivity of the surface
$\eta$	Fin efficiency (in sensible heat transfer mode) or pump efficiency
$\lambda$	Thermal conductivity (W/m°C) or friction factor
$\mu$	Viscosity (Pa.s)
$\sigma$	Stefan-Boltzmann constant (W/m <sup>2</sup> K <sup>4</sup> )
$\delta$	Thickness of fin (m)
$\delta_v$	Measurement noise
$\delta_w$	Process noise
$\varphi$	Factor
$\xi$	Frictional factor
$\Omega$	Factor identified based on heater heat transfer coefficient test (W/m°C)

## Subscripts

a	Air
b	Boiler
bmt	Basement
c	Cover
C	Thermal capacity
cd	Lower cover of right side
ce	Cell
ceil	Ceiling
conv	Convection
cov	Cover
cr	Right cover of baseboard heater
crt	Correction
ct	Top cover of baseboard heater
ctd	Below top cover
ctu	Above top cover
cu	Upper cover of right side
d	Design condition
e	East direction
ele	Electricity
emd	Estimated
eq	Equivalent
f	Fuel or friction factor

fin	Fin
fit	Fitting
flr	Floor
F	Fault
h	Horizontal
htr	Baseboard heater
i	Internal or integer
in	Into
int	Internal heat sources
low	Lower
lowbnd	Lower boundary
m	Motor
mod	Model
msd	Measured
n	Factor identified based on baseboard heater heat transfer coefficient test or north direction
N	Normal
max	Maximum
min	Minimum
o	Outside
opt	Optimal
out	Output from control volume
p	Pipe

r	Return
rm	Room
s	Supply water or south direction
sf	Surface
soil	Soil
sol	Solar radiation
sov	Overall sensible
sp	Set point
t	Tube
tot	Total
top	Top of control volume or top cover
up	Upper
upbnd	Upper boundary
v	Vertical
val	Valve
w	Water or west direction
win	Window
wl	Wall
y	y axis direction
z	Zone

## Acronyms

AC	Alternating current or air conditioning
AHU	Air handling unit
ANN	Artificial neural network
ASHRAE	American society of heating, refrigerating and air-conditioning engineers
CFD	Computational fluid dynamics
COG	Center of gravity
CRI	Compositional rule of reference
DC	Direct current
DDC	Direct digital control
DP	Differential pressure
EKF	Extended Kalman filter
FDD	Fault detection and diagnosis
FFSI	Functioning fuzzy subset inference
FIS	Fuzzy inference system
FLAC	Fuzzy logic adaptive control
FLC	Fuzzy logic control
FOM	Figure of merit
FTC	Fault tolerant control
HVAC	Heating, ventilating and air-conditioning
HWH	Hot water heating
ICS	Inferential control scheme

KF	Kalman filter
LCC	Life cycle cost
MAC	Model algorithmic control
MFMZ	Multi-floor multi-zone
MIMO	Multi-input multi-output
NN	Neural network
PDD	Percentage persons dissatisfied
PID	Proportional, integral and derivative
PMV	Predicted mean vote
SFMZ	Single floor multi-zone
SISO	Single input single output
SQP	Sequential quadratic programming
VAV	Variable air volume
VSD	Variable speed drive

# **Chapter 1 Introduction, Objectives and Contributions**

## **1.1 Introduction**

In order to provide thermal comfort and maintain desired indoor environment conditions, heating, ventilating and air-conditioning (HVAC) systems have been increasingly used throughout the world. These systems are run for keeping desired environment in winter, in summer, even in transient seasons, and they, as such, consume huge amounts of energy such as oil, natural gas, coal and electricity etc. It is well acknowledged that 25~35% of the total energy use is consumed by buildings, and space heating systems account for up to 50~60% of the total building energy consumption.

From the data described in the “Energy Use Data Handbook 1990 and 1998 to 2004”, it can be seen that, in Canada, residential and commercial buildings consumed 30.3% of the total energy use, and space heating systems represent 55% of the building energy use in 2004. Investigating the reasons for this huge energy consumption of HVAC systems is important. A number of factors such as heat transfer processes, HVAC system design methods and control strategies, the influence of actual operations (such as part load conditions), over sizing of the selected equipment, non-optimal operation and, various component and system faults have been found to impact energy efficiency. Since the energy crisis in 1970s, and the oil crisis in the beginning of 2005, interest in reducing energy consumption, decreasing pollution and improving the environment have been the key motivating factors for developing energy efficient operating strategies. To achieve these aims, two main strategies could be utilized. One approach is to adopt energy efficient components and HVAC systems, such as the selection of high efficiency boilers,

the implementation of variable speed drives (VSD), the use of variable flow systems instead of constant flow system, and the optimal design of systems. The other strategy is to use innovative energy management techniques to achieve better performance, such as implementation of suitable control strategies, optimal control, intelligent controllers, together with fault detection and diagnosis (FDD).

Hot water heating (HWH) systems have been employed extensively in high latitude regions of the world. Because of their importance and economic impact, this research focuses on dynamic modeling, advanced control strategies, and fault tolerant control of HWH systems.

## **1.2 Hot water heating systems**

The capacity of HWH systems operated nowadays varies from small size such as 10KW to huge size such as 1.5GW. Generally speaking, HWH systems consist of three main sub-systems: a heat source, a distribution network, and the end user. The heat source can be classified by the type of heat source (single or multiple heat sources) and energy source: fossils (coal, oil and natural gas) and electricity. The distribution network can be either a direct or indirect pipe system. The end user could be divided into residential and commercial building users. From practical point of view, a very popular high-rise building HWH system with single heat source is shown in Figure 1.1. In this figure, the hot water from the boiler is supplied to the high-rise building heating system, and each floor sub-heating system is connected by the riser using direct return loop. The heaters in the rooms emit heat to the building indoor environment. All of the return water from the sub-heating system returns to the circulation pump, and then is pumped to the boiler in order to be heated again. A makeup water system is employed to maintain

certain water pressure in the circuit. The boiler output varies based on heating load. The water flow rate in the loops could be either constant or variable. Several disturbances (outdoor air temperature, solar radiation and internal gains) acting on the heating system affect the system performance.

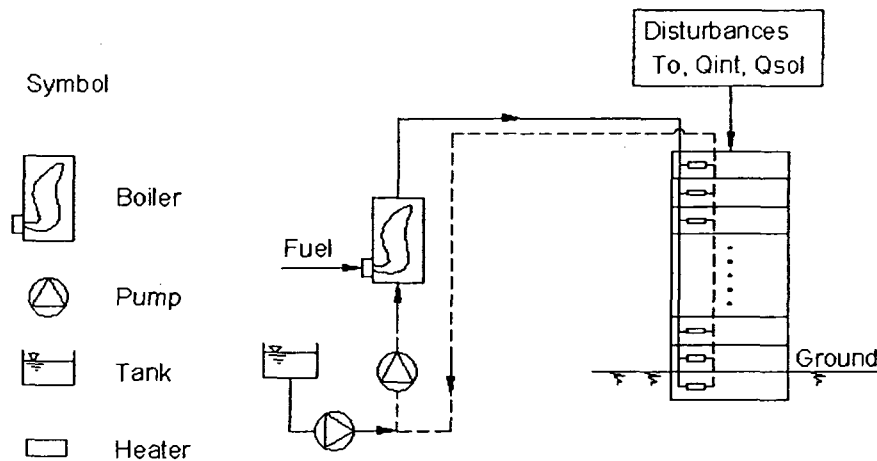


Figure 1.1 A typical HWH system for a high-rise building

In order to improve energy savings and the system performance, four different aspects will be explored: (i) adding proper controllers to modulate either supply water temperature or water flow rate or both in the heating system, (ii) using solar radiation and internal gains as kinds of beneficial heat gains to decrease energy consumption, (iii) computing and using optimal set points, and (iv) employing fault detection and diagnosis (FDD) to improve operating performance of the HWH system.

Improving energy efficiency of HWH systems is a challenging control problem because the dynamic systems consist of time-varying parameters, acted upon by multiple disturbances, involving transportation delay process, off-design operation, water leakage and strong non-linear properties etc. Control failures could lead to large swings in indoor air temperature, hydraulic and thermal unbalances, lower reliability, the breakdown of

heating devices and low energy efficiency. Component faults could result in large energy wastage and undesirable performance of HWH systems.

### **1.3 HWH System Control**

Based on the development of computer technology and control devices, computer control systems are utilized to control HWH systems in recent decades. Generally, large HWH systems involve two level controls: a supervisory level and a local level control, which are implemented in the form of direct digital control (DDC). In the supervisory level control, historical weather data, system parameters and operational information are recorded, analyzed and utilized to make decisions satisfying the requirement of system control and operation under varied situations. The local level controllers catch control information from either supervisory level or pre-programmed logic. Examples of local controls are supply water temperature reset control, night set-back control, makeup water pressure control, return water temperature reset control and water mass flow rate control etc. These control strategies are mostly used in large HWH systems; however, they are employed independently without taking into account the interaction among control variables in HWH systems.

A typical HWH system control configuration is depicted in Figure 1.2. From this figure, it can be seen that the fuel firing rate is regulated by measuring the indoor air temperature in one of the multi-zones by a local controller. The controller could be proportional (P) or proportional and integral (PI) control. Generally speaking, the dynamics of HWH systems with large heat capacity do not change rapidly; therefore, the derivative (D) control does not significantly improve control system performance. For this reason, a properly designed PI controller is adequate to track the temperature set

points in practice. The controller may also be of other type such as a fuzzy logic controller for instance. It should also be noted that in a small system such as the one in Figure 1.2, the control signal comes from one zone temperature. This could be a problem if a HWH system is large and consists of several zones. In such cases measuring all zone air temperatures, transportation and treatment of all signals should be taken into account.

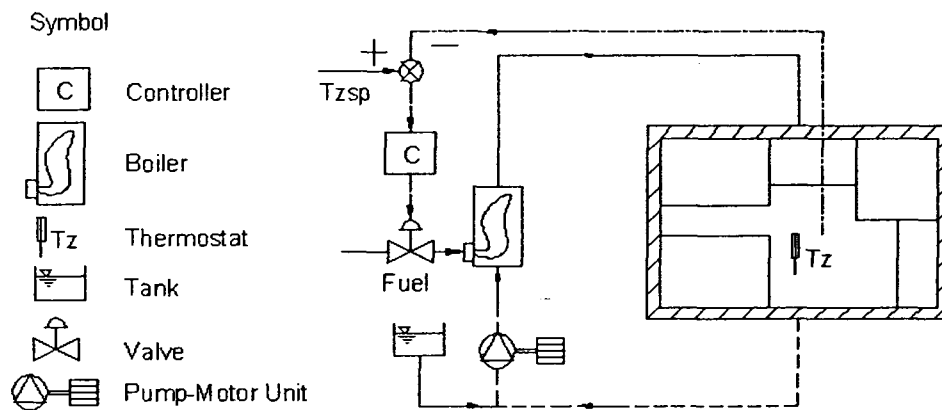


Figure 1.2 HWH system control configuration

HWH system processes are highly interactive coupled time-varying processes. For instance, in a zone air temperature control based on regulating water mass flow rate, when the zone air temperature is higher than the set point, the zone air temperature controller tends to reduce the water flow rate. However, if the supply water temperature output from the boiler is not controlled, it could fluctuate rapidly even crossing over the upper limit of the boiler supply water temperature. Another property of HWH systems is that the building loads and operating characteristics of systems vary with time. Hence, in order to achieve the objectives of using the least energy, obtaining better performance and satisfying thermal comfort, HWH system control strategies should be considered at system level with individual local control loops embedded in the overall system.

Although PI controllers have been widely used in HWH systems because of their cost effectiveness, robustness and reliability, they still have problems that cause poor operation of systems, especially due to the practice of tuning one loop at a time. The local controllers cannot maintain good performance all the time with fixed gains or default settings. This is due to the fact that HWH systems consist of multiple control loops that interact with each other and, as such, the controller gains should be adjusted according to the different operating conditions to track set points.

In practice, two methodologies have been employed to overcome the obstacles. One is called the “gain scheduling approach”; the other is named the “self-adaptive approach”. In the gain scheduling approach, the gains of the controllers are adjusted based on a lookup table that is calibrated under different operating situations. Astrom and Wittenmark (1989) showed that this approach works well in HVAC control systems. The dynamic models of HWH systems developed either from theoretical principles or from system identification techniques exhibit uncertainties. The models do not compare well with the actual processes; hence, control systems based on those models cannot give good performance. The self-adaptive approach on the other hand can automatically tune the parameters of controllers by identification of the dynamic responses of the systems. This approach has many applications described in next chapter because this method is simple to implement, saves energy and deals with most control problems. Nevertheless, for highly coupled non-linear systems, such as HWH systems, tuning a local controller could affect the performance of other controllers. To handle this problem, it is desirable to utilize a multi-input and multi-output (MIMO) control strategy.

Since 1970s, advanced control systems such as model algorithmic control (MAC), adaptive control, robust control, artificial intelligent control and FDD have been developed. MAC is a computer control algorithm that consists of a dynamic model, a feedback control loop and an online optimization to generate the output of the controller. System uncertainty and measurement noise could be handled by combining the Kalman filter (KF) for linear systems and the extended Kalman filter (EKF) for non-linear systems. Intelligent control such as fuzzy control, expert control, neural network control and fuzzy identification, is based on the knowledge and understanding of control systems, and plays very important role. Fuzzy control utilizes mathematical techniques for dealing with imprecise dynamic knowledge using linguistic language (if-then rules). With fuzzy logic, propositions can be represented with degrees of truthfulness and falsehood (0~1). Many fuzzy logic controllers have been employed as set point regulators in HVAC system applications, and have improved system operation very much. It should also be noted that energy savings and optimal operation are dependent on the reliability and safety of HWH system operation. Thus, FDD technology is also used to identify and handle system failures. Moreover, fault tolerant control (FTC) that combines FDD can be employed in HWH systems to improve system performance, e.g., thermal comfort and energy savings.

#### **1.4 The importance of this research**

In the recent decades, due to rapid economic development all over the world, the amount of primary energy use such as coal, crude oil and natural gas etc has been increasing rapidly. As a result, reducing primary and secondary energy consumption as well as lowering environment pollution (such as toxic waste creation, waste disposal etc.)

become an increasingly important consideration in the HVAC field. This is especially for those countries and regions of the world where HWH systems have been used in large numbers. Recently, according to statistical data from China statistic organization, residential building energy consumption accounts for approximately 32% of the entire energy consumption, and energy consumption for heating reaches about 57% of residential building energy consumption, and the energy used for heating residential buildings in China is about 3 times that of developed countries under similar conditions. Secondly, the need to improve the indoor air environment has received much attention recently. Thirdly, because HWH systems have become larger and larger, there is a need to employ FDD to identify problems and take corrective actions. Finally, designing appropriate FTC systems based on advanced control strategies and FDD information has advantages for both energy customers and energy suppliers.

## **1.5 Scope & objectives**

In this study, dynamic modeling, intelligent control and FTC based on the FDD approach are studied for HWH systems.

The motivation is: achieving potential energy savings and the prospect of improving the indoor environment. The main objectives of this study are to develop and simulate advanced control strategies and FTC techniques for HWH systems. The specific objectives are to:

- (1) *Develop an overall dynamic model for a HWH system for a high-rise building.*

The component models include those for a boiler, motor-pump unit, control valve, finned-tube baseboard heater and pipe network etc. The component models are combined and extended in order to develop the overall HWH dynamic model

from zone (room) level to floor level and building level. The entire system model can be used to predict the system dynamics, evaluate the control strategies, compute the energy consumption, detect and isolate different faults and simulate fault tolerant control strategies.

- (2) Design advanced control strategies utilizing fuzzy logic theory and adaptive control strategies for both temperature and fluid flow control to improve system performance.
- (3) Design a supervisory control strategy for the overall system.
- (4) Develop fault isolation strategies for the measurement and process faults in HWH systems.
- (5) Devise FTC strategies based on FDD information to improve system performance, save energy and extend the operating range of the system.
- (6) Simulate the HWH system dynamics with various control strategies. Evaluate energy efficiency and thermal comfort for occupants.

## **1.6 Contributions and summary**

The primary contributions of this thesis are summarized as follows:

1. By applying first principles of mass, momentum and energy balances, a large scale overall HWH system model for a high-rise building is developed by considering temperature, fluid flow, current and motor speed dynamics. The overall dynamic model is obtained by model order reduction and aggregation techniques and extended from a one room level model to a single floor multi-zone model and finally to a multi-floor multi-zone model.

2. A zonal model is developed and utilized for model condition verification and correcting room air temperature measurement.
3. Advanced control strategies utilizing fuzzy-PI and fuzzy logic adaptive PI (FLA-PI) controllers were designed in order to regulate the supply water temperature from the boiler and the water mass flow rate entering the zones. The intelligent control systems improved system performance and saved energy. The measurement and process noises were dealt with the EKF technique, and smooth performance was realized by employing the estimated state variables.
4. Supervisory control based on optimization technique was developed for the HWH control system. By utilizing this strategy, energy savings were achieved.
5. Model-based FDD and model-based FTC techniques were developed for the high-rise building HWH system. Measurement and process faults were determined and isolated according to a fuzzy inference engine. The FDD information such as fault and fault level were used in the FTC strategies.

The rest of this thesis is arranged into six chapters. In the next chapter, a literature review on HWH system modeling, system control strategies, FDD and FTC is presented.

In Chapter 3, the detailed component level models of a HWH system for a high-rise building are developed. By using a model order reduction technique, the model order is reduced. The open loop tests are carried out to study system performances.

In Chapter 4, the single-floor multi-zone model is extended to a multi-floor multi-zone dynamic system for the high-rise building based on order reduction and aggregation techniques. Also, the open loop tests were made to study the dynamic responses of the system.

In Chapter 5, advanced control strategies using fuzzy logic adaptive control (FLAC) systems were designed for the HWH system. The effect of parameter uncertainties and noises from measurement and process were examined by using the EKF technique. A methodology for computing optimal set points is also presented.

In Chapter 6, model-based FTC systems are developed and tested based on FDD information combined with measurement signal and process faults. Measurement faults such as a supply water temperature sensor fault, a process faults such as heater efficiency degradation and control valve faults are studied.

Conclusions, contributions of this investigation and recommendations for future research are stated in Chapter 7.

## **Chapter 2 Literature Review**

### **2.1 Introduction**

Based on the motivation and objectives of this study, developing successful control strategies for HVAC systems, especially focused on HWH systems, is necessary to realize better FDD embedded control systems. As a result, the literature review of this research will be divided into the following sections: (i) system design considerations and operation, (ii) dynamic models and simulations, (iii) system control strategies, (iv) the Kalman filtering techniques, (v) fault detection and diagnosis and (vi) fault tolerant control strategies.

### **2.2 System design consideration and operation**

Proper HVAC system design plays an important role in both first cost and system operation. Suitable design consideration improves performance avoiding undesirable thermal environments, poor operation, large energy consumption and even system failures. A number of researchers have addressed these aspects.

Six residential heating systems in Hungary were studied by Zoltan and Robert (2002) for the purposes of maintaining indoor air temperature and saving energy. They state that three important conditions have to be satisfied in HVAC systems such as (1) the design flow must be available at all terminals, (2) the differential pressure across the control valves must not vary excessively, and (3) the flow must be compatible at system interfaces. Heating systems with one-pipe and two-pipe, built-in thermostatic and balancing valves were recommended. They showed that the heating system not only

fulfilled the design indoor air temperature requirements, but also the heat consumption was reduced by 10% to 25%.

The use of variable water flow under the control of the space temperature sensor at each terminal is necessary in HVAC systems. Considerations for the hydraulic system design such as the use of control valves and balancing valves, the selection of the size, pressure drop of the control valves and valve authority etc. have been described by Richard (1998). Moreover, the author stated that the use of a differential pressure control device across the most resistant terminal and the location should be taken into account. Proper balancing should be based on the minimum set point of the  $\Delta P$  control valve for all branches. In addition, Roy (1998) addressed how to select and set balancing valves for HVAC hydraulic systems in order to save pumping cost.

Space heating and domestic hot water control systems sometimes are connected together. As a result, special design considerations should be taken into account for this type of combination to handle the effect of interactions. Burd (1997) presented the design requirement and actual modes of operation for a combined heating system to satisfy spikes in the domestic hot water load and to decrease the first and operating cost of the district heating system due to the small diameter pipe network and the lower circulating water flow rate.

Jaćimovic et al (1998) described a supply water temperature calculation method for both direct and indirect district hot water heating systems. The impact of the heat exchanger type and its fouling on the heat output was considered. The supply water temperature in the primary and secondary systems was computed using a linear function between heat losses from heated objects and outdoor air temperature. The assumptions

include: constant indoor air temperature and constant heat exchanger overall heat transfer coefficient. However, the heat exchanger overall heat transfer coefficient is not constant because of fouling in practice.

Accessibility analysis of district heating networks was introduced by Xuzhong et al (2001). An accessibility measure was defined for a multi-loop district heating network, when all control valves in the loops were regulated to the proper opening position, resulting in great pumping cost reduction. A steady state mathematical method was developed based on graph theory and principles of hydraulic networks. A maximum-minimum optimization method with linear constraints was applied to obtain suitable pressure difference of each terminal.

## **2.3 Dynamic models and simulations**

Because of uncertainty of building enclosure parameters and time varying disturbances acting on the systems, it is almost impossible to obtain complete and accurate data from measurement of actual system operation; nevertheless, mathematical models and numerical simulations offer a low cost solution to overcome those difficulties. Extensive models of HVAC systems and their components can be found in the literature. These models are used in the field of design, analysis, control, optimization as well as energy estimation etc. These models could be either steady state or dynamic models. Most HVAC system models are built from bottom-up approach. In other words, component models are developed firstly, and then they are integrated to build whole system models. Major components in HWH systems are boiler, pipe network, heat exchanger, control valve, heater, building enclosure and conditioned zone and rotating equipment such as fan, pump and motor.

### 2.3.1 Component level models

#### *Boiler model*

Boilers in HVAC systems are one of the most important components not only because they are the biggest energy consuming devices, but they also play an important role in regulating HVAC system performance. Due to the complexity of boiler combustion process and dominant radiation heat transfer processes in boiler chambers, most boiler models are developed based on steady state heat balance principles. These models are used to predict the fuel consumption with/without fuel controller under different operating condition. Many researchers employed steady state models or simplified dynamic models instead of complex boiler models in simulations. It should be noted that, the combustion process in the boiler chamber is relatively faster than other heat transfer processes such as water-to-water, water-to-air and air-to-air; therefore, simplified boiler models could be used.

Boiler efficiency is the ratio of the energy output and energy input. Generally, the efficiency can be obtained by two methods: curve fitting from experimental data and using energy balance method. Curve fitting models are based on the real measurement under different operating situations. The other model depends on the viewpoint of energy flow: input-output method and heat loss method. All heat losses from boiler such as stack gas, chemical incomplete combustion, physical incomplete combustion, and radiation of combustion and natural convection should be taken into account. When heating loads of the systems vary, not only boiler efficiency changes, but also air mass flow rate of the combustion process has to match the load. A simple method of calculating efficiency of boilers was presented by Lianzhong (2003).

Niu and Wong (1998) presented a simple boiler model for an industrial boiler unit that can be used to simulate power plant performance. In this model, the heat transfer in the combustion chamber was considered by the zone method; while the heat transfer in the secondary super-heater, the re-heater, the primary super-heater and the economizer was simulated by lump parameter analysis. Main components of the system model were formed based on the boiler system configuration. However, because of the complexity of the boiler system, a steady state model was adopted and several modification factors were made. Relatively complicated models of boiler combustion for a coal fired boiler with a fixed bed were developed by Biyikoğlu et al (2005). One was the analytical model which solved the governing equations of 2-D turbulent flow in the combustion chamber and 1-D coal combustion in the fixed bed; the other was the fuzzy logic model which predicted temperature distribution in the chamber based on data obtained from numerical solution for charging coal and air feeding rates. The author employed control volume method to state the equations in the combustion chamber and the fixed bed. The simulation results were found to be satisfactory. Although fuzzy logic approaches could be an easier approach instead of solving complex mathematical equations, related information has to be obtained from the experts or based on experience.

#### ***Finned-tube baseboard heater model***

Hot water baseboard heaters are commonly structured by finned-tube with different geometry of fins and tube diameter. Moreover, heat output from baseboard heaters varies depending on the geometry of fins, finned-tube manufacturing method and material used. Hence, a finned-tube dynamic model is necessary to obtain the dynamic responses of temperature, pressure, mass flow rate and heat output from the baseboard

heaters. Some studies used steady state models based on NTU effectiveness of straight finned-tube and simplified dynamic models based on some assumptions. Also, empirical models have been proposed in the literature. However, few studies focused on detailed finned-tube baseboard heater models.

Delnero et al (2004) proposed an exact solution for a water to air finned-tube cross-flow heat exchanger. The dynamic model was developed based on mass and energy balance principles in one dimension. Major assumptions were described as follows: constant air and water density, independent of temperature for convective heat transfer coefficients, one dimensional water flow, constant air temperature and velocity through the entrance cross section to the heat exchanger, and constant fin effectiveness. The mathematical equations were solved by separating the PDEs into a boundary value problem and an initial-boundary value problem, then combining the solutions of these sub-problems by superposition to obtain the general solution.

A dynamic model of a finned-tube heat exchanger used in an air handling unit (AHU) was developed and validated by Yu et al (2003) based on energy balance principles in order to investigate an FDD strategy. To increase the accuracy of the dynamic model, the heat exchanger was split into 32 small elements deferred from straight finned-tube and bends. The responses of the model were compared with the measurement, and a correction factor was used in order to improve the simulation results.

An empirical study was investigated by Chuah et al (2004). In the study, 15 finned-tube heat exchangers with different fin pitches, tube numbers and fin geometry were chosen. Natural convection heat transfer of the heat exchangers was investigated by varying the hot water temperature, water velocity in the tube and the finned-tube

configuration. The experimental results showed that inlet water temperature was a significant factor in heat transfer; while water velocity in the tube was a weak factor in heat transfer. Furthermore, large number of tubes and smaller fin pitch resulted in lower heat transfer coefficient. Although the experimental study was obtained by using chilled water, it is still meaningful for use in hot water in heating systems.

### ***Pump/Fan-motor model***

Electrical motors are used in HVAC systems in running devices such as fans and pumps. Large amounts of electricity are consumed by these electrical motors.

Fan-motor units are usually used in a HWH system boiler house to transport air into and carry out flue gas from a boiler combustion system. In the past, although constant speed fans were employed widely, variable speed fans have increasingly been used these days due to the development of variable speed drives (VSD). Because of small time constant of fans compared with other components of HWH systems, they are usually described in steady state form based on theoretical fan laws. At actual operation, especially at lower speed, the energy consumption of fans is somehow greater than theoretical value due to the losses in electrical motor windings. Fan head coefficient (pressure head) and fan efficiency could be estimated by curve fitting the performance data from the manufacturer's catalog (Hill, 1985, and Wang and Xinqiao, 2000). For instance, Mei and Levermore (2002) developed two models to predict the pressure rise of a variable speed fan under steady state condition; one was based on polynomial curve fitting method, the other is a ten neurons sigmoid neural network (NN) model with two inputs. From control point of view, model of fans can be expressed as a first-order dynamic equation with different time constants for different operational ranges. With

experimental data under step change of the control voltage, the fan dynamics were expressed by a first order equation with different time constants for different operational ranges. Considering the losses in the frequency converter and the motor, the fan efficiency was not constant. Engdahl and Johannsson (2004) employed a quadratic function to describe the correlation between the fan power consumption and the supply air flow by assuming that half of the fan electricity was converted into an increase in the supply air temperature.

Pump-motor units have the similar properties as fan-motor units except the transported medium is water to air. According to experimental data, pumping costs in HVAC systems vary between 10~35% of total system operation costs depending on the system design, operating method and control strategies etc. However, this cost could be decreased by proper selection of set point and by applying VSD. An example of using pump differential pressure set point reset according to the position of chilled water valves was introduced by Brain and Fisher (2003). For conventional control, the chilled water valve was controlled to maintain the discharge air temperature set point for each air-handling unit, and the pump was regulated to keep a fixed differential pressure. The new control strategy could save pumping cost since the tertiary pump speed is regulated based on at least one chilled water valve almost fully open, and the pump differential pressure was optimized associated with the position of the control valve. This method could be applied to HWH systems. On the other hand, in order to apply variable speed control for pumps in HVAC field, several aspects such as the variation of the water system pressure head, suitable methods of regulating pump speed and sequential control for multi-pump operation have to be considered carefully. These situations, which were based on the pipe

network, the variation of the load as well as the control method of the whole system, were presented by James (2003).

Motors used in HVAC systems can be classified into two categories. Direct current (DC) motors that convert electrical power provided by a voltage source to mechanical power via magnetic coupling; the other is single or three phase alternating current (AC) induction motors. Permanent magnet DC motors are constructed by two major parts: the rotor or armature and the stator, and they are very commonly utilized in many industrial systems such as variable speed and torque control applications. On the other hand, the speed of the AC motors varies depending on three parameters i.e., the fixed number of poles, the frequency of line voltage and the amount of torque loading on the motor. A simple DC motor dynamic model with armature current, motor torque, back emf and rotor angular velocity was given by Benjamin (1991). In addition, the author described the factors of the torque constant and the back emf constant are identical with their units respectively expressed in Nm/A and Vs/rev.

#### *Zone (space) model*

Zone models for space conditioning vary from simple to very complex. Simple zone models normally utilize lumped parameters with well-mixed assumption in the conditioned space; while complex zone models employ computational fluid dynamics (CFD) methodology which identifies zone air flow and temperature distributions based on partial differential equations in space and time. The complexity of zone model were presented by Serbric et al (2000) and Huang and Haghighat (2005). On the other hand, simple zone models are suitable for control purpose with acceptable accuracy; while

complex zone models are preferred in more complex investigations such as indoor air quality requiring air flow rate, velocity, humidity and temperature distribution.

Four simple zone dynamic models were developed by Borresen (1987) for air temperature control analysis. The differences in these models were based on the treatment of the walls in the zone. The first model neglected the influence of the walls; the second model considered the influence of the walls by introducing their areas and U values. The last two models considered constant wall temperature and time constant of walls respectively. According to the empirical data, all models gave good short-term responses and steady state responses. For instance, the first and third models had similar steady state responses. However, the dynamics of the models showed different response.

Kasahara et al (2000) stated that zone models could be reduced to first order plus dead time models based on lumped parameters. Moreover, time constants for the zone dynamic responses were divided into two categories: fast and slow responses. This is due to the difference in the thermal capacities of materials. From control point of view, simplified time constant models were adopted with well-mixed zone air assumption.

In addition, a simplified model based on a zonal model approach was developed and validated (Inard 1998) in different heating system configurations for energy consumption and thermal comfort evaluation. The investigated heating systems included localized hot water and electrical heaters, a distributed hot water heated floor and a distributed electrical heated ceiling. Results showed that the distributed hot water heat source could achieve better compromise in both energy consumption and thermal comfort. However, the results obtained based on the particular case might vary if the heating system parameters change.

### 2.3.2 System level models

Since HWH systems are becoming larger and larger with huge energy consumption, interest in optimal operation, optimal control strategies and fault detection and diagnosis has received increased attention in recent decades. However, to establish the objectives of energy savings, optimal operation, control strategies and end-user demand management, system level HVAC dynamic models rather than component level dynamic models are required for investigation and applications. Many studies have considered the steady state and dynamic system models based on first principles. Most system level models are modular based. In other words, component models were integrated together depending on the input and output connecting the entire system.

For example, an 11-order dynamic model of a HWH system, consisting of boiler model, zone model, outside wall model and roof model, was developed by Kanarachos and Geramanis (1998). This dynamic model was used to simulate the responses of designed single input single output (SISO) and multi-input multi-output (MIMO) control strategies. Because of the nonlinearities such as uncertainties, saturation of the actuators and long system delay, adaptive controllers were designed by employing neural networks and evaluated with simulations. Detailed controller design procedures and learning law of the two kinds of control systems were introduced. Two days of simulation tests showed that the control systems could overcome the difficulties by using the adaptive controllers.

A direct district HWH system dynamic model was developed by Lianzhong and Zaheeruddin (2004). In this constant flow model, component models such as boiler model, underground pipe model, pump-motor model, heater model, zone air model and building enclosure model were combined to develop a dynamic system model. Heating

system characteristics, optimal parameters and control strategies were investigated based on the overall system model. Transport delay in the district heating systems was dealt with by use of the Smith predictor technique. Simulation results showed that energy savings of 19~32% could be obtained if the proper control strategy, with optimal supply water temperature set point for the boiler was used, and the zone air temperature was maintained within acceptable level for thermal comfort.

A dynamic model of a hydraulic heating system considering boiler, finned-tube baseboard heaters, heat exchanger coil and zone was developed by Zaheeruddin and Monastiriakos (1998). The baseboard heater was modeled as 1-D equations and discretized along the water flow direction. The simulated responses of the analytic model were compared with an existing on-off controlled HWH system. The validated model was utilized to design feedback controllers for controlling the zone air temperature, the boiler water temperature and the domestic hot water temperature. A load matching approach based on the relationship between the supply water temperature and outdoor air temperature to obtain the supply water set point was used. The boiler supply water temperature was controlled by regulating the fuel firing rate of the boiler, and the zone temperature was controlled by regulating water flow rate in the heaters.

A grey-box modeling technique which used physical knowledge with statistical database was used for a large district heating system (Nielsen and Madsen, 2006). This model was used to connect energy consumption to climate and calendar information. The database included heat consumption and weather data for a certain period based on hourly measurement. The overall model structure was selected based on physical

characteristics of the heating system during the statistical modeling process. The grey-box approach showed to be powerful to improve the energy efficiency of the system.

Many types of zone (room) air temperature modeling techniques were introduced in literature. Single air node models for zone air dynamics usually make assumptions such as well-mixed zone air and neglected stratification phenomena. However, these kinds of models give no information about air flow pattern such as temperature and mass flow rate distribution. On the other hand, detailed temperature and flow distribution may be obtained by using computational fluid dynamic (CFD) models with extremely long computational time and large amount of computer memory. Between single air node models and CFD models, intermediate methodologies that are entitled as zonal model techniques not only can give accurate heat transfer information than single air node models, they also could present temperature and flow distribution information for the purpose of predicting thermal comfort, control investigation and energy consumption.

From a zonal model, air temperature and mass flow distribution in a room could be obtained with enough accuracy. The number of the cells in a room is usually taken into account from the simplest such as 3 to relatively complex such as on the order of 100. The principles of mass and energy balance are applied to all cells in order to calculate heat and mass transfers between them. By solving the set of coupled equations, the distributions of air temperature and mass flow rate are carried out.

The first generated zonal models by Howarth (1985) and Inard (1988) were based on fixed air flow directions and considered with specific flow laws for the types of boundary, plume and jet cells. Obviously, there was a limitation due to the assumption of fixed air flow directions. After that, zonal models (Wurtz et al 1999) were developed

consisting of air flow rates that were function of pressure distribution in the neighborhood of the cells. Though these models have given more general application, it has been shown that the approaches cannot predict the driving flow momentum with adequate confidence (Musy et al 1997). Since then, hybrid zonal models were developed based on specific laws for driving flows and power law pressure distribution for all cells (Grelat 1987, Dalicieux and Bouia 1991, Huang et al 2003). These approaches could be found for several simple configurations.

### **2.3.3 Available simulation software packages**

Computer simulation software packages for buildings are effective analytical tools for dynamic response, energy analysis and the evaluation of HVAC systems. Nowadays, many simulation software packages are available such as DOE-2 (1981), EnergyPlus, EnergyExpress, TRNSYS (Klein et al, 1983), HVACSIM (Park et al, 1985), BLAST (1979) and ESP-r etc.

One of the well known building energy simulation programs is DOE-2, which is based on an hourly, whole-building energy analysis calculation of energy performance and life cycle cost (LCC) assessment. Another popular program is EnergyPlus, which is based on most popular features and capabilities of BLAST and DOE-2. It can be utilized to model heating, cooling, lighting, ventilation and other energy flows in buildings. Recently, it includes the new capacities such as multi-zone air flow and thermal comfort etc. EnergyExpress can be used to simulate energy consumption and predict peak loads in commercial buildings.

However, due to the fact that source codes of public domain simulation software are not available, the advantages of programming such as easily changing source codes and flexible programming cannot be implemented in these software packages.

## **2.4 System control strategies**

In this section, control strategies, optimal operation and controller tuning methods utilized in HVAC systems are reviewed. Intelligent control such as fuzzy logic control is also the focus of this section.

### **2.4.1 System control and optimal operation**

Many types of control strategies for HVAC systems have been studied by researchers such as neural networks, genetic algorithms, predictive control, optimal control, expert control, grey model control etc. In spite of all these, PID control continues to be the most popular and successful controller. Although it is well known that optimization methodologies could be used to obtain better control performance, the major objectives of optimal operation in HVAC systems are to improve system performance which is commonly described by energy use and thermal comfort. Many studies focused on the methodologies based on various optimal solutions. Constraints in HVAC systems could be linear, nonlinear, equality and inequality equations. Also, boundaries of system variables have to be given for proper system operation. An optimization algorithm has to be chosen to obtain the solution. The optimal results are generally employed as set points or optimal system parameters in order to improve system operation. A number of papers focused on optimization could be found in HVAC area. Most papers used steady state optimization approach; while a few dealt with dynamic optimization problems. Note that

many optimization approaches and system control strategies can be combined in order to reach better performance.

Traditional two-position (on-off) control has been widely employed in space heating systems in the past. Kulkarni and Feng (2004) developed a state space dynamic model for simulating and comparing transient responses of residential building control systems with a single-zone, two-position control. An objective function based on energy consumption was utilized to minimize energy use. From the simulation results, it was shown that PI control has better performance than the traditional two-position control although they do not reveal much difference in energy consumption.

Spreitzer et al (2002) stated control approaches for regulating water flow rate in a variable water flow rate HWH system. Conventional PI controllers with fixed gain parameters regulate boiler supply water temperature based on measured outdoor air temperature. Two kinds of observers namely a disturbance observer and parameter observer were studied in order to obtain the water flow rate. The disturbance observer was based on rewriting the equations of the state space model; thus, the water flow rate was seen as a disturbance. The parameter observer was used to get the water flow rate based on the relationship between water flow rate and supply water temperature. They showed that two observers improved the control system performance.

Two different observer-based schemes for the estimation of the water mass flow rate through a central heating boiler in a central hot water heating system were developed (Karsten 2002). One scheme was based on a simple dynamic model; the other was based on supply water temperature prediction error. The supply water temperature from the boiler was controlled by a typical fixed gain PI controller. Simulation results presented

that the water mass flow rate had a great influence on the boiler's capacity to transfer energy to the circulating water in the heat transfer process. Nevertheless, the control system performance could be affected by the accuracy of the observers.

An overall air-conditioning system dynamic model (Michael et al. 2007) considering five subsystems consisting of a blower model, a mixing box model, a boiler model, a water flow control valve model and heating coil model, were taken into account and verified by employing experimental data. The overall model was used to test advanced controllers in order to improve system performance. The simulation and testing results in the simple HVAC system addressed that the temperature and the flow rate of the discharge air were able to be regulated by the advanced MIMO control system to handle multi-variable interactions. The advanced control strategy such as robust control theory may be used in HWH systems.

In order to simulate control system responses and achieve robustness of hot water heating and cooling systems, Gouda et al (2003) developed two controllers. Component models such as the building envelope, the heater, the control valve, the actuator and the measuring instrument were modeled to describe the overall HVAC system. The controllers were tuned according to a gradient-descent-based optimization procedure, and the robustness quantities were analyzed with HVAC system operating conditions. Moreover, the simulation runs showed flexibility, transparency and computational efficiency of the developed dynamic model. In addition, a robust adaptive controller was designed by Singh et al (2000) based on solving the robust servomechanism problem for a fan-coil heating system.

Investigations on potential energy savings in heating systems that could be achieved by improving boiler controls were addressed by Liao and Detxer (2004). The boiler supply water temperature controls in HWH systems were grouped into three main categories such as fixed set point, set point compensated according to outdoor air temperature and fixed set point but fuel firing was delayed for a fixed period. The heating system performance was evaluated based on two parameters: total energy consumption and thermal comfort in the zone. Both simulation results and experimental data showed that the potential energy saving might be as high as 20% by using an inferential control scheme (ICS) described by Liao and Dexter (2003) to the boiler in uncontrolled radiator heating systems. Moreover, an estimation model of an average zone air temperature based on dynamics of temperatures in multi-zone heating systems was developed and validated by Liao and Dexter (2003). The boiler firing rate, outdoor air temperature and solar radiation were considered in the estimator. The estimator was validated according to the available data from heating systems. The ICS was presented in order to control the system performance. However, large set of training data was required to improve the commissioning of the estimator. A simplified dynamic model for examining the average zone air temperature in heating systems was also introduced. An experimental study was made by Liao and Dexter (2005).

Optimization is a popular technique that is applied to HWH systems. A method of obtaining optimal hot water supply temperature in a district heating system was introduced by Benonysson et al (1995) based on minimizing operational costs. In the optimization model, both transportation delay and customer demand were considered. The optimization problem was solved according to interplay between the nodal method

and a standard optimization package. Tatsuo (2002) developed an optimization method and applied to a HVAC system for an office building. Several objective functions were defined such as energy consumption, peak energy demand through a year and energy cost for one year in order to attain better control strategy. A new calculation procedure was developed in order to improve computational efficiency. The method was based on several assumptions such as the second order model for the sensible heat absorption in the zone, dynamics associated with latent heat storage and the appliance were neglected.

#### **2.4.2 PID tuning methods**

Traditional PID controllers used in HVAC systems are designed for design conditions. However, HVAC systems run under off-design conditions almost all of the time. To this end, PID parameters have to be updated at different operating conditions to avoid large energy consumption and poor system performance. Researchers such as Kitamori (1979 and 1980), Kasahara et al (1999), Kamimura (2002), Ozawa (2003), Noda (2003), and Masakazu (2005) etc. developed many strategies to tune PID parameters.

Kasahara et al (1999) designed robust PID controllers considering model uncertainty in HVAC systems. They utilized a first-order plus dead time equation that is commonly employed to model plant transfer function in HVAC domain. This approximate plant was used to design a robust PID controller by solving a two-disk type of mixed sensitivity problem. The gains of PID controllers were expressed by linear functions of ratio of dead time to time constant. Moreover, Kamimura et al (2002) designed PID controllers and compared with three tuning methods such as the Ziegler-Nichols rule, partial model matching method and optimization method for control

performance. Based on the comparison, it was found that the control performance due to PI and I-P control was superior to that of PID and I-PD control, and I-P and I-PD control strategies were more practical than PI and PID control for energy savings.

Ozawa (2003) proposed a tuning method for PID controllers using optimization approach subject to constraints on control input using a first-order lag plus a dead time system. A secondary loop employing integral control with proportional-plus-derivative (I-PD) action was introduced in order to avoid overshoot of the response to reference input changes, and compared with those by applying the partial model matching method introduced by Kitamori (1979 and 1980). Simulation results showed that the PID controller tuned by using optimal technique was robust and useful in simulation.

Another tuning method for PID controllers based on the optimization approach was described by Masakazu et al (2005). This approach considered two kinds of constraints such as the integral of squared time multiplied by squared error (ISTE) for response to load disturbances and the integral of squared time derivatives of control input (ISTC). The performance index was defined and minimized to obtain the optimal PID parameters. The simulation results showed that very little difference in control performance between the PI controller and the  $H_\infty$  compensator designed by Noda et al (2003) for the same dynamic system.

#### - 2.4.3 Fuzzy control

Because of parameter uncertainty in HVAC model simulation, exact thermal dynamic analysis of this kind of system is rarely accurate. For accurate modeling, a large number of nonlinear equations may be needed. In other words, this task is almost impossible in practice due to the computational time and effort. However, there are two

ways, namely artificial neural network (ANN) and fuzzy logic, which could be employed to overcome the obstacle and analyze HVAC system responses. Itzhak and Reddy (2003) gave a detailed literature review focused on HVAC&R area about the applications of artificial intelligence and knowledge-based expert systems.

Fuzzy Logic Control (FLC) systems, which were first introduced by Mamdani and Assilian (Ying, 2000), are considered as one of the most significant applications of fuzzy logic set theory by Zadeh in 1965. This theory is based on the notion of fuzzy sets, which can take values between interval  $[0, 1]$ , that are used to represent the degree of membership. Fuzzy variables are expressed in linguistic form, such that the inputs and outputs could be extrapolated in terms of linguistic variables, which are not exact mathematical functions. There are two kinds of fuzzy inference systems (FIS), which were named as Mamdani and Sugeno types.

Three major parts for a typical fuzzy logic inference system structure are formed such as fuzzifier, inference engine and defuzzifier. The knowledge base is used to support the inference system operation. The non-fuzzy output is conducted according to the fuzzy logic based on the non-fuzzy input. The major advantages of fuzzy logic controllers compared with traditional PID controllers are summarized as follows: (1) easier to develop, (2) extensive range under different operating conditions, and (3) readily customizable in natural language.

Fuzzy inference systems applied to different types of HVAC systems and comparisons with different types of controllers were described in many papers such as Nagib et al (1992), Altrock et al (1994), Haissig (1999), Mesbah and Pang (1999), Gouda et al (2001), Kolokotsa (2003) and Jili (2003a and 2003b).

Nagib et al (1992) stated that a fuzzy controller could be utilized for a nonlinear thermal process based on a set of rule bases to derive fuzzy control action. The fuzzy rule base was obtained by the empirical knowledge from the operator and engineer. Altrock et al (1994) developed another fuzzy controller used in a HWH system in order to improve both energy use and thermal comfort level. In the fuzzy control, 405 rules which derived based on a knowledge-based evaluation of existing measurement data to obtain the set point of the hot water supply temperature. Both the fuzzy logic controller and a traditional controller were implemented and the performance of the control systems was compared.

An innovative adaptive fuzzy control strategy for controlling zone air temperature in HWH systems was developed by Haissig (1999). The variable water flow rate entering each heater was controlled by a motor-driven control valve. The water flow rate controllers were implemented by using fuzzy logic based on the relationship between water flow rate and valve opening position. In another study, five fuzzy controllers such as fuzzy P, fuzzy PID, fuzzy PI, fuzzy PD and adaptive fuzzy PD were designed by Kolokotsa (2003). The performance of the building by using different fuzzy controllers was simulated based on the performance indexes of subsystem responses and the energy consumption. Simulation results showed that the adaptive PD fuzzy controller based on scaling factors could achieve the best energy saving. Moreover, the advantages of fuzzy logic control such as uncertainty in building characteristics and modification of controller structure were addressed by the author.

Gouda et al (2001) developed a Mamdani type of fuzzy logic controller and a PID controller for a HWH system and compared with system performance. In the simulations

conducted both mean radiant temperature and relative humidity were considered to compute thermal comfort level based on Fanger's predicted mean vote (PMV) and percentage persons dissatisfied (PPD). As a reference model, a PID-based controller was first developed with the PMV as control variable, and then a PMV-based fuzzy logic controller was employed to replace the PID-based controller. Simulation results showed that fuzzy-based control system could achieve better performance and robustness than the normal PID controller.

Different fuzzy logic control strategies such as the compositional rule of inferences (CRI) and the functioning fuzzy subset inference (FFSI) were designed, analyzed, and compared with a conventional PID controller by Jili (2003a) in a HVAC system. The control systems based on fuzzy logic theory used in a low-temperature hot water testing bed were described by Jili (2003b). According to the simulation results, in the calculation of fuzzy reasoning process, CRI required more computation than FFSI. Also, the FFSI was more concise than the CRI with fuzzification in discrete domain; therefore, no stable error exists in the control process. Moreover, by using the fuzzy control strategies, the performance was better than that of the PID controller. From the experimental results by using a single-chip fuzzy controller, the FFSI control in zone air temperature had fast response, high control precision and good stability.

A fuzzy-neural method used for a bang-bang controller in a house heating system was presented by Mesbah and Pang (1999). Both a fuzzy controller and a fuzzy neural network controller were designed. In the fuzzy neural network approach, multi-layered structure such as fuzzification layer, rule reasoning layer and defuzzification layers were described in this paper to resemble the fuzzy rule base system. The robust property was

achieved by utilizing the fuzzy logic controllers rather than a standard on-off switching control scheme. However, fine-tuning of the fuzzy controllers was required to improve control system performance.

## **2.5 The Kalman filtering techniques**

Kalman filtering technologies have been the subject of extensive research and applications, especially in the areas of autonomous or assisted navigation since 1960. This is due to the fact that a recursive solution to deal with discrete-data linear filtering problems was developed by Kalman (1960). The Kalman filter is a set of mathematical equations that provide an efficient computational (recursive) KF to estimate the state of a process, in a way that minimizes the mean of the squared error. The filter is very powerful not only does it support estimations of past, present and even future states, but it can also deal with the precise nature of the system when the model is unknown. The KF is distinguished based on the problems to be handled. The KF states the general problems of estimating linear controlled processes that are governed by linear stochastic difference equations. In contrast, non-linear Kalman filter technology which is named extended Kalman filter (EKF) should be used instead of the linear KF for nonlinear systems. EKF could linearize the estimation around the current mean and covariance by using Taylor series. Very popular formulations of the KF and the EKF were introduced by Welch and Bishop (2004). Since nonlinearity exists in almost all HVAC systems, the applications of the EKF are more suitable for the systems. Applications of the KF in HVAC systems can be found in some papers such as heat exchanger analysis using this technique described by Jonsson (1994) and Al-Haik (1999).

Application of the KF estimation techniques was presented by John and Ray (1983) for a large power generation plant which included four 500MW oil-fired boiler/turbine units. The biases from both external disturbances and dynamic model errors were considered carefully in the use of the KFs. The KFs were modified to meet the needs in the systems. From the comparisons with a PID controller, the KF-based controller was shown to improve disturbance rejection, decrease the sensitivity to measurement noise and be more robust for control performance.

A state space method for estimation of continuous-time models for thermal dynamics of buildings based on discrete time building measuring performance data was represented by Madsen and Holst (1995). The KF was utilized to compute the likelihood function that used to estimate the parameters of this model. The model of the heat dynamics was described by the stochastic differential equation. The measurement error distributed white noise with zero mean and variance was assumed. Moreover, mutually independent of system noise and measurement noise was also assumed. The KF predicted and corrected the variables recursively. According to this approach the problems associated with the dynamic modeling methods were decreased.

Homme and Gillet (2001) presented an improvement at both structural and control level for increasing entire efficiency of solar kits in a domestic hot water supply system. A predictive control strategy was designed and validated based on an optimization approach to achieve better performance. The EKF was used to update the user's demand every day. The nonlinear model was linearized around the nominal trajectory in order to employ the KF technique.

One of the advantages of the KF is that it removes system and measurement noises and retains useful information. It can be utilized as a tool to estimate variables existing in wide range of processes. Not only does it work well in linear systems, but it is also suitable for nonlinear systems. The basic concepts concerned on the design and implementation of the KFs were presented by Simon (2001). In order to control system process accurately, process variables have to be correctly estimated; to this end, the KF was often implemented in embedded control systems.

Application of FDD with the embedded KF was presented by Tudoroiu and Zaheeruddin (2005) for a discharge air temperature system commonly used in HVAC area. In this nonlinear dynamic model, the discharge air temperature from the heating coil was controlled by the PI controller. A fault detection and diagnosis approach for the valve actuator failures was developed based on an interactive KF estimation algorithm. First-order Markov chain of the system model sequence was assumed in the algorithm.

## **2.6 Fault detection and diagnosis (FDD)**

Faults are very general problems in HVAC system commissioning, operation and maintenance. Faults in a system can be detected and diagnosed by comparing the values of output variables against a set of rules that establish the values expected under various combinations of input variables. FDD has been focused on identifying changes in a system as it operates over extended time periods. Faults could be classified in terms of two types: measurement and process faults. Moreover, combined multi-faults appear and pose more challenging problems for detection and isolation in HVAC systems.

FDD techniques applied to HVAC area have received growing interest in recent years. This is not only due to the development of computer technology and the increasing

computational efficiency, but also much of energy consumed by improperly operated buildings (Katipamula and Brambley, 2005a and 2005b). McKellar (1987) studied automated FDD for a vapor-compression-based refrigeration system. In the 1990s, many researchers focused on FDD for refrigeration systems and equipment and applied to air-handling units (AHU) based on temperature and/or pressure measurements to detect and diagnose common faults. ASHRAE Technical Committee on Smart Building Systems sponsored several projects on FDD (Comstock et al (2001), Norford et al (2002), Reddy and Andersen (2002) and Reddy et al (2003)).

A clear picture of the FDD and prognosis was described by Katipamula and Brambley (2005a). There were four steps for the applications of FDD technique. The first step was to monitor the physical system or equipment and to determine any problems occurred in system processes. The second step was utilized to examine the faults and find out their causes. This step could be subdivided into two sections: fault isolation and fault identification. The first two steps were entitled as FDD generally. After that, fault evaluation was utilized to identify the impact of the faults on the system performance based on several factors. The final step was related to decision making, which means how to respond to the faults. In addition, some diagnosis methods could be utilized to judge what kinds of faults occurred. Two methodologies were discussed by Richard et al (2005a).

Following the FDD, evaluations of the impacts of the faults should be taken into account to make decision on operation and maintenance. Greitzer et al (2002) stated that the degree of fault could be quantified in term of a method named figure of merit (FOM).

However, most literature focused on the methods for FDD itself rather than evaluation and decision making process in HVAC field.

Venkatasubramanian (2003a, 2003b and 2003c) addressed a classification scheme for FDD methods entitled by the terminologies of quantitative model-based, qualitative model-based and process history based methods according to the knowledge used in these approaches and presented by Katipamula and Brambley (2005a). Quantitative models were a set of quantitative mathematical equations related to the processes; while qualitative models consisted of the relationships among the process parameters (variables). On the other hand, a large amount of empirical data was assumed to be available in order to create process history based FDD models.

Quantitative model-based FDD approach is based on understandings of an a priori knowledge in the physical principles governing the behavior of HVAC systems. Bendapudi and Braun (2002) stated that detailed physical models using a set of detail mathematic equations rely on mass, momentum and energy balance principles could be developed and solved. These merits could be represented such as modeling accurate estimation of outputs when the models were well formulated, easily distinguishing from normal and fault operation, and simulating transient responses of the system. A model-based FDD was studied by Kelso and Wright (2005).

Although the applications of FDD techniques in the HVAC domain existed for many years, many researchers have focused on air-conditioning (AC) systems rather than heating systems. However, by investigating the applications employed in AC systems, the underlying principles can be extended to heating system FDD.

An improved statistical rule-based FDD method for a rooftop air conditioner was stated by Haorong et al (2003). The results were compared with those from Breuker and Braun (1998). New fault detection and diagnostic classifiers were presented with easier implementation and improved FDD sensitivity. Rule-based FDD approach for AC systems could also be found in the publications from Bin and James (2001), John et al (2001), Richard et al (2005a and 2005b) and Peng et al (2005).

A real AHU reference model was developed based on first principles and empirical relationships by Richard et al (2005b). The developed thermal models, pressure and flow models were used in automated functional testing during commissioning of the AHU. The concepts of model-based automated testing were described by Richard et al (2005a). In addition, a component level model-based method introduced with a mixing box and an air-handling unit fan for automated functional testing were addressed by Peng et al (2005).

Transient pattern analysis should be taken into account in condition monitoring processes in large HVAC systems. Incorrect FDD results could happen during online monitoring if transient responses were not taken into account. Investigation based on this point for FDD in a variable air volume (VAV) system was presented by Cho et al (2005a). Several conditions were tested in an environmental chamber test facility. From the experimental results, it showed that the dynamic system exhibited fast and slow patterns, and faults in neighboring elements strongly influenced each other. Online fault diagnosis should consider transient properties of HVAC systems. Model uncertainty for model-based FDD in HVAC systems was introduced by Buswell and Wright (2004).

FDD in multi-fault cases is a difficult task in HVAC systems because of the strong coupled nonlinear time-varying dynamics of the systems. Cho et al (2005b) presented a pattern diagnosis method using pattern classification and residual ratios based on measurements of real temperatures, pressure, damper position and air flow rate in a VAV system to detect and isolate single-faults and/or multi-faults.

A fault direction space method used to detect and diagnose faults for HVAC components and subsystems was presented by Yi et al (1995). The fault direction space method was based on the variation of the on-line characteristic parameter identification and did not require component and system models. However, the threshold in this FDD method was only suitable for indicating a significant fault. A resistance coefficient region contraction method for hydraulic process fault detection and diagnosis and parameter identification in district heating networks was developed by Yi and Xuzhong (2000). In the method, the resistance coefficient value in each branch was calculated based on steady state pressure balance principle according to different branch connection types.

A FDD strategy for temperature sensor faults in an air conditioning system based on past operation data was developed (Zhijian, 2006). Data mining technique combining a rough set approach and an artificial neural network was used to deduce appropriate parameters. Simulation results showed that for air handling units the temperature and humidity measurements were enough to distinguish the sensor faults of the supply chilled water and the return chilled water. On the other hand, Zhimin and Xinqiao (2007) stated that some faults were influenced in control loops due to feedback control actions; therefore, real sensor faults might be hidden to discover.

A FDD method for detecting abnormal energy consumption in building HVAC systems based on daily readings of energy consumption and peak energy consumption was presented (John, 2007) to decrease fault detecting time and save energy. The data analysis method utilized robust statistic estimation of the mean and standard deviation from normal and abnormal building energy consumption. However, heating/cooling loads of buildings may be affected by inside environment and outside climate, sometimes FDD based on daily energy consumption cannot be applied to isolate faults on time.

An artificial neural network was developed by Xiaoming et al (1996a, 1997) to detect and diagnose faults for heating systems in non-permanently occupied buildings. Six type of faults related to gas-fired boiler, control valve and control system were selected. This investigation showed that the FDD approach using neural network was feasible for such heating system. An application of neural networks for FDD method used in complex heating systems was also presented by Xiaoming et al (1996b).

## **2.7 Fault tolerant control (FTC)**

In the recent three decades from 1980's, research related to reconfigurable/restructable fault tolerant control systems has increased gradually. However, the research on FDD and FTC systems was developed in parallel. It is known that FTC systems can deal with certain degree of failures automatically with stable and acceptable performance in overall system level. A few studies on FDD in HWH system area can be found in the literature; nevertheless, the research on FTC in HWH systems has not been explored.

Literature review of FTC systems focused on reconfigurable/restructable controller design techniques was presented by Youmin and Jin (2003). The FTC systems

were divided into two categories: passive and active FTC systems. In passive FTC systems, the controllers were designed with robustness against failure conditions. On the other hand, active FTC systems were designed to be able to reconfigure control actions so that acceptable system performance could still be maintained in the presence of faults. The major objectives of designing FTC systems were concerned of both normal operation and fault conditions. Existing reconfigurable control approaches were cataloged based on control algorithms and application field; while existing FTC methods were classified depending on the criteria such as mathematical tool used, design approach used and reconfiguration method.

Due to the fact that faults always exist in real system operation, it is necessary to develop fault tolerant software for handling both fault-free and fault conditions. A formal model-driven FTC system approach was proposed by Linas and Elena (2004) based on integration of the FTC system into an automated refinement process. A case study by using this scheme for a deviation of safe and fault tolerant controller in a heating system was proposed to construct the FTC system.

A fuzzy model-based fault tolerant control system was developed by Xiongfu and Arthur (1999) for an air-conditioning system. This control system was utilized to operate in the presence of degradation faults such as air or water-side fouling, and minimize the energy consumption in the system. Considering the influence of high degree of uncertainty from fault isolation scheme, the developed fuzzy models were not only employed to predict the overall system performance but also to identify suitable set points of the supply air and the chilled water temperature. The results stated the ability of the fuzzy model prediction for the system operation. In addition, the temperature set

points were adapted in the fuzzy model-based FTC supervisory control strategy to attain better system operation.

A multi-model approach in a FTC system was demonstrated by Silva et al (2006) for a VAV terminal unit. The FTC system was composed of three modules: a bank of models, a bank of controllers, and the FDD and controller reconfiguration algorithms. The FTC scheme was utilized to seek the best representation of the plant characteristics and controller reconfiguration to provide fault tolerance under faulty situations. The cost function based on weighting factors was solved by using an optimization methodology, and the optimal weighting factors were employed to quantify the degree of model activation. Experimental results by using the proposed FTC strategy indicated that the system performance was improved compared with a traditional PI controller.

Prakesh et al (2002) developed a basic FTC scheme in order to deal with faults from sensor and actuator biases, and abrupt faults such as unmeasured or process parameters. An appropriately integrating fault detection and identification method with the controller in the FTC system was employed to correct the offset introduced by the faults. Results showed that the FTC system gave good performance under the occurrence of soft faults. In addition, a FTC system, which was a robust adaptive predictive control strategy combined with a FDD system, was addressed by David et al (2007) for a sensor fault in a nonlinear chemical process.

An integration of fault detection, feedback control and supervisory control subject to control actuator failures was addressed by Prashant (2006) for nonlinear process FTC system implementation. A set of control configurations constructed by Lyapunov-based controllers were designed first. Then, a fault detection filter was utilized to acquire the

control system behaviour with a fault free condition, and the deviation of the process states from the control system was employed for detecting the faults. After that, a high level supervisory switch was utilized according to the stability region in order to arrange the essential control system configuration and ensure the system under stable operation with fault situations. Finally, simulations based on the FTC system were studied to demonstrate the idea behind the proposed approach.

## **2.8 Summary**

From the above literature review the following conclusions and observations are made.

Steady state models may over estimate energy consumption of HVAC systems because of time-varying operating situations. Although simplified component level models can be used to form system level models based on energy balance principles, simulations and control design based on simplified dynamic models could also lead to incorrect dynamic responses and results. A full order system model is necessary to study (both dynamic responses and energy consumption) and to design better control strategies.

Due to high nonlinear processes, time-varying features, control loop interactions and part load operating conditions of HVAC systems, fixed gain PID controllers are not suitable in operation. Moreover, system uncertainty and inaccurate mathematical models also result in poor performance, undesired indoor environment and poor energy efficiency. Thus, adaptive control and intelligent control such as the use of fuzzy logic theory should be used to design improved control strategies to overcome these difficulties.

Since faults can happen in HVAC system operation in any time, obtaining correct system operating information will play a significant role in fault conditions of HVAC systems. There is a need to utilize FDD for overall systems. Moreover, it is essential to design control systems, which not only can work well in fault-free systems, but also can give good performance under fault conditions.

Although extensive investigations have been done on the system control and FDD of HVAC systems, there still exists several limitations derived from the literature review related to HWH systems. The limitations are stated as follows:

(1) Most studies use steady state or over simplified dynamic component models to form system level models in HWH systems. However, several important component models such as the boiler model, the finned-tube model and the pipe network model are over simplified or neglected. A detailed finned-tube baseboard heater dynamic model cannot be found in the literature.

(2) Most studies dealt with the FDD techniques in air conditioning systems; while few investigations described the applications of FDD based on steady state models.

(3) Some papers focused on PID control and fuzzy logic control used at the local level, not many studies can be found for supervisory control level.

(4) Modeling of HWH systems for high-rise buildings for control and diagnostic studies has not been studied.

(5) FTC system for HWH systems has not been found in the literature.

With this as the background, the objectives defined in section 1.5 were undertaken. In the following chapters, dynamic modeling, control system strategy design, FDD and FTC for the high-rise building HWH system will be discussed in detail.

## **Chapter 3 Dynamic Modeling of a One Room HWH System**

The first objective of this research is to develop an overall HWH system dynamic model for a high-rise building. To this end, the modeling problem will be broken down in three steps: (i) development of a one room heating system model, (ii) development of a multi-zone heating system model describing one floor of a commercial building, and (iii) development of a large scale multi-floor multi-zone system model. In this chapter, the first step, namely, development of a one room heating system model will be described. Next, a zonal model will be developed in order to study the room air temperature distribution and deduce a correction factor that can be used in designing control system strategies. Finally, a model reduction technique will be utilized to reduce the model order. The reduced-order model will be employed to extend the modeling processes to the multi-zone HWH system in the following chapter. Open loop simulation results will be presented and explained showing the responses from the one room model and the reduced-order model respectively.

### **3.1 Dynamic modeling of a one room heating system**

#### **3.1.1 Baseboard heater model in a room**

Finned-tube baseboard heaters are one of the important components. The temperature of hot water in the heater decreases while the heat is transferred to the indoor air. From an operation point of view, the baseboard heater acts like an interface between the hot water inside the tube and indoor air acting on the outside. In the heater with its cover, the column of warm air will flow up from bottom acting like a “stack” within the cavity. Such a configuration could be modeled like a vertical air channel. From an

optimization and control point of view, it is important to study the heating system and the terminal baseboard heater characteristics, so that the objectives of efficient energy management can be met. Therefore, a dynamic model of the finned-tube baseboard heater is required.

The physical model of a hot water heating system with a baseboard heater in a zone or room is composed of several subsystems (i) baseboard heater with cover; (ii) bare pipe with cover; (iii) indoor environmental zone; (iv) outside wall. A schematic diagram of the room with the baseboard heater is illustrated in Figure 3.1. Also shown in this figure are the components of heat transfer to and from the room air. In order to accurately model the rate of heat transfer from the heater, the baseboard heater was divided into ten segments along the length shown in Figure 3.2. In other words, there are 12 vertical channels, which are two bare pipe vertical channels one at each end and ten finned-tube consecutive vertical channels. Each segment was treated like a vertical channel carrying air. Each vertical channel as shown in Figure 3.3(a) was divided into four control volumes along the height of the heater. The mass, energy balance and momentum equations were formulated for each control volume to build an overall model of the baseboard heating system (Lianzhong and Zaheeruddin, 2005).

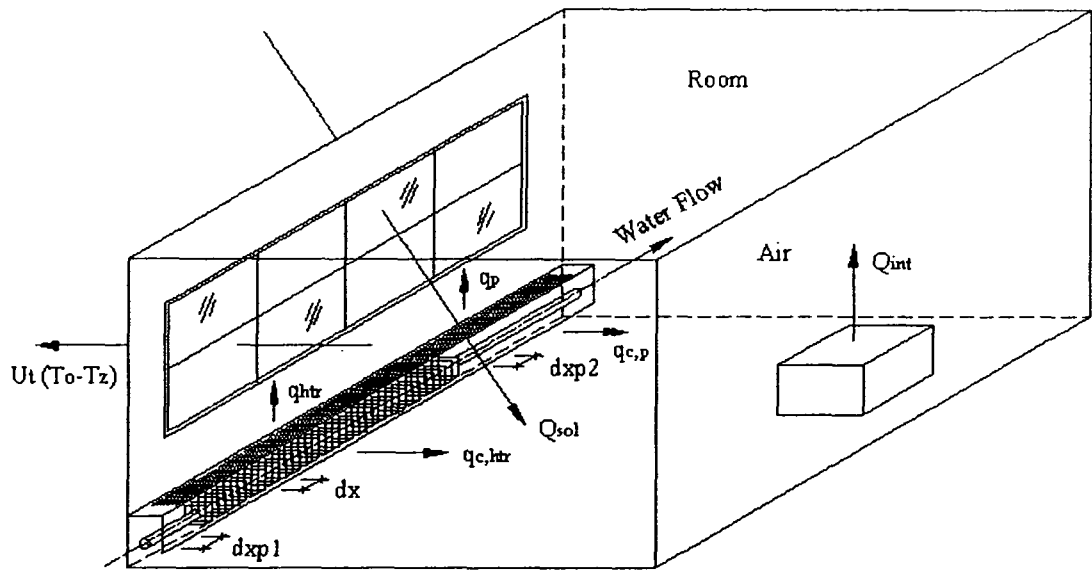


Figure 3.1 Schematic diagram of the room with the baseboard heater

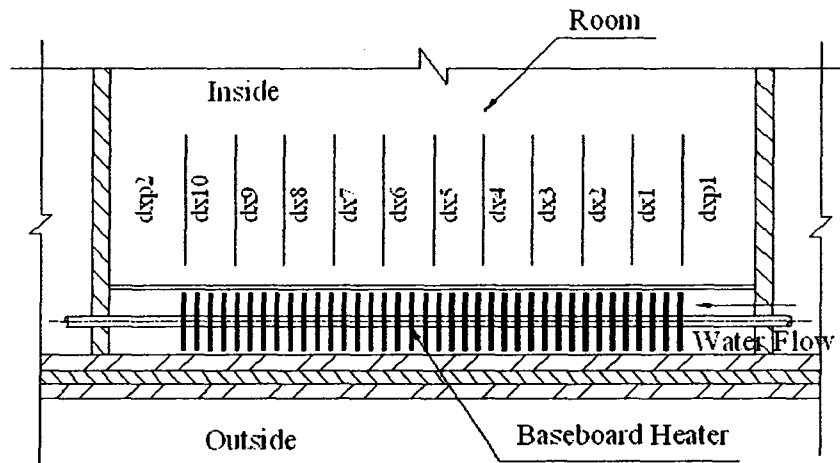


Figure 3.2 Separation of the vertical channels for the baseboard heater and the connections

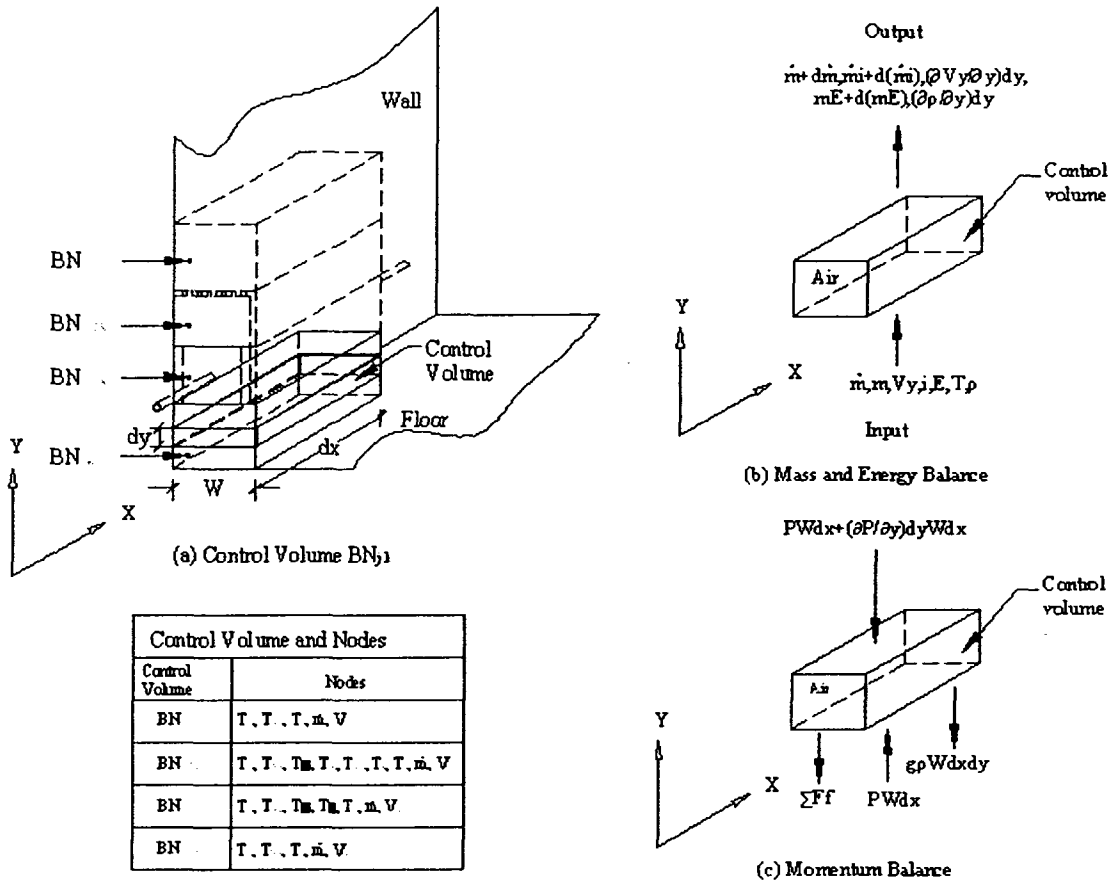


Figure 3.3 Schematic diagram of the vertical channel and the control volume

In order to develop the dynamic models of a finned-tube baseboard heater with a cover and a bare pipe with a cover, some basic assumptions were made. These are:

- (a) Uniform conditions of the air and the water in the control volume.
- (b) The air flow from the heater is completely mixed with the indoor air.
- (c) The air temperature entering the bottom of the baseboard heater is less than the indoor air temperature by  $1.5^{\circ}\text{C}$ .
- (d) The velocity of the air in the control volume changes only in y-direction.

- (e) Heat transfer (natural convection) inside the cover from the bottom to the top is assumed to occur in the vertical direction only; therefore, the heat transfer along horizontal direction is ignored.
- (f) The changes in indoor air humidity were neglected.
- (g) The internal surface of the outside wall was assumed to have uniform temperature.
- (h) The inside wall temperature was assumed to be equal to the room temperature.

***The Baseboard Heater and Control Volumes***

The baseboard heater with its cover was modeled as a natural convection heating device by using two direction heat transfer and fluid flow analysis. A typical control volume ( $W \cdot dx \cdot dy$ ) is shown in Figure 3.3(a), in which  $dx$  and  $dy$  are the intervals in  $x$  and  $y$  directions. Note that  $dx$  and  $dy$  are along the directions parallel with the supply water pipe and the vertical wall of the enclosure respectively.

By applying the mass, energy and momentum balance principles introduced by Zaheeruddin and Zheng (1994) to each control volume, the following dynamic Equations (3.1)~(3.3) were derived.

***Mass, Energy Balance and Momentum Equations***

$$\frac{\partial m}{\partial t} + \frac{\partial \dot{m}}{\partial y} = 0 \tag{3.1}$$

$$\frac{d(mE)}{dt} = \frac{dq}{dy} - \frac{d(\dot{m}i)}{dy} \tag{3.2}$$

$$\frac{\partial \dot{m}}{\partial t} dy + d\left(\frac{\dot{m}^2}{m}\right) = -gWdx dy \phi - \sum F_f \tag{3.3}$$

The mass balance in Equation (3.1) expresses the fact that on a per unit volume basis there is a balance between mass flow rates of air in and out and the rate of change of mass within the control volume. In Equation (3.2), changes in the density of air along the air flow direction and as a function of time are considered. This equation describes that the rate of energy stored in the control volume is equal to the net flow of energy transferred across the control surfaces. Equation (3.3) represents the force balance on the control volume where the product of mass and acceleration is equal to exterior forces acting on the control volume.

#### ***Dynamic Model of the Baseboard Heater***

Each vertical channel of the baseboard heater was divided into four control volumes of width  $dx$  and height  $dy$ . One of the control volumes is depicted in Figure 3.3(a) with a listing of state variables or nodes in each vertical channel and the placement of nodes in the control volumes is shown in Figure 3.4(a). The notation  $BN_{j,k}$  refers to the  $j^{\text{th}}$  row and  $k^{\text{th}}$  column of the control volume. In the following, the equations at each control volume  $BN_{j,k}$ ,  $BN_{j+1,k}$ ,  $BN_{j+2,k}$  and  $BN_{j+3,k}$  will be developed.



$$dq_a = h_{wfs} dx dy (T_{wfsi} - T_a) \quad (3.7)$$

where  $h_{ws}$  is the heat transfer coefficient of air and  $dx dy$  is the heat transfer area. By neglecting the indoor air humidity, the enthalpy of air can be expressed as

$$i_a = c_p T_a \quad (3.8)$$

and the energy change of the air in y direction can be represented by

$$d(\dot{m}_a i_a) = c_p d(\dot{m}_a T_a) = c_p \dot{m}_a \frac{\partial T_a}{\partial y} dy + c_p T_a \frac{\partial \dot{m}_a}{\partial y} dy \quad (3.9)$$

where,  $c_p$  is the specific heat of air at constant pressure.

The total energy of air in the control volume (Equation (3.6)) is computed from

$$E_a = c_v T_a + 0.5 V_{ya}^2 + gy \quad (3.10)$$

where,  $c_v$  is the specific heat of air at constant volume. The second term is the kinetic energy due to change in velocity and the third term is the potential energy. The rate of energy transfer is

$$\frac{d(m_a E_a)}{dt} = c_v m_a \frac{\partial T_a}{\partial t} + m_a V_{ya} \frac{\partial V_{ya}}{\partial t} + (c_v T_a + 0.5 V_{ya}^2 + gy) \frac{\partial m_a}{\partial t} \quad (3.11)$$

Since  $\frac{\partial V_{ya}}{\partial t} = 0$  and substituting Equations (3.4), (3.7), (3.9) and (3.11) into

Equation (3.6) and rearranging, we have

$$c_v m_a \frac{\partial T_a}{\partial t} + c_p \dot{m}_a \frac{\partial T_a}{\partial y} + (c_p T_a - c_v T_a - 0.5 V_{ya}^2 - gy) \frac{\partial \dot{m}_a}{\partial y} = h_{wfs} dx (T_{wfsi} - T_a) \quad (3.12)$$

Equation (3.12) is the statement of the energy balance on the air in the control volume. The rate of change of energy is equal to the rate of heat transfer between the air and the interior surface of the outside wall. It was assumed that the inlet air temperature to the baseboard heater is colder than the room air temperature. That is

$$T_{ain} = T_z - 1.5 \quad (3.13)$$

#### Control Volume BN<sub>j+1,k</sub>

The equations of mass balance and velocity of the air are the same as those given by Equations (3.4) and (3.5). The convective rate of heat transfer, dq, can be described by

$$dq_a = h_{cda} dx dy (T_{cd} - T_a) + h_t A_t dx (T_t - T_a) + h_{wtsf} dx dy (T_{wtsfi} - T_a) + \left[ \int_{A_{fin}} h_t (T_{fin} - T_a) dA_{fin} \right] dx \quad (3.14)$$

where  $A_{fin}$  and  $A_t$  are the heat transfer area of the fins and the tube per unit length; while  $T_{cd}$ ,  $T_t$  and  $T_{fin}$  are the temperatures of the cover, the tube and the fins respectively.

Equation (3.14) describes the total heat transfer by convection from the control volume. The total rate of heat transfer is equal to the sum of the rate of heat transfer between the air and the inside surface of the cover, between the air and the outside tube surface, between the air and the interior surface of the outside wall as well as between the air and the fin surfaces.

By defining the fin efficiency and assuming sensible heat transfer, we can write

$$\eta_s = \frac{\int_{A_{fin}} h_t (T_{fin} - T_a) dA_{fin}}{h_t (T_t - T_a) A_{fin}} = \frac{\tanh(Mr\varphi)}{Mr\varphi} \quad (3.15)$$

where  $M = \left(\frac{2h_t}{k_{fin}\delta}\right)^{0.5}$  and  $\varphi = \left(\frac{R_{eq}}{r} - 1\right)[1 + 0.35 \ln\left(\frac{R_{eq}}{r}\right)]$  described by McQuiston and

Parker (2005).  $\delta$  is the thickness of the fin; while  $k_{fin}$  is the conductivity of the fin material. Note that an equivalent annular fin with radius  $R_{eq}$  based on equal areas was assumed to model the square fin. The sum of the tube and the fin area is the total area, that is

$$A_0 = A_t + A_{fin} \quad (3.16)$$

Substituting Equations (3.15) and (3.16) into Equation (3.14) and rearranging, the total heat transfer is

$$dq_a = h_{cda} dx dy (T_{cd} - T_a) + h_t dx A_0 \left[1 - \frac{A_{fin}}{A_0} (1 - \eta_s)\right] (T_t - T_a) + h_{wtsf} dx dy (T_{wtsf} - T_a) \quad (3.17)$$

By defining the surface effectiveness

$$\eta_{sov} = 1 - \frac{A_{fin}}{A_0} (1 - \eta_s) \quad (3.18)$$

and using Equation (3.18), Equation (3.17) becomes

$$dq_a = h_{cda} dx dy (T_{cd} - T_a) + h_t dx A_0 \eta_{sov} (T_t - T_a) + h_{wtsf} dx dy (T_{wtsf} - T_a) \quad (3.19)$$

Thus, the energy balance equation can be written as

$$c_v m_a \frac{\partial T_a}{\partial t} + c_p \dot{m}_a \frac{\partial T_a}{\partial y} + (c_p T_a - c_v T_a - 0.5 V_{ya}^2 - gy) \frac{\partial \dot{m}_a}{\partial y} = h_{cda} dx (T_{cd} - T_a) + h_{wtsf} dx (T_{wtsf} - T_a) + \frac{h_t dx A_0 \eta_{sov} (T_t - T_a)}{dy} \quad (3.20)$$

In Equation (3.20), the rate of energy change in the control volume is equal to the rate of heat transfer between the air and the surfaces of the interior cover of the baseboard heater, the interior of the outside wall and the finned-tube.

The rate of energy stored in the fins and the tube is equal to the net rate of heat transferred to the air and the water inside the tube. This process can be represented by

$$c_{fin} m_{fin} \frac{1}{A_{fin}} \frac{\partial}{\partial t} \left( \int_{A_{fin}} T_{fin} dA_{fin} \right) + c_t m_t \frac{\partial T_t}{\partial t} = h_t A_0 \eta_{sov} (T_a - T_t) + h_w A_w (T_w - T_t) \quad (3.21)$$

where,  $c_{fin}$ ,  $c_t$ ,  $m_{fin}$  and  $m_t$  represent the specific heat and mass of the fins and finned-tube per unit length in the direction of water flow;  $h_w$  is the convective heat transfer coefficient between the inside tube wall and the water, and  $A_w$  is the water side heat transfer area per

unit length in the direction of the water flow. By making use of the definition of the fin efficiency (Equation (3.15)), the integral term in Equation (3.21) was expressed as

$$\frac{\partial}{\partial t} \left( \int_{A_{fin}} T_{fin} dA_{fin} \right) = \frac{\partial}{\partial t} [T_a + \eta_s (T_t - T_a)] A_{fin} \quad (3.22)$$

Substituting Equation (3.22) into Equation (3.21) and rearranging, we have

$$(1 - \eta_s) \frac{\partial T_a}{\partial t} + \left( \eta_s + \frac{c_t m_t}{c_{fin} m_{fin}} \right) \frac{\partial T_t}{\partial t} = \frac{1}{c_{fin} m_{fin}} [h_t A_0 \eta_{sov} (T_a - T_t) + h_w A_w (T_w - T_t)] \quad (3.23)$$

Equation (3.23) describes the energy balance on the finned-tube. The rate of energy stored in the finned-tube is equal to the rate of heat transfer between the air and the finned-tube surface as well as between the finned-tube and the water.

The energy balance equations for the cover and the water flow inside the finned-tube were also developed. These equations are

$$c_c m_{cd} \frac{dT_{cd}}{dt} = h_{cda} dy (T_a - T_{cd}) + h_{cdz} dy (T_z - T_{cd}) + dy \varepsilon \sigma F_{vf} (T_z^4 - T_{cd}^4) \quad (3.24)$$

$$c_w m_w \frac{\partial T_w}{\partial t} + c_w \dot{m}_w \frac{\partial T_w}{\partial x} = h_w A_w (T_t - T_w) \quad (3.25)$$

Note that  $T_z$  and  $T_{cd}$  in the 3<sup>rd</sup> term in Equation (3.24) refer to absolute temperature. Also, the view factor was assumed to be equal to 1.

#### Control Volume BN<sub>i+2,k</sub>

Mass balance and velocity equations for this control volume are the same as those for the control volume BN<sub>j,k</sub>. The energy balance equation can be written as

$$\frac{dq_a}{dy} = \frac{h_{wfsf} dx dy (T_{wfsf} - T_a) + h_{cuu} dx dy (T_{cu} - T_a) + h_{ctd} WR_{top} dx (T_{ct} - T_a)}{dy} \quad (3.26)$$

$$\frac{d(\dot{m}_a i_a)}{dy} = c_p \dot{m}_a \frac{\partial T_a}{\partial y} + c_p T_a \frac{\partial \dot{m}_a}{\partial y} \quad (3.27)$$

$$\frac{d(m_a E_a)}{dt} = c_v m_a \frac{\partial T_a}{\partial t} + (c_v T_a + 0.5 V_{ya}^2 + gy) \frac{\partial m_a}{\partial t} \quad (3.28)$$

By employing the mass balance of the air in Equation (3.4), we have

$$c_v m_a \frac{\partial T_a}{\partial t} + c_p \dot{m}_a \frac{\partial T_a}{\partial y} + (c_p T_a - c_v T_a - 0.5 V_{ya}^2 - gy) \frac{\partial \dot{m}_a}{\partial y} =$$

$$h_{wfsf} dx (T_{wfsf} - T_a) + h_{cua} dx (T_{cu} - T_a) + h_{ctd} (T_{ct} - T_a) WR_{top} \frac{dx}{dy} \quad (3.29)$$

where,  $T_{cu}$  and  $T_{ct}$  are the temperatures of the right side cover and the top cover respectively. In addition,  $h_{cua}$  is the convective heat transfer coefficient of the vertical surfaces on the control volume; while  $R_{top}$  is the ratio of the non-hole width of the top cover to the whole width  $W$  of the top cover. The cover temperature equations for the right side cover and the top cover are

$$c_c m_{cu} \frac{dT_{cu}}{dt} = h_{cua} dy (T_a - T_{cu}) + h_{cuz} dy (T_z - T_{cu}) + dy \varepsilon \alpha_{vf} (T_z^4 - T_{cu}^4) \quad (3.30)$$

$$c_c m_{ct} \frac{dT_{ct}}{dt} = h_{ctu} WR_{top} (T_{aj+3,k} - T_{ct}) + h_{ctd} WR_{top} (T_a - T_{ct}) \quad (3.31)$$

where,  $m_{cu}$  and  $m_{ct}$  are the mass of the right side and top cover material per unit length;  $h_{ctu}$  is the convective heat transfer coefficient at the top cover surface.  $T_{aj+3,k}$  is the air temperature above the control volume. The heat transfer by radiation from the right cover surface was also considered.

#### Control Volume BN<sub>j+3,k</sub>

Mass balance and velocity equations on this control volume are the same as those before. The energy balance equations are also similar to those for the control volume BN<sub>j+2,k</sub> except for the convective heat transfer term. Accordingly, the air temperature in the control volume can be expressed as

$$c_v m_a \frac{\partial T_a}{\partial t} + c_p m_a \frac{\partial T_a}{\partial y} + (c_p T_a - c_v T_a - 0.5 V_{y_a}^2 - gy) \frac{\partial \dot{m}_a}{\partial y} =$$

$$h_{wsf} dx (T_{wsf} - T_a) + \frac{h_{cta} WR_{top} dx (T_{ct} - T_a)}{dy} \quad (3.32)$$

Since the air flow rate is constant along the y axis, the mass flow rate of the air in the vertical direction does not vary over dy. In other words, the momentum balance in all four control volumes can be expressed by using a single momentum balance equation.

That is

$$\frac{\partial \dot{m}_a}{\partial t} dy + d\left(\frac{\dot{m}_a^2}{m_a}\right) = -g W dx dy \phi_a - \sum F_f \quad (3.33)$$

where

$$\sum F_f = C_{f1} \left(dx \int_0^{H_1} dy\right) \left(\frac{\rho_{a1}}{2} V_{ya1}^2\right) + C_{f2} \left(dx \int_0^{H_2} dy\right) \left(\frac{\rho_{a2}}{2} V_{ya2}^2\right) + C_{f3} \left(dx \int_0^{H_3} dy\right) \left(\frac{\rho_{a3}}{2} V_{ya3}^2\right)$$

$$+ C_{f4} \left(dx \int_0^{H_4} dy\right) \left(\frac{\rho_{a4}}{2} V_{ya4}^2\right) + C_{f5} \left(dx \int_0^{H_2} dy\right) \left(\frac{\rho_{a2}}{2} V_{ya2}^2\right) + C_{f6} \left(dx \int_0^{H_3} dy\right) \left(\frac{\rho_{a3}}{2} V_{ya3}^2\right) \quad (3.34)$$

$$+ C_{f7} W dx (1 - R_{ft}) \left(\frac{\rho_{a2}}{2} V_{ya2}^2\right) + C_{f8} W dx (1 - R_{top}) \left(\frac{\rho_{a3}}{2} V_{ya3}^2\right)$$

The friction coefficients were computed at several locations in the vertical channel (Figure 3.4(b)).  $C_{fx}$  in Equation (3.34) is the friction coefficient of each surface, and  $R_{ft}$  is the ratio of the face area of the finned-tube to the total area of the top cover on the control volume. The force balance equation on the vertical channel expresses the fact that the forces due to non-steady flow and convective components are equal to external forces acting on the control volume. The external forces resulting from the buoyancy term and friction force terms on the wall surface, right side cover surface, top of cover and finned-tube segment were considered.

Both heat transfer and friction coefficients are not only related to Reynolds Number (Re), Prandtl Number (Pr), Grashof Number (Gr) and Nusselt Number (Nu), but also are functions of the geometry of the heater cavity. The heat transfer correlations for various configurations were obtained by Roshenow and Choi (1965), Zhang and Ren (1979), Holman (1981) and ASHRAE F. (2001). These are listed in Tables 3.1 and 3.2. The detailed meanings of the notation in the tables are presented in the literature. Note that because the ratio of width to height for the baseboard heater is greater than 0.3, the natural convection heat transfer in this case can be considered as an unlimited space convective heat transfer process as discussed by Zhang and Ren (1979).

Table 3.1 Convection heat transfer correlations for air and water

Configuration	Correlation	Characteristic dimension	Ref.
For air: Vertical flat surface	$h_v = 0.56 \left( \frac{k_a}{L_{eq}} \right) (Gr_a Pr_a)^{0.25}$ $(10^4 \leq Gr_a Pr_a \leq 10^8)$ $h_v = 0.13 \left( \frac{k_a}{L_{eq}} \right) (Gr_a Pr_a)^{0.33}$ $(10^8 < Gr_a Pr_a \leq 10^{12})$	$\frac{1}{L_{eq}} = \frac{1}{L_v} + \frac{1}{L_h}$ <p>Properties at fluid temperature.</p>	ASHRAE F. (2001)
Upper surface of heated plates or lower surface of cooled plates	$h_{cnu} = 0.54 \left( \frac{k_a}{L_{eq}} \right) (Gr_a Pr_a)^{0.25}$ $(2 * 10^4 \leq Gr_a Pr_a \leq 8 * 10^6)$ $h_{cnu} = 0.15 \left( \frac{k_a}{L_{eq}} \right) (Gr_a Pr_a)^{\frac{1}{3}}$ $(8 * 10^6 < Gr_a Pr_a \leq 10^{11})$	$\frac{1}{L_{eq}} = \frac{1}{L_v} + \frac{1}{L_h}$ <p>Properties at film temperature.</p>	Holman (1981)
Lower surface of heated plates or upper surface of cooled plates	$h_{cnd} = 0.58 \left( \frac{k_a}{L_{eq}} \right) (Gr_a Pr_a)^{0.2}$ $(10^5 \leq Gr_a Pr_a \leq 10^{11})$	$\frac{1}{L_{eq}} = \frac{1}{L_v} + \frac{1}{L_h}$ <p>Properties at film temperature.</p>	Holman (1981)
Horizontal pipe	$h_t = 0.36 + \frac{0.518 (Gr_a Pr_a)^{\frac{1}{4}}}{\left[ 1 + \left( \frac{0.559}{Pr_a} \right)^{\frac{9}{16}} \right]^{\frac{4}{9}}}$ $(10^{-6} \leq Gr_a Pr_a \leq 10^9)$	<p>Parameter: exterior diameter of the pipe and properties at film temperature.</p>	Holman (1981)
For water:	$Nu_w = \frac{h_w D_{pi}}{k_w}$ $Nu_w = 1.86 \left( \frac{Re_w Pr_w D_{pi}}{L_p} \right)^{\frac{1}{3}} \left( \frac{\mu_w}{\mu_t} \right)^{0.14}$ $(Re_w \leq 2300)$ $Nu_w = 0.023 Re_w^{0.8} Pr_w^{0.3}$ $(0.5 < Pr_w < 120, 2300 < Re_w < 10^7, \text{ and } \frac{L}{D_{pi}} > 50)$	All fluid properties at bulk temperature except T at tube temperature.	ASHRAE F. (2001), Roshenow and Choi (1965)

Table 3.2 Correlations for computing friction coefficients for air and water

Configuration	Correlation	Characteristic dimension	Ref.
For air: Vertical flat surface	$C_{fv} = \frac{1.292}{Re_{va}^{0.5}}$ $Re_{va} \leq 5 * 10^5$	$L_v$ Properties at fluid temperature.	Zhang and Ren, (1979)
Section change on top cover	$C_f = \alpha_1 R_{fa}^3 + \alpha_2 R_{fa}^2 + \alpha_3 R_{fa} + \alpha_4$		ASHRAE F. (2001)
Outside horizontal finned-tube pipe	$C_f = \alpha_5 R_{fa}^2 + \alpha_6 R_{fa} + \alpha_7$		ASHRAE F. (2001)
Outside horizontal pipe	$C_f = \alpha_8 R_{ea}^3 + \alpha_9 R_{ea}^2 + \alpha_{10} R_{ea} + \alpha_{11}$	Properties at film temperature.	Holman (1981)
For water: Inside tube	$C_{fw} = \frac{64}{Re_w}$ ( $Re_w \leq 2300$ ) $C_{fw} = \frac{0.3164}{Re_w^{0.25}}$ ( $2300 < Re_w \leq 10^5$ ) $C_{fw} = 0.0032 + \frac{0.221}{Re_w^{0.237}}$ ( $10^5 < Re_w \leq 3 * 10^6$ )	Parameter: interior diameter of the pipe and properties at film temperature.	ASHRAE F. (2001)

### 3.1.2 Dynamic model of heat transfer from the bare pipe with the cover to the room air

The model of the bare pipe with the cover was divided into three control volumes of width  $dx$ : (i) the bare pipe with the cover and inside air ( $PN_{j+1,k}$ ); (ii) the air above the cover ( $PN_{j+2,k}$ ), and (iii) the air below the cover ( $PN_{j,k}$ ). Note that the model equations differ from those given above. These equations were derived and are given below.

$$c_v m_a \frac{\partial T_a}{\partial t} + c_p \dot{m}_a \frac{\partial T_a}{\partial y} + (c_p T_a - c_v T_a - 0.5 V_{ya}^2 - gy) \frac{\partial \dot{m}_a}{\partial y} =$$

$$h_{wtsf} dx (T_{wtsf} - T_a) + h_{ca} dx (T_{cr} - T_a) + [h_{cid} (T_{ci} - T_a) WR_{top} + h_l A_p (T_i - T_a)] \frac{dx}{dy} \quad (3.35)$$

$$c_c m_{cr} \frac{\partial T_{cr}}{\partial t} = h_{ca} dy (T_a - T_{cr}) + h_{cz} dy (T_z - T_{cr}) + dy \epsilon \alpha F_{vf} (T_z^4 - T_{cr}^4) \quad (3.36)$$

$$c_c m_{cl} \frac{\partial T_{cl}}{\partial t} = h_{clu} WR_{top}(T_{aj+2,k} - T_{cl}) + h_{clid} WR_{top}(T_a - T_{cl}) \quad (3.37)$$

$$c_w m_w \frac{\partial T_w}{\partial t} + c_w \dot{m}_w \frac{\partial T_w}{\partial x} = h_w A_w (T_i - T_w) \quad (3.38)$$

$$\frac{\partial \dot{m}_a}{\partial t} dy + d\left(\frac{\dot{m}_a^2}{m_a}\right) = -g W dx dy \phi_a - \sum F_f \quad (3.39)$$

where

$$\begin{aligned} \sum F_f = & C_{f1} (dx \int_0^{H1} dy) \left(\frac{\rho_{a1}}{2} V_{ya1}^2\right) + C_{f2} (dx \int_0^{H2+H3} dy) \left(\frac{\rho_{a2}}{2} V_{ya2}^2\right) + C_{f3} (dx \int_0^{H4} dy) \left(\frac{\rho_{a3}}{2} V_{ya3}^2\right) \\ & + C_{f4} (dx \int_0^{H2+H3} dy) \left(\frac{\rho_{a2}}{2} V_{ya2}^2\right) + C_{f5} W dx (1 - R_{tb}) \left(\frac{\rho_{a2}}{2} V_{ya2}^2\right) + C_{f6} W (1 - R_{top}) dx \left(\frac{\rho_{a2}}{2} V_{ya2}^2\right) \end{aligned} \quad (3.40)$$

Note that  $R_{tb}$  is the ratio of the face area of the bare pipe to the total area of the top cover in the control volume.

### 3.1.3 Room model

The schematic diagram of the room with the baseboard heater is shown in Figure 3.1. The heat losses from the building enclosure, the capacity of the heating equipment and environmental factors can affect the indoor air temperature balance. Furthermore, internal heat sources such as heat gains from people, lights, appliances and heat gain from solar radiation also influence the indoor air temperature. Under these circumstances, an energy balance on the indoor air consists of all three mechanisms of heat transfer namely conduction, convection and radiation. By identifying the energy transfer terms to and from the indoor air, an energy balance equation was developed, that is

$$\begin{aligned}
C_z \frac{dT_z}{dt} = & \left\{ \sum c_p \dot{m}_a (T_{atop} - T_z) + \int_0^{H_2} \int_0^{L_{hr}} [h_{cdz} (T_{cd} - T_z) + \varepsilon \sigma F_{vf} (T_{cd}^4 - T_z^4)] dx dy \right. \\
& + \left. \int_0^{H_3} \int_0^{L_{hr}} [h_{cu} (T_{cu} - T_z) + \varepsilon \sigma F_{vf} (T_{cu}^4 - T_z^4)] dx dy \right\}_{hr} \\
& + \left\{ \sum [c_p \dot{m}_a (T_{atop} - T_z) + \int_0^{H_2+H_3} \int_0^{L_p} [h_{cz} (T_{cr} - T_z) + \varepsilon \sigma F_{vf} (T_{cr}^4 - T_z^4)] dx dy] \right\}_p \\
& + Q_{sol} A_{win} + Q_{int} A_{flr} + U_{win} A_{win} (T_o - T_z) + U_{wf} A_{wf} (T_o - T_z) + \sum [U_{wlsfi} A_{wf} (T_{wlsfi} - T_o)]
\end{aligned} \tag{3.41}$$

where, the subscripts htr and p denote the baseboard heater and the bare pipe. This equation describes the fact that the rate of heat stored in the room air is equal to the difference between rate of heat gains and rate of heat losses. The heat gains from the solar radiation and the internal gains were considered in the closed loop simulations of the heating system with control strategies; however, they were set to zero in the open loop simulations.

### 3.1.4 Outside wall model

The dynamics of the outside wall behind the baseboard heater for the four control volumes are taken into account. The outside wall is divided into two layers according to the wall structure. The equations are given in Equations (3.42) and (3.43) for the outside and inside layers respectively. Similarly, the outside wall dynamics behind the bare pipe control volumes can be formed by the same structure as in Equations (3.42) and (3.43).

$$C_{wlo} \frac{dT_{wlo}}{dt} = U_{wlo} A_{wl} (T_o - T_{wlo}) + U_{wlot} A_{wl} (T_{wli} - T_{wlo}) \tag{3.42}$$

$$C_{wli} \frac{dT_{wli}}{dt} = U_{wlot} A_{wl} (T_{wlo} - T_{wli}) + U_{wli} A_{wl} (T_{wlsfi} - T_{wli}) \tag{3.43}$$

In Equation (3.42), the net energy stored in the outside layer of the outside wall is equal to the heat transferred between the outside air and the inside layer of the outside

wall. The dynamic heat transfer between the outside layer of the outside wall and the interior surface of the outside wall is considered in Equation (3.43).

To conclude, the set of Equations (3.1)–(3.40) developed above describe the rate of heat transfer from one segment of the baseboard heater and the bare pipe to the room air. Thus, these equations are applied to each segment of the heater and the bare pipe. It was noted that these equations together with the room model and wall model equations, have multiple time constants and behaved like stiff equations. The full order model of the one room HWH system with 135 dynamic equations, which are 100, 16, 18 and 1 equation for the baseboard heater, the bare pipe, the outside wall and the room respectively, is numerically integrated to obtain the output responses.

### **3.2 Zonal model with full order baseboard heater model**

In order to solve the developed one room heating system model, the inlet air temperature to the heater (boundary condition in Equation (3.13)) was assumed. However, it is well known that, the room air temperature is not the same at all points in the room when the heating system is operational. Therefore, it is necessary to verify the assumption made in Equation (3.13) by using a more detailed room air temperature model. To this end, a zonal modeling approach will be used. The zonal model details are presented in Appendix A.

### **3.3 Model reduction of the one room heating system**

Based on the full order hot water baseboard heater model equations described in the previous section, it is noted that the full order baseboard heater model with the zonal model can present more detailed information related to the room air temperature

distribution. However, extending the full order models to develop multi-zone dynamic models of the heating system will result in large number of equations and will increase computational time. Therefore, it is instructive to reduce the order of the baseboard heater model such that the reduced-order model predictions remain close to those of the full order model.

Generally speaking, many model order reduction methodologies deal with linear systems. Some reduction approaches calculate Hankel singular values of state space variables in dynamic models to estimate the “energy” of them; while eigenvalues are used to define the stability of dynamic systems. Large Hankel singular values preserve the most important characteristics in dynamic systems. Reduced-order models should keep the significant properties of dynamic systems. However, because of the difficulties of the stiff nonlinear system and sensitive responses of the developed full order baseboard heater model, it is difficult to attain the Hankel singular values from the model.

To this end, a physical approach is used. Since the heat output from the baseboard heater changes depending on the water temperature, the water mass flow rate and the room air temperature, a curve fitting technique was applied to the detailed simulations of the full order baseboard heater model to predict the heat output from the heater. The relationship among heat output, temperature and water mass flow rate is given in Equation (3.44).

$$Q_{hr} = f(T_w, T_{rm}, \dot{m}_w) \quad (3.44)$$

The same room was used for the reduced-order dynamic model. The heater was divided into three segments of same length as shown in Figure 3.5. The state variables of

temperature presented in Figure 3.5 include the outside wall (2 nodes), the room air (1 node) and the water inside the tube (3 nodes).

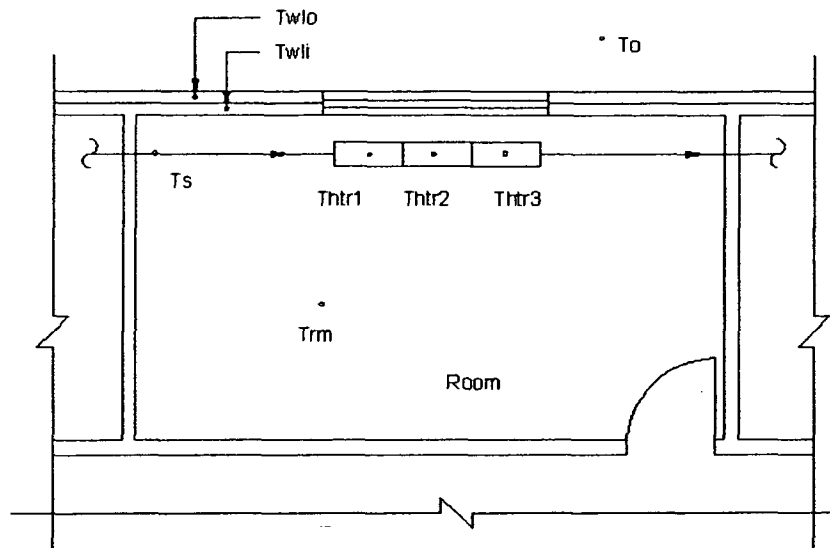


Figure 3.5 Layout of the one room heating system

According to energy balance principle, the dynamics of the temperatures including the room air, the water and the outside wall can be computed and expressed in the following equations.

**Outside surface temperature of the outside wall**

$$T_{wlsfo} = \frac{h_o T_o + U_{wlsfo} T_{wlo}}{h_o + U_{wlsfo}} \quad (3.45)$$

**Room air temperature**

$$C_{rm} \frac{dT_{rm}}{dt} = c_w \dot{m}_w (T_s - T_{htr3}) + Q_{int} A_{rm} + Q_{sol} A_{win} + U_{wli} A_{wl} (T_{wli} - T_{rm}) + U_{win} A_{win} (T_o - T_{rm}) \quad (3.46)$$

In Equation (3.46), the net energy stored in the room air is equal to the heat output from the hot water, internal gains and solar radiation minus the heat losses from the building enclosure such as the outside wall and the window.

### ***Baseboard heater segments***

$$C_{hr1} \frac{dT_{hr1}}{dt} = c_w \dot{m}_w (T_s - T_{hr1}) - f_w L_{hr1} \Omega_{hr} \left( \frac{T_s + T_{hr1}}{2} - T_{rm} \right)^{(1+n)} \quad (3.47)$$

Equation (3.47) describes that the net energy stored in the water of the first segment of the heater is equal to the heat supplied from the hot water minus the heat emission from the outside surface of the heater to the room air. Similarly, the dynamics of the second and third segments of the heater are expressed in Equations (3.48) and (3.49).

$$C_{hr2} \frac{dT_{hr2}}{dt} = c_w \dot{m}_w (T_{hr1} - T_{hr2}) - f_w L_{hr2} \Omega_{hr} \left( \frac{T_{hr1} + T_{hr2}}{2} - T_{rm} \right)^{(1+n)} \quad (3.48)$$

$$C_{hr3} \frac{dT_{hr3}}{dt} = c_w \dot{m}_w (T_{hr2} - T_{hr3}) - f_w L_{hr3} \Omega_{hr} \left( \frac{T_{hr2} + T_{hr3}}{2} - T_{rm} \right)^{(1+n)} \quad (3.49)$$

### ***Outside wall***

$$C_{wlo} \frac{dT_{wlo}}{dt} = U_{wio} A_{wl} (T_{wli} - T_{wlo}) + U_{wifo} A_{wl} (T_{wifo} - T_{wlo}) \quad (3.50)$$

$$C_{wli} \frac{dT_{wli}}{dt} = U_{wli} A_{wl} (T_{rm} - T_{wli}) + U_{wlio} A_{wl} (T_{wlo} - T_{wli}) \quad (3.51)$$

## **3.4 Simulation results of the one room heating system**

### **3.4.1 Simulation results of the room heating system**

In order to study the dynamic responses of the baseboard heating system, open loop simulation runs were made. A room in a commercial building with a hot water

baseboard heater (Multi/Pak 95-10, C-440, Commercial Fin-Tube Radiation Selection Guide, 2004) of 3.8m designed length was considered. The baseboard heater was divided into ten finned-tube segments of 0.38m long and two bare pipe sections of 1.15m long. The design parameters of the hot water baseboard heating system are depicted in Table 3.3.

Table 3.3 Design parameters

Variable	Unit	Data	Variable	Unit	Data
$V_z$	$m^3$	134.3	$C_t$	$J/^\circ C$	$1.17 \cdot 10^3$
$A_{nr}$	$m^2$	38.37	$C_{fin}$	$J/^\circ C$	$6.89 \cdot 10^3$
$q_{rmd}$	W	3002	$C_p$	$J/^\circ C$	$1.46 \cdot 10^3$
$L_{hr}$	m	3.8	$C_z$	$J/^\circ C$	$1.62 \cdot 10^5$
$m_t$	$Kg/m$	1.226	$A_t$	$m^2/m$	0.084
$A_{fin}$	$m^2/m$	2.936	$m_{fin}$	$Kg/m$	2.023
$R_{tb}$		0.785	$R_{top}$		0.75
$R_{ft}$		0.745			

The dynamic responses of the air in the heater cavity (vertical control volumes in Figure 3.3(a)) are presented in Figures 3.6(a)~(f). The hot water supply temperature was  $T_s=83^\circ C$ , and the water mass flow rate was  $\dot{m}_w=0.5776Kg/s$ . Under these conditions, the air temperature in the cover, from bottom to top, reached 12.69, 46.88, 45.94 and  $45.05^\circ C$  (Figure 3.6(a)) respectively in about 600s. The air in control volume 2 attained the highest temperature since it is in this control volume that the finned-tube section delivers heat to the air and therefore acts like a heat source. The cover surface temperature responses at the top, upper right and lower right sections are shown in Figure 3.6(c); these are 35.32, 24.03 and  $24.44^\circ C$  respectively. The density of air as a function of temperature in the heater is shown in Figure 3.6(d). Note that control volume 2 has the smallest air density; while control volume 1 has the highest air density. The mass flow

rate of air in the vertical direction reached 0.0147Kg/s within 600s as depicted in Figure 3.6(e). The air velocity in the control volumes did not change significantly as shown in Figure 3.6(f). From Figure 3.6(b), it can be seen that the temperatures of water in the tube and the finned-tube wall reached 82.78 and 80.06°C within 200s. Also it is of interest to note the speed of the dynamic responses (Figure 3.6). It is noted that the temperature responses of water in the tube, the finned-tube wall, the mass flow rate of the air and the air temperature in control volume 2, 3 and 4 are faster than other responses. The zone temperature response was the slowest reaching steady state in about 3 hours.

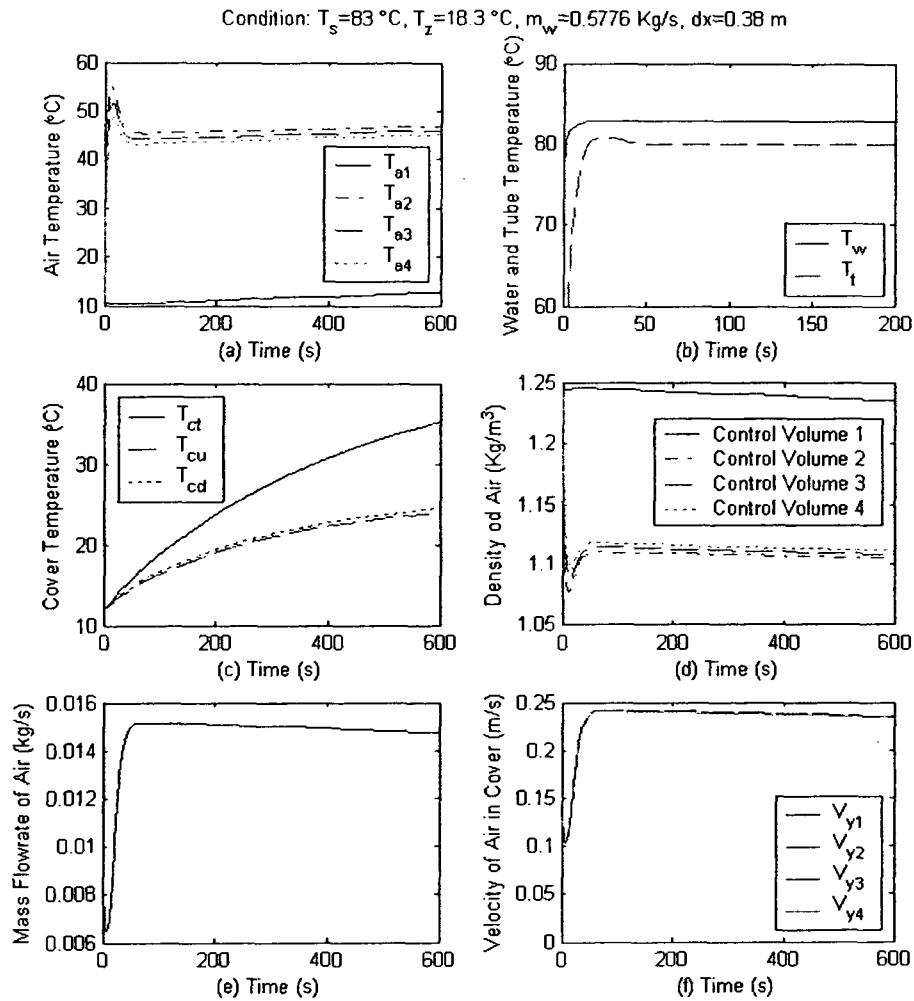


Figure 3.6 Dynamic responses of the outputs in the finned-tube vertical channel

The tube, the air and the cover temperatures, the density, velocity and mass flow rate of the air as a function of supply water temperature are depicted in Figures 3.7 (a) and (b) for control volume 2 of the finned-tube vertical channel. From the figures, it is noted that the temperatures of the finned-tube, the lower cover and the air, the mass flow rate and the velocity of the air all increase as the supply water temperature is increased. However, the density of the air decreases as the supply water temperature is increased.

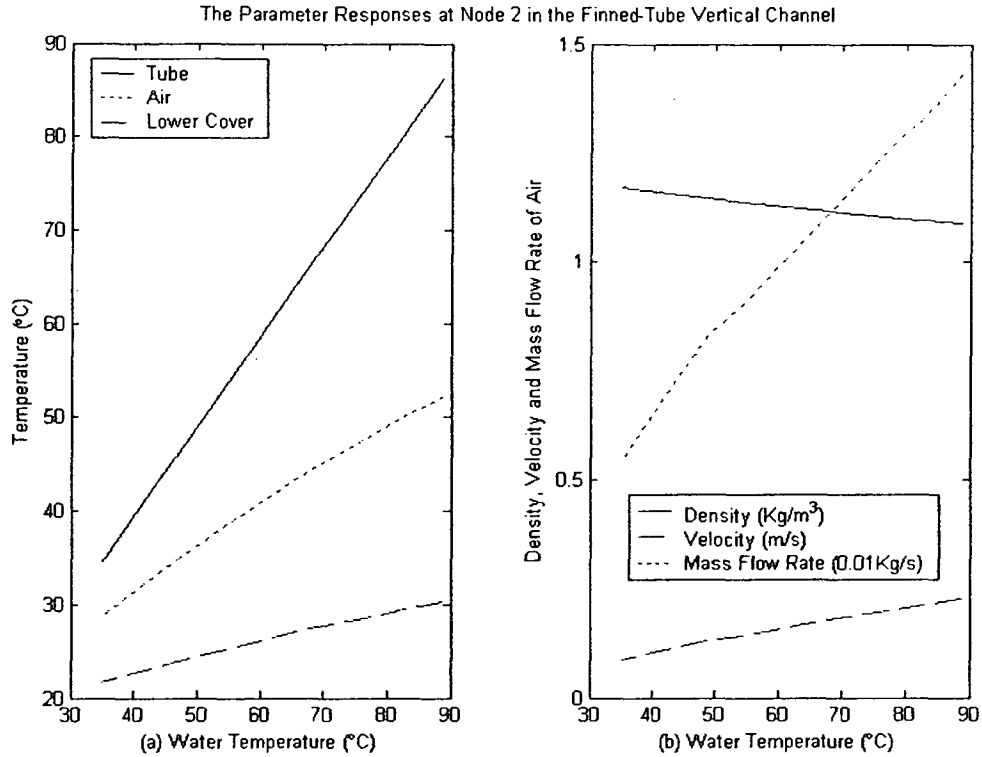


Figure 3.7 Output responses as a function of water supply temperature at control volume 2

From the simulation results the outputs such as total heat output from the vertical channel, the heat output to the indoor air, the air flow resistance as well as the air mass flow rate were obtained for different zone air and supply water temperatures. The results are illustrated in Figures 3.8(a)~(d). It was found that the rate of heat delivered to the room air was slightly less than the rate of heat output from the heater. This is due to the heat loss from the outside wall behind the heater. This case is shown in Figures 3.8(a) and (b). Moreover, it can be seen in Figure 3.8(d) that the air flow rate is higher at higher water temperature than that at lower water temperature.

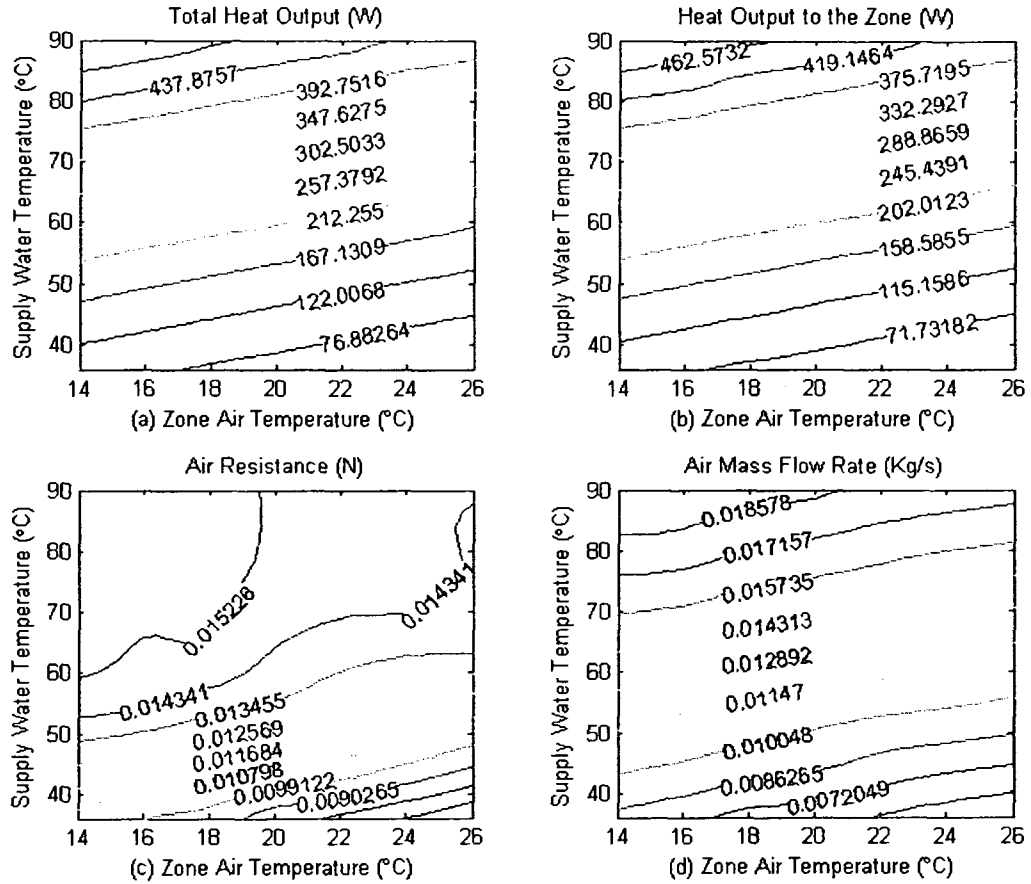


Figure 3.8 Lines of constant outputs in zone air and supply water temperature plane

The heat outputs from one meter bare pipe vertical channel are simulated and given in Figure 3.9. Not only is the heat transferred from the hot water to the bare pipe, from the pipe to the air inside and outside of the cover by nature convection and emission, but it also transfers heat to inside surface of the outside wall. The relationship between the heat outputs from the bare pipe vertical channel and the supply water temperature is linear within the range of the supply water temperature from 30 to 89°C.

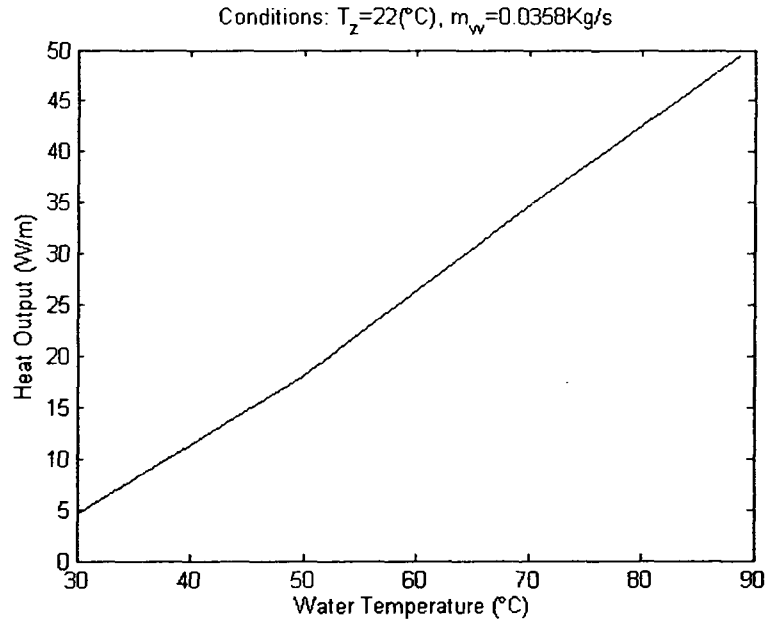


Figure 3.9 Heat outputs from the bare pipe vertical channel

The dynamic responses of the temperature and the air mass flow rate for the baseboard heater vertical channels and the room air are depicted in Figure 3.10 for design conditions of  $T_s=90^{\circ}\text{C}$  and  $\dot{m}_w=0.0358\text{Kg/s}$  with the bare pipe  $2*1.15\text{m}$  and the finned-tube baseboard heater  $3.8\text{m}$  long. The water temperature responses from the bare pipe and finned-tube vertical channels are presented in Figure 3.10(a). It can be seen that the water temperature decreases along the water flow direction. Note that the water temperature difference between the first bare pipe vertical channel and the first finned-tube vertical channel is larger than that between the last finned-tube vertical channel and the last bare pipe vertical channel. This is due to the higher heat output as water temperature increases. In other words, the heat output from the finned-tube vertical channels is larger than that from the bare pipe vertical channels in terms of comparing with the water temperature reduction in finned-tube and bare pipe vertical channels. The air temperature responses from the first and the last finned-tube and bare pipe sections are

depicted in Figure 3.10(b). The leaving air temperature decreases along the length of the heater from 39.36 to 36.19°C in the finned-tube section. Likewise, the leaving air temperatures were 28.72 and 26.73°C at the beginning and the end of the bare pipe sections. Since the heat transferred by the bare pipe segments is less than that by the finned-tube segments, the highest leaving air temperature occurs in the first finned-tube segment in the direction of water flow. The highest air mass flow rate (0.0239Kg/m) happens in the first finned-tube vertical channel shown in Figure 3.10(c) because of the greatest heat transfer process. The zone air temperature response is shown in Figure 3.10(d). The zone air temperature reached 24.09°C in an hour and attained steady state in about 3 hours. Note that the zone temperature is higher than the design zone air temperature (22°C) because the actual installed length of the baseboard heater was greater than the designed length as it included a safety factor.

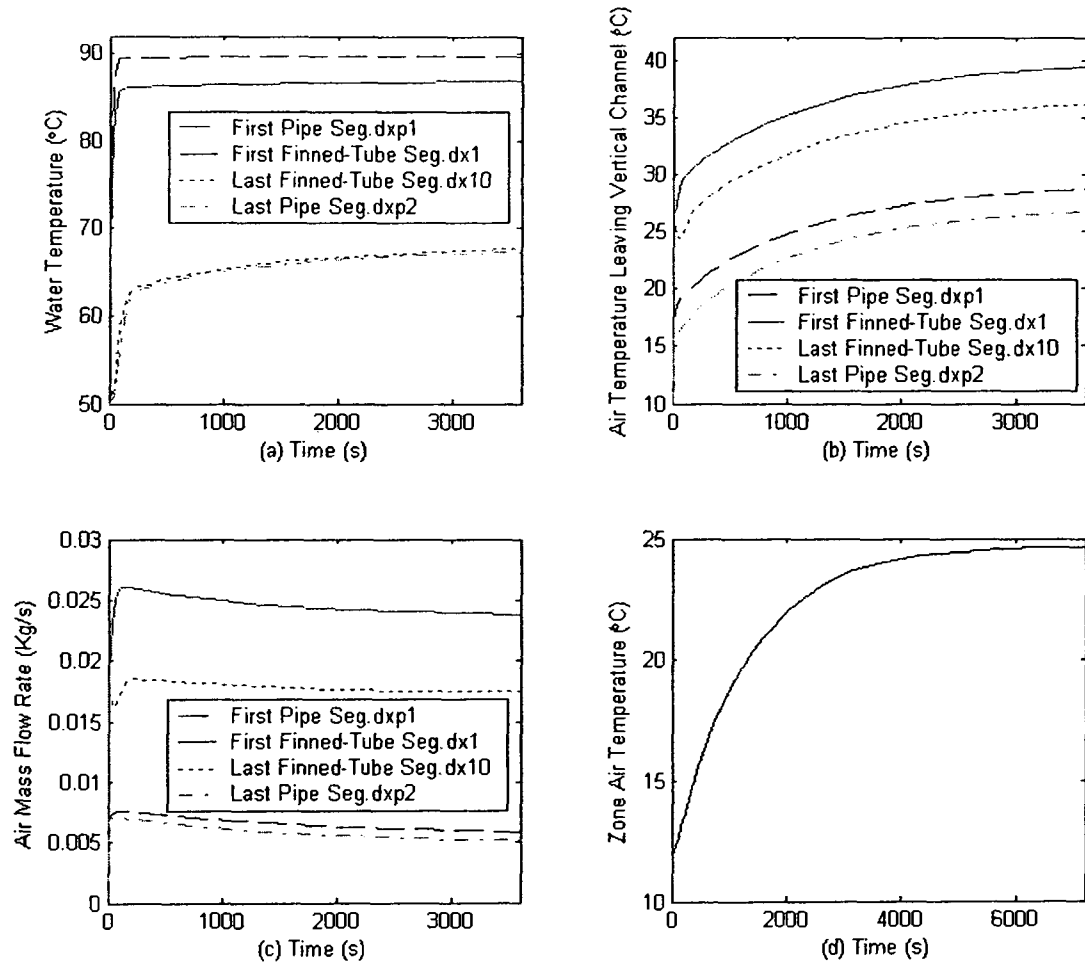


Figure 3.10 Dynamic responses of the baseboard heater and the room at  $T_s=90^\circ\text{C}$  and  $\dot{m}_w=0.0358\text{Kg/s}$

[dxp1: first segment of bare pipe; dx1: first segment of finned-tube; dx10: last segment of finned-tube; dxp2: last segment of bare pipe. (See Figure 3.2)]

In order to attain the design room air temperature, an alternative way is to reduce the supply water temperature to the baseboard heater. This situation was made by changing the supply water temperature from 90 to  $84.1^\circ\text{C}$ . Compared with the responses of the water temperature, air temperature leaving the vertical channels and the air mass

flow rate, the steady state values are less than those in Figures 3.10. Note that in this situation, the room air temperature reaches 21.96°C.

The rate of heat output from the heater at different supply water temperatures was simulated and is illustrated in Figure 3.11. The magnitudes of the air friction coefficients in the model were adjusted such that the difference in heat outputs between the predictions from the model and the manufacturer's data given (Commercial Fin-Tube Radiation Selection Guide, 2004) was less than 3%. As a result, it is noted that this matching of data does not validate the model instead the manufacturer's data was used to develop a reasonably accurate heater model.

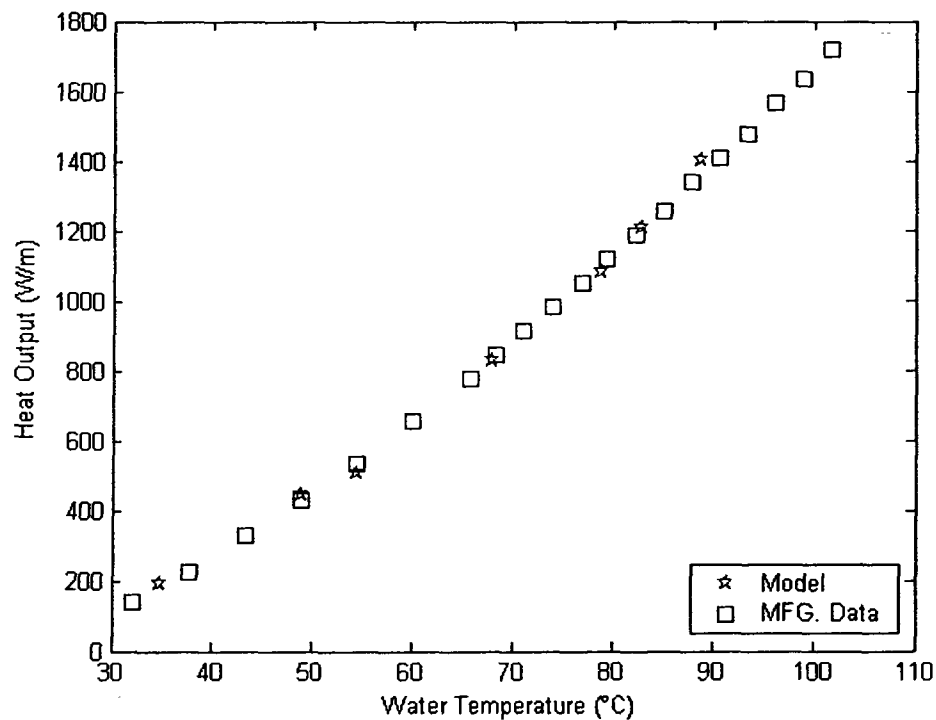


Figure 3.11 Comparison of heat output between the model and the manufacture data

On the other hand, not only do the heat outputs from the baseboard heater change according to the supply water temperature and the room air temperature, but they also

vary based on the mass flow rate of water. This is due to the variation of the heat transfer coefficient inside the finned-tube wall. Simulation results showed that the heat outputs increase when the velocity inside the tube and the supply water temperature increase, and the room air temperature decrease.

From the simulation results related to the finned-tube baseboard heater, it can be seen that the density driven air flow rate in the baseboard cavity ranged between 0.007 to 0.019Kg/s with the corresponding water temperatures ranging between 30 to 85°C. Moreover, the baseboard heating system exhibits a two time scale property. In other words, the overall dynamic responses from the baseboard heater consist of fast-natural-convection driven air flow responses and slow zone air temperature response. The ratio of time scale was between 6 and 12. The results also show that the temperature of the supply water has significant influence on the rate of heat transfer from the heater. As such temperature control strategy is likely to improve the regulation property of HWH systems. The developed model can be used to examine such control strategies.

### **3.4.2 Simulation results of the reduced-order one room model**

For the one room heating system, three dynamic models, namely the full order baseboard heater model, the full order baseboard heater model with the zonal model (see Appendix A) and the reduced-order model, were developed. The major motivation was to replace the full order one room model by the reduced-order model so that a more manageable high-rise building HWH system model could be developed.

To this end, it is necessary to compare the dynamic responses of the three models. The simulation results are depicted in Figure 3.12 under the conditions of  $T_o=-21.8^\circ\text{C}$ ,  $T_s=84.1^\circ\text{C}$  and  $\dot{m}_w=0.0358\text{Kg/s}$ . It can be seen from Figure 3.12(a) that, after 12 hours,

the steady state values reach 21.98, 21.9 and 22.02°C for the full order baseboard heater model, the full order baseboard heater model with the zonal model and the reduced-order model respectively. In addition, the water temperatures  $T_{hr1}$ ,  $T_{hr2}$  and  $T_{hr3}$  achieve their steady state values of 81.65, 79.35 and 77.15°C respectively given in Figure 3.12(b). Note that the measured air temperature (in Cell 7) in the zonal model has a small difference about 0.1°C compared with the air temperature from the full order baseboard heater model and the reduced-order model.

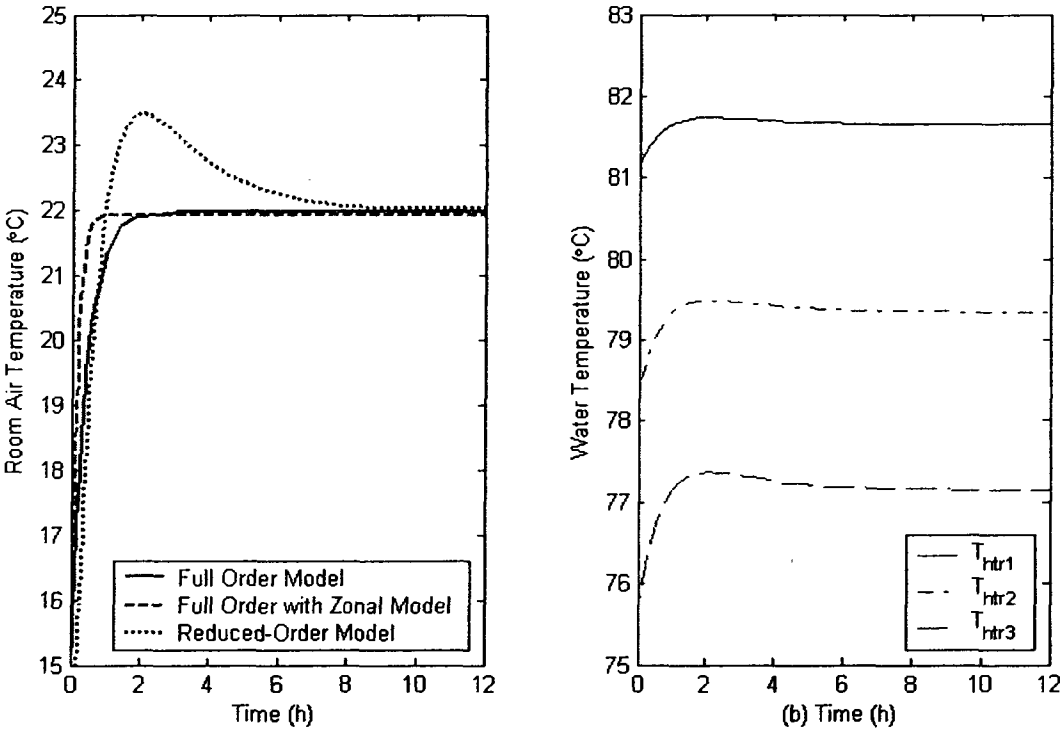


Figure 3.12 Comparison with dynamic responses of the room models

From the open loop tests, it can be seen that, the reduced-order one room heating system model has enough accuracy compared with the other two full order models. As a result, the reduced-order model will be used to develop multi-zone high-rise building HWH system model in the next chapter.

## **Chapter 4 Dynamic Modeling of Multi-Zone HWH Systems**

The reduced-order one room model was used as the basis for developing a multi-zone HWH system model. In this chapter, the multi-zone HWH system models are separated and presented in two sections: one describes a single floor multi-zone (SFMZ) dynamic model; the other describes a multi-floor multi-zone (MFMZ) dynamic model. The developed MFMZ system model will be used to design intelligent control strategies, FDD and FTC strategies.

### **4.1 Dynamic modeling of a SFMZ HWH system**

#### **4.1.1 Physical model of the SFMZ system**

The SFMZ HWH system layout designed for the high-rise building is illustrated in Figure 4.1. There are four zones in each above-ground floor, which respectively face the north, east, south and west direction. The number of rooms in each zone is also identified in the figure. Each zone has a different heating load; while each room in the zone has similar heating load.

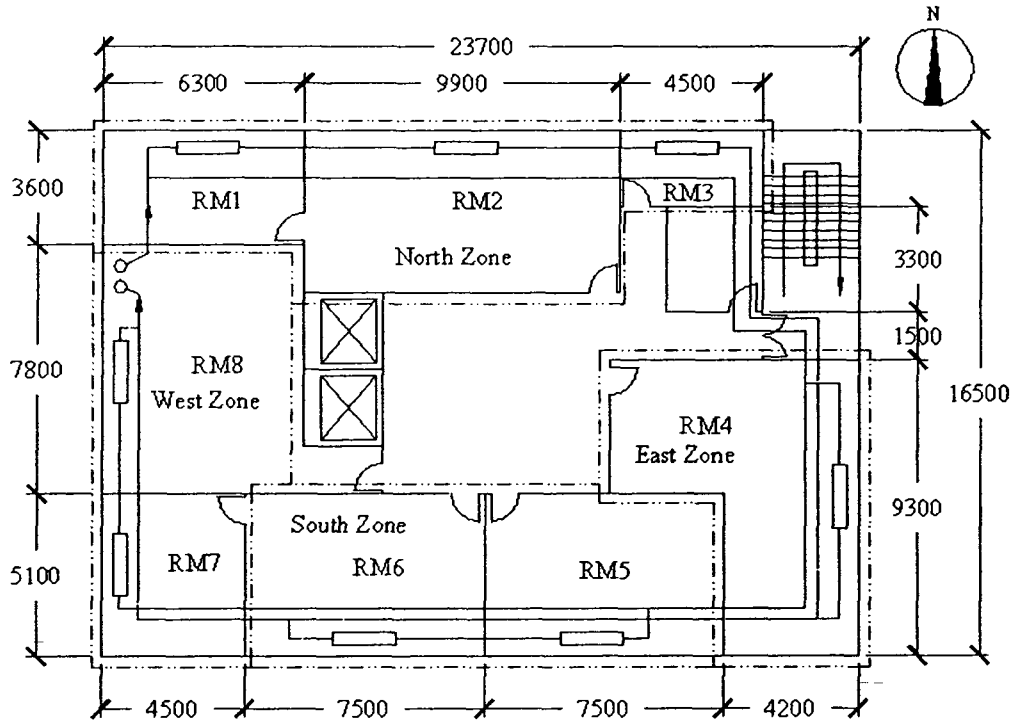


Figure 4.1 HWH system layout of the SFMZ system

In order to develop the dynamic model of the SFMZ system, mass, energy and momentum balance principles are utilized. The schematic diagram with nodes for the HWH system is given in Figure 4.2. There are four circulating water loops: (i) Loop n: A-B-B1-B2-B3-B4-B5-e-d-c-b-a, (ii) Loop e: A-B-C-C1-d1-d-c-b-a, (iii) Loop s: A-B-C-D-D1-D2-D3-c1-c-b-a, and (iv) Loop w: A-B-C-D-E-E1-E2-E3-b1-b-a, sharing the same pressure difference ( $\Delta P_{Aa}$ ). The HWH system model consists of reverse-return pipe network.

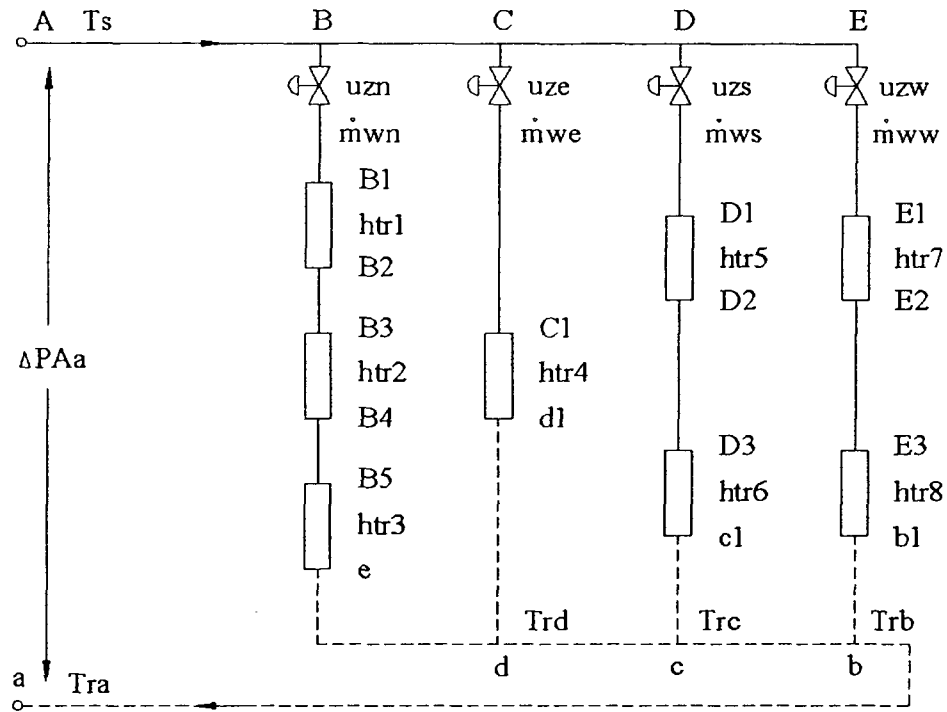


Figure 4.2 Schematic drawing with nodes for the HWH system

Temperature and water mass flow rate dynamics are the focus of the SFMZ system model. They are described as follows.

#### 4.1.2 Temperature dynamics

Six or eight equations for each room are used to develop the air and water temperature dynamics depending on the number of outside wall(s) of the rooms. Because the air and water temperature dynamic equations in each room are the same as described in the one room model reduction section, only return water temperature calculation is given in Equations (4.1)~(4.4) based on steady state approach. Note that the heat loss from the pipe network is neglected.

$$T_{rd} = \frac{\dot{m}_{wn}T_{re} + \dot{m}_{we}T_{rd1}}{\dot{m}_{wn} + \dot{m}_{we}} \quad (4.1)$$

$$T_{rc} = \frac{(\dot{m}_{wn} + \dot{m}_{we})T_{rd} + \dot{m}_{ws}T_{rc1}}{\dot{m}_{wn} + \dot{m}_{we} + \dot{m}_{ws}} \quad (4.2)$$

$$T_{rb} = \frac{(\dot{m}_{wn} + \dot{m}_{we} + \dot{m}_{ws})T_{rc} + \dot{m}_{nw}T_{rb1}}{\dot{m}_{wn} + \dot{m}_{we} + \dot{m}_{ws} + \dot{m}_{nw}} \quad (4.3)$$

$$T_{ra} = T_{rb} \quad (4.4)$$

#### 4.1.3 Water mass flow rate dynamics

Generally, one of the most commonly installed HWH hydraulic systems is a closed loop system. The closed water flow systems must satisfy the following three principles: (i) the continuity has to hold for all closed circuits and all junctions in the network, (ii) the momentum balance has to be satisfied for all pipe segments in the loop, and (iii) the cyclic integral of pressure drops around independent circuit must be zero. All components in each independent circuit should be considered, and their pressure drops should be computed according to the water mass flow rate.

By applying the momentum balance theory and the frictional resistance calculation method of water, the dynamic equations for Loop n are expressed in detail. Note that the formulation for pressure drops from pipe segments, fittings and equipment is presented in Appendix B.

Dynamic equations of the water mass flow rates in pipe segments AB, BB1, B1B2, B2B3, B3B4, B4B5, B5e, ed, dc, cb and ba can be obtained by applying Equation (B.2, Appendix B) to each pipe segment. Therefore, a set of momentum equations are given in Equations (4.5)~(4.15).

$$\frac{L_{AB}}{A_{AB}} \frac{d(\dot{m}_{wn} + \dot{m}_{we} + \dot{m}_{ws} + \dot{m}_{nw})}{dt} = P_A - P_B - \sum f_{AB} \quad (4.5)$$

$$\frac{L_{BB1}}{A_{BB1}} \frac{d\dot{m}_{wn}}{dt} = P_B - P_{B1} - \sum f_{BB1} \quad (4.6)$$

$$\frac{L_{B1B2}}{A_{B1B2}} \frac{d\dot{m}_{wn}}{dt} = P_{B1} - P_{B2} - \sum f_{B1B2} \quad (4.7)$$

$$\frac{L_{B2B3}}{A_{B2B3}} \frac{d\dot{m}_{wn}}{dt} = P_{B2} - P_{B3} - \sum f_{B2B3} \quad (4.8)$$

$$\frac{L_{B3B4}}{A_{B3B4}} \frac{d\dot{m}_{wn}}{dt} = P_{B3} - P_{B4} - \sum f_{B3B4} \quad (4.9)$$

$$\frac{L_{B4B5}}{A_{B4B5}} \frac{d\dot{m}_{wn}}{dt} = P_{B4} - P_{B5} - \sum f_{B4B5} \quad (4.10)$$

$$\frac{L_{B5e}}{A_{B5e}} \frac{d\dot{m}_{wn}}{dt} = P_{B5} - P_e - \sum f_{B5e} \quad (4.11)$$

$$\frac{L_{ed}}{A_{ed}} \frac{d\dot{m}_{wn}}{dt} = P_e - P_d - \sum f_{ed} \quad (4.12)$$

$$\frac{L_{dc}}{A_{dc}} \frac{d(\dot{m}_{wn} + \dot{m}_{we})}{dt} = P_d - P_c - \sum f_{dc} \quad (4.13)$$

$$\frac{L_{cb}}{A_{cb}} \frac{d(\dot{m}_{wn} + \dot{m}_{we} + \dot{m}_{ws})}{dt} = P_c - P_b - \sum f_{cb} \quad (4.14)$$

$$\frac{L_{ba}}{A_{ba}} \frac{d(\dot{m}_{wn} + \dot{m}_{we} + \dot{m}_{ws} + \dot{m}_{ww})}{dt} = P_b - P_a - \sum f_{ba} \quad (4.15)$$

Applying the principle of cyclic integral of pressure drops around each circuit must be zero, the momentum equations for Loop n are added from Equations (4.5) to (4.15), and is rearranged, it becomes

$$\begin{aligned}
& \left( \frac{L_{AB}}{A_{AB}} + \frac{L_{BB1}}{A_{BB1}} + \frac{L_{B1B2}}{A_{B1B2}} + \frac{L_{B2B3}}{A_{B2B3}} + \frac{L_{B3B4}}{A_{B3B4}} + \frac{L_{B4B5}}{A_{B4B5}} + \frac{L_{B5e}}{A_{B5e}} + \frac{L_{ed}}{A_{ed}} + \frac{L_{dc}}{A_{dc}} + \frac{L_{cb}}{A_{cb}} + \frac{L_{ba}}{A_{ba}} \right) \frac{d\dot{m}_{wn}}{dt} + \\
& \left( \frac{L_{AB}}{A_{AB}} + \frac{L_{dc}}{A_{dc}} + \frac{L_{cb}}{A_{cb}} + \frac{L_{ba}}{A_{ba}} \right) \frac{d\dot{m}_{we}}{dt} + \left( \frac{L_{AB}}{A_{AB}} + \frac{L_{cb}}{A_{cb}} + \frac{L_{ba}}{A_{ba}} \right) \frac{d\dot{m}_{ws}}{dt} + \left( \frac{L_{AB}}{A_{AB}} + \frac{L_{ba}}{A_{ba}} \right) \frac{d\dot{m}_{wv}}{dt} \\
& = P_A - P_a - \left( \sum f_{AB} + \sum f_{BB1} + \sum f_{B1B2} + \sum f_{B2B3} + \sum f_{B3B4} + \sum f_{B4B5} + \sum f_{B5e} \right. \\
& \quad \left. + \sum f_{ed} + \sum f_{dc} + \sum f_{cb} + \sum f_{ba} \right)
\end{aligned} \tag{4.16}$$

Using matrix form, Equation (4.16) can be rewritten as

$$\left( \frac{L}{A} \right)_{loopn} \begin{bmatrix} \frac{d\dot{m}_{wn}}{dt} \\ \frac{d\dot{m}_{we}}{dt} \\ \frac{d\dot{m}_{ws}}{dt} \\ \frac{d\dot{m}_{wv}}{dt} \end{bmatrix} = f_{loopn} = f_1'(T, \dot{m}_{wn}, \dot{m}_{we}, \dot{m}_{ws}, \dot{m}_{wv}, u_{zn}) \tag{4.17}$$

Similarly, by the application of the momentum balance to Loop e, Loop s and Loop w respectively, the mass flow rates for these loops are shown as

For Loop e:

$$\begin{aligned}
& \left( \frac{L_{AB}}{A_{AB}} + \frac{L_{dc}}{A_{dc}} + \frac{L_{cb}}{A_{cb}} + \frac{L_{ba}}{A_{ba}} \right) \frac{d\dot{m}_{wn}}{dt} + \left( \frac{L_{AB}}{A_{AB}} + \frac{L_{BC}}{A_{BC}} + \frac{L_{CC1}}{A_{CC1}} + \frac{L_{C1d1}}{A_{C1d1}} + \frac{L_{d1d}}{A_{d1d}} + \frac{L_{dc}}{A_{dc}} + \frac{L_{cb}}{A_{cb}} + \frac{L_{ba}}{A_{ba}} \right) \frac{d\dot{m}_{we}}{dt} \\
& + \left( \frac{L_{AB}}{A_{AB}} + \frac{L_{BC}}{A_{BC}} + \frac{L_{cb}}{A_{cb}} + \frac{L_{ba}}{A_{ba}} \right) \frac{d\dot{m}_{ws}}{dt} + \left( \frac{L_{AB}}{A_{AB}} + \frac{L_{BC}}{A_{BC}} + \frac{L_{ba}}{A_{ba}} \right) \frac{d\dot{m}_{wv}}{dt} \\
& = P_A - P_a - \left( \sum f_{AB} + \sum f_{BC} + \sum f_{CC1} + \sum f_{C1d1} + \sum f_{d1d} + \sum f_{dc} + \sum f_{cb} + \sum f_{ba} \right)
\end{aligned} \tag{4.18}$$

For Loop s:

$$\begin{aligned}
& \left( \frac{L_{AB}}{A_{AB}} + \frac{L_{cb}}{A_{cb}} + \frac{L_{ba}}{A_{ba}} \right) \frac{d\dot{m}_{wn}}{dt} + \left( \frac{L_{AB}}{A_{AB}} + \frac{L_{BC}}{A_{BC}} + \frac{L_{cb}}{A_{cb}} + \frac{L_{ba}}{A_{ba}} \right) \frac{d\dot{m}_{we}}{dt} \\
& + \left( \frac{L_{AB}}{A_{AB}} + \frac{L_{BC}}{A_{BC}} + \frac{L_{CD}}{A_{CD}} + \frac{L_{DD1}}{A_{DD1}} + \frac{L_{D1D2}}{A_{D1D2}} + \frac{L_{D2D3}}{A_{D2D3}} + \frac{L_{D3c1}}{A_{D3c1}} + \frac{L_{c1c}}{A_{c1c}} + \frac{L_{cb}}{A_{cb}} + \frac{L_{ba}}{A_{ba}} \right) \frac{d\dot{m}_{ws}}{dt} \\
& + \left( \frac{L_{AB}}{A_{AB}} + \frac{L_{BC}}{A_{BC}} + \frac{L_{CD}}{A_{CD}} + \frac{L_{ba}}{A_{ba}} \right) \frac{d\dot{m}_{ww}}{dt} \tag{4.19} \\
= & P_A - P_a - (\sum f_{AB} + \sum f_{BC} + \sum f_{CD} + \sum f_{DD1} + \sum f_{D1D2} + \sum f_{D2D3} \\
& + \sum f_{D3c1} + \sum f_{c1c} + \sum f_{cb} + \sum f_{ba})
\end{aligned}$$

For Loop w:

$$\begin{aligned}
& \left( \frac{L_{AB}}{A_{AB}} + \frac{L_{ba}}{A_{ba}} \right) \frac{d\dot{m}_{wn}}{dt} + \left( \frac{L_{AB}}{A_{AB}} + \frac{L_{BC}}{A_{BC}} + \frac{L_{ba}}{A_{ba}} \right) \frac{d\dot{m}_{we}}{dt} + \left( \frac{L_{AB}}{A_{AB}} + \frac{L_{BC}}{A_{BC}} + \frac{L_{CD}}{A_{CD}} + \frac{L_{ba}}{A_{ba}} \right) \frac{d\dot{m}_{ws}}{dt} \\
& + \left( \frac{L_{AB}}{A_{AB}} + \frac{L_{BC}}{A_{BC}} + \frac{L_{CD}}{A_{CD}} + \frac{L_{DE}}{A_{DE}} + \frac{L_{EE1}}{A_{EE1}} + \frac{L_{E1E2}}{A_{E1E2}} + \frac{L_{E2E3}}{A_{E2E3}} + \frac{L_{E3b1}}{A_{E3b1}} + \frac{L_{b1b}}{A_{b1b}} + \frac{L_{ba}}{A_{ba}} \right) \frac{d\dot{m}_{ww}}{dt} \tag{4.20} \\
= & P_A - P_a - (\sum f_{AB} + \sum f_{BC} + \sum f_{CD} + \sum f_{DE} + \sum f_{EE1} + \sum f_{E1E2} + \sum f_{E2E3} \\
& + \sum f_{E3b1} + \sum f_{b1b} + \sum f_{ba})
\end{aligned}$$

Combining Equations (4.17)~(4.20) by using matrix formulation, the four water mass flow rate dynamic equations become

$$\begin{bmatrix} \left(\frac{L}{A}\right)_{loopn} \\ \left(\frac{L}{A}\right)_{loope} \\ \left(\frac{L}{A}\right)_{loops} \\ \left(\frac{L}{A}\right)_{loopw} \end{bmatrix} \begin{bmatrix} \frac{d\dot{m}_{wn}}{dt} \\ \frac{d\dot{m}_{we}}{dt} \\ \frac{d\dot{m}_{ws}}{dt} \\ \frac{d\dot{m}_{ww}}{dt} \end{bmatrix} = \begin{bmatrix} f_{loopn} \\ f_{loope} \\ f_{loops} \\ f_{loopw} \end{bmatrix} = \begin{bmatrix} f_1'(T, \dot{m}_{wn}, \dot{m}_{we}, \dot{m}_{ws}, \dot{m}_{ww}, u_{zn}) \\ f_2'(T, \dot{m}_{wn}, \dot{m}_{we}, \dot{m}_{ws}, \dot{m}_{ww}, u_{ze}) \\ f_3'(T, \dot{m}_{wn}, \dot{m}_{we}, \dot{m}_{ws}, \dot{m}_{ww}, u_{zs}) \\ f_4'(T, \dot{m}_{wn}, \dot{m}_{we}, \dot{m}_{ws}, \dot{m}_{ww}, u_{zw}) \end{bmatrix} \tag{4.21}$$

Note that the first term (L/A) is a 4\*4 square matrix. Equation (4.21) can be solved as

$$\begin{bmatrix} \frac{dm_{nn}}{dt} \\ \frac{dm_{ne}}{dt} \\ \frac{dm_{ns}}{dt} \\ \frac{dm_{nw}}{dt} \end{bmatrix} = \begin{bmatrix} \left(\frac{L}{A}\right)_{loopn} \\ \left(\frac{L}{A}\right)_{loope} \\ \left(\frac{L}{A}\right)_{loops} \\ \left(\frac{L}{A}\right)_{loopw} \end{bmatrix}^{-1} \begin{bmatrix} f_{loopn} \\ f_{loope} \\ f_{loops} \\ f_{loopw} \end{bmatrix} = \begin{bmatrix} f_1(T, \dot{m}_{nn}, \dot{m}_{ne}, \dot{m}_{ns}, \dot{m}_{nw}, u_{zn}) \\ f_2(T, \dot{m}_{nn}, \dot{m}_{ne}, \dot{m}_{ns}, \dot{m}_{nw}, u_{ze}) \\ f_3(T, \dot{m}_{nn}, \dot{m}_{ne}, \dot{m}_{ns}, \dot{m}_{nw}, u_{zs}) \\ f_4(T, \dot{m}_{nn}, \dot{m}_{ne}, \dot{m}_{ns}, \dot{m}_{nw}, u_{zw}) \end{bmatrix} \quad (4.22)$$

In summary, the SFMZ HWH dynamic system consists of 58 dynamic equations, which is composed of 8, 22, 24, 4 equations for the rooms, the outside walls, the baseboard heaters and the water mass flow rates respectively.

## 4.2 Parameter aggregation for model reduction

### 4.2.1 Aggregation model of the SFMZ system

Because the developed SFMZ HWH system dynamic model is still too large, it requires a technique to decrease the order of the model so that it can be utilized to build a multi-floor system model. This was achieved by applying a parameter aggregation method for temperature dynamics; while the fluid flow dynamics in the zones remain the same as described in the section of the SFMZ HWH system model.

Based on this method, the energy stored in the outside walls, the zone air and the water inside of the baseboard heaters were aggregated for north, east, south and west zones. Thus, the dynamic state variables consisting of the temperature and the mass flow rates of north, east, south and west zones are described in the schematic diagram shown in Figure 4.3.

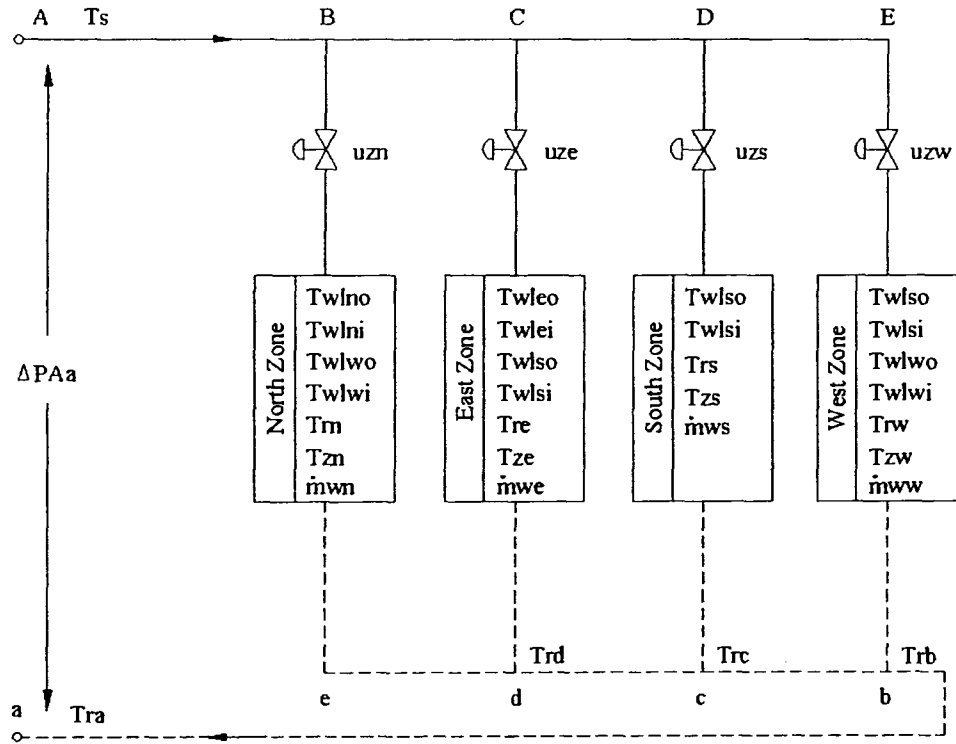


Figure 4.3 Schematic diagram showing states of the aggregated SFMZ HWH system

By applying the mass and energy balance principles to each zone, a set of equations were determined as follows.

For the return water temperatures:

$$T_{rd} = \frac{\dot{m}_{wn}T_{rn} + \dot{m}_{we}T_{re}}{\dot{m}_{wn} + \dot{m}_{we}} \quad (4.23)$$

$$T_{rc} = \frac{(\dot{m}_{wn} + \dot{m}_{we})T_{rd} + \dot{m}_{ws}T_{rs}}{\dot{m}_{wn} + \dot{m}_{we} + \dot{m}_{ws}} \quad (4.24)$$

$$T_{rb} = \frac{(\dot{m}_{wn} + \dot{m}_{we} + \dot{m}_{ws})T_{rc} + \dot{m}_{ww}T_{rw}}{\sum_{j=1}^k (\dot{m}_{wj})} \quad (4.25)$$

Note that  $T_{ra} = T_{rb}$  when applying the assumption of no heat losses from the pipe networks.

For the zone air temperature:

$$C_{zj} \frac{dT_{zj}}{dt} = c_w \dot{m}_w (T_s - T_{rj}) + Q_{solj} A_{winj} + Q_{intj} A_{zj} + \sum [U_{wlj} A_{wlj} (T_{wlj} - T_{zj}) + U_{win} A_{winj} (T_o - T_{zj})]_{jk} \quad (4.26)$$

In Equation (4.26), j and k refer to the direction of the zones and the number of the outside wall respectively. The net energy stored in the zone air is equal to the heat output from the hot water, the solar radiation from the windows and the internal heat gains minus the heat losses from the building enclosure.

For the baseboard heater:

$$C_{htrj} \frac{dT_{rj}}{dt} = c_w \dot{m}_{wj} (T_s - T_{rj}) - f_{wj} L_{htrj} \Omega_{htr} \left( \frac{T_s + T_{rj}}{2} - T_{zj} \right)^{(1+n)} \quad (4.27)$$

Equation (4.27) states that the net energy stored in the water inside of the heater tube in each zone is equal to the heat supplied from the hot water minus the heat emission from the outside surface of the heater(s) to the zone air.

For the outside wall:

$$C_{wljo} \frac{dT_{wljo}}{dt} = U_{wli\sigma} A_{wlj} (T_{wlji} - T_{wljo}) + U_{wlsf} A_{wlj} (T_{sff} - T_{wljo}) \quad (4.28)$$

$$C_{wlji} \frac{dT_{wlji}}{dt} = U_{wli\sigma} A_{wlj} (T_{zj} - T_{wlji}) + U_{wli\sigma} A_{wlj} (T_{wljo} - T_{wlji}) \quad (4.29)$$

Equations (4.28) and (4.29) express the temperature dynamics of the two layers of the outside wall.

The mass flow rate dynamic equations remained unchanged, and the matrix formulation is given as

$$\frac{d\dot{m}_{wj}}{dt} = f_j(T, \dot{m}_{wn}, \dot{m}_{we}, \dot{m}_{ws}, \dot{m}_{ww}, u_{zj}) \quad (4.30)$$

With this approach, the aggregated SFMZ system model is composed of 26 dynamic equations.

#### **4.2.2 Aggregation model of the basement heating system**

By applying aggregation technique, a dynamic model of the basement HWH system was also developed. The details are presented in Appendix C.

### **4.3 Dynamic model of a MFMZ HWH system**

#### **4.3.1 Physical model of the high-rise building HWH system**

In the dynamic modeling for the high-rise building HWH system, the major consideration is to employ the dynamic model for designing and analyzing control and FTC strategies. Therefore, the overall model will consider the fluid flow and temperature dynamics for the entire perimeter loop baseboard heating system. A section view of the high-rise building with the HWH system is presented in Figure 4.4. The HWH system is connected by water risers from the mechanical room at each floor. The HWH systems in the above-ground floors have the same configurations. Details of the mechanical room hydraulic system and the differential pressure position are illustrated in Figure 4.5. A schematic diagram of the entire system with parameter notation is given in Figure 4.6.

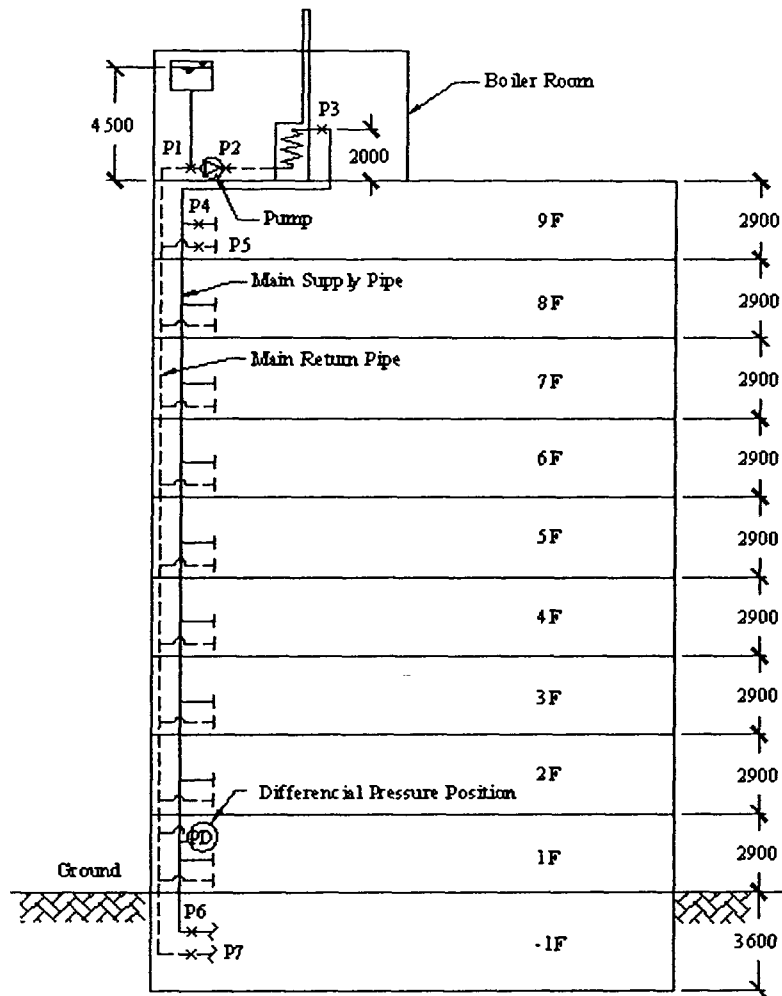


Figure 4.4 Hydraulic system of the ten-floor high-rise building HWH system

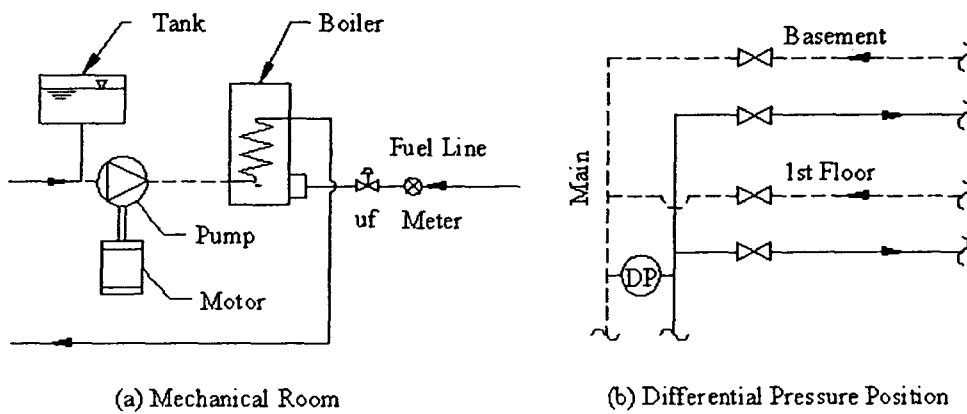


Figure 4.5 Details of mechanical room and differential pressure position

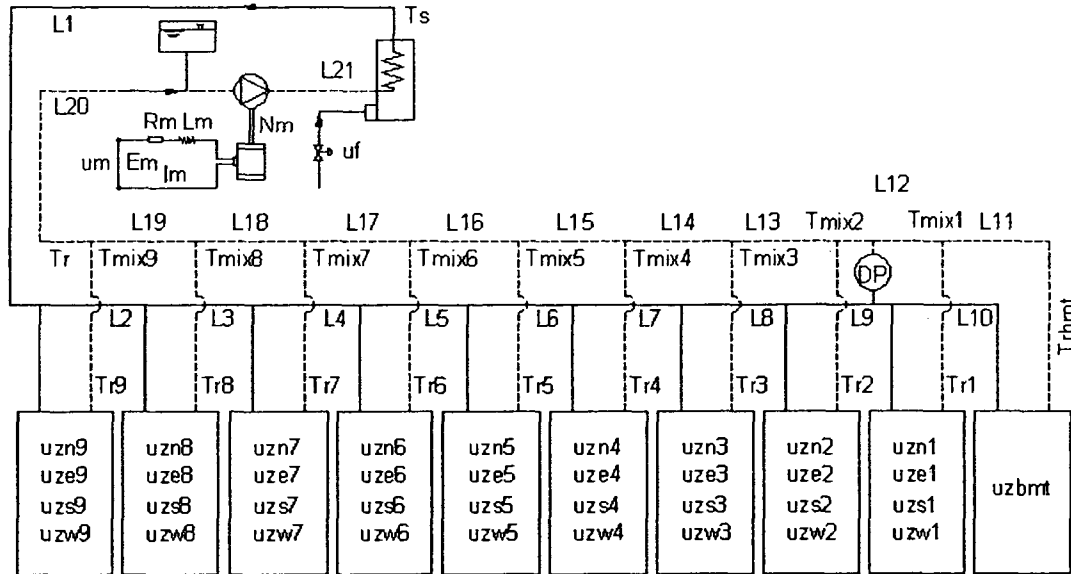


Figure 4.6 Schematic diagram of the entire HWH system

#### 4.3.2 Dynamic modeling of the MFMZ system

Based on mass, energy and momentum balance principles, the overall dynamic model of the high-rise building HWH system is developed and presented in four parts: temperature, water mass flow rate, motor speed and current dynamics. These are described as follows.

##### *Temperature dynamics*

The temperature dynamics of the above-ground floors remain the same as given in the aggregated SFMZ model; while those of the basement are given by the basement heating system model (Appendix C).

The return water and the boiler output temperatures are calculated in the following equations.

For the mixing return water:

$$T_{mix} = \frac{\dot{m}_{win1}T_{in1} + \dot{m}_{win2}T_{in2}}{\dot{m}_{win1} + \dot{m}_{win2}} \quad (4.31)$$

The subscripts in1 and in2 refer to the water flows that are mixed after the connection point. Note that there are 37 return water temperature mixing nodes for the entire system.

For the boiler:

$$C_b \frac{dT_s}{dt} = u_f \dot{m}_{fmax} HV (\gamma_1 R_{load}^2 + \gamma_2 R_{load} + \gamma_3) - c_w \dot{m}_{tot} (T_s - T_r) \quad (4.32)$$

In this equation, the net energy stored in the water of the boiler body is equal to the effective heat input in terms of the fuel minus the heat absorbed by the circulating water through the boiler. The boiler efficiency is obtained depending on the ratio of the boiler heating load.

#### ***Water mass flow rate dynamics***

Total pressure of water is composed of gravity pressure, velocity pressure and static pressure. The gravity pressure relates to the position of the water. However, if the water is in a closed loop, the gravity pressure for computing frictional losses can be neglected due to the closed loop property. On the other hand, velocity pressure in a pipe segment also has a small value compared with static pressure in a typical HWH system operation process. This is due to the fact that the water velocity in a pipe segment is around 1m/s in general.

By applying the momentum balance principle to the overall hydraulic system, a set of 37 water mass flow rate dynamic equations including all independent circulating loops can be computed. As an example, the closest loops (the 9<sup>th</sup> floor heating system) with the associated main pipes shown in Figure 4.7 are taken into account to illustrate the

fluid flow dynamics. There are four loops indicated as Loop 1, Loop 2, Loop 3 and Loop 4 respectively.

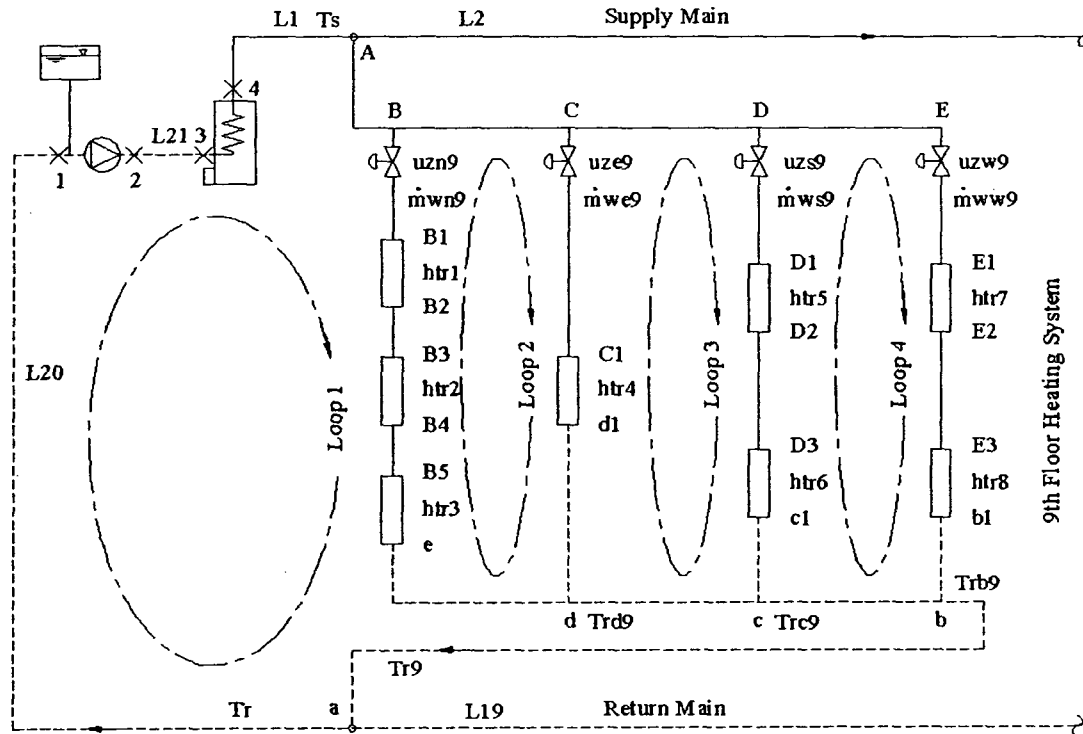


Figure 4.7 Diagram of the closest circulating water loops

Loop 1: (1-2-3-4-A-B-B1-B2-B3-B4-B5-e-d-c-b-a-1)

For pipe segment L20:

$$\frac{L_{20}}{A_{L20}} \frac{dm_{\text{water}}}{dt} = P_a - P_1 - f_{L20} \quad (4.33)$$

This equation expresses that the change of the total water mass flow rate is related to the pressure difference between the beginning and the end of the pipe segment and its frictional losses. The same concept can be applied for each pipe segment below.

For pipe segment L21:

$$\frac{L_{21}}{A_{L21}} \frac{d\dot{m}_{\text{mol}}}{dt} = P_2 - P_3 - f_{L21} \quad (4.34)$$

For pipe segment L1:

$$\frac{L_1}{A_{L1}} \frac{d\dot{m}_{\text{mol}}}{dt} = P_4 - P_A - f_{L1} \quad (4.35)$$

For pipe segment AB:

$$\frac{L_{AB}}{A_{AB}} \frac{d(\dot{m}_{\text{wn}9} + \dot{m}_{\text{we}9} + \dot{m}_{\text{ns}9} + \dot{m}_{\text{nw}9})}{dt} = P_A - P_B - f_{AB} \quad (4.36)$$

For pipe segments B~B1~d:

$$\begin{aligned} & \left( \frac{L_{BB1}}{A_{BB1}} + \frac{L_{B1B2}}{A_{B1B2}} + \frac{L_{B2B3}}{A_{B2B3}} + \frac{L_{B3B4}}{A_{B3B4}} + \frac{L_{B4B5}}{A_{B4B5}} + \frac{L_{B5e}}{A_{B5e}} \frac{L_{ed}}{A_{ed}} \right) \frac{d\dot{m}_{\text{wn}9}}{dt} \\ & = P_B - P_d - (f_{\text{valv}} + f_{BB1} + f_{B1B2} + f_{B2B3} + f_{B3B4} + f_{B4B5} + f_{B5e} + f_{ed})_9 \end{aligned} \quad (4.37)$$

For pipe segment dc:

$$\frac{L_{dc}}{A_{dc}} \frac{d(\dot{m}_{\text{wn}9} + \dot{m}_{\text{we}9})}{dt} = P_d - P_c - f_{dc} \quad (4.38)$$

For pipe segment cb:

$$\frac{L_{cb}}{A_{cb}} \frac{d(\dot{m}_{\text{wn}9} + \dot{m}_{\text{we}9} + \dot{m}_{\text{ns}9})}{dt} = P_c - P_b - f_{cb} \quad (4.39)$$

For pipe segment ba:

$$\frac{L_{ba}}{A_{ba}} \frac{d(\dot{m}_{\text{wn}9} + \dot{m}_{\text{we}9} + \dot{m}_{\text{ns}9} + \dot{m}_{\text{nw}9})}{dt} = P_b - P_a - f_{ba} \quad (4.40)$$

For the circulating pump:

$$P_2 - P_1 = H_{\text{pump}} = C_h \rho_w D_{\text{pump}}^2 N_m^2 \quad (4.41)$$

Note that the pressure head of the pump is depending on both its geometrical parameter and the motor speed.

For the boiler:

$$P_3 - P_4 = f_{bd} \left( \frac{\dot{m}_{wtot}}{\dot{m}_{wbd}} \right)^2 \quad (4.42)$$

The pressure drop for the boiler is calculated by using its design values.

By adding Equations (4.33)~(4.40), and replacing  $P_2-P_1$  and  $P_3-P_4$  using Equations (4.41) and (4.42), the water mass flow rate dynamic equation for Loop 1 becomes

$$\begin{aligned} & \left( \frac{L_1}{A_{L1}} + \frac{L_{21}}{A_{L21}} + \frac{L_{20}}{A_{L20}} \right) \left( \frac{d\dot{m}_{wn1}}{dt} + \frac{d\dot{m}_{we1}}{dt} + \frac{d\dot{m}_{vs1}}{dt} + \frac{d\dot{m}_{nw1}}{dt} + \frac{d\dot{m}_{wn2}}{dt} + \frac{d\dot{m}_{we2}}{dt} + \frac{d\dot{m}_{vs2}}{dt} + \frac{d\dot{m}_{ww2}}{dt} + \frac{d\dot{m}_{wn3}}{dt} + \right. \\ & \frac{d\dot{m}_{we3}}{dt} + \frac{d\dot{m}_{vs3}}{dt} + \frac{d\dot{m}_{nw3}}{dt} + \frac{d\dot{m}_{wn4}}{dt} + \frac{d\dot{m}_{we4}}{dt} + \frac{d\dot{m}_{vs4}}{dt} + \frac{d\dot{m}_{nw4}}{dt} + \frac{d\dot{m}_{wn5}}{dt} + \frac{d\dot{m}_{we5}}{dt} + \frac{d\dot{m}_{vs5}}{dt} + \frac{d\dot{m}_{nw5}}{dt} + \\ & \frac{d\dot{m}_{wn6}}{dt} + \frac{d\dot{m}_{we6}}{dt} + \frac{d\dot{m}_{vs6}}{dt} + \frac{d\dot{m}_{nw6}}{dt} + \frac{d\dot{m}_{wn7}}{dt} + \frac{d\dot{m}_{we7}}{dt} + \frac{d\dot{m}_{vs7}}{dt} + \frac{d\dot{m}_{nw7}}{dt} + \frac{d\dot{m}_{wn8}}{dt} + \frac{d\dot{m}_{we8}}{dt} + \frac{d\dot{m}_{vs8}}{dt} + \\ & \frac{d\dot{m}_{nw8}}{dt} + \frac{d\dot{m}_{wn9}}{dt} + \frac{d\dot{m}_{we9}}{dt} + \frac{d\dot{m}_{vs9}}{dt} + \frac{d\dot{m}_{nw9}}{dt} + \frac{d\dot{m}_{vbtot}}{dt} \left. \right) + \frac{L_{AB}}{A_{AB}} \left( \frac{d\dot{m}_{wn9}}{dt} + \frac{d\dot{m}_{we9}}{dt} + \frac{d\dot{m}_{vs9}}{dt} + \right. \\ & \frac{d\dot{m}_{nw9}}{dt} \left. \right) + \left( \frac{L_{BB1}}{A_{BB1}} + \frac{L_{B1B2}}{A_{B1B2}} + \frac{L_{B2B3}}{A_{B2B3}} + \frac{L_{B3B4}}{A_{B3B4}} + \frac{L_{B4B5}}{A_{B4B5}} + \frac{L_{B5e}}{A_{B5e}} + \frac{L_{ed}}{A_{ed}} \right) \frac{d\dot{m}_{wn9}}{dt} + \frac{L_{dc}}{A_{dc}} \left( \frac{d\dot{m}_{wn9}}{dt} + \right. \\ & \frac{d\dot{m}_{we9}}{dt} \left. \right) + \frac{L_{cb}}{A_{cb}} \left( \frac{d\dot{m}_{wn9}}{dt} + \frac{d\dot{m}_{we9}}{dt} + \frac{d\dot{m}_{vs9}}{dt} \right) + \frac{L_{ba}}{A_{ba}} \left( \frac{d\dot{m}_{wn9}}{dt} + \frac{d\dot{m}_{we9}}{dt} + \frac{d\dot{m}_{vs9}}{dt} + \frac{d\dot{m}_{nw9}}{dt} \right) \\ & = H_{pump} - f_{bd} \left( \frac{\dot{m}_{wtot}}{\dot{m}_{wbd}} \right)^2 - f_{L1} - f_{L21} - f_{L20} - (f_{AB} + f_{BB1} + f_{B1B2} + f_{B2B3} + f_{B3B4} + f_{B4B5} + \\ & f_{B5e} + f_{ed} + f_{dc} + f_{cb} + f_{ba} + f_{vbtot})_9 \end{aligned} \quad (4.43)$$

The change of the water mass flow rates in Loop 1 is equal to the pressure increased by the circulating pump minus all frictional losses resulted from the closed loop. Note that the total water mass flow rate is equal to the summation of all water mass flow rates in branches. The subscribe 9 in the right part of the equation indicates the 9<sup>th</sup> floor heating system.

Loop 2: (d-e-B5-B4-B3-B2-B1-B-C-C1-d1-d)

For pipe segment BC:

$$\frac{L_{BC}}{A_{BC}} \frac{d(\dot{m}_{we9} + \dot{m}_{ws9} + \dot{m}_{ww9})}{dt} = P_B - P_C - f_{BC} \quad (4.44)$$

For pipe segments C~C1~d:

$$\left( \frac{L_{CC1}}{A_{CC1}} + \frac{L_{C1d1}}{A_{C1d1}} + \frac{L_{d1d}}{A_{d1d}} \right) \frac{d\dot{m}_{we9}}{dt} = P_C - P_d - (f_{vale} + f_{CC1} + f_{C1d1} + f_{d1d})_9 \quad (4.45)$$

By adding Equations (4.44) and (4.45), and subtract from Equation (4.37), it becomes

$$\begin{aligned} & \left( \frac{L_{BB1}}{A_{BB1}} + \frac{L_{B1B2}}{A_{B1B2}} + \frac{L_{B2B3}}{A_{B2B3}} + \frac{L_{B3B4}}{A_{B3B4}} + \frac{L_{B4B5}}{A_{B4B5}} + \frac{L_{B5e}}{A_{B5e}} + \frac{L_{ed}}{A_{ed}} \right) \frac{d\dot{m}_{wn9}}{dt} - \\ & \frac{L_{BC}}{A_{BC}} \left( \frac{d\dot{m}_{we9}}{dt} + \frac{d\dot{m}_{ws9}}{dt} + \frac{d\dot{m}_{ww9}}{dt} \right) - \left( \frac{L_{CC1}}{A_{CC1}} + \frac{L_{C1d1}}{A_{C1d1}} + \frac{L_{d1d}}{A_{d1d}} \right) \frac{d\dot{m}_{we9}}{dt} \\ & = -(f_{BB1} + f_{B1B2} + f_{B2B3} + f_{B3B4} + f_{B4B5} + f_{B5e} + f_{ed} + f_{valn})_9 + (f_{BC} + \\ & \quad f_{CC1} + f_{C1d1} + f_{d1d} + f_{vale})_9 \end{aligned} \quad (4.46)$$

Loop 3: (c-d-d1-C1-C-D-D1-D2-D3-c1-c)

For pipe segment CD:

$$\frac{L_{CD}}{A_{CD}} \frac{d(\dot{m}_{ws9} + \dot{m}_{ww9})}{dt} = P_C - P_D - f_{CD} \quad (4.47)$$

For pipe segments D~D1~c:

$$\begin{aligned} & \left( \frac{L_{DD1}}{A_{DD1}} + \frac{L_{D1D2}}{A_{D1D2}} + \frac{L_{D2D3}}{A_{D2D3}} + \frac{L_{D3c1}}{A_{D3c1}} + \frac{L_{c1c}}{A_{c1c}} \right) \frac{d\dot{m}_{ws9}}{dt} \\ & = P_D - P_c - (f_{vals} + f_{DD1} + f_{D1D2} + f_{D2D3} + f_{D3c1} + f_{c1c})_9 \end{aligned} \quad (4.48)$$

For pipe segment dc:

$$\frac{L_{dc}}{A_{dc}} \frac{d(\dot{m}_{wn9} + \dot{m}_{we9})}{dt} = P_d - P_c - f_{dc} \quad (4.49)$$

By adding Equations (4.45) and (4.49), Equation (4.47) and (4.48), then subtract each other, it gives

$$\begin{aligned} & \left( \frac{L_{CC1}}{A_{CC1}} + \frac{L_{C1d1}}{A_{C1d1}} + \frac{L_{d1d}}{A_{d1d}} \right) \frac{d\dot{m}_{we9}}{dt} + \frac{L_{dc}}{A_{dc}} \left( \frac{d\dot{m}_{wn9}}{dt} + \frac{d\dot{m}_{we9}}{dt} \right) - \frac{L_{CD}}{A_{CD}} \left( \frac{d\dot{m}_{ws9}}{dt} + \frac{d\dot{m}_{wn9}}{dt} \right) - \\ & \left( \frac{L_{DD1}}{A_{DD1}} + \frac{L_{D1D2}}{A_{D1D2}} + \frac{L_{D2D3}}{A_{D2D3}} + \frac{L_{D3c1}}{A_{D3c1}} \right) \frac{d\dot{m}_{ws9}}{dt} \quad (4.50) \\ & = -(f_{CC1} + f_{C1d1} + f_{d1d} + f_{dc} + f_{vale})_9 + (f_{CD} + f_{DD1} + f_{D1D2} + f_{D2D3} + f_{D3c1} + f_{c1c} + f_{vals})_9 \end{aligned}$$

Loop 4: (b-c-c1-D3-D2-D1-D-E-E1-E2-E3-b1-b)

For pipe segment cb:

$$\frac{L_{cb}}{A_{cb}} \frac{d(\dot{m}_{wn9} + \dot{m}_{we9} + \dot{m}_{ws9})}{dt} = P_c - P_b - f_{cb} \quad (4.51)$$

For pipe segments D~E~b:

$$\begin{aligned} & \left( \frac{L_{DE}}{A_{DE}} + \frac{L_{EE1}}{A_{EE1}} + \frac{L_{E1E2}}{A_{E1E2}} + \frac{L_{E2E3}}{A_{E2E3}} + \frac{L_{E3b1}}{A_{E3b1}} + \frac{L_{b1b}}{A_{b1b}} \right) \frac{d\dot{m}_{wn9}}{dt} \quad (4.52) \\ & = P_D - P_b - (f_{vahw} + f_{DE} + f_{EE1} + f_{E1E2} + f_{E2E3} + f_{E3b1} + f_{b1b})_9 \end{aligned}$$

In terms of adding Equations (4.48) and (4.51), and subtract from Equation (4.52), it turns into

$$\begin{aligned} & \left( \frac{L_{DD1}}{A_{DD1}} + \frac{L_{D1D1}}{A_{D1D2}} + \frac{L_{D2D3}}{A_{D2D3}} + \frac{L_{D3c1}}{A_{D3c1}} \right) \frac{d\dot{m}_{ws9}}{dt} + \frac{L_{cb}}{A_{cb}} \left( \frac{d\dot{m}_{wn9}}{dt} + \frac{d\dot{m}_{we9}}{dt} + \frac{d\dot{m}_{ws9}}{dt} \right) - \\ & \left( \frac{L_{DE}}{A_{DE}} + \frac{L_{EE1}}{A_{EE1}} + \frac{L_{E1E2}}{A_{E1E2}} + \frac{L_{E2E3}}{A_{E2E3}} + \frac{L_{E3b1}}{A_{E3b1}} \right) \frac{d\dot{m}_{wn9}}{dt} \quad (4.53) \\ & = -(f_{DD1} + f_{D1D2} + f_{D2D3} + f_{D3c1} + f_{c1c} + f_{dc} + f_{cb} + f_{vals})_9 + (f_{DE} + f_{EE1} + f_{E1E2} + \\ & f_{E2E3} + f_{E3b1} + f_{b1b} + f_{vahw})_9 \end{aligned}$$

To conclude, the water flow rate dynamics from the heat source to the nearest floor heating system can be calculated by using the set of four equations (Equations (4.43), (4.46), (4.50) and (4.53)). For other independent loops, the same principle is employed to compute their water mass flow rates. Because there are 37 independent

circulating loops in the entire HWH system, it has to be given the same number of equations in order to solve the water mass flow rates anywhere.

In general, the obtained equations for the water mass flow rate can be formulated as a matrix form with size

$$(M_1)_{37 \times 37} \left( \frac{dm_w}{dt} \right)_{37 \times 1} = (M_2)_{37 \times 1} \quad (4.54)$$

where matrix  $M_1$  includes all  $\left(\frac{L}{A}\right)$  terms; while matrix  $M_2$  has the pressure head of the pump and all frictional losses such as the pipe segments, the equipment (the boiler and control valves) and fittings.

#### ***Motor speed and current dynamics for the pump-motor unit***

Assuming the condition of a directly connected pump-motor unit utilized in the heating system, according to Zheng (1997), the governing equations of the DC motor are

$$J_{eq} \frac{dN_m}{dt} = \frac{K_i I_m}{2\pi} - B_{eq} N_m - \frac{\dot{m}_{water} H_{pump}}{(2\pi)^2 \rho_w \eta_{pump} N_m} \quad (4.55)$$

$$L_m \frac{dI_m}{dt} = u_m E_m - R_m I_m - 2\pi K_b N_m \quad (4.56)$$

In Equation (4.55), the power which accelerates the pump can be expressed by the torque of the motor, frictional loss in the pump and the load power required. Equation (4.56) represents the application of Kirchhoff's law for the circuit. Note that the values of  $K_i$  and  $K_b$  are identical if the units of  $K_i$  and  $K_b$  are used in Nm/A and Vs/rev respectively.

#### ***Entire large scale dynamic model***

All state space variables used in the overall system including temperatures, mass flow rate, motor speed and current are expressed in Equations (4.57)~(4.60).

$$M_c \frac{dT}{dt} = f_1(T, \dot{m}_w, u, Q) \quad (4.57)$$

$$M_{\dot{m}_w} \frac{d\dot{m}_w}{dt} = f_2(T, \dot{m}_w, N_m, u) \quad (4.58)$$

$$M_{N_m} \frac{dN_m}{dt} = f_3(\dot{m}_w, N_m, I_m) \quad (4.59)$$

$$M_{I_m} \frac{dI_m}{dt} = f_4(I_m, N_m, u) \quad (4.60)$$

In Equations (4.57)~(4.60), the symbols such as  $T$ ,  $\dot{m}_w$ ,  $u$ ,  $N_m$  and  $I_m$  refer to the temperature, the water mass flow rate, the control signal, the motor speed and the current of the HWH system respectively. Note that the first two equations are written in matrix formulation.

In summary, the large scale overall MFMZ system model consists of 342 equations, which include 241 dynamic equations focused on the fluid flow of the water and the temperatures of the air and water. The breakdown of equations respectively are: 127 equations for the outside wall temperature, 37 equations for the zone air temperature, 37 equations for the water temperatures of the heaters, 37 equations for the water mass flow rate in the independent loops, 1 equation for the boiler supply water temperature, 1 equation for the motor speed and 1 equation for the current. The overall dynamic system model will be utilized to simulate and analyze the system responses described in the section below.

#### 4.4 Simulation results of the MFMZ HWH system

The dynamic responses of temperature, water mass flow rate, motor speed and current were simulated by carrying out open loop tests. Also, comparisons are made

between the SFMZ model and its aggregated model. The simulation results are plotted in the following figures with explanation.

#### **4.4.1 Results from the SFMZ heating system**

The open loop zone air temperature dynamic responses are shown in Figure 4.8. From the figure it can be seen that, under the conditions of  $T_s=90^{\circ}\text{C}$ ,  $T_o=-21.8^{\circ}\text{C}$ , with control valves fully open and  $\Delta P_{Aa}=20\text{KPa}$ , all the room air temperatures reach their steady state values within the range from 23.39 to 25.8 $^{\circ}\text{C}$  after 12 hours. These values are greater than the design indoor air temperature value. This is due to the over-sized heat transfer area of the baseboard heaters. Decreasing the supply water temperature and/or reducing the entering water mass flow rate into the zones can bring the room air temperatures back to the design condition.

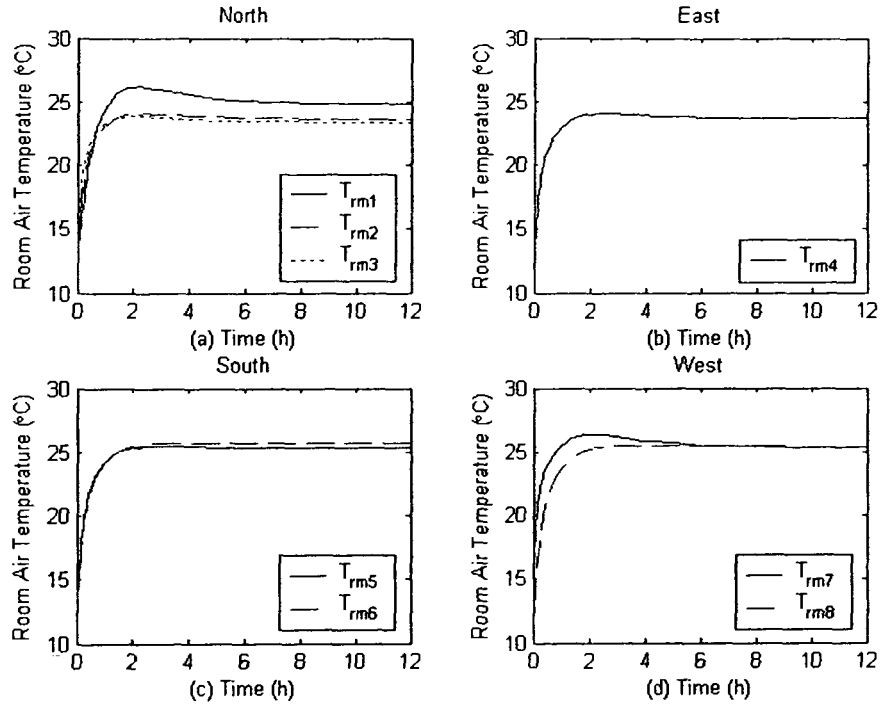


Figure 4.8 Room temperature responses in the SFMZ heating system

In order to decrease zone air temperature, it is possible to adjust the supply water temperature and/or the water mass flow rate into the heaters. For this case, the tests are made and depicted in Figure 4.9 under the conditions:  $T_o = -21.8^\circ\text{C}$  and  $\Delta P_{Aa} = 20\text{KPa}$ . All control valve openings in the four zones are set to 100% in the first 12 hours. The supply water temperature is set to  $86.4^\circ\text{C}$  in order to achieve the room air temperature in the east zone (RM4) at its design temperature ( $22^\circ\text{C}$ ). This is because the east zone has the lowest zone air temperature compared with the others. In order to satisfy the design indoor air temperature requirement for all zones as much as possible, the supply water temperature is controlled first. Then, the water mass flow rates entering the zones are regulated according to the zone temperature responses. Based on this consideration, the openings of

the control valves in north, east, south and west were positioned at 74%, 80%, 33% and 32% respectively in the last 12 hours.

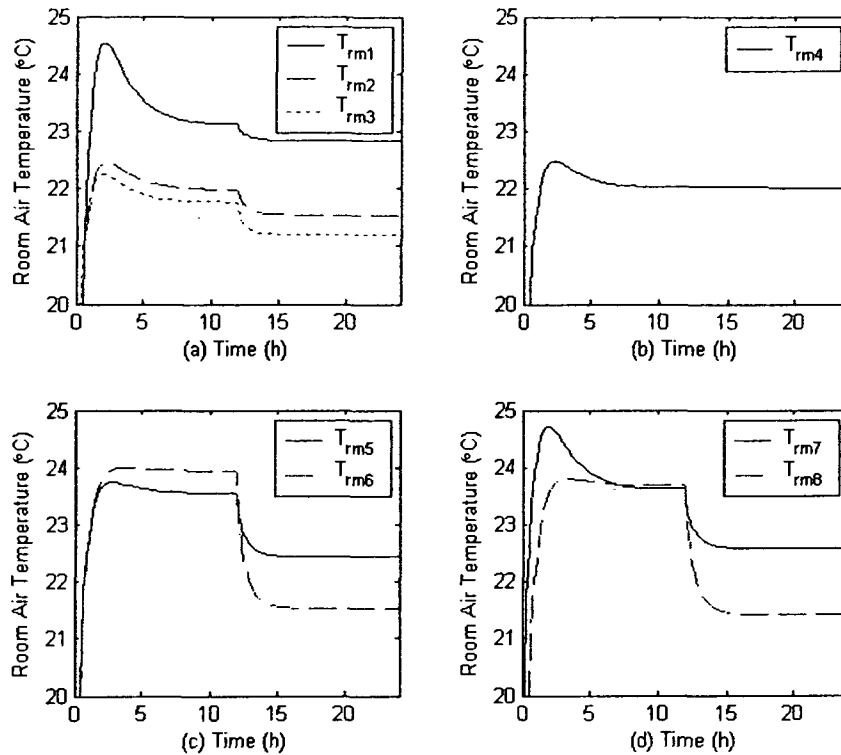


Figure 4.9 Room temperature responses of the zones

This result shows that if the supply water temperature is controlled by a supervisory controller, and the water mass flow rates to the zones are regulated by local controllers, the room air temperatures can be maintained within a reasonable range, especially with disturbances such as solar radiation and internal gains acting on the zones.

Based on the design of the HWH system for the SFMZ system, the heaters are arranged in series in the zones. Because of this configuration and the nonlinear property of the heat output from the baseboard heater, changes of either the supply water temperature or the water mass flow rate will not give the heat outputs from the heaters proportionally. The case for north zone with three rooms is tested and presented in Figure

4.10 with  $T_s=86.4^\circ\text{C}$ ,  $T_o=-21.8^\circ\text{C}$ ,  $\Delta P_{Aa}=20\text{KPa}$  and the control valves fully open. The room temperatures in Room 1, 2 and 3 reach their steady state values of 23.12, 21.98 and  $21.76^\circ\text{C}$  respectively. This means that all room air temperatures in north zone cannot satisfy their design room temperature at the same time.

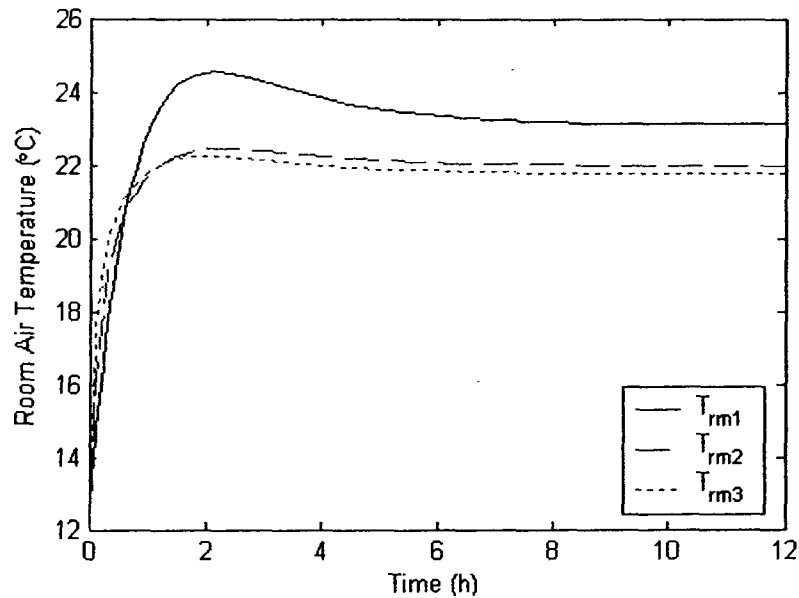


Figure 4.10 Room air temperature responses in north zone

Differential pressure acting on the heating system will affect the water mass flow rate distribution in the circulating loops. In general, the differential pressure should be maintained about 5~30KPa in order to overcome the water resistances of device, fittings and pipe networks. In order to estimate the influence of the differential pressure, the dynamic responses of the water mass flow rates of the system are simulated and shown in Figure 4.11 under the following conditions:  $T_s=90^\circ\text{C}$ ,  $T_o=-21.8^\circ\text{C}$ , the control valves fully open and the differential pressure in the water loops set at 5, 10, 20 and 30KPa. From the figures it can be seen that the water mass flow rates achieve their steady state values in 10s. The lower pressure difference gives less water mass flow rate, vice versa. The steady

state values of the water mass flow rates for north, east, south and west zones are given in Table 4.1.

The variation of the differential pressure will cause the change in the water mass flow rate. By analyzing the simulation results given in Table 4.1, turbulent flow loop, which obeys the square power law relationship between the differential pressure and the water mass flow rate, can be identified.

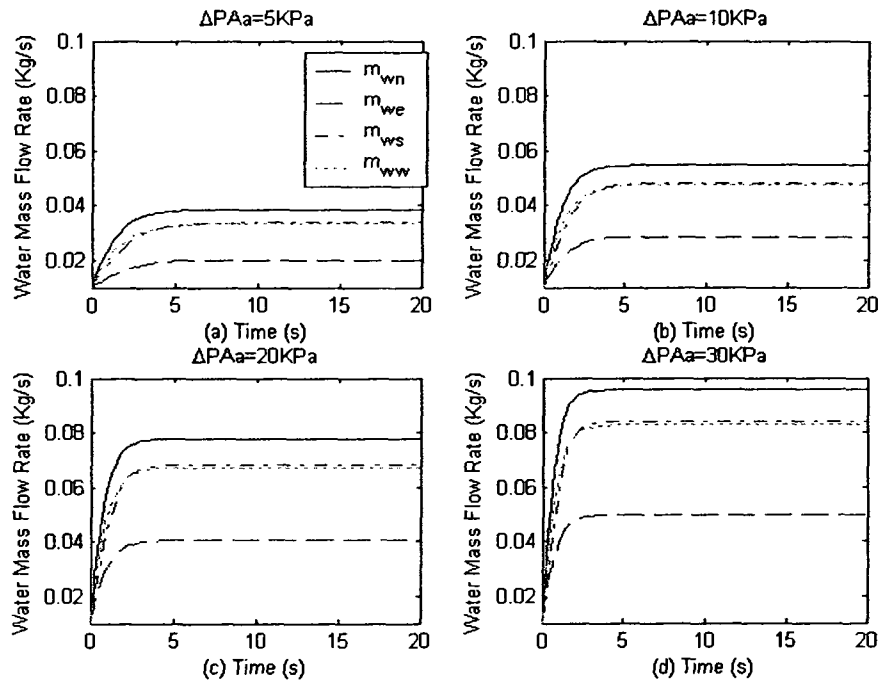


Figure 4.11 Water mass flow rates at differential pressures

Table 4.1 Water mass flow rates with variation of differential pressures

Zone		Differential pressure (KPa)			
		5	10	20	30
North	Kg/s	0.0386	0.0547	0.0779	0.0958
East	Kg/s	0.0200	0.0285	0.0405	0.0497
South	Kg/s	0.0337	0.0481	0.0685	0.0842
West	Kg/s	0.0333	0.0474	0.0674	0.0827

The pressure distribution of the water in pipe network was computed for the SFMZ heating system. The total pressure is composed of velocity, static and gravity pressure, and the total pressure difference between the points in the pipe network is resulted from the frictional losses. By assuming the gravity pressure has the same value on the given single floor, for example, 0KPa, simulation runs were made under the following conditions:  $T_s=90^{\circ}\text{C}$ ,  $T_o=-21.8^{\circ}\text{C}$ , the control valves fully open and 20KPa differential pressure. The responses of the total, the static and the velocity pressures in Loop n are depicted in Figure 4.12. Note that x axis expresses the length along the water flow direction. Figure 4.12(a) shows that the static pressure decreases from point “A” to “a” given in Figure 4.2. The pressure drop from the control valve is about 45% of the total offered differential pressure for the single floor heating system. In general, pressure drop in a control valve between 40% and 60% of the total piping system frictional drop is desirable. From Figure 4.12(b), it can be noted that the velocity pressure varies according to both the water flow rate and the diameter associated with pipe segments. Moreover, the velocity pressure has very small values compared with those of the static and total pressure; therefore, it is usually ignored in measuring water pressure in HWH systems.

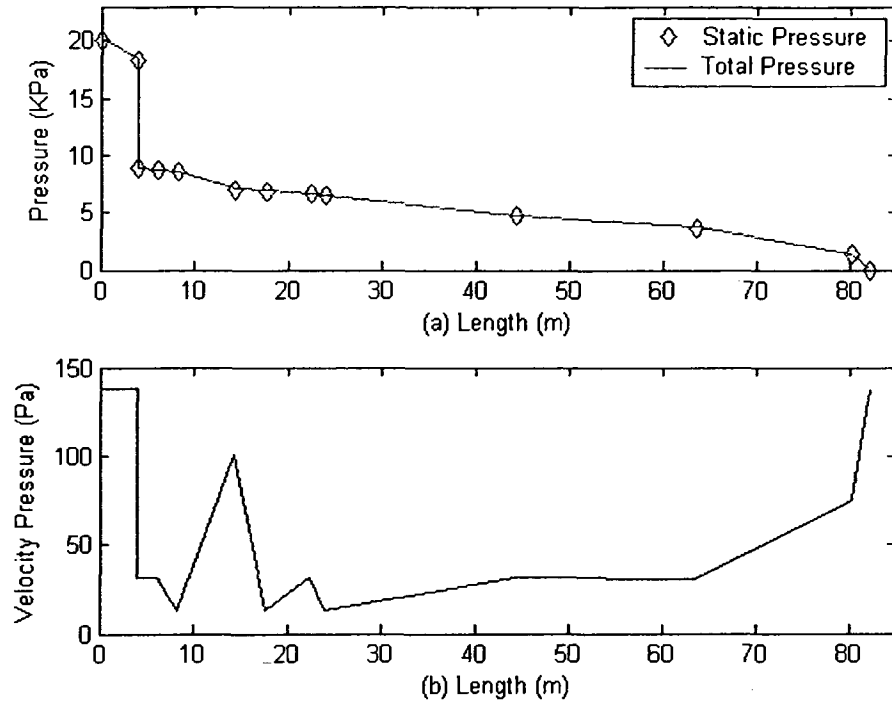


Figure 4.12 Total, static and dynamic pressures in Loop n

It is interesting to observe the pressure losses for all loops along the water flow direction in the SFMZ system. The water pressure drops are mainly resulted from the frictional losses in the hydraulic loops. Under the design conditions and by maintaining 20KPa water differential pressure ( $\Delta P_{Aa}$ ), the water pressure drops of the loops are simulated and given in Figure 4.13. From this figure, both the pressure losses associated with the length of the loops and the pressure drops from the control valves are within desirable range.

In addition, the pressure reference point of the circulating loop is assumed at point “a” located in the end of the return main pipe network (See Figure 4.2) in the hydraulic system, and its value is equal to 0KPa. Note that the reference pressure does not change the dynamic system responses under system operating conditions. In other words, if the

reference pressure has a non-zero value, all the loop pressure should be adjusted with the same value, but the pressure drops for all elements remain identical.

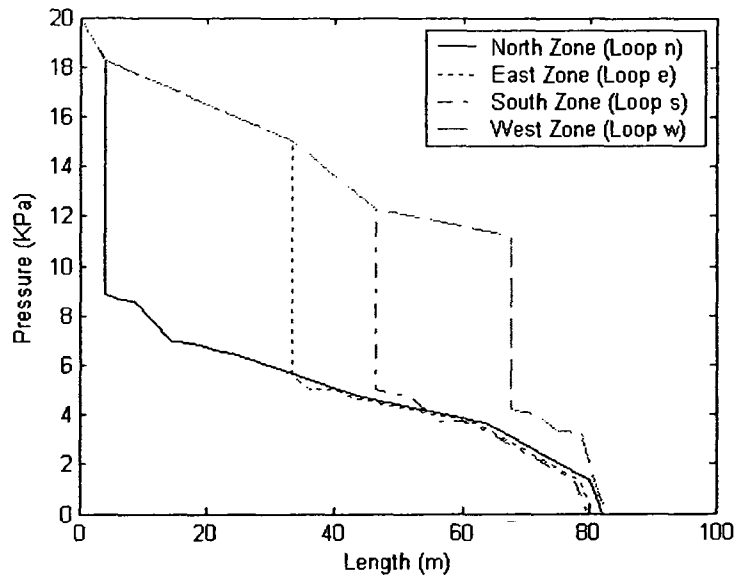


Figure 4.13 Static pressure drops in all loops

#### 4.4.2 Results from the aggregated heating system

For the purpose of comparison the SFMZ model and its aggregated model were simulated as below under the conditions:  $T_s=90^{\circ}\text{C}$ ,  $T_o=-21.8^{\circ}\text{C}$ ,  $\Delta P_{Aa}=20\text{KPa}$  and the control valves fully open. The air temperature responses are depicted in Figure 4.14 for the SFMZ and its aggregated model. The thick lines in the figures indicate the responses from the aggregated SFMZ models. From the figures, it can be seen that not only the air temperature dynamics have the similar responses, but also the steady state values reached are almost identical in the models. In addition, the water mass flow rates remain the same from the two models.

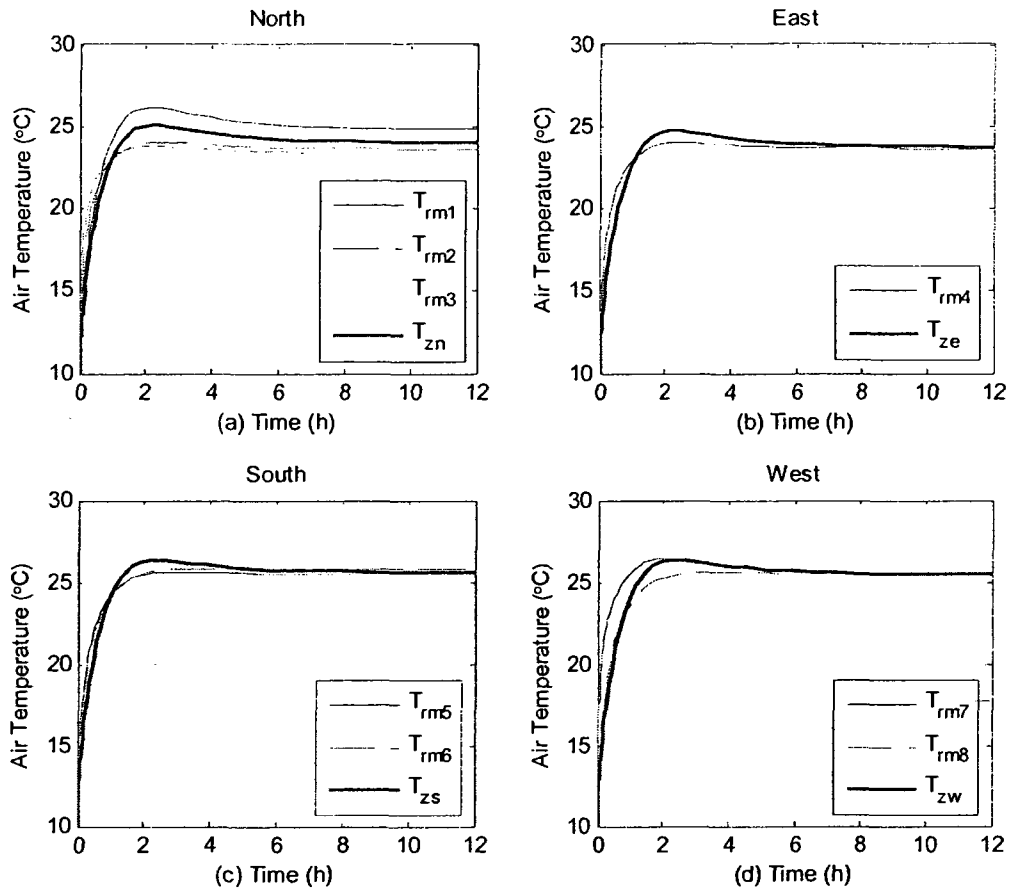


Figure 4.14 Comparison of dynamic responses with two SFMZ models

Hence, the aggregated SFMZ system model consisting of temperature and water mass flow rate dynamics could be employed to extend the modeling process with enough precision.

#### 4.4.3 Results from the MFMZ heating system

In order to study the entire HWH system temperature and fluid flow dynamic responses, several open loop tests are made and given as follows.

Under the conditions of  $T_o = -21.8^\circ\text{C}$ ,  $u_f = 1$ , no additional gains and all water mass flow rate control valves fully open, the simulation results are shown in Figures 4.15 and 4.16 respectively. Floors such as on the 9<sup>th</sup> floor (the closest floor), the 5<sup>th</sup> floor (the

middle floor), the 1<sup>st</sup> floor and the basement (the farthest floor) are chosen to observe the dynamic responses. From Figures 4.15 (a)~(d), it can be seen that all zone air temperatures reach their steady state values above the design zone air temperature (22°C), and the temperatures in east zones on all floors have the lowest values (from 24.78 to 25.59°C) at 12 hour. The steady state values of the supply and return water temperatures from and to the boiler reached 92.68 and 72.55°C as shown in Figure 4.15(e). The reason for the supply water temperature to reach in excess of 90°C is due to the fully open fuel control valve. Therefore, the water temperature from the boiler should be regulated to reduce the zone air temperatures of the entire heating system. In addition, the dynamic responses of the motor speed, the current and the input power are depicted in Figure 4.15(f). The motor speed, the current and the power fluctuates in the first 10 seconds. After that time, the electrical circuit is stable. The ratio of the stable electrical load to the peak load taking place at the first wave is 1:9.1. Thus, there is a need to decrease the start up electrical load to avoid the transient shock to the electrical motor.

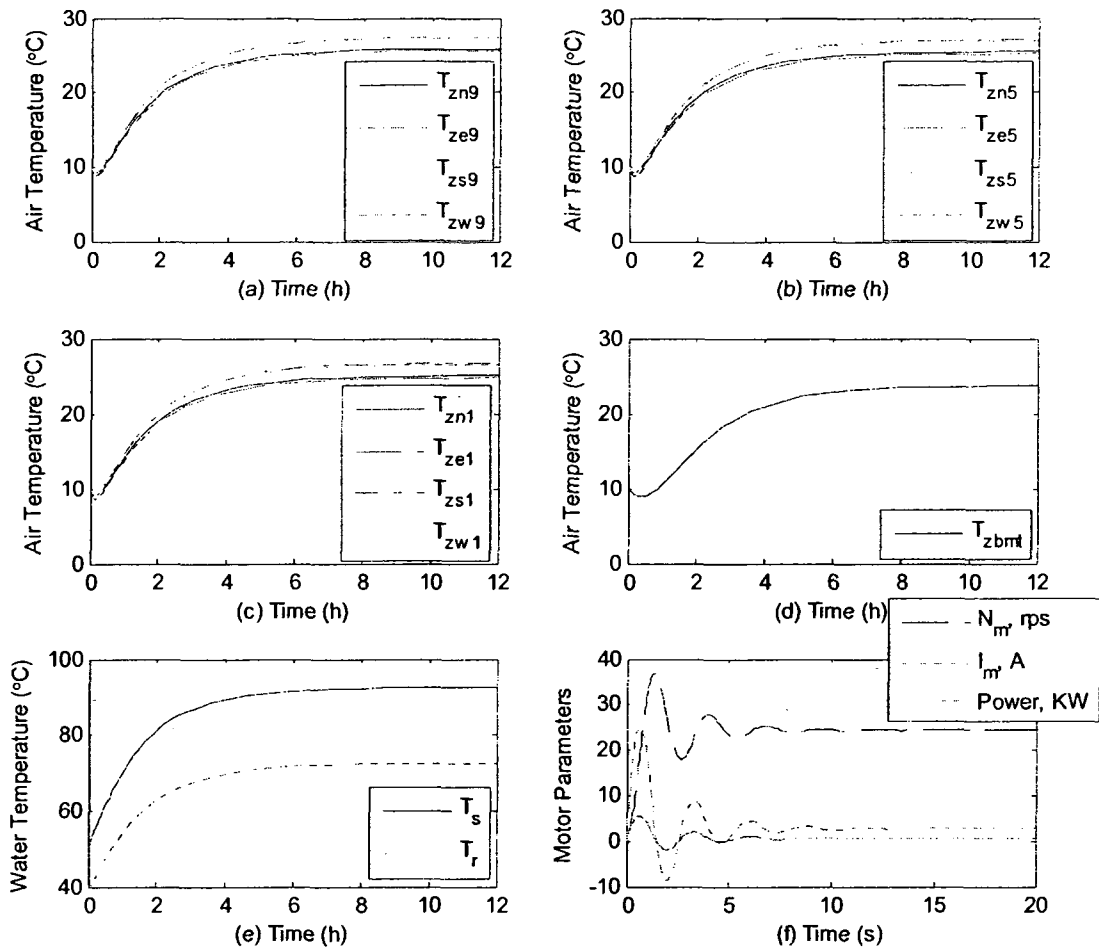


Figure 4.15 Dynamic responses of the floor heating systems and the pump-motor unit

### *Fluid flow responses*

With the same conditions as used in Figure 4.15, the dynamic responses for the fluid flow are illustrated in Figure 4.16 for the chosen zones. In Figures 4.16(a)~(d), the water mass flow rates fluctuate corresponding to the changes of the motor speed in the first 10 seconds. The steady state values of the water mass flow rate are different based on the frictional losses resulting from pipe segments, equipment (boiler, control valves), and fittings (shutoff valves, 3-way connection and elbows etc.) in the circuits. By comparing the water mass flow rate dynamics of the zones on the 9<sup>th</sup>, the 5<sup>th</sup> and the 1<sup>st</sup> floor shown in Figures 4.16(a)~(c), it is noted that the water mass flow rates of the zones

on the 9<sup>th</sup> floor have the highest values; while they have the lowest values on the first floor. This is because the differential pressure of the water in the former loops is greater than that in the rear loops. This also causes the increase of zone air temperature in the former zones. The dynamic response of the output water mass flow rate from the pump is given in Figure 4.16(e), and it reaches the steady state value of 2.471Kg/s.

From the dynamic responses of the zone air temperatures and the water mass flow rates, it can be seen that the dynamic system has two time scales: a fast response system (fluid flow of water) and slow response systems (zone air and water flow temperature).

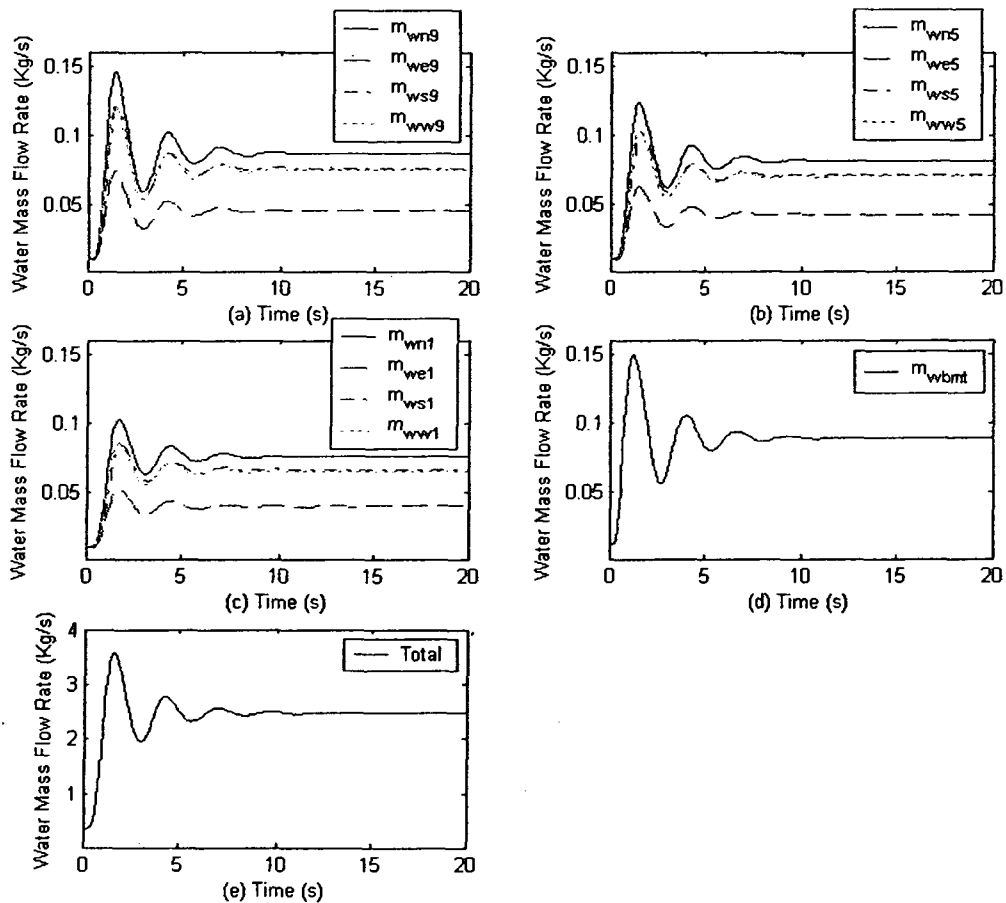


Figure 4.16 Dynamic responses of water mass flow rates

### *Effect of supply water temperature*

Since the supply water temperature needs to be supplied reasonably to keep away from overheating zone air, to this end, it is decreased based on the lowest zone temperature (east zones on the floors). If east zones achieve their designed zone temperature, the others will be greater than the design values. Under the same conditions used in Figure 4.15 except for setting the fuel control signal  $u_f$  to 0.95, the test results are depicted in Figure 4.17 for four floors. As shown in the figures, the air temperatures in north, south and west zones are above 22°C. The supply and return water temperatures from and to the boiler are 86.4 and 67.6°C respectively.

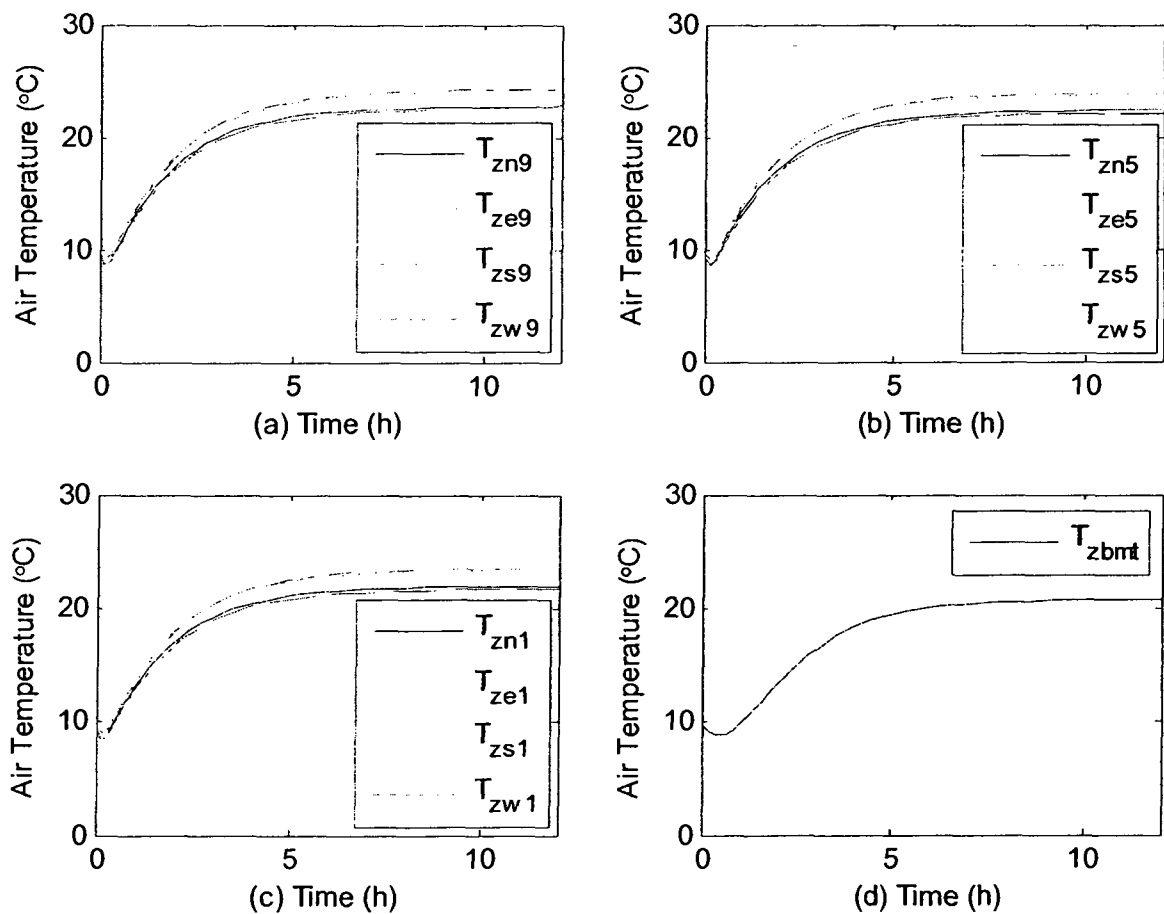


Figure 4.17 Zone air temperatures under decreased supply water temperature

In order to match the required heating loads in the heating system, the supply water temperature should be varied according to different outdoor air temperature. To maintain the design zone temperature in east zones, the relationship between the supply water temperature and the outside temperature is tested and depicted in Figure 4.18. The supply water temperature appears an approximate linear function of the outside temperature.

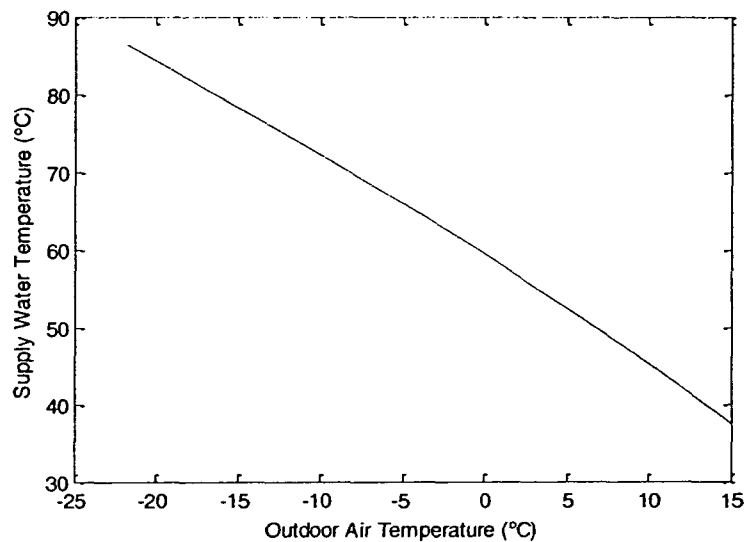


Figure 4.18 Relationship between supply water temperature and outside temperature

#### ***Water pressure dynamic responses***

The water pressure dynamics in the entire hydraulic system are also of interest in this study. The total pressure including gravity, static and velocity pressure can be calculated based on the system dynamic model. Several cases such as frictional losses in the pipe networks, pressure at points, and variation of control valve opening and changes of the motor voltage are considered in the open loop tests. The main circulating loop is defined by the longest pipe network passing through the basement heating system.

The total pressures at different points in the hydraulic system are varied not only based on their locations but also according to their static and velocity pressures. The dynamics of the total pressure are presented in Figure 4.19 for the selected seven points (from  $P_1$  to  $P_7$ ) given in Figure 4.4. The selected points consider the major devices, the highest and the lowest floor of the heating systems. The simulation are tested under the conditions of  $u_m=1$ ,  $u_f=0.951$  and fully open control valves. In the mechanical room, the total pressure entering to and leaving from the pump, and leaving from the boiler are presented in Figure 4.19(a). The pressure head of the pump achieves 90.4KPa with the water mass flow rate of 2.471Kg/s. Comparing Figure 4.19(a) with Figure 4.19(b), the highest total pressure takes place at  $P_6$  because it has the greatest gravity pressure, while the lowest total pressure occurs at  $P_1$  due to its location. In addition, the total pressure differences between the supply and return water on the 9<sup>th</sup> floor ( $P_4$ - $P_5$ ) and the basement ( $P_6$ - $P_7$ ) reach 24.7 and 18.4KPa respectively.

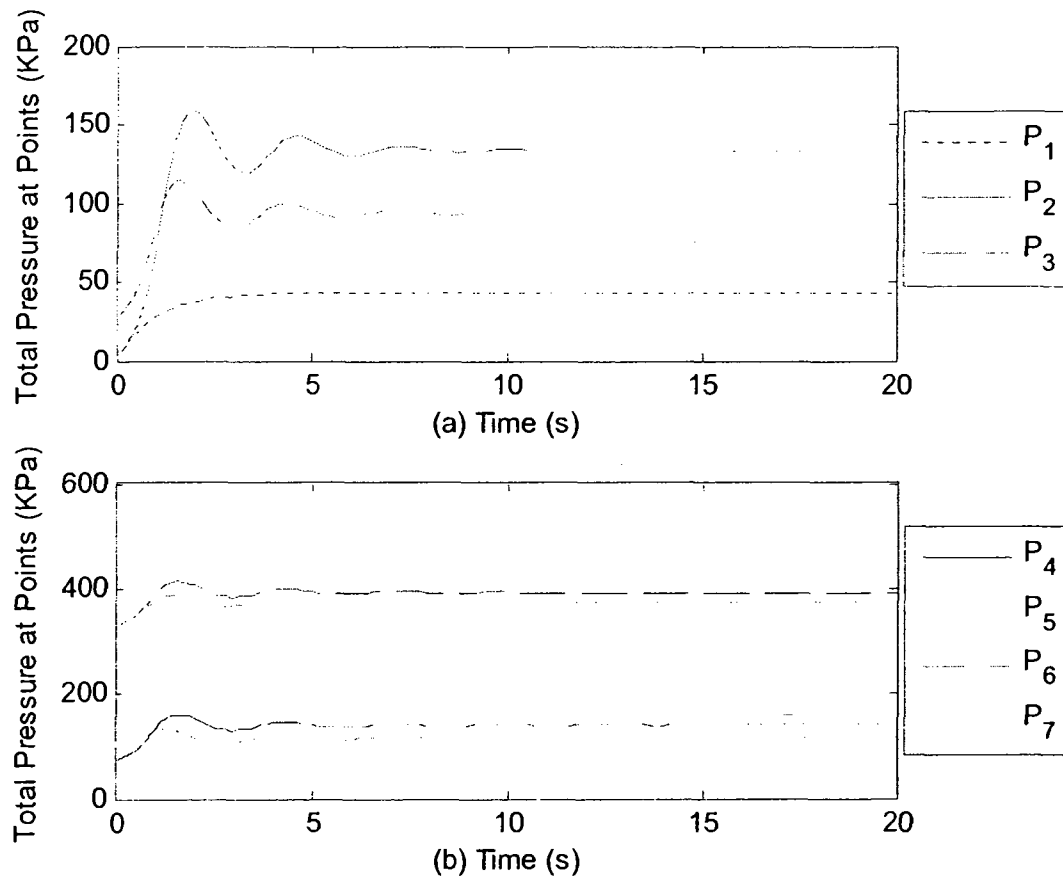


Figure 4.19 Dynamic responses of total pressure at different points

### *Pressure drops in the system*

In Figure 4.20, the pressure drops (static and velocity pressures) for the main pipe network thru the basement system, the 9<sup>th</sup>, the 5<sup>th</sup> and the first floor heating systems are simulated at 20 second under the same conditions employed in Figure 4.19. The x axis refers to the distance from point P<sub>1</sub> along the water flow direction of the main pipe network. It can be seen that, in the main loop, the pressure of water is increased by the circulation pump (90.4KPa) and decreased by the frictional losses such as the boiler (63.4KPa), the control valve at the basement (12.1KPa) and the pipe segments and the fittings (14.9KPa). The pressure at the entrance of the pump (P<sub>1</sub>) is maintained at 43.04KPa because of the height of the suction tank. The differences in pressure between

the supply and return water on the 9<sup>th</sup>, the 5<sup>th</sup> and the first floor heating system are 24.7, 21.7 and 18.4KPa respectively, according to their location in the system.

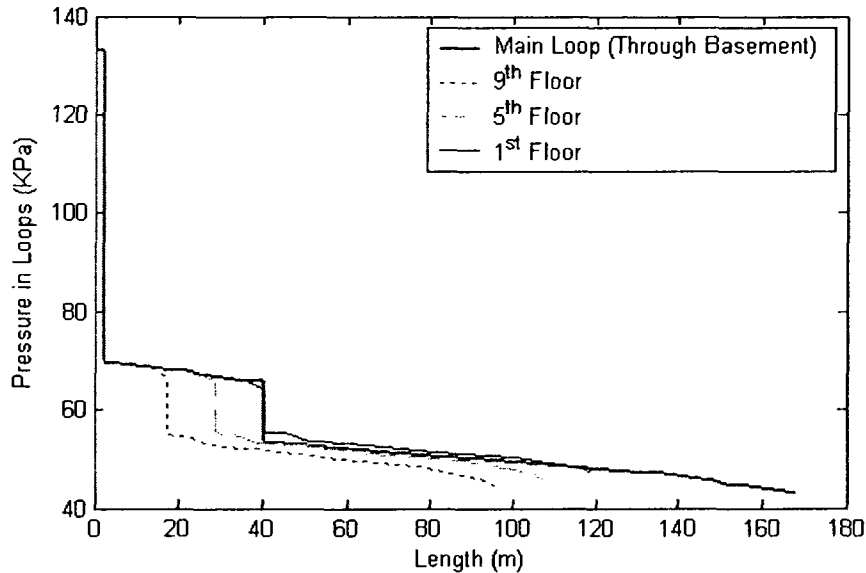


Figure 4.20 Pressure drops without gravity pressure in the hydraulic system

### ***Effect of motor speed***

The applications of VSDs such as for pump-motor units are widely used in HVAC field not only due to the lower equipment cost and electrical shock but also due to energy saving. To this end, the dynamic responses of the system parameters such as the motor speed, the water mass flow rate, the total pressure at point P<sub>2</sub> (output pressure of the pump) and the electrical power input are simulated and presented in Figure 4.21 with different motor voltage control signals. As shown in Figure 4.21(a), the motor speed attains 24.38, 18.34 and 14.7rps associated with the voltage control signal  $u_m$  as 1, 0.75 and 0.6. When  $u_m$  is equal to 1, the peak values of the motor speed, the water mass flow rate, the total pressure at point P<sub>2</sub> and the power input reach 1.47, 1.46, 1.2 and 9.02 times higher than their steady state values respectively at the starting period. Moreover, under

ideal conditions, the water mass flow rate, the pressure head and the power used should obey the power law for pump-motor units. To check the power law in this case, the simulated data is given in Table 4.2. From the calculation, the water mass flow rate and the pressure head of the pump agree with the power law perfectly; nevertheless, the electrical power consumption is more than the power law values because of the lower efficiency of the pump-motor unit.

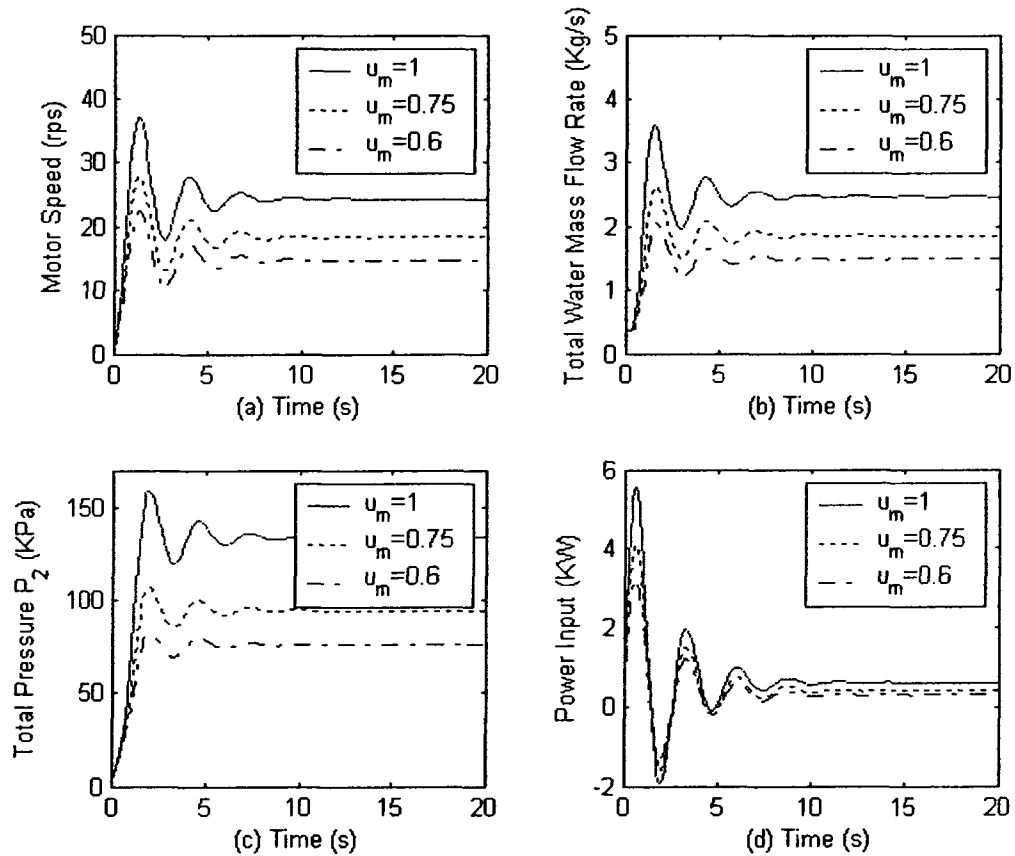


Figure 4.21 Dynamic responses of changing electrical voltage control signal

Table 4.2 Comparison of the pump-motor operation parameters with the power law

Motor speed		Water mass flow rate		Pressure head		Power input	
rpm	%	Kg/s	%	KPa	%	KW	%
24.38	100	2.471	100	90.4	100	0.61	100
18.34	75.23	1.856	75.11	51.25	56.69	0.403	66.07
14.7	60.3	1.485	60.1	32.87	36.36	0.298	48.85

The results presented in this section give expected trends from the HWH system and the hydraulic system responses. The results also showed the scope and application of the model in studying various dynamic responses of the system under realistic load conditions.

## Chapter 5 Design of Control Strategies for the HWH System

### 5.1 Introduction

The major reason for requiring control in HWH systems is that system operation is influenced by disturbances such as solar radiation, internal gains and outdoor air temperature and process and measurement noises. In other words, if there are no disturbances and noises acting on the systems, it is not essential to build control systems. As motioned before, outside air temperature has the most significant effect on HWH systems. The objectives of control of HWH systems are to improve thermal comfort, obtain better operation and save energy.

In order to achieve the objectives suitable control strategies should be designed for the HWH system in the high-rise building. The considered configuration of the control system used for the heating system is presented in Figure 5.1. For example, the supply water temperature from the boiler is regulated by the fuel controller  $C_f$ ; the voltage to the motor is controlled by the controller  $C_m$  based on the differential pressure (DP) signal to adjust the motor speed. In addition, all zone air temperatures could be monitored by the controllers ( $C_z$ ) to regulate the water mass flow rates entering the zones. The outputs from the controllers were computed by PI control algorithm based on intelligent inference systems. From control and operation points of view, the disturbances, process and measurement noises acting on the entire system were handled by using advanced adaptive PI controllers and the EKF technique.

In addition, in order to establish optimal operation of the HWH system, a supervisory optimal control strategy will be designed in this chapter.

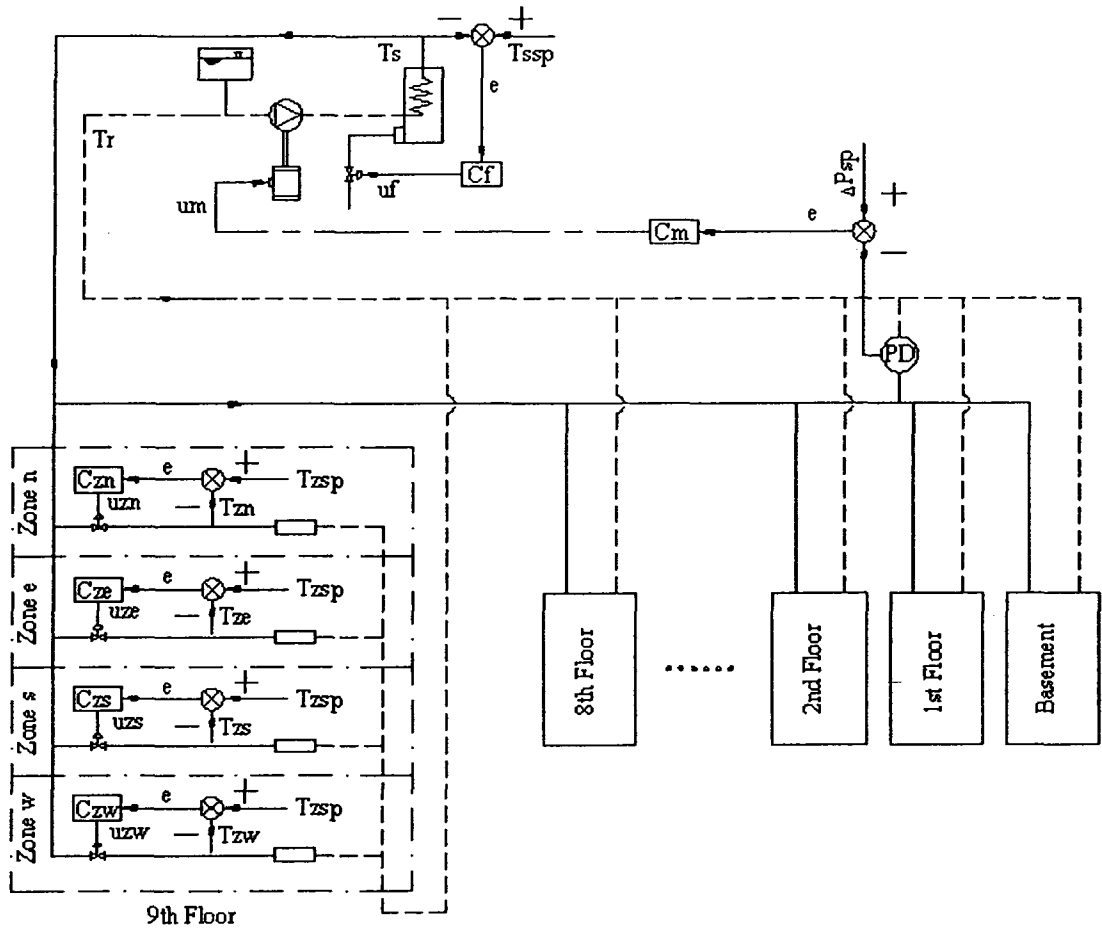


Figure 5.1 Configuration of control strategies used for the HWH system

In order to design the control strategies for the overall HWH system, the high-rise building shown in Figure 4.4 was chosen. The building is composed of one top floor, eight typical floors above-ground and one basement floor. The layouts of the floors are identical and depicted in Figure 4.1. There are four zones on each floor above the ground and one zone for the basement. The design parameters of the system are given in Table 5.1.

Table 5.1 Parameters of the HWH system

Item	Unit	Data
Total heated floor area of the building	m <sup>2</sup>	3910.5
Heated floor area of each floor	m <sup>2</sup>	391.05
Height of each floor	m	2.8
Design supply water temperature	°C	90
Design return water temperature	°C	70
Design outside air temperature	°C	-21.8
Design inside air temperature	°C	22
Soil temperature	°C	1
Total design heating load	KW	191.04
Heat capacity of the boiler	KW	210
Thermal capacity of the boiler	MJ/°C	8.1648
Efficiency of the boiler	%	89
Heat value of the fuel	MJ	37.62
Total design circulating water flow rate	Kg/s	2.2811
Design heating load on the top floor	KW	24.9
Design heating load on the typical floor	KW	19.43
Design heating load on the basement	KW	10.7
Thermal resistance of outside window	m <sup>2</sup> °C/W	0.34
Thermal resistance of outside wall	m <sup>2</sup> °C/W	0.79
Factor n (shown in Equation (3.47)) identified based on the baseboard heater heat transfer coefficient test	-	0.341
Armature voltage	V	220
Equivalent frictional factor	Kgm <sup>2</sup> /s	0.013
Equivalent moment of inertia	Kgm <sup>2</sup>	0.124
Armature inductance	H	3
Armature resistance	Ω	2
Back emf constant	Vs/rev	1.4
Torque constant	Nm/A	1.4

To simulate the responses of the control system, three kinds of disturbances such as the outside air temperature, solar radiation and internal gains were considered. The profiles of the disturbances are presented in Figure 5.2 for one day. The ranges of the outdoor air temperature, solar radiation and internal gains are from -12.1 to 0.6°C, from 0 to 112.5W/m<sup>2</sup> and from 5.4 to 17.4W/m<sup>2</sup> respectively. It is noted that the solar radiation intensity is different for different zones based on the direction of the zones.

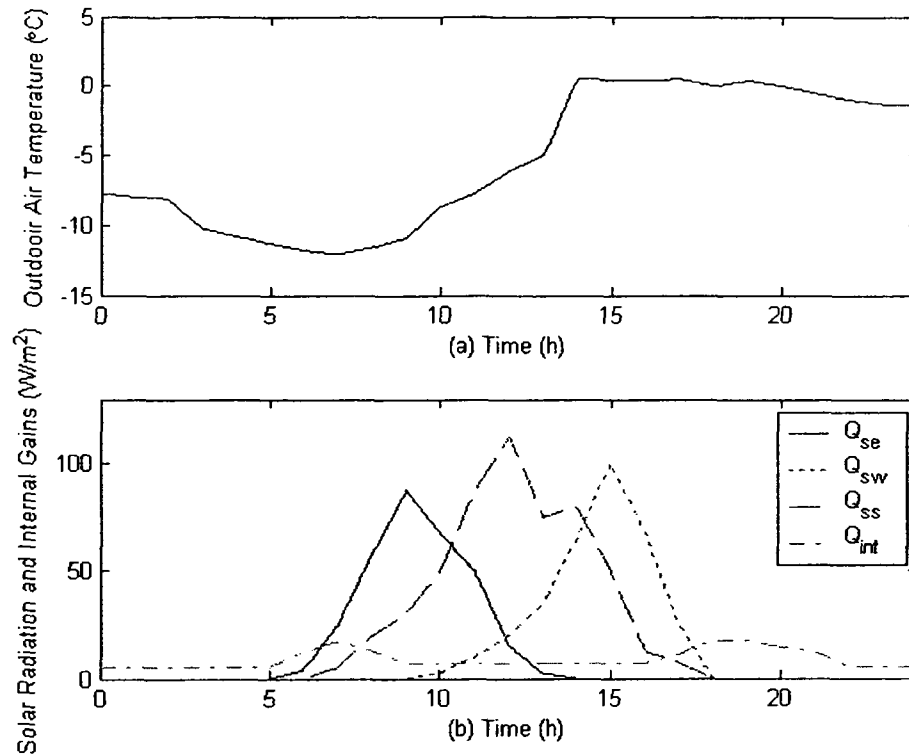


Figure 5.2 Disturbances acting on the heating system

In this study, four control strategies are investigated. In a widely used control strategy for the boiler, the fuel firing rate is regulated by the average temperature of the supply and return water from and to the boiler. Then, in addition to the fuel firing rate controlled by the supply water temperature, the water mass flow rates are regulated using fuzzy logic adaptive controllers. Next, the process and measurement noises are taken into account by using hybrid EKF technique in the control system design to improve system performance. Finally, a supervisory control strategy is designed and simulated by using optimization approach. These control strategies are described and tested in the following sections.

## 5.2 Control strategy design

### 5.2.1 Design of boiler control strategy based on average water temperature

In this design strategy, only the average temperature of the supply and return water is controlled by regulating the fuel firing rate to the boiler. This strategy is typically installed and operated in many high-rise building HWH systems currently. The control system configuration is shown in Figure 5.3 with the fuel firing controller ( $C_f$ ). A typical PI controller is employed with fixed gains such as  $k_{pf}=0.1$  and  $k_{if}=0.0001$  respectively. The reference points of the average supply and return water temperature are obtained according to the relationship between the average temperatures of the supply and return water temperature and the average outside air based on previous 24 hours.

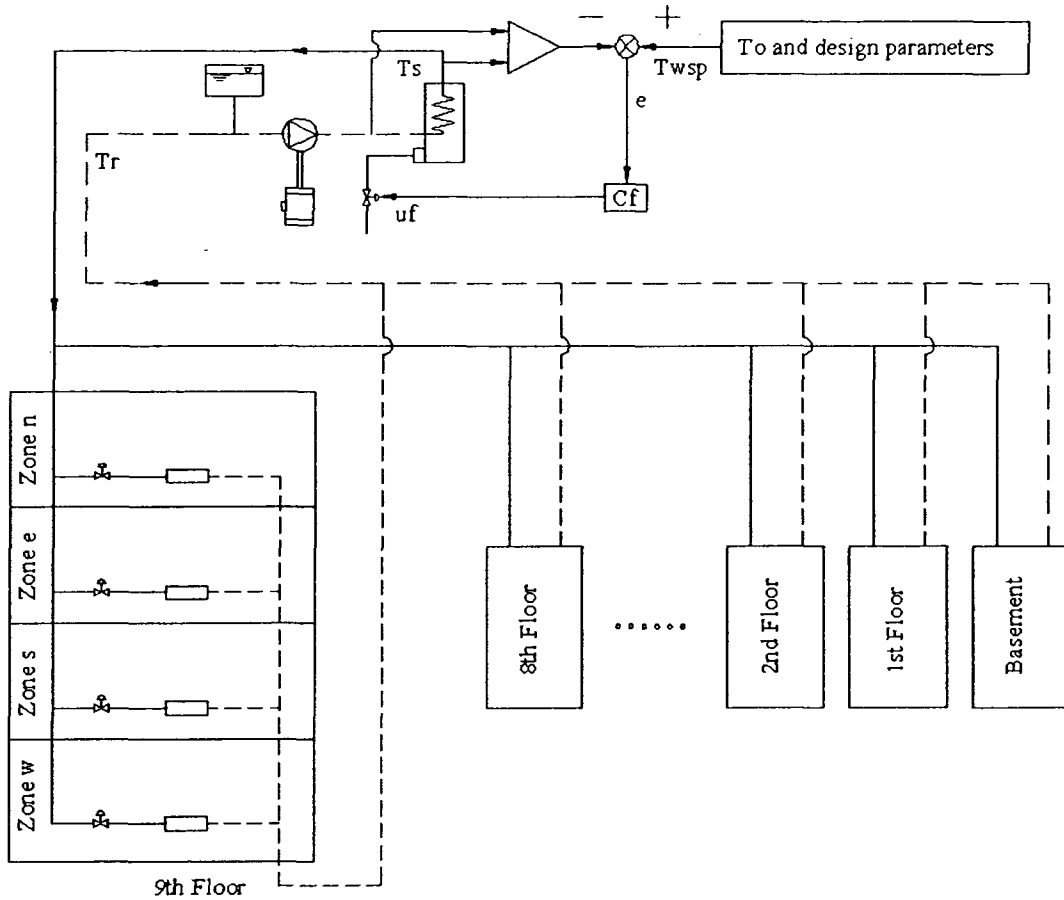


Figure 5.3 Control system configuration in the boiler control strategy

The reason for using the average outside air temperature is due to the large heat capacity of the building and the heating system itself. The heating load does not depend on the instantaneous outside temperature. Thus, the relationship between the average supply and return water temperature set point and the average outside air temperature was expressed as in Equation (5.1) and plotted in Figure 5.4. From this figure, it is clear that the average outside air temperature varies smoothly.

$$T_{wsp} = 0.5(T_{sd} + T_{rd}) - \left[ \frac{0.5(T_{sd} + T_{rd}) - T_{zd}}{T_{zd} - T_{od}} \right] \left( \frac{1}{24} \sum_{l=1}^{24} T_o - T_{od} \right) \quad (5.1)$$

In Equation (5.1),  $T_{wsp}$  indicates the average supply and return water temperature set points. It is noted that the water temperature set point profile is smooth because the change of the average outside air temperature is not too much as shown in Figure 5.4.

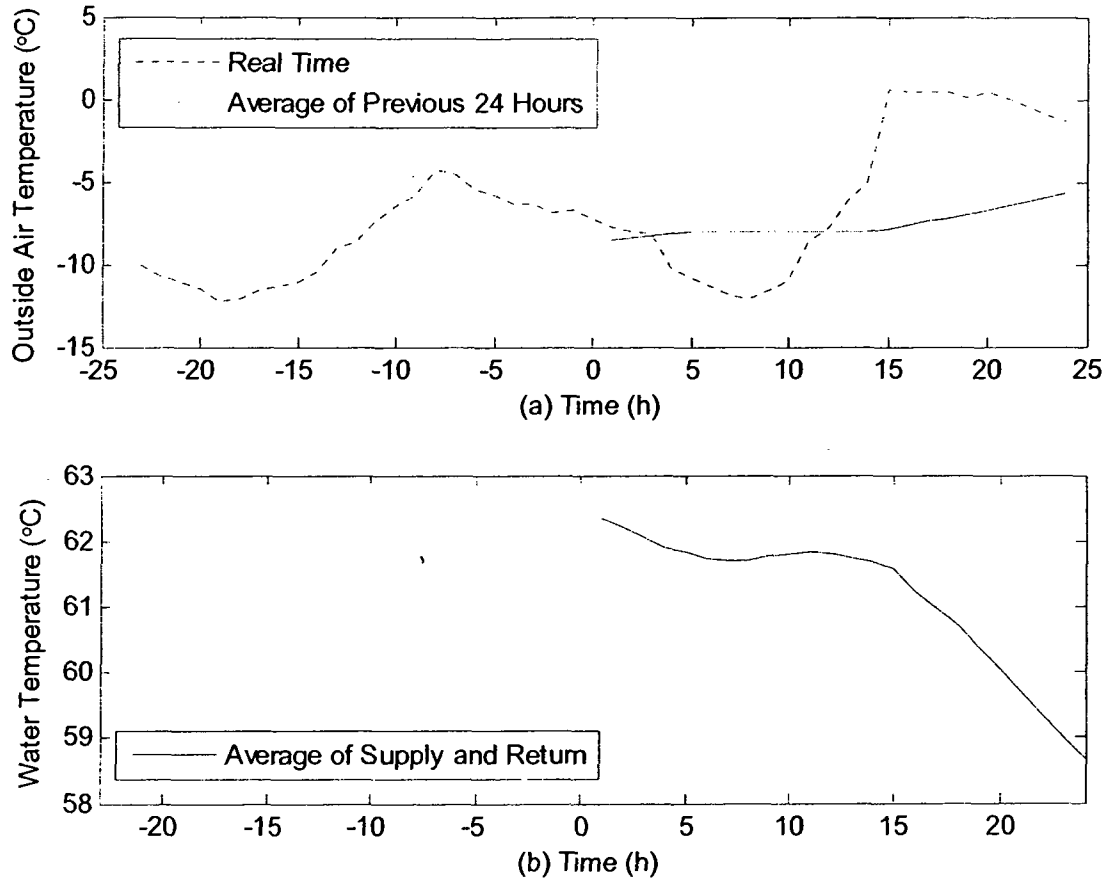


Figure 5.4 Average water temperature set points

In the control strategy, a typical PI controller for the fuel firing rate of the boiler is utilized. The output signal from the PI controller is calculated using Equation (5.2). The proportional and integral gains  $k_{pf}$  and  $k_{if}$  are considered as constant values.

$$u_f = k_{pf}[T_{wsp} - 0.5(T_s + T_r)] + k_{if} \int_0^t [T_{wsp} - 0.5(T_s + T_r)] dt \quad (5.2)$$

The dynamic responses of the temperature and the fuel control signal are simulated and presented in the following figures, Figures 5.5 and 5.6.

The responses of the water temperatures from and to the boiler, the return water temperatures from the zones and the fuel control signal are shown in Figure 5.5. As shown in Figure 5.5(a) except for the first three hours, the supply water temperature varies from 68.67 to 63.86°C; while the temperature difference between the supply and return water ranges from 13.22 to 9.13°C. Although the outdoor air temperature fluctuates from -12.1 to 0.6°C in the day, the average outside temperature within previous 24 hours changes from -8.47 to -5.68°C. As a result, the supply water temperature from the boiler does not swing rapidly. On the other hand, the return water temperature from each zone on the 5<sup>th</sup> floor heating system for example differs from each other given in Figure 5.5 (b) especially in the daytime. The biggest return water temperature difference among the return water temperatures (2.3°C) occurs between the south zone and the north zone. The major reason is that the zone air temperatures are influenced by different solar radiation to the zones and then the return water temperatures are affected by the zone air temperatures. The fuel firing rate varies from 0.55 to 0.70 as depicted in Figure 5.5(c).

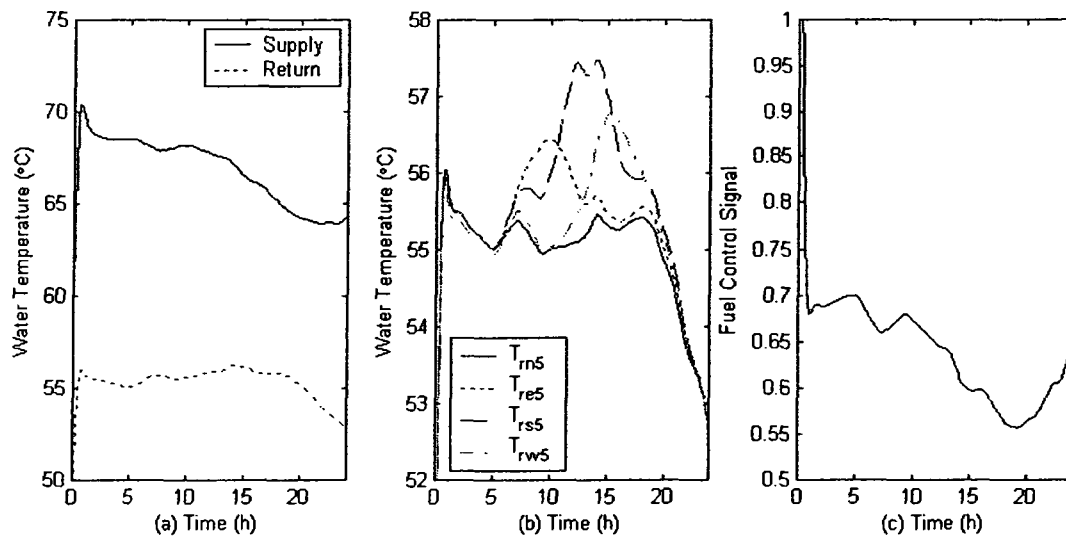


Figure 5.5 Dynamic responses of water temperature and fuel control signal

The zone air temperature responses are given in Figure 5.6 for the different zones on the 5<sup>th</sup> floor. Compared with the north zone air temperature, the zone air temperatures in other zones are greater between 7:00 to 21:00. This is caused by the additional heat gains (solar radiation and internal heat gains) acting on the zones, and are not compensated by the control strategy. Note that the peak variation of the zone air temperature between the north zone and the other zones is distinctly different depending on the zone direction. The largest deviations from the design zone air temperature (22°C) are 7.95, 8.76, 10.35 and 10.06°C for north, east, south and west zones respectively.

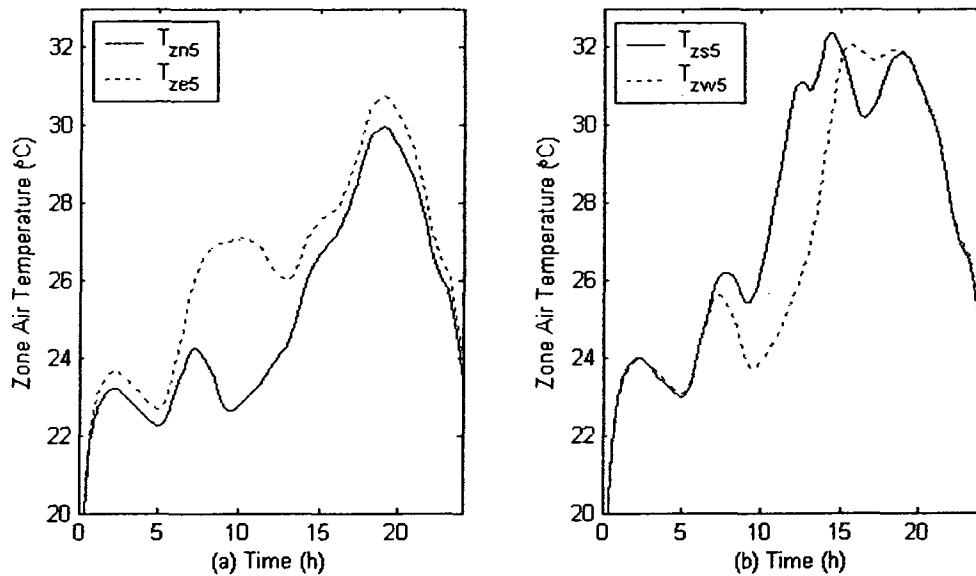


Figure 5.6 Dynamic responses of the zone air temperatures (boiler control only)

From the simulation results it can be seen that, in order to improve energy efficiency and thermal comfort, not only the supply water temperature should track the variation of the outside air temperature quickly, but also the additional heat gains have to be compensated by using advanced control strategies.

### 5.2.2 Design of fuzzy logic adaptive PI control (FLAC) strategy

Generally, HWH systems are controlled by typical PI controllers; however, there is increasing interest these days in the use of fuzzy logic control (FLC) strategies since fuzzy inference systems (FIS), which are based on the understanding and knowledge of the physical systems, have intelligent properties and therefore they are well suited for designing energy efficient control strategies. More and more real-world applications of FLC in HVAC field have been found (Lianzhong and Zaheeruddin, 2007).

In order to improve control system performance and thermal comfort level and save operating energy, the zone air temperature could also be regulated based on varying water mass flow rate in the HWH system. This control strategy is studied by designing and simulating fuzzy logic adaptive PI controllers (FLAC). The control system configuration is depicted in Figure 5.7. Since the exact relationship between the supply water temperature from the boiler and the outside air temperature is unknown, the fuzzy logic theory was employed to infer this relationship. Two types of fuzzy logic inference systems such as Mamdani and Sugeno types were employed and embedded in the control system. Mamdani type FIS infers the supply water temperature set point of the overall HWH system based on the understanding of the nature of relationship between the supply water temperature and the outside air temperature. On the other hand, Sugeno types of FISs deduce the proportional and integral gains for the adaptive PI controllers used in the zone controllers of the heating system. The reason of using Sugeno type FIS for the zone air temperature control is due to its superior computational efficiency. In all 38 controllers were used in the overall HWH control system. In other words, one fuzzy-PI

controller is used for the fuel firing rate control; while 37 fuzzy logic adaptive PI controllers are utilized to regulate the zone air temperatures in the high-rise building.

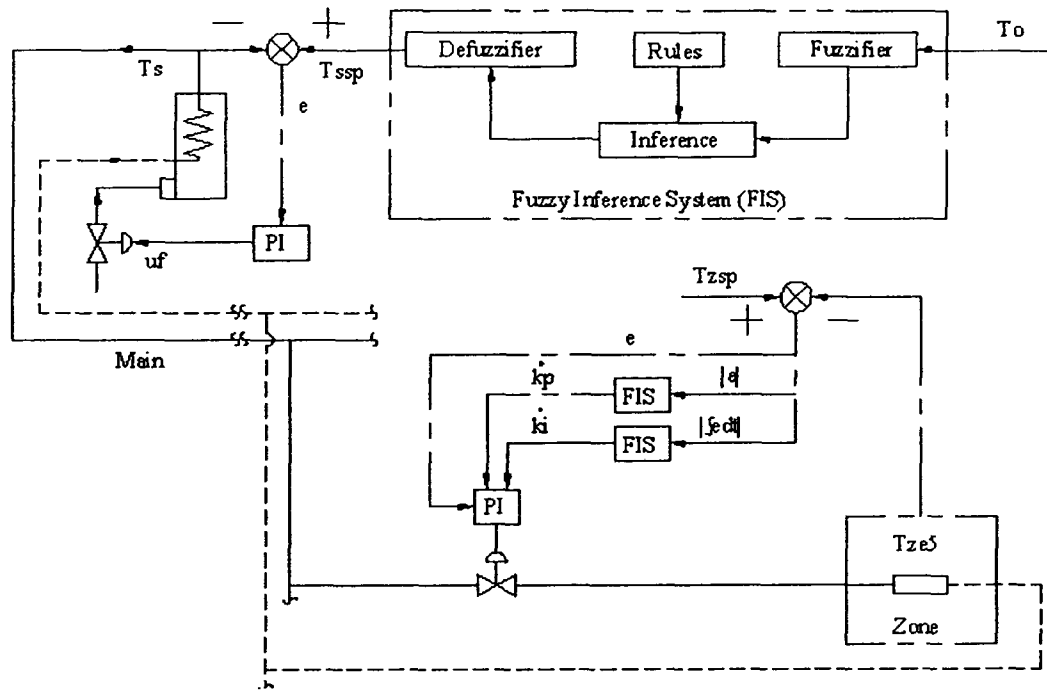


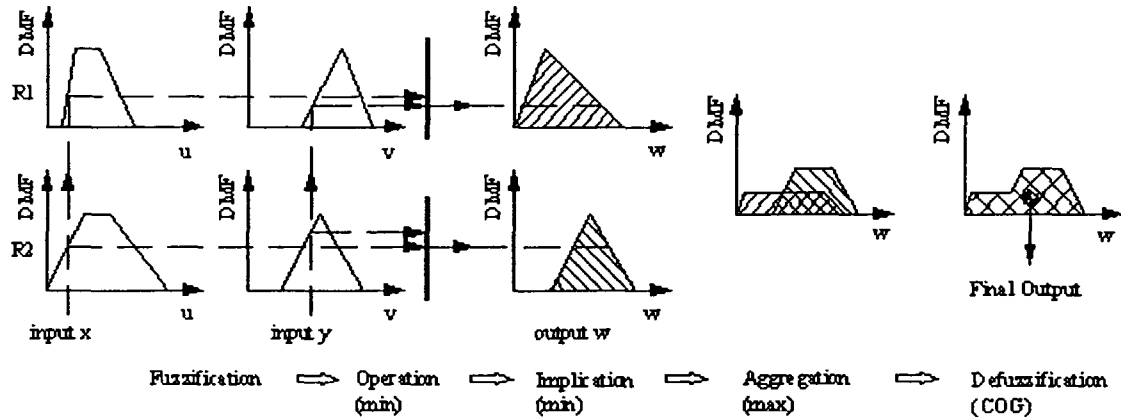
Figure 5.7 Fuzzy logic adaptive control system configuration

Typical FISs such as Mamdani and Sugeno types are depicted in Figure 5.8. From this figure it can be seen that, the final output in Mamdani type is obtained in five steps: fuzzification by fuzzifier, fuzzy operation (min), implication (min), aggregation (max) and defuzzification (Center Of Gravity, COG) by defuzzifier. The middle three steps with the rules are called fuzzy inference engine. Sugeno type of FIS, which was introduced by Sugeno (Takagi and Sugeno, 1985) is similar to Mamdani type in many respects. The first two steps are exactly identical. The major distinction between them is that Sugeno type output membership functions are either linear or constant.

The process from fuzzification to defuzzification can be interpreted as follows. Consider two inputs  $u$  and  $v$  such as outdoor air temperature and total heat from solar

radiation and internal heat gains. To model their impact on output such as boiler water temperature set point, one can use the degree of membership function (fuzzification). The effect of each input on the output is thus captured in the operation and implication steps.

Mamdani Type of FIS



Sugeno Type of FIS

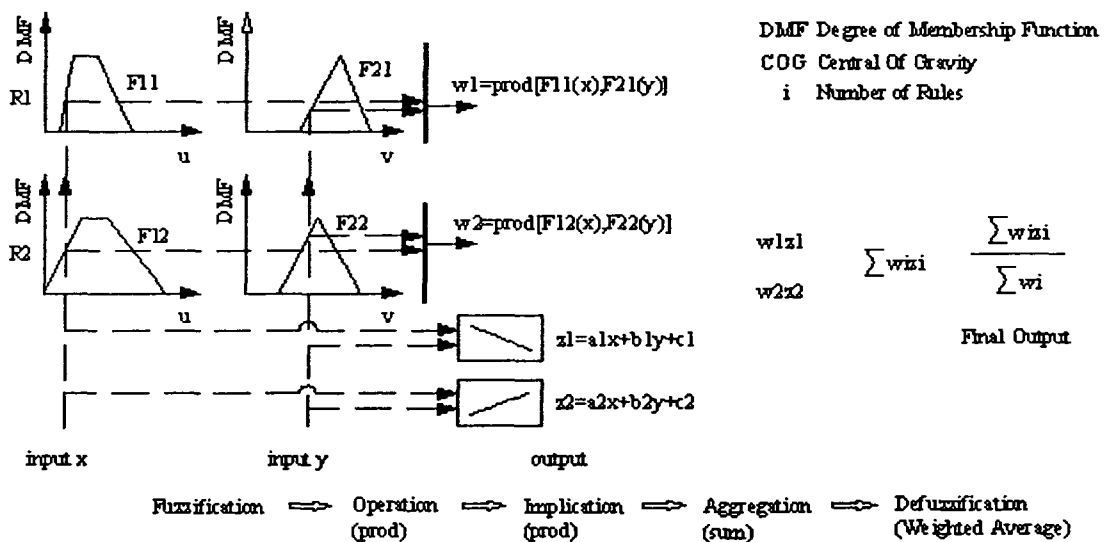


Figure 5.8 Two types of fuzzy systems

Due to the assumption of unknown relationship between the supply water temperature and outside air temperature, Mamdani type of FIS is employed to infer the set points of the supply water temperature. In the design of the FLC system, the set points

of the supply water temperature are determined according to physical understanding of correlation between variables  $T_{ssp}$  and  $T_o$ . Based on this knowledge, a set of linguistic membership functions were defined and depicted in Figure 5.9. The abbreviation such as VCD, CD, CL, LCL, WM, HT, VHT, VL, LW, LMD, MD, LH, H and VH expresses very cold, cold, cool, little cool, warm, hot, very hot, very low, little warm, little middle, middle, little high, high and very high respectively.

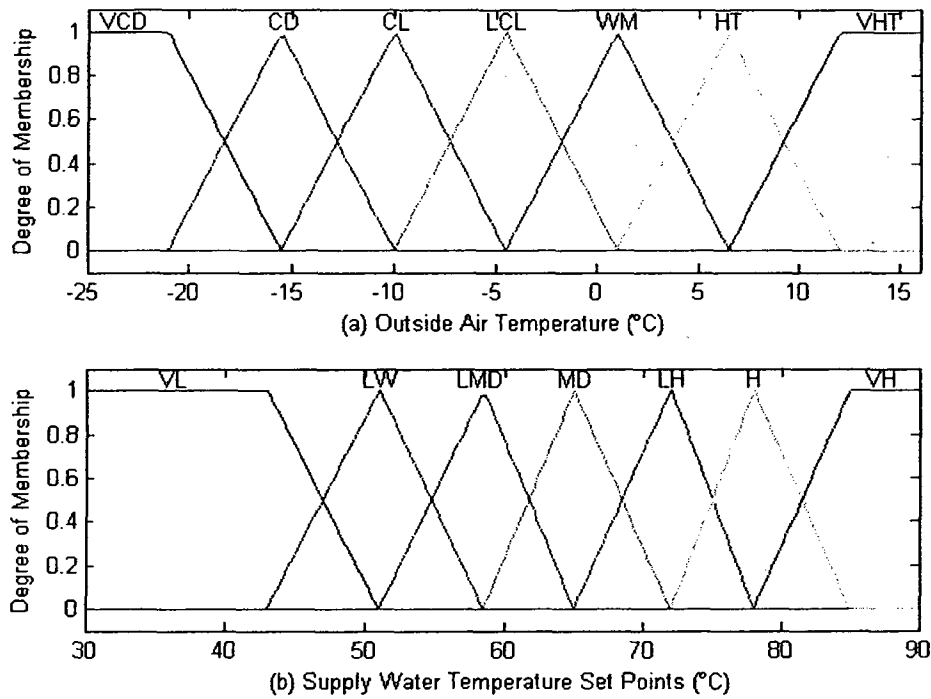


Figure 5.9 Membership functions for  $T_{ssp}$

The use the linguistic functions in fuzzy logic is inferred due to the assumption that the exact relationship between the variables is unknown and/or sometimes the functional relationship cannot be identified. This relationship between input and output is called a rule base in a FIS. For example, seven different rules with single antecedent were

defined between the supply water temperature set point and the outdoor air temperature, such as:

- (1) If  $T_o$  is VCD, then the supply water temperature set point is VH
- (2) If  $T_o$  is CD, then the supply water temperature set point is H
- (3) If  $T_o$  is CL, then the supply water temperature set point is LH
- (4) If  $T_o$  is LCL, then the supply water temperature set point is MD
- (5) If  $T_o$  is WM, then the supply water temperature set point is LMD
- (6) If  $T_o$  is HT, then the supply water temperature set point is LW
- (7) If  $T_o$  is VHT, then the supply water temperature set point is VL

The output of the supply water temperature set point ( $T_{ssp}^*$ ) from the FIS can be indicated as

$$T_{ssp}^* = [T_{o1}(T_o) \cap T_{ssp1}(T_{ssp})] \cup \dots \cup [T_{o7}(T_o) \cap T_{ssp7}(T_{ssp})] \quad (5.3)$$

A PI controller embedded with the FIS such as this is easy to implement since the operator could adjust the input command signals of the system based on a linguistic interface which may describe outdoor conditions as very cold, cold, mild etc., and the FIS would then translates these linguistic functions to appropriate control signals. The control signals of  $u_f$  and  $u_z$  can be computed as

$$u_f = k_{pf}(T_{ssp}^* - T_s) + k_{if} \int_0^t (T_{ssp}^* - T_s) dt \quad (5.4)$$

$$u_z = k_{pz}(T_{zsp} - T_z) + k_{iz} \int_0^t (T_{zsp} - T_z) dt \quad (5.5)$$

Note that the proportional and integral gains of the zone air temperature controllers are self-adaptive, based on the absolute values of the zone air temperature

deviation ( $T_{zsp}-T_z$ ) and their integrant utilized in the FISs. The proportional and integral gains ranged between 0.05 to 0.6 and 0.00005 to 0.0003 respectively for the two Segeno types of FISs. The main reason for using self-adaptive gains is to obtain fast response and avoid overshoot of the control system. The controller adaptive gains were updated using Equations (5.6) and (5.7) according to Figure 5.8. Note that the terms:  $f(|e|)$  and

$f\left(\left|\int_0^t edt\right|\right)$  are linear functions related to the error signal.

$$\dot{k}_{pz} = f_p[|e| + f(|e|)] \quad (5.6)$$

$$\dot{k}_{iz} = f_i\left[\left|\int_0^t edt\right| + f\left(\left|\int_0^t edt\right|\right)\right] \quad (5.7)$$

The dynamic responses of the major outputs such as the supply and return water temperatures from and to the boiler, total water mass flow rate and the fuel control signal are simulated and depicted in Figure 5.10. In Figure 5.10(a), the supply water temperature varies from 74.54 to 58.44°C; while the temperature difference between the supply and return water fluctuates from 19.57 to 40.36°C. The temperature difference between the supply and return water in this control strategy is increased greatly compared with that in the control system designed in Section 5.2.1 especially when the additional heat gains become larger. Hence, total water mass flow rate is reduced and fluctuated compared with that in Section 5.2.1 (constant water mass flow rate at 2.2811Kg/s). Larger water temperature difference between the supply and return water implies less water mass flow rate circulating in the heating system. Total water mass flow rate response is given in Figure 5.10(b). The change of the water mass flow rate is associated with the additional heat gains. The fuel control signal ranges from 0.73 to 0.37 shown in

Figure 5.10(c). By observing the energy consumption such as pump energy and fuel use with those in the boiler control system, great energy savings can be realized by intelligently using the additional heat gains.

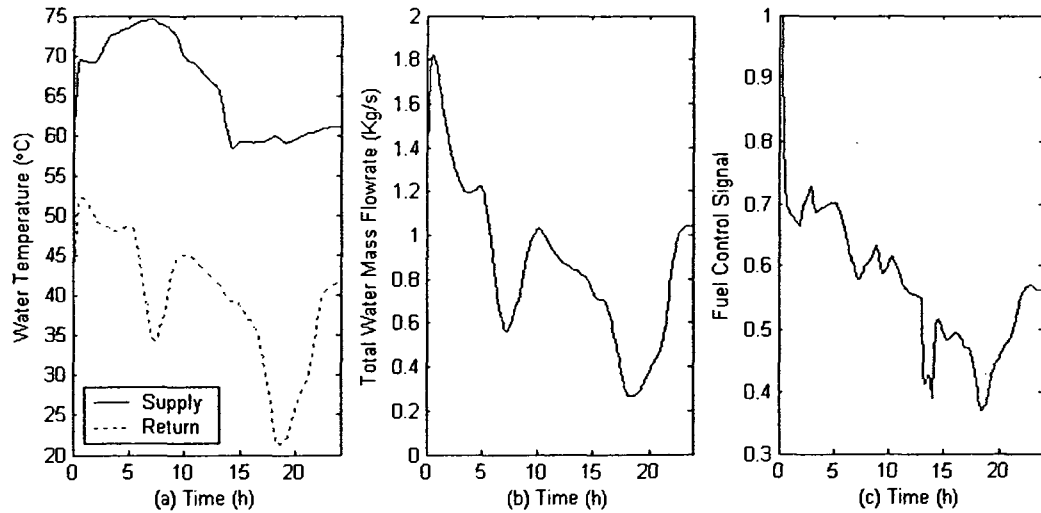


Figure 5.10 Dynamic responses of the major outputs

The dynamic responses of the return water temperatures and the water mass flow rate control signals on the 5<sup>th</sup> floor heating system for example are shown in Figure 5.11 for the north, east, south and west zone respectively. Due to the fact that no solar radiation acts on the north zone, the return water temperature has the highest value compared with those in other zones. The biggest return water temperature difference between the north zone and the others is 32.35°C taking place in the south zone. Note that the dynamic responses of the water mass flow rate control signals have similar trends as the responses of the return water temperatures.

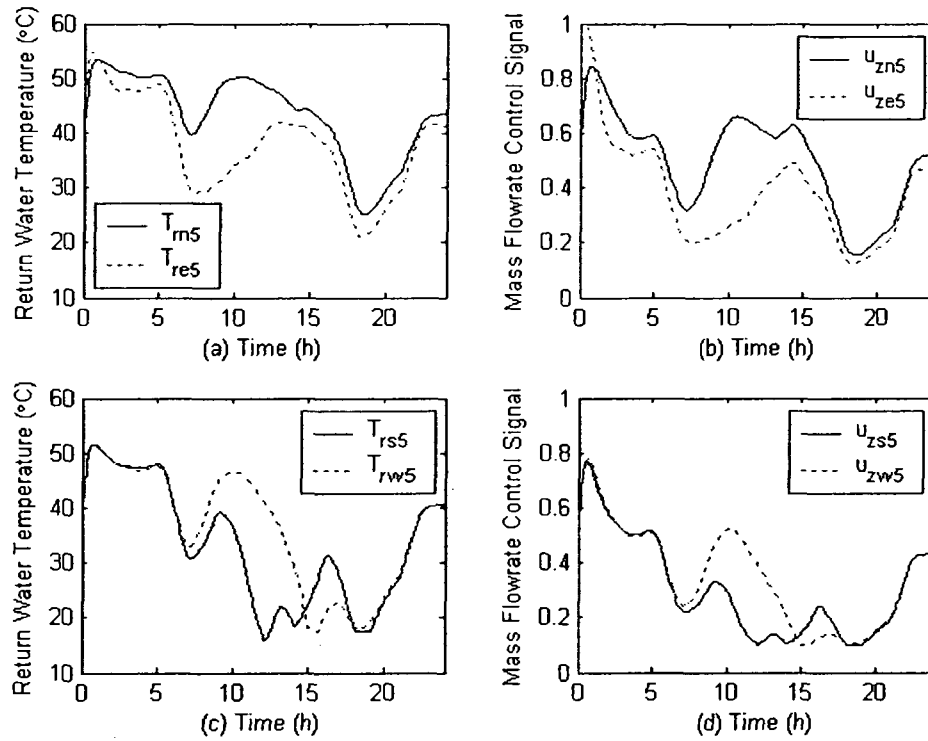


Figure 5.11 Dynamic responses of zone water temperatures and water flow control signals

The air temperature responses of the four zones are presented in Figures 5.12. Except for the influence of the initial conditions in the first three hours, the air temperature fluctuations for the north, east, south and west zones are 1.12, 0.71, 1.08 and 1.02°C respectively. In other words, the temperature swing ranges from 21.70 to 22.40°C most of time. Compared with those air temperatures in Section 5.2.1, the thermal comfort is improved greatly in this case.

Additional merit of the adaptive PI control strategy is demonstrated in Figure 5.12(a). In this figure, the zone air temperature responses with fixed PI gains ( $T_{ze5b}$ ) and with adaptive PI gains ( $T_{ze5a}$ ) are depicted. Compared with the fixed gain PI controller for

the east zone, the swing in the zone air temperature is 1.24°C less by using the adaptive PI controller.

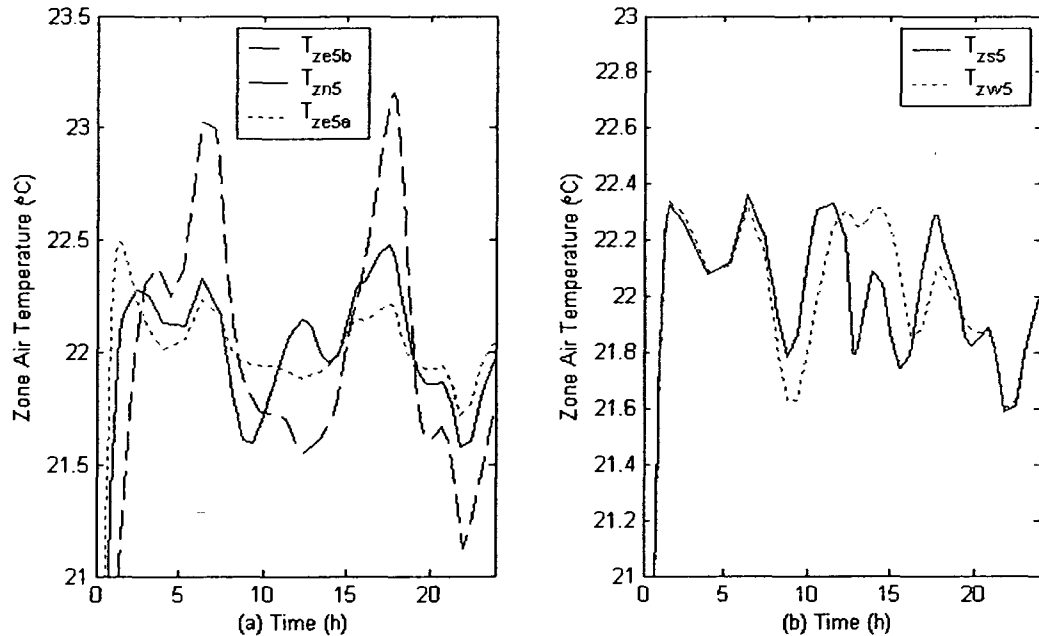


Figure 5.12 Dynamic responses of the zone air temperatures (FLAC)

### 5.2.3 Design of hybrid control strategy with the EKF

In a real HWH system, noises such as measurement noise and process noise always exist and affect system operation. For example, measurement signals could be degraded by electromagnetic field and electric voltage etc. Process noise acting on the system can be taken into account as system uncertainty acting on state variables. Large noises would cause additional energy consumption, zone air temperature fluctuation and pressure shock in the hydraulic system. Furthermore, since the air temperature sensor is usually positioned close to the interior wall, the actual air temperature measurement will be different compared with the air temperature with the assumed well-mixed assumption. This is due to the zone air temperature distribution (stratification) that was mentioned in

the zonal model (Appendix A). To this end, considerations for handling process and measurement noises and zone air temperature distribution have to be taken into account in the control strategy. The noises will be dealt with the EKF for the large scale nonlinear dynamic system, and the relationship among the zone air temperature measurement, indoor air temperature under well-mixed assumption and outside air temperature will be utilized in this simulation study.

The reasons of applying for the EKF can be described as follows. By using the EKF the state variables affected by process and measurement noises could be estimated based on their measurement data at past and current time. In other words, it is an extension of recursive least square approach according to state variables of dynamic systems. Second, sometimes not all state variables can be measured by sensors, or the measurement is too expensive. Finally, the noises acting on the dynamic process and the measurement not only influence control system performance but also increase system energy consumption. Hence, for nonlinear dynamic systems, the EKF approach, which provides a powerful mathematical framework used for state variable evaluation, should be utilized to take care of the noises. By involving the EKF technique, it is possible to include additional effects in dynamic models to achieve better system performance.

Compared with other state variable estimation methods, there are several advantages of using the EKF technique in the HWH system. To begin with, it is not necessary to develop a very accurate dynamic system model, even when the precise nature of the dynamic system is unknown (Welch and Bishop 2004). Second, this technique not only can handle linear dynamic systems but also can handle nonlinear dynamic processes by applying Taylor series equation. Third, it could directly estimate

unmeasured system dynamics with noises to attain suitable state space variable estimation. It is an efficient recursive program consuming less computation time, which means that it is good for use as an online estimator (observer) and simple to implement. Also, it is easy to analyze state variable covariance and address the quality of the results. Finally, it offers an advantage of determining up-to-date uncertainties of the estimates for real-time quality assessments or for off-line system design investigation.

A block diagram depicted in Figure 5.13 is utilized to describe the overall HWH system control configuration with FL adaptive PI controllers and the EKF. In the control system, the dynamics of the entire system is influenced by the process noise, and one of the system outputs ( $T_{ze5}$  under well-mixed assumption) is corrected based on the zonal model information to obtain the corrected zone air temperature ( $T_{ze5crt}$ ). The measured zone air temperature ( $T_{ze5msd}$ ) is gathered by adding measurement noise. Then, the process and measurement noises acting on the dynamic system are evaluated according to the EKF, and the estimated state variables ( $y_{emd}$ ) are obtained. The estimated state variables such as the supply water temperature from the boiler ( $T_s$ ) and the zone air temperature ( $T_z$ ) are compared with their set points ( $T_{ssp}$  and  $T_{zsp}$ ). Note that the set point of  $T_s$  is deduced based on a FIS with two antecedents: outside temperature and additional heat gains. In addition, the adaptive proportional and integral gains of the zone air temperature PI controllers are inferred by two Sugeno types of FISs. The advantages of this control strategy are that it not only improves energy efficiency and thermal comfort but also compensates for the degradation in operation resulting from the noises. In total there are 38 PI controllers, one fuzzy-PI controller for the boiler control and 37 fuzzy

logic adaptive PI controllers for the zone air temperature regulation, which are combined with the EKF in the control system.

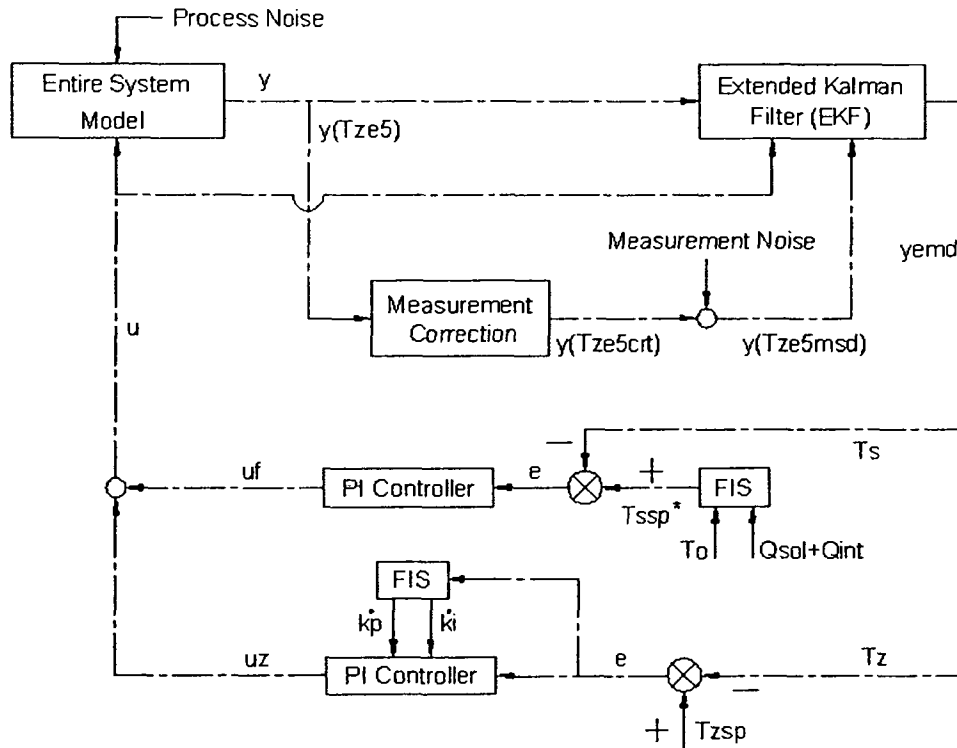


Figure 5.13 Control system configuration with the EKF

In the FIS for the supply water temperature set point, three linguistic variables such as outside air temperature, ratio of additional heat gains and supply water temperature set point are employed. There are seven membership functions for each linguistic variable and these are depicted in Figure 5.14. The rule-base for the FIS with two antecedents is given in Table 5.2. Mamdani type of FIS is used to obtain the supply water temperature set point after defuzzification.

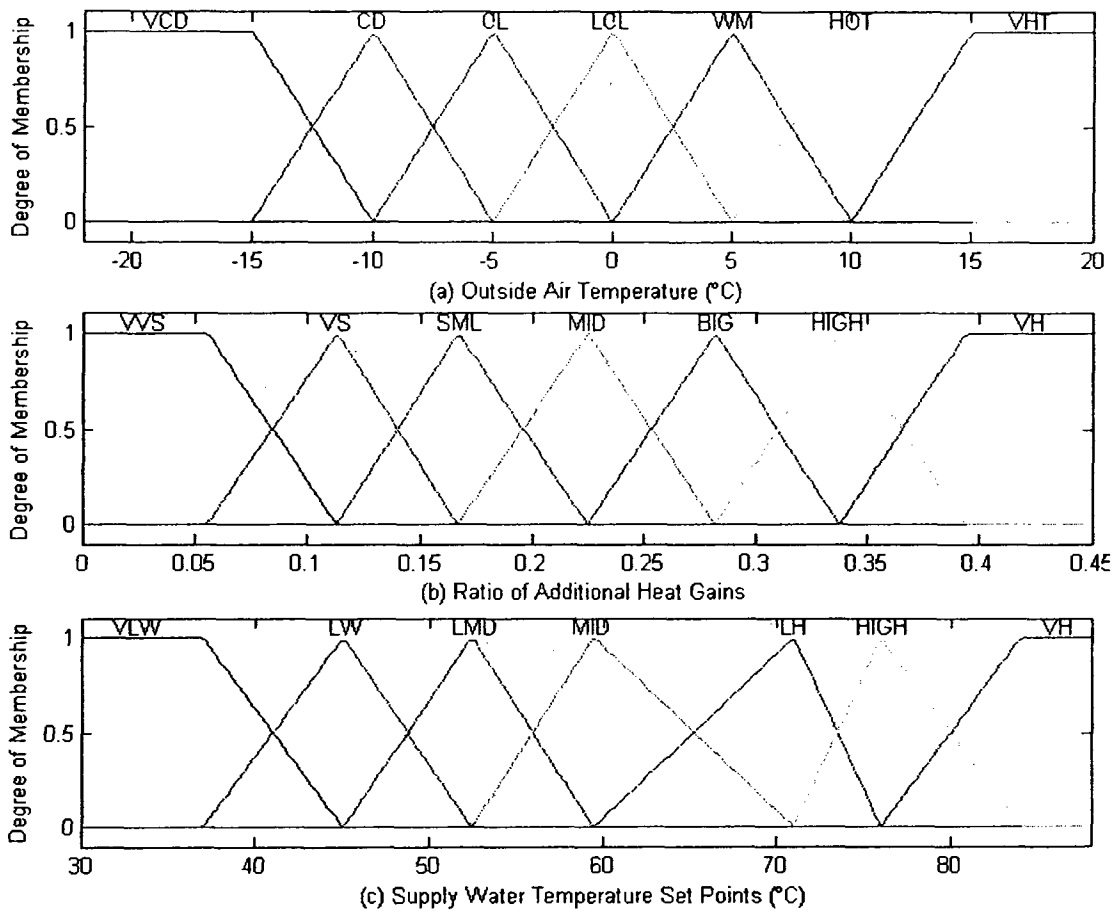


Figure 5.14 Memberships functions of the linguistic variables for  $T_{ssp}$

Table 5.2 Rule-base for the FIS

Water temperature set point		Ratio of additional heat gains						
		VVS	VS	SML	MID	BIG	HIGH	VH
Outside air temperature	VCD	VH	HIGH	LH	MID	MID	LMD	LW
	CD	LH	LH	LH	MID	LMD	LW	VLW
	CL	MID	MID	MID	LMD	LMD	LW	VLW
	LCL	LMD	LMD	LMD	LMD	LW	VLM	VLW
	WM	LW	LW	LW	LW	VLM	VLM	VLM
	HOT	LW	VLM	VLM	VLM	VLM	VLM	VLM
	VHT	VLM	VLM	VLM	VLM	VLM	VLM	VLM

In order to diminish the influence of the process and measurement noises, the EKF technique is applied for the overall HWH system. Note that this technique could be

employed for all measurement of the HWH system in the same manner although the measurement noise is applied only for the east zone air temperature on the 5<sup>th</sup> floor in this study. The measurement noise for the zone air temperature is assumed as stationary, uncorrelated, zero expectation, and Gaussian white noise with 0.40°C difference. The magnitude of process and measurement noise covariance is assumed as  $10^{-5}$  and 0.16 respectively. The outputs of the fuel and the water mass flow rate control signals were calculated from Equations (5.4) and (5.5).

Two sets of equations introduced by Welch and Bishop (2004), which are time and measurement update equations, are utilized for the EKF. These Equations (5.8)~(5.12) are given below.

Time update equations:

$$\hat{x}_k^- = f(\hat{x}_{k-1}, u_{k-1}, 0) \quad (5.8)$$

$$P_k^- = A_k P_{k-1} A_k^T + W_k Q_{k-1} W_k^T \quad (5.9)$$

Measurements update equations:

$$K_k = \frac{P_k^- H_k^T}{H_k P_k^- H_k^T + V_k R_k V_k^T} \quad (5.10)$$

$$\hat{x}_k = \hat{x}_k^- + K_k [z_k - h(\hat{x}_k^-, 0)] \quad (5.11)$$

$$P_k = (I - K_k H_k) P_k^- \quad (5.12)$$

where A, W, H and V are defined in Equations (5.11)~(5.14) as

$$A_k = \frac{\partial f}{\partial x}(\hat{x}_{k-1}, u_{k-1}, 0) \quad (5.13)$$

$$W_k = \frac{\partial f}{\partial w}(\hat{x}_{k-1}, u_{k-1}, 0) \quad (5.14)$$

$$H_k = \frac{\partial h}{\partial x}(\hat{x}_k^-, 0) \quad (5.15)$$

$$V_k = \frac{\partial h}{\partial v}(\hat{x}_k^-, 0) \quad (5.16)$$

where  $A$ ,  $W$ ,  $H$  and  $V$  refer to the Jacobian matrixes of partial derivatives of function  $f$  and  $h$  with respect to  $x$ ,  $w$ ,  $x$  and  $v$  respectively. Note that  $f$  and  $h$  state the nonlinear stochastic difference equations for the process and the measurement; while  $\hat{x}_k^-$  and  $\hat{x}_k$  indicate the priori and posteriori estimation of state vectors.

The complete set of the EKF equations described in Equations (5.8)~(5.16) function as a predictor (Equations (5.8)~(5.9)) and a corrector (Equations (5.10)~(5.11)) for the heating system. The predictor assigns the state vectors and their covariance estimates from the previous time step  $k-1$  to the current time step  $k$  according to the overall system model. Note that the Jacobian matrices  $A_k$  and  $W_k$  vary at step  $k$ ; while the process noise covariance  $Q_k$  changes at each time step. On the other hand, the corrector is utilized to generate estimated state vectors  $\hat{x}_k$  on the Kalman gain  $K_k$ , the zone air temperature measurement  $T_{ze5}$  and the *posteriori* estimate error covariance  $P_k$ . Also note that the Kalman gain, the estimated values, the *posteriori* estimate error covariance, the Jacobian matrices  $H_k$  and  $V_k$  and the measurement noise covariance  $R_k$  vary at time step  $k$ .

The dynamic responses with process and measurement noises of the HWH system were simulated and are depicted in Figures 5.15~5.18. Note that only the east zone on the 5<sup>th</sup> floor is chosen to show the results.

The *posteriori* estimate error covariance ( $P_k$ ) is plotted in Figure 5.15. The error covariance is reduced rapidly associated with the time from the initial value of  $10^{-2}$  to the

final value of  $2.6 \cdot 10^{-4}$  within 2 hours. However, it should be noted that the choice of the initial value is not critical except for zero because the EKF will converge eventually.

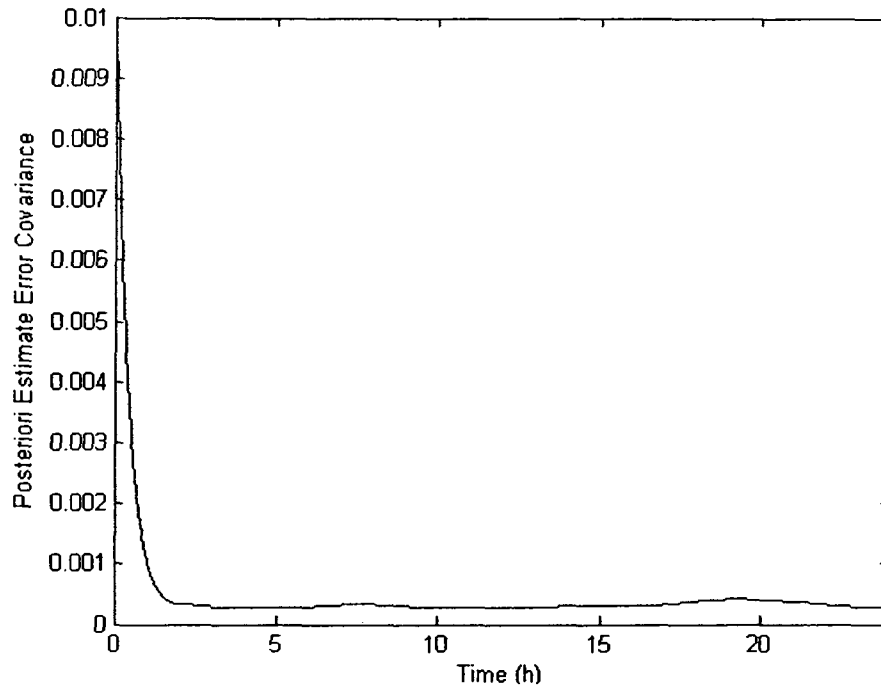


Figure 5.15 The *posteriori* estimate error covariance

The dynamic responses of the system outputs such as the supply and return water temperatures from and to the boiler, total water mass flow rate and the fuel control signal are presented in Figure 5.16. As shown in Figure 5.16(a), the supply and return water temperatures vary from 74.92 to 57.95 and from 50.1 to 41.8°C respectively except for the influence of the initial conditions in the first three hours. The response of total water mass flow rate given in Figure 5.16(b) is decreased from the design value of 2.2811Kg/s to between 1.402 to 1.169Kg/s. The water mass flow rate reduction is due to the use of the additional heat gains. The response of the fuel firing rate of the boiler given in Figure 5.16(c) fluctuated between 0.746 and 0.434; while the control system was tracking the changes in the heating load.

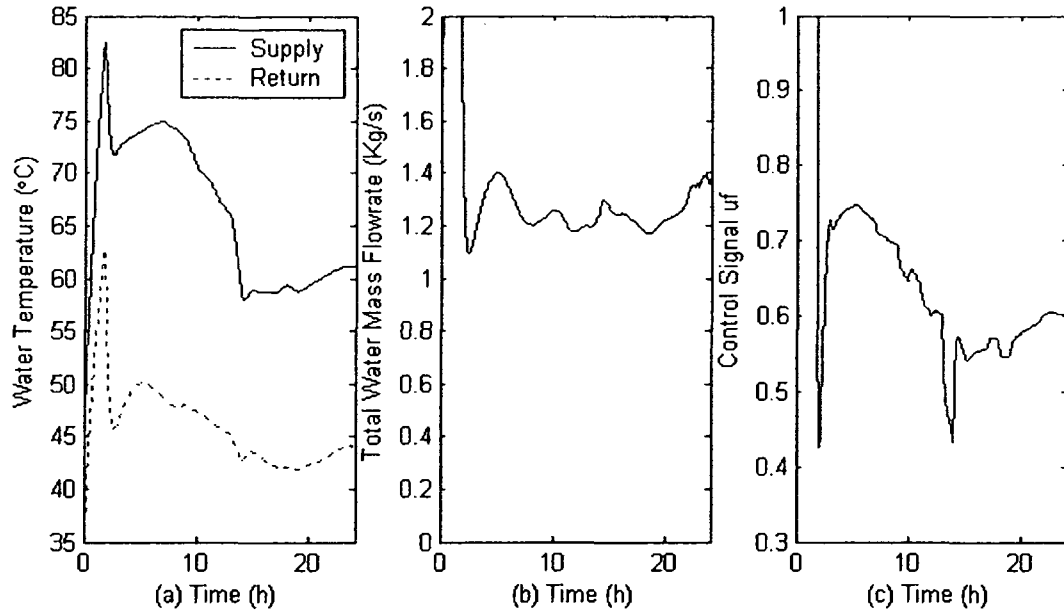


Figure 5.16 Dynamic responses of the outputs in the control system with the EKF

The dynamic responses of the return water temperature and the mass flow rate control signals are depicted in Figure 5.17 for the four zones on the 5<sup>th</sup> floor heating system. From the return water temperature responses shown in Figures 5.17(a) and (c) it can be seen that, in the north zone, the water temperature has the highest value compared with those in the others in the daytime because of no solar radiation acting in this zone. The biggest water temperature difference reaches 26.08°C. Note that the water mass flow rate control signals of the zones presented in Figures 5.17(b) and (d) display the similar trends associated with the return water temperature responses.

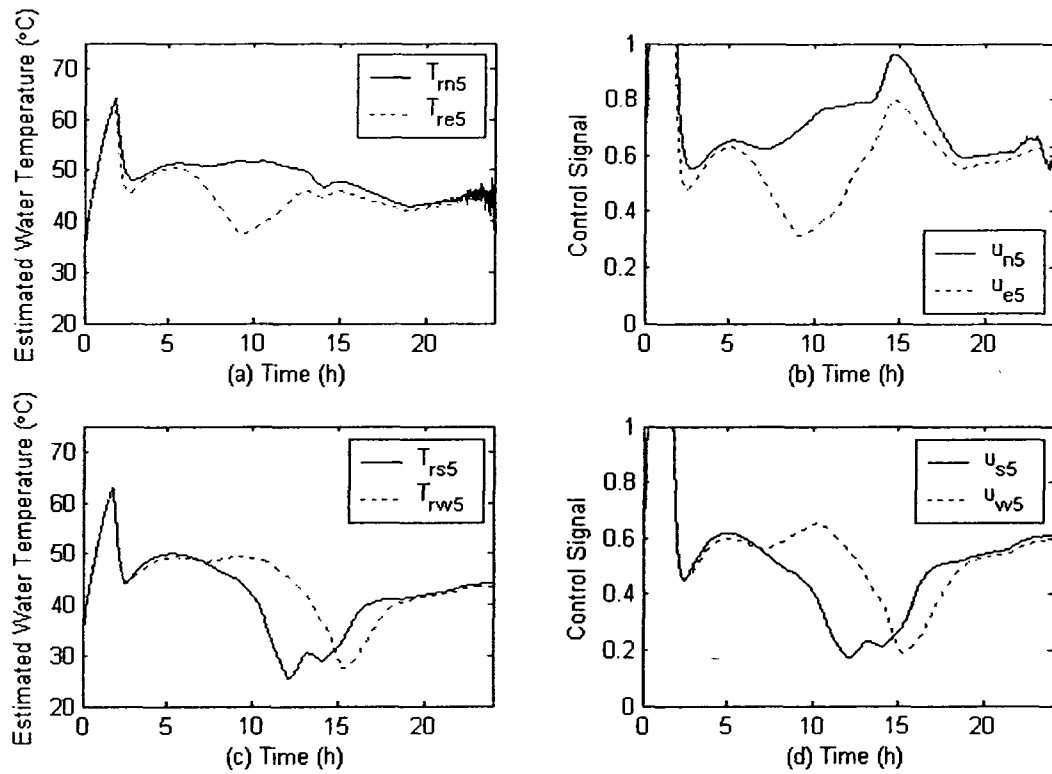


Figure 5.17 Responses of return water temperatures and mass flow rate control signals

The action of the EKF can be illustrated by comparing the dynamic responses of the measured and estimated state variables with and without the EKF. The simulation results are shown in Figure 5.18. In Figures 5.18(a) and (b), the measured and estimated state variables of  $T_s$  and  $T_{ze5}$  with the EKF are plotted. From Figure 5.18(a), it can be seen that the supply water temperature measurement is fluctuated  $3.60^\circ\text{C}$  due to the influence of the system noises; while the temperature estimated by the EKF shows smoothly moving signal. In addition, as shown in Figure 5.18(b), the swing in the zone air temperature is also reduced by the EKF estimation, although the fluctuation of the temperature is mainly caused by the measurement noise. In Figures 5.18(c)~(f), the measured state variables of  $T_s$  and  $T_{ze5}$  are compared with and without the EKF

respectively. The fluctuation in the supply water temperature is decreased from  $6.40^{\circ}\text{C}$  without the EKF to  $3.60^{\circ}\text{C}$  with the EKF as shown in Figures 5.18(e) and (c); while the swing in the zone air temperature is reduced from  $3.50^{\circ}\text{C}$  without the EKF to  $1.80^{\circ}\text{C}$  with the EKF as depicted in Figures 5.18(f) and (d). The results show that the EKF could be employed to deal with process and measurement noises effectively.

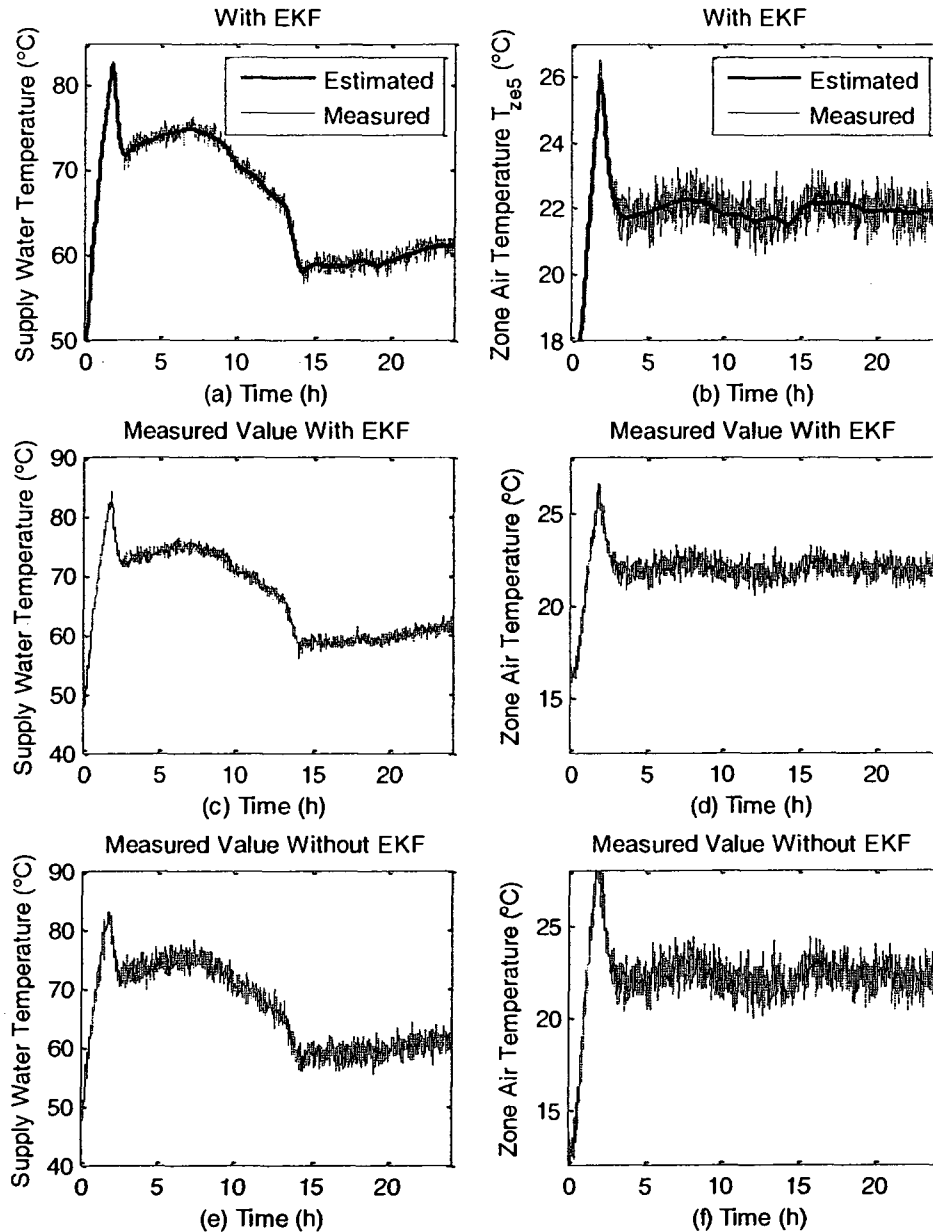


Figure 5.18 Temperature dynamic responses with and without the EKF

Likewise, the dynamic response of the zone air temperature  $T_{ze5}$  is depicted in Figure 5.19(a). The dot points indicate the zone air temperature measurement; while the solid line refers to the estimated zone air temperature. From this figure, it is noted that the air temperature measurement fluctuated about  $2^{\circ}\text{C}$  (zone air temperature set point is

22°C); while the estimated values ranged from 21.72 to 22.15°C. The simulation results imply two aspects. One is the process and measurement noises can be compensated by the intelligent controllers; the other is that the EKF can decrease the influence of the noises acting on the control system and obtain smooth estimated values of state space variables for the control action.

By comparisons, the dynamic responses of the zone air temperature  $T_{ze5}$  without process and measurement noises are plotted in Figure 5.19(b). It shows that the air temperature measurement and the estimated values are identical. In addition, comparing the zone air temperature responses in Figures 5.19(a) and (b), it is apparent that the performance of the heating system is affected by the noises greatly; hence, the noises should be regulated by advanced control strategies with suitable filtering techniques such as the EKF.

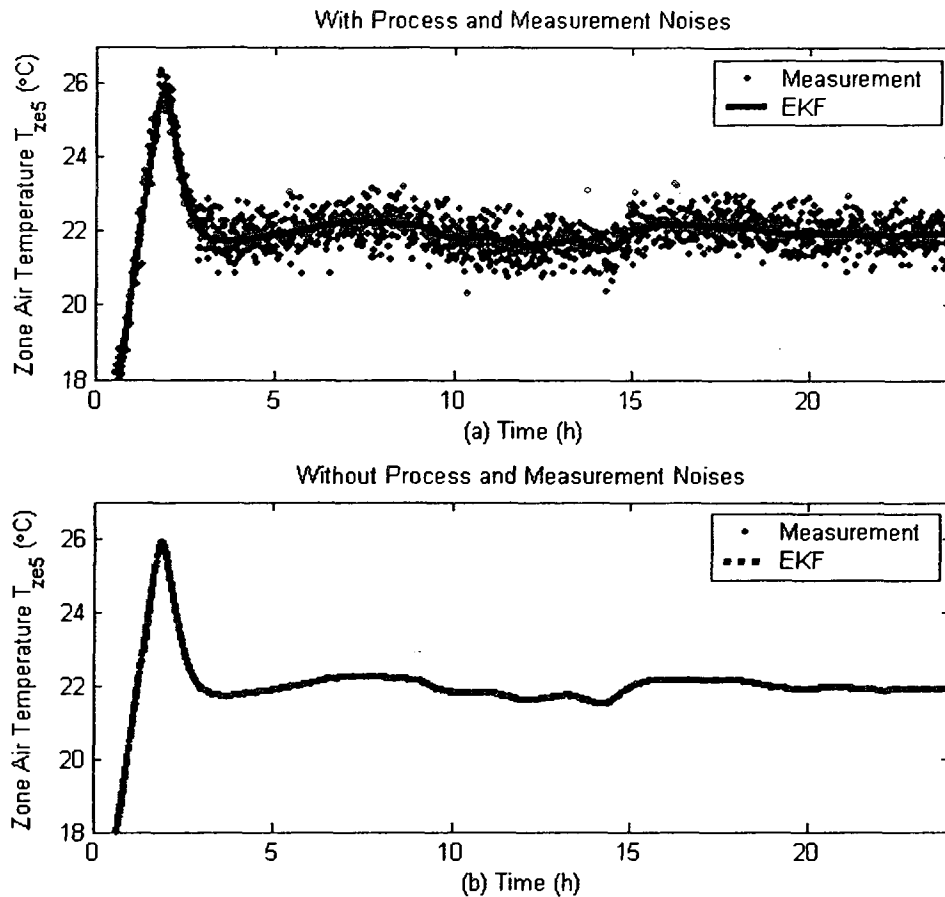


Figure 5.19 Comparisons of zone air temperature responses with and without noises

The process and the measurement noises were varied in the overall system. When the noises remain as white noises and the covariance for the process error and measurement error were changed from 0.1 and 0.4 to 0.05 and 0.1 respectively, the simulated dynamic responses of the system are shown in Figure 5.20. Comparing the results in Figure 5.16 and Figure 5.20, it can be seen that the dynamic responses of the supply and return water temperatures, total mass flow rate and the fuel control signal do not change too much; while the zone air temperature fluctuation decreases from 2.97°C

(Shown in Figure 5.19(a)) to 1.15°C (Shown in Figure 5.20(d)) for the different noise levels.

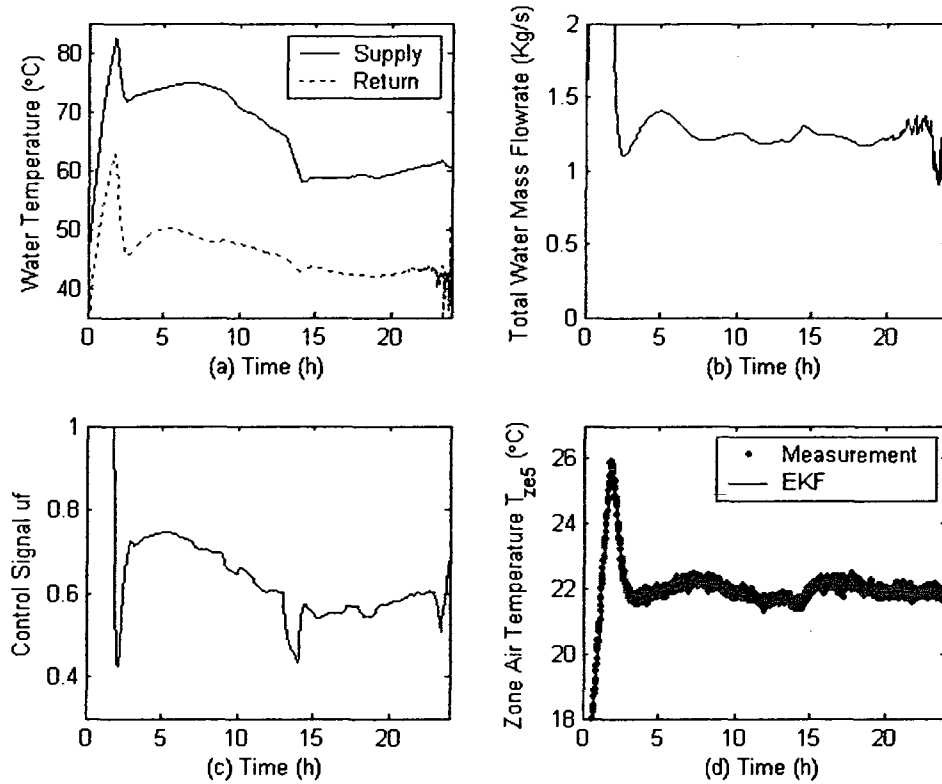


Figure 5.20 Dynamic responses of the system by changing noise levels

To evaluate the process and measurement noises affecting the system dynamic responses with the EKF, the simulations were made for different conditions. The dynamic responses of the supply and return water and the zone air temperatures are presented in Figures 5.21(a) and (b) with process noise and without measurement noises; while the temperature dynamic responses are depicted in Figures 5.21(c) and (d) without process noise and with measurement noises. It can be seen from the estimated values from the

EKF that, the temperature responses with the process noise is more influenced compared with those with measurement noise.

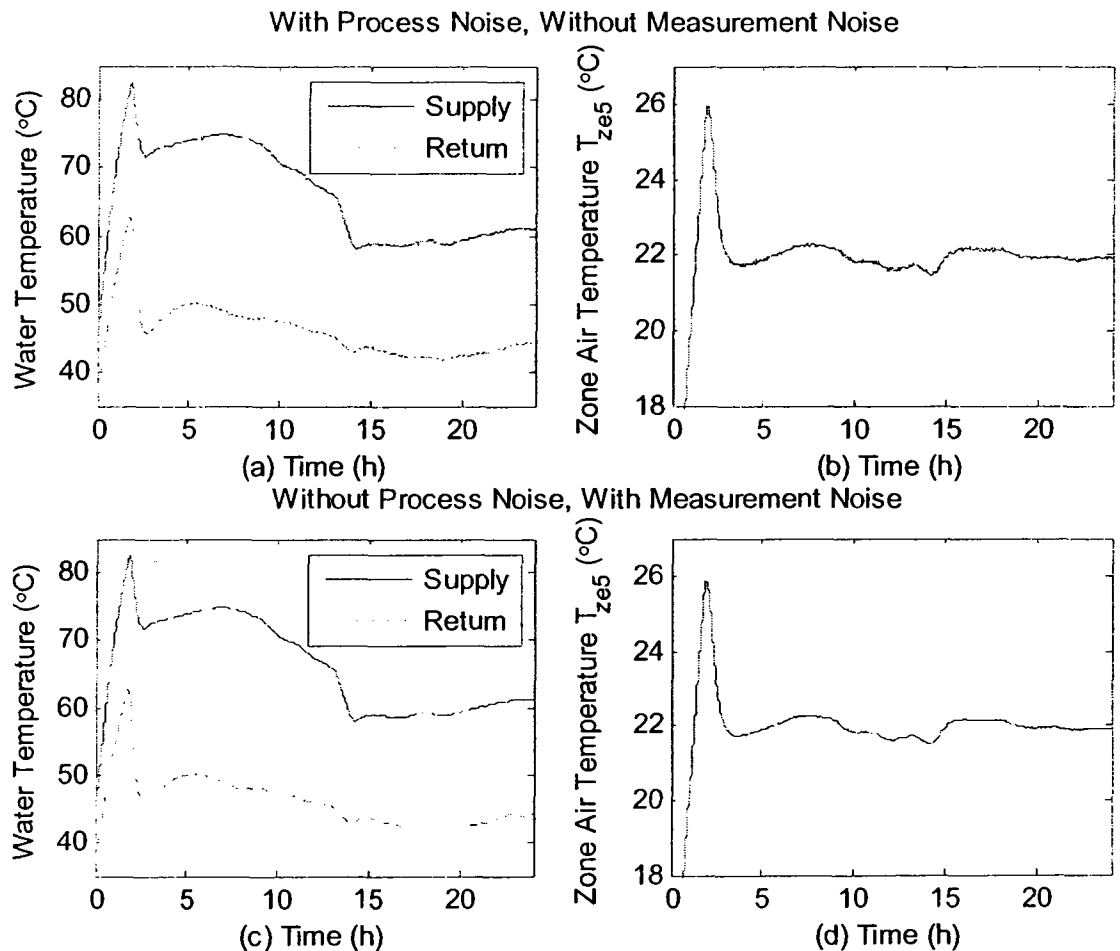


Figure 5.21 Temperature dynamic responses for different noise conditions

Strictly speaking, it is incorrect that all information in physical HWH systems can be obtained. In other words, uncertainty does exist in all parameters that have been used in the overall dynamic model equations. However, estimating all the parameter uncertainty is difficult not only because of the computational time but also due to the unavailability of some parameters of the system. Such parameters include heat transfer coefficient of baseboard heaters from water side to air side, thermal conductivity of building enclosure and heating load etc. To demonstrate the feasibility of the EKF

method, three important parameters such as thermal conductivity of the outside wall, overall heat transfer coefficient of the baseboard heater and the efficiency of the boiler, were selected as uncertain parameters in the case study.

The simulation runs were made in order to observe the overall control system responses. The parameter uncertainties were assumed as follows: the overall heat transfer coefficient of the baseboard heater from water to air side is decreased by 10%, the overall heat transfer coefficient of the outside wall is increased by 20%, and the boiler efficiency reduced by 5%. The simulation results are presented in Figures 5.22 and 5.23.

Since the heating load is increased by varying the uncertain parameters, shown in Figure 5.22(a), the water temperature difference between the supply and return water is reduced with the parameter changes compared that without parameter changes, and the water mass flow rates are increased (Illustrated in Figure 5.23(b)). In addition, the fluctuation of the zone air temperature is increased with uncertain parameters (Figure 5.22(b)). Therefore, the uncertainty in parameters indeed affects the system performance. The increase in heating load and the decrease in both the heat transfer coefficient of the heater and the boiler efficiency could lead to more energy consumption. This situation is presented in Figure 5.23(a) which shows additional fuel consumption of about 4.70% with the changed parameters; while the pumping energy is also increased in this case (see Figure 5.23(b)). It is important to note that this kind of parameter uncertainty in the system could also be handled by the EKF.

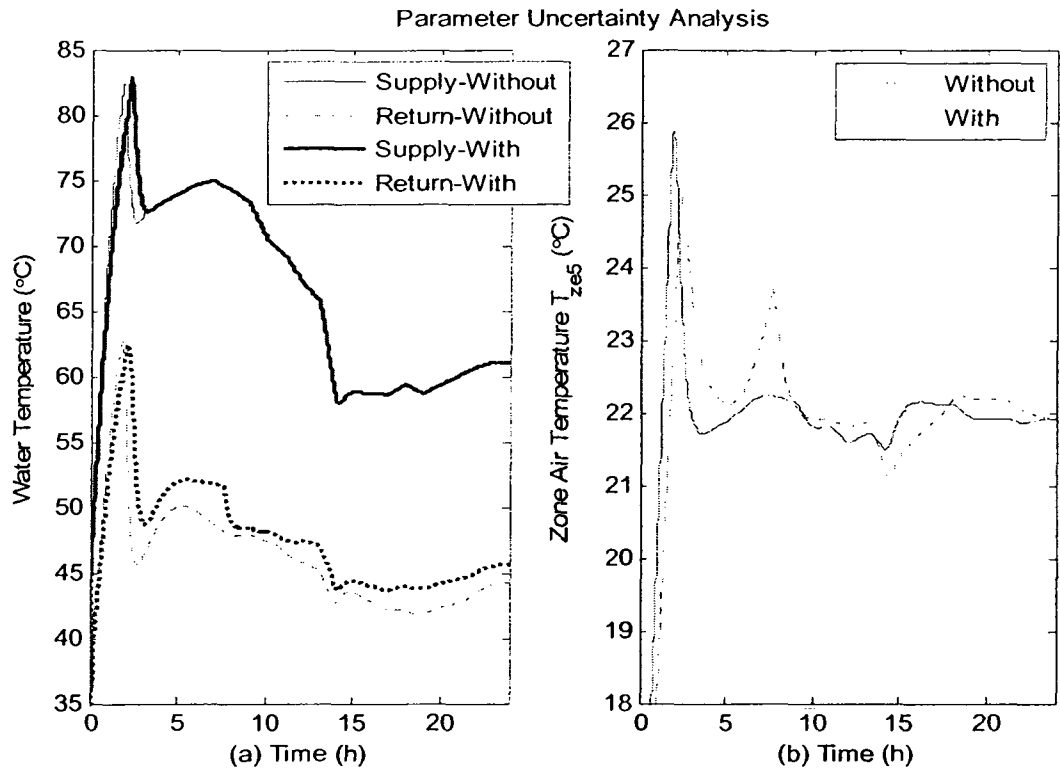


Figure 5.22 Dynamic responses of the system outputs considered uncertain parameters

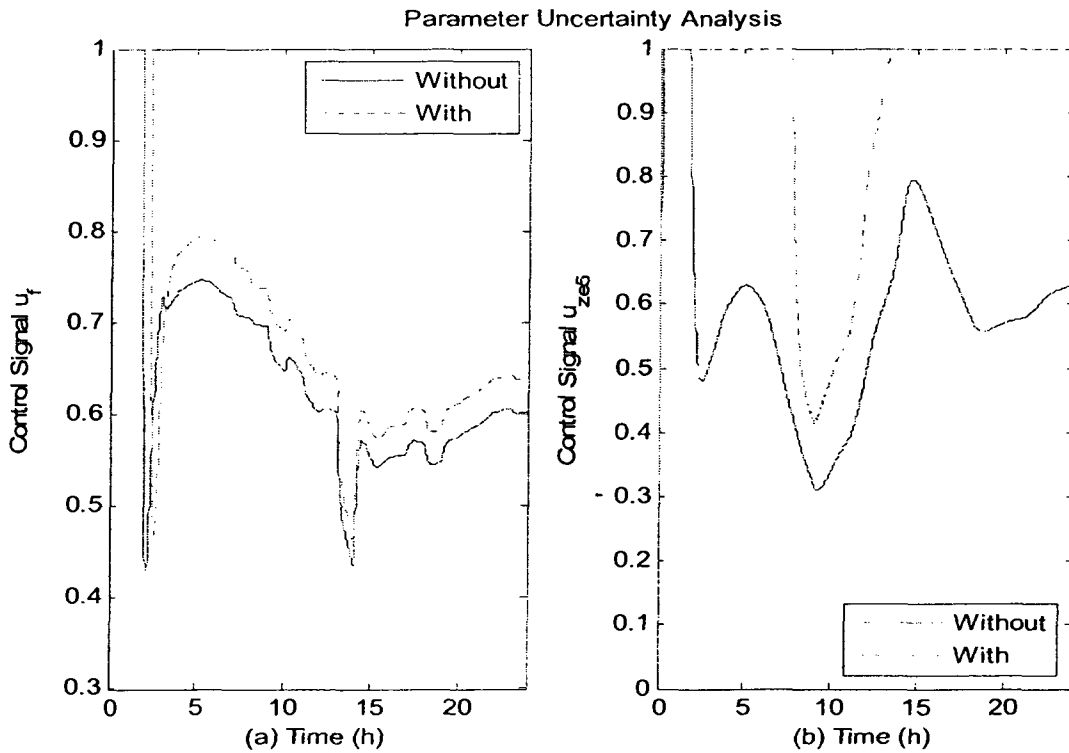


Figure 5.23 Dynamic responses of the system control signals

From the analysis of above results, it can be concluded that the designed control strategies based on the fuzzy-PI controller, the fuzzy logic adaptive PI controllers and the use of the EKF estimation improve the robustness property of the control systems.

### **5.3 Energy efficiency and set point accuracy evaluation**

#### **5.3.1 Energy efficiency evaluation**

The designed control strategies were applied for the high-rise building shown in Figure 4.4 for energy use calculation and comparison over one day. The parameters of the building are given in Table 5.1. The mechanical room with a boiler is located at the top of the building. The baseboard heaters are connected by reverse-return piping network on each floor heating system; while the main piping network is designed vertically as direct-return type. The closed hydraulic hot water system is driven by a centrifugal circulation pump.

The energy consumptions of pump such as electricity and fuel for the boiler for the designed control strategies were computed, and the results are presented in Table 5.3. Comparing with the energy use from this table, the pump energy and the fuel could be saved up to 88.35% and 15.78% by using the fuzzy-PI controller for the supply water temperature and the FLAC control strategy for the water mass flow rate control.

Table 5.3 Energy consumptions over one day

Control strategy	Electricity		Fuel		Daily comfort level	Remark
	KWH	%	GJ	%	%	
Boiler control	13.91	100	12.55	100	20.86	Base
FLAC	1.62	11.65	10.57	84.22	83.84	Adaptive PI gains
FLAC	2.39	17.18	11.84	94.34	70.98	Fixed PI gains
Control with the EKF	2.76	19.84	11.21	89.32	79.88	$\delta_v=0.1, \delta_w=0.4$
Control with the EKF	2.47	17.76	10.89	86.77	80.03	$\delta_v=0.05, \delta_w=0.1$
Control with the EKF	2.35	16.89	11.79	93.94	76.44	With parameter uncertainty

### 5.3.2 Set point accuracy evaluation

Estimation of set point accuracy of different designed control strategies is essential. To this end, a scale is defined based on zone air temperature fluctuation with a fuzzy inference engine. The dynamic response of the zone temperature ( $T_z$ ) is divided into six regions according to its absolute deviation from its set point value such as less than and equal to  $0.25^\circ\text{C}$ , between  $0.25$  and  $0.50^\circ\text{C}$  and equal, between  $0.50$  and  $1^\circ\text{C}$  and equal, between  $1$  and  $1.50^\circ\text{C}$  and equal, between  $1.50$  and  $2^\circ\text{C}$  and equal, and greater than and equal to  $2^\circ\text{C}$  as illustrated in Figure 5.24.

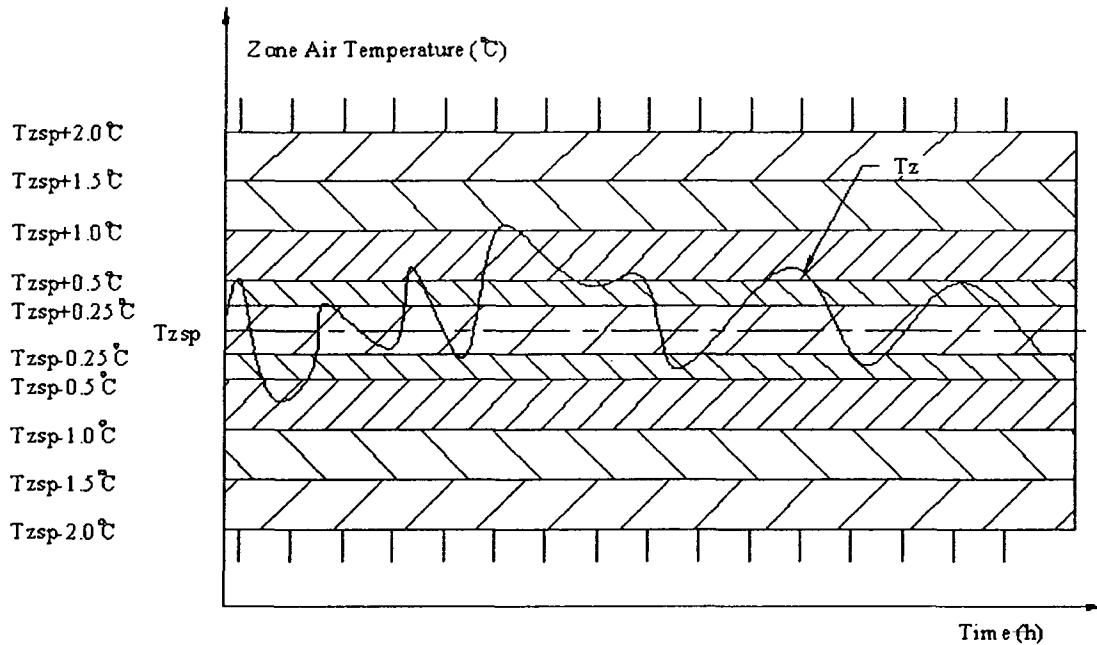


Figure 5.24 Definition of set point accuracy for zone air temperature

By applying fuzzy logic set theory, set point accuracy of a zone can be estimated when a heating system is operating. There are two linguistic variables: zone air temperature deviation and set point accuracy, which are divided into five membership functions respectively. If-then rules of the FIS are given as follows:

If ND of zone air temperature, then set point accuracy is VVA

If SD of zone air temperature, then set point accuracy is VA

If MD of zone air temperature, then set point accuracy is AT

If BD of zone air temperature, then set point accuracy is IA

If VBD of zone air temperature, then set point accuracy is VIA

The abbreviation such as ND, SD, MD, BD, VBD, VVA, VA, AT, IA and VIA indicates no deviation, small deviation, middle deviation, big deviation, very big deviation, very very accurate, very accurate, accurate, inaccurate and very inaccurate

respectively. The degree of membership functions of the linguistic variables are depicted in Figure 5.25. The interval [0, 1] can be utilized to examine the set point accuracy in zones. For instance, if the level value is more close to 1, more accuracy will be achieved, and vice versa.

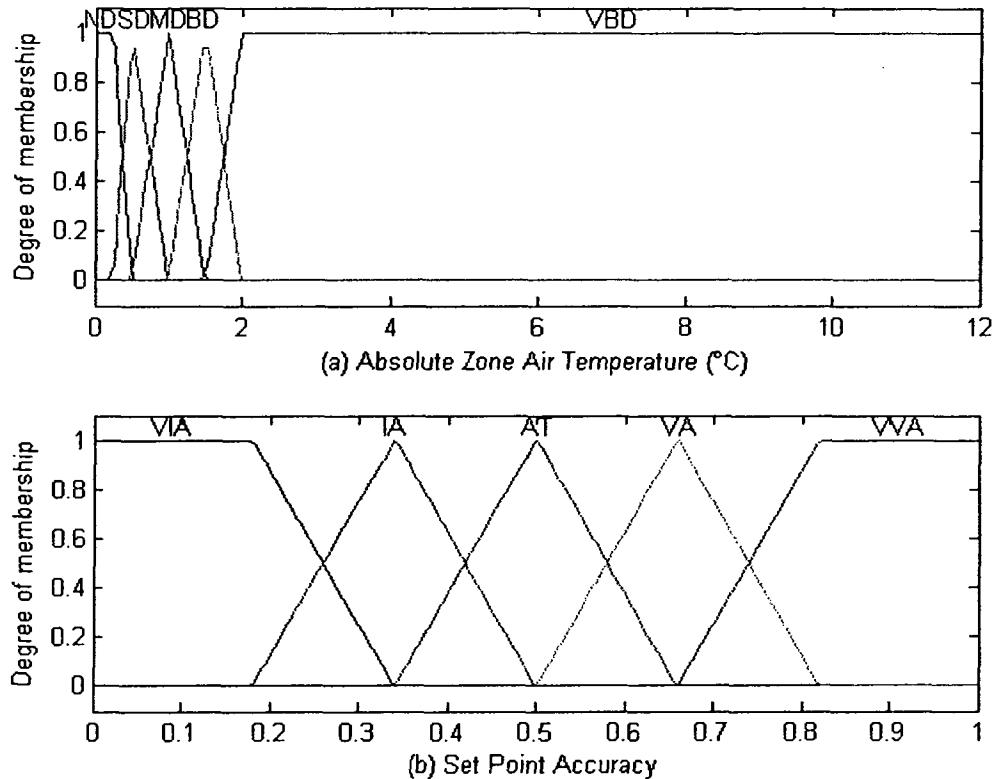


Figure 5.25 Degree of membership functions for set point accuracy estimation

Set point accuracy estimation approach was applied to the east zone on the 5<sup>th</sup> floor heating system. The results are depicted in Figures 5.26~5.28. It can be seen from Figure 5.26 that the set point accuracy in the boiler control strategy given in Section 5.2.1 is very low in the day. The values are small especially after 6 hours because of the disturbances acting on the system caused the larger zone air temperature deviation. This

situation could be improved based on both water temperature and mass flow rate regulation.

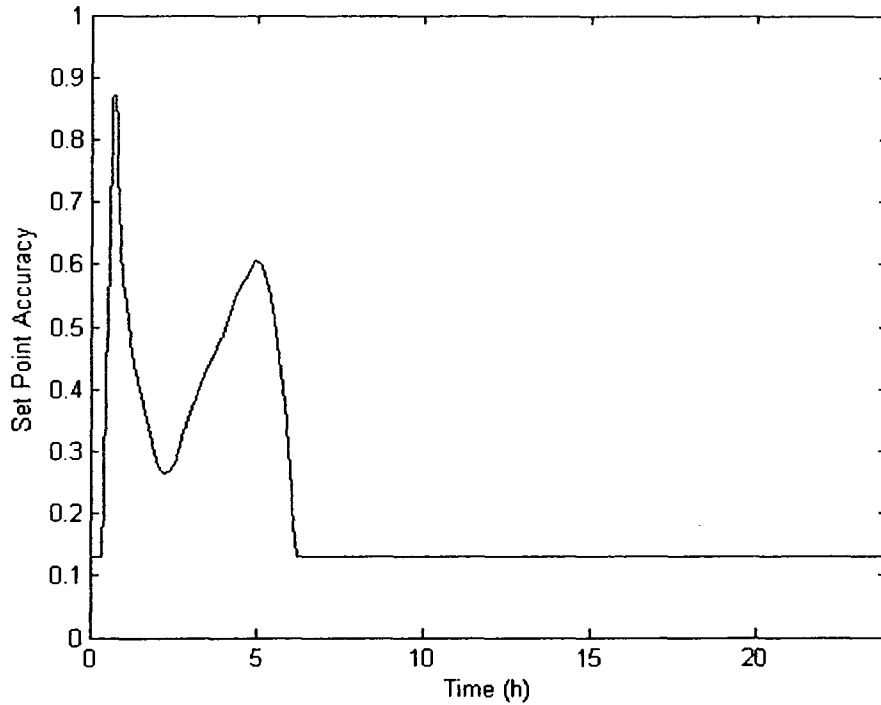


Figure 5.26 Set point accuracy estimation in the boiler control strategy

By employing advanced control strategy such as fuzzy logic adaptive controllers to the HWH system, the set point accuracy was evaluated and the result is depicted in Figure 5.27. It reaches higher value (0.88) most of time. The improvement is due to the fact that the supply water temperature from the boiler was regulated based on the current outside air temperature, and the zone air temperatures were controlled by adjusting the water mass flow rate entering the heaters.

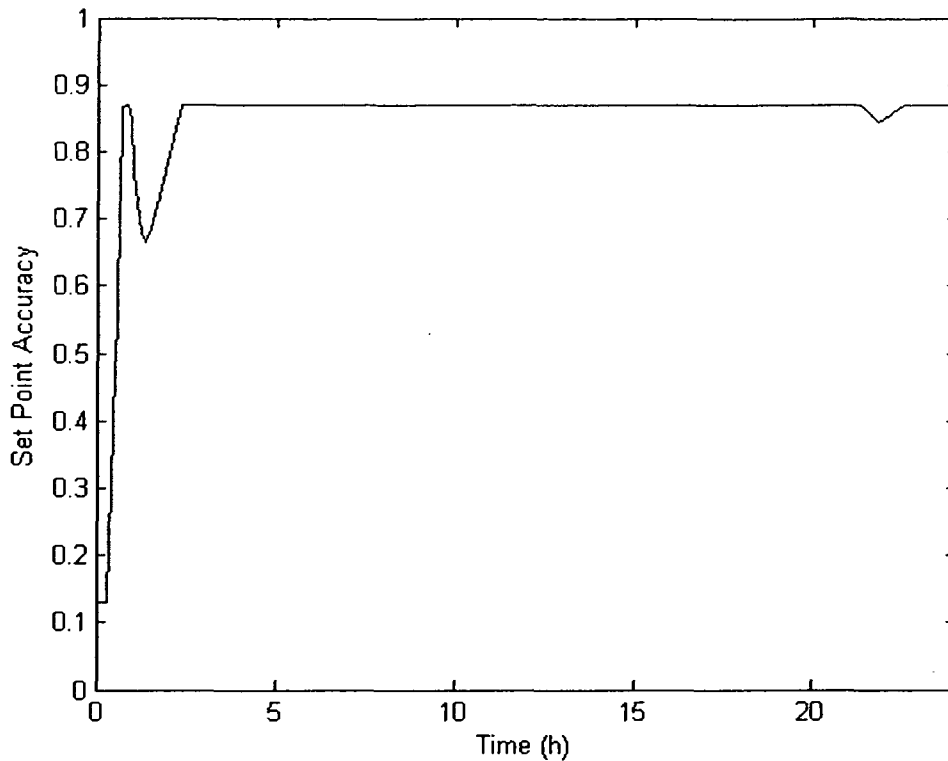


Figure 5.27 Set point accuracy estimation by using FLAC strategy

The nonlinear properties of the dynamic system and the process and measurement noises acting on the entire system make the control task difficult. However, by employing the hybrid control strategy combining the EKF, the system performance was improved. The set point accuracy obtained with this strategy is shown in Figure 5.28. Most of time, the zone air temperature remains steady with higher level during the occupied hours. Note that in addition to set point accuracy estimation, a thermal comfort estimation method that concerns about zone air temperature, air velocity and humidity etc. can also use the above fuzzy logic approach. However, such tests were not conducted in this thesis.

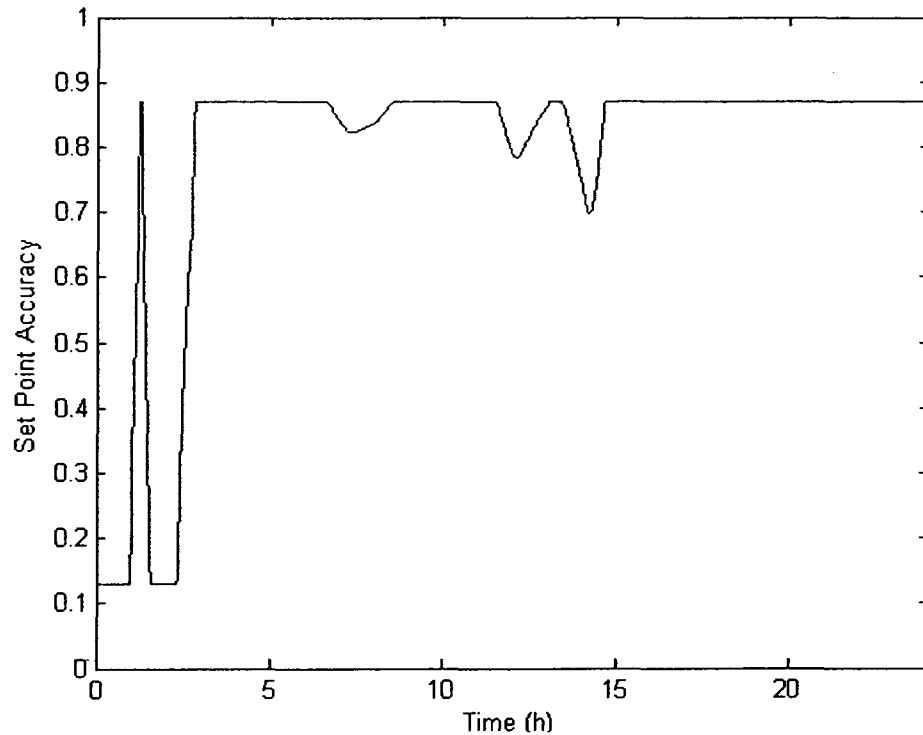


Figure 5.28 Set point accuracy estimation in the control strategy with the EKF

## 5.4 Design of supervisory control system

Generally, a supervisory control system is very essential for large system operation such as the high-rise building HWH system. The supervisory control system ensures optimal operation of the entire system. First, the optimal set points of operating parameters have to be calculated by an optimization methodology, which can then be supplied to the local controllers. Every local controller will track the optimal set point trajectory, which functions as a reference signal in the local control system. The two-level control can maintain thermal comfort for occupants, improve system performance and is expected to save energy.

Optimal operation can be achieved by tracking optimal set points using local controllers. To this end, a nonlinear constraint optimization problem with a multi-

objective function is formulated and solved. The idea behind this is that if the local controllers such as the supply water temperature controller and the zone air temperature controllers can follow their optimal profiles, great energy savings could be realized.

The configuration of the supervisory control system is depicted in Figure 5.29. In the control system, there are two types of local controllers: one is used for the supply water temperature control, and the others (37 controllers) are employed for the zone air temperature regulation. The optimal set points for the controllers are computed first with all disturbances based on the optimization approach. Then, the set points are utilized as reference signals for the PI controllers and the results are compared with associated measured parameters from the system dynamic model. The error ( $e$ ) between the set point and the measurement is sent to the fuzzy logic adaptive PI controllers (FLAC) for both the supply water temperature and the zone air temperature controllers to obtain the output control signals. The output control signals are used for the control system to attain system outputs.

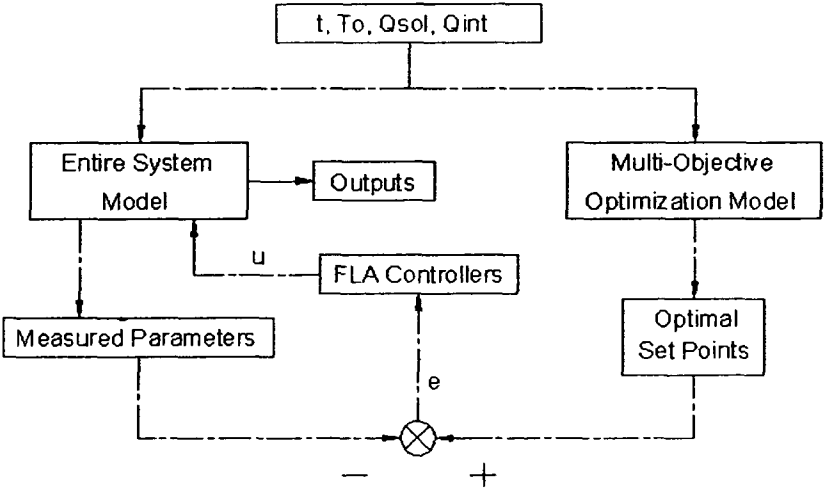


Figure 5.29 Configuration of the supervisory control system

In the nonlinear constraint multi-objective optimization approach, the multi-objective functions composed of the pumping energy, the fuel consumption and the zone air temperature deviation are defined and minimized in the optimization process. The multi-objective functions are given in Equation (5.17). The optimization problem is defined as the minimization of all of the objectives subject to the constraints represented in Equation (5.18). Note that the square value of the zone air temperature deviation is considered. In order to decrease the computational time, a simplified steady state HWH system model based on lumped parameters is utilized. Consequently, 33 optimal variables ( $x$ ) such as  $T_{z\text{bmt}}$ ,  $T_{zn}$ ,  $T_{ze}$ ,  $T_{zs}$ ,  $T_{zw}$ ,  $T_s$ ,  $T_{rbmt}$ ,  $T_m$ ,  $T_{re}$ ,  $T_{rs}$ ,  $T_{rw}$ ,  $\dot{m}_f$ ,  $\dot{m}_{bmt}$ ,  $\dot{m}_n$ ,  $\dot{m}_e$ ,  $\dot{m}_s$ ,  $\dot{m}_w$ ,  $N_m$ ,  $I_m$  and 19 outside wall temperature nodes are selected, and six optimal values of  $T_{\text{sopt}}$ ,  $T_{z\text{bmtopt}}$ ,  $T_{zn\text{opt}}$ ,  $T_{ze\text{opt}}$ ,  $T_{zs\text{opt}}$ ,  $T_{zw\text{opt}}$  are chosen as optimal reference points for the local controllers in the control system shown in Figure 5.29. The constraints of the optimal variables are given in Table 5.4. The optimal solution minimizes the worst-case value of the set of multi-objective functions from an initial estimation. This approach is generally referred to as the *minimax* problem. The algorithms of sequential quadratic programming (SQP) procedure (Brayton 1979), Quasi-Newton and line search are utilized, and modifications are made to the line search and Hessian matrix. In the line search an exact merit function is used together with the merit function proposed by researchers (Han 1977, Powell 1978, Madsen and Schjaer-Jacobsen 1979, Grace et al 1989). When the merit function shows improvement, the line search is terminated.

Table 5.4 Constraints of the optimal variables

Optimal variable	$T_{zbmt}$	$T_{zn}$	$T_{ze}$	$T_{zs}$	$T_{zw}$	$T_s$	$T_{rbmt}$
Unit	°C	°C	°C	°C	°C	°C	°C
Upper limit	23	23	23	23	23	90	70
Lower limit	21	21	21	21	21	25	25
Optimal variable	$T_m$	$T_{re}$	$T_{rs}$	$T_{rw}$	$\dot{m}_f$	$\dot{m}_{bmt}$	$\dot{m}_n$
Unit	°C	°C	°C	°C	Kg/s	Kg/s	Kg/s
Upper limit	70	70	70	70	0.01	0.15	0.75
Lower limit	25	25	25	25	0	0	0
Optimal variable	$\dot{m}_e$	$\dot{m}_s$	$\dot{m}_w$	$N_m$	$I_m$	$T_{wlo}$ (19)	
Unit	Kg/s	Kg/s	Kg/s	rpm	A	°C	
Upper limit	0.45	0.6	0.6	1450	5	22	
Lower limit	0	0	0	0	0	-25	

$$J_{\min} = \begin{bmatrix} J_{fuel} \\ J_{ele} \\ J_{Tz} \end{bmatrix}_{\min} = \begin{bmatrix} \int_0^t \dot{m}_f HV dt \\ \int_0^t E_m I_m dt \\ \int_0^t \sum_0^j (T_{zsp} - T_{zj})^2 dt \end{bmatrix}_{\min} \quad (5.17)$$

$$\min_x \max_{J_i} [J_i(x)]$$

such that

$$C(x) \leq 0 \quad (\text{Nonlinear inequality constraints})$$

$$C_{eq}(x) = 0 \quad (\text{Nonlinear equality constraints}) \quad (5.18)$$

$$A_{ineq} x \leq b_{ineq} \quad (\text{Linear inequality constraints})$$

$$A_{eq} x = b_{eq} \quad (\text{Linear equality constraints})$$

$$x_{lowbnd} \leq x \leq x_{upbnd} \quad (\text{Boundary conditions})$$

where  $x$ ,  $b_{ineq}$ ,  $b_{eq}$ ,  $x_{lowbnd}$ , and  $x_{upbnd}$  are vectors; while  $A_{ineq}$  and  $A_{eq}$  are matrices.  $C(x)$  and  $C_{eq}(x)$  are the nonlinear inequality and equality functions.  $J(x)$  is the multi-objective functions with the optimal variables  $x$ .

An example is given hereby to represent how the optimization approach works. At time equal to 3000s, the optimization iteration process is presented in Figure 5.30. After 21 iterations and 791 function calls, the solution converged. The optimal variables became stable and satisfied the terminal condition.

Iter	F-count	Max {F,constraints}	Step-size	Directional derivative	Procedure
1	71	2.145e+004	1	0.467	
2	107	57.48	1	0.000674	Hessian modified
3	143	1.012	1	2.14e-005	
4	179	0.4759	1	-3.39e-006	
5	215	0.4731	1	-9.87e-006	Hessian modified
6	251	0.4725	1	-1.83e-005	Hessian modified twice
7	287	0.4679	1	-4.6e-006	Hessian modified
8	323	0.5199	1	-7.77e-005	Hessian modified
9	359	0.4677	1	-5.2e-007	Hessian modified twice
10	395	0.4721	1	-2.02e-005	Hessian modified twice
11	431	0.4685	1	-6.48e-007	Hessian modified twice
12	467	0.4684	1	-9.73e-006	Hessian modified twice
13	503	0.474	1	-2.17e-005	Hessian modified twice
14	539	0.4676	1	-8.4e-007	Hessian modified twice
15	575	0.4676	1	-5.02e-007	Hessian modified twice
16	611	0.4676	1	-6.05e-007	Hessian modified twice
17	647	0.4676	1	-8.65e-007	Hessian modified twice
18	683	0.4676	1	-1.76e-006	Hessian modified twice
19	719	0.4679	1	-7.14e-006	Hessian modified twice
20	755	0.4676	1	-1.38e-006	Hessian modified twice
21	791	0.4676	1	-3.5e-007	Hessian modified twice

Optimization terminated successfully:  
Magnitude of directional derivative in search direction  
less than 2\*options.TolFun and maximum constraint violation  
is less than options.TolCon

Figure 5.30 Optimization process at t=3000s

The optimization utilized in the designed control strategy is called at each time step in the entire system dynamic simulation. Under the condition of  $u_m=1$ , the dynamic responses of the overall HWH system are depicted in Figure 5.31 and Figure 5.32.

The temperature difference between the supply and return water remained between 14.31 to 27.21°C as illustrated in Figure 5.31(a). The return water temperature from the east zone ( $T_{zes}$ ) presented in Figure 5.31(b) shows lower values around 9:00 and 18:00. This is due to additional heat gains in the zone at those periods. From Figure 5.31(c), it can be seen that the east zone air temperature tracks the optimal set points very well except for the influence of the initial conditions in the first few hours. Note also that the optimization failed between 17:30 to 18:30 because the zone air temperature set points are lower than the lower boundary. The reason behind this is that the optimization approach cannot always strictly satisfy all constraints. In other words, the optimization for the HWH system is not able to obtain the feasible solution (optimal values) all of the time. In spite of this, the total circulating water mass flow rate in the optimal case (Figure 5.31(d)) is 43.6% less than the total design value.

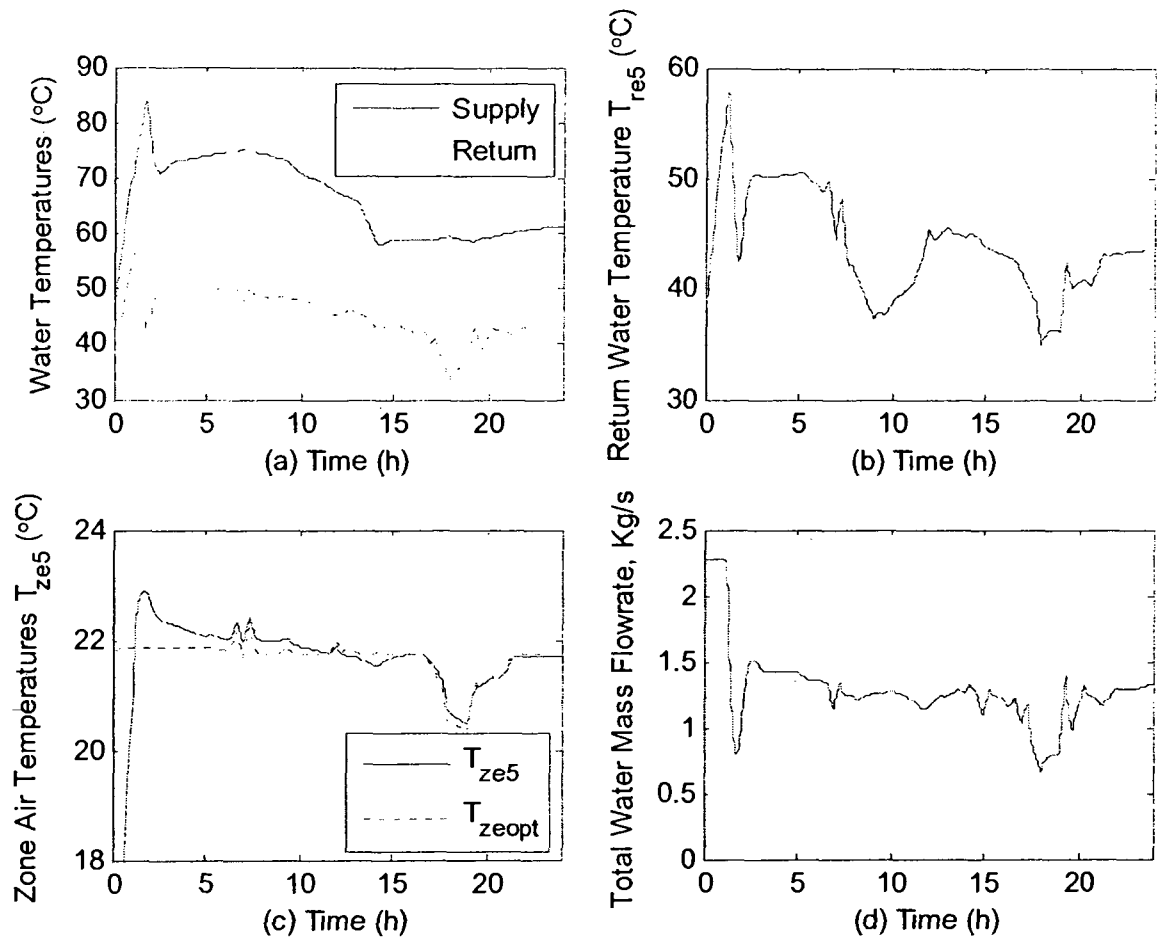


Figure 5.31 Dynamic responses of the optimal system outputs

The dynamic responses of the optimal control signals are depicted in Figure 5.32. It can be seen from Figure 5.32(a) that the fuel control signal response follows the variation of the heating load. By comparing the water mass flow rates in the four zones on the 5<sup>th</sup> floor heating system, it is noted that the peak water mass flow rate occurs at different time. This is due to the fact that the additional gains such as solar radiation and internal heat gains in the four zones occur at different time. As a result, not only thermal comfort is improved, but also the energy consumption is decreased because of the utilization of the additional heat gains and the reduction in the circulating mass flow rate of water.

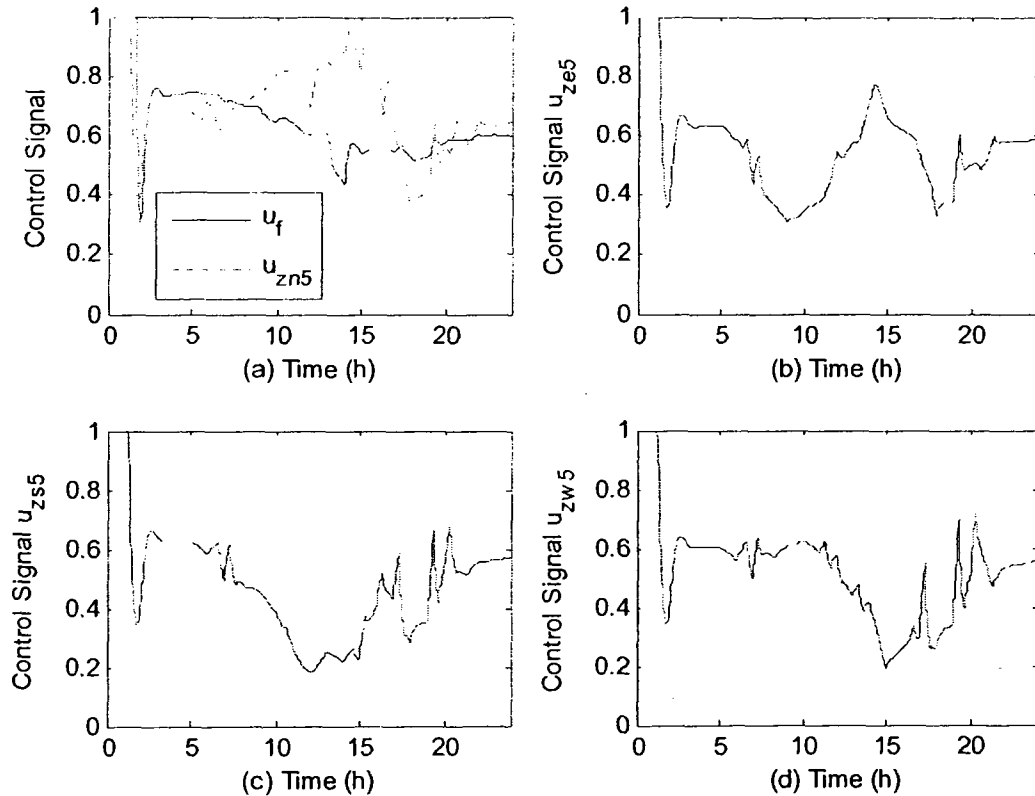


Figure 5.32 Dynamic responses of the control signals in the optimal control system

In order to evaluate the energy savings resulting from the designed optimal control strategy, comparisons were made with a typical operation strategy for the HWH system. In the typical HWH control strategy, the supply water temperature from the boiler is controlled by a fixed gain PI control. The set points of the supply water are chosen as a constant value, and the water mass flow rate in the overall system remained at the design value. The typical daily outside air temperature ranged from  $-13.2$  to  $-5^{\circ}\text{C}$ ; while the solar radiation and internal gains were within  $0\sim 112.5\text{W/m}^2$  and  $5.4\sim 17.4\text{W/m}^2$  respectively.

The results from simulation runs are plotted in Figure 5.33 for comparisons. From Figures 5.33(a) and (b), it is noted that the supply and return water in the optimal operation decreased by  $14.91$  and  $21.31^{\circ}\text{C}$  on average compared with those in the typical

control strategy. The temperature difference between the supply and return water in the optimal operation is increased compared with that in the typical operation. These results imply that energy savings can be achieved by using the optimal control strategy. The fluctuation in the zone air temperature ranged from 25.01 to 31.82 °C in the typical operation. This was not only caused by uncontrolled zone air temperatures but also resulted from the high set points of the supply water temperature. However, these disadvantages are overcome by the optimal control results displayed in Figure 5.33(c). The control signals of the fuel and the mass flow rate of water ( $u_{ze5}$ ) are plotted in Figures 5.33(d) and (e) respectively. Lower fuel consumption resulted from lower heating load requirement in the optimal system. It is also noted that, about half of total mass flow rate of water is required (Figure 5.33(f)) for running the HWH system with the optimal control strategy compared with that in the typical control strategy.

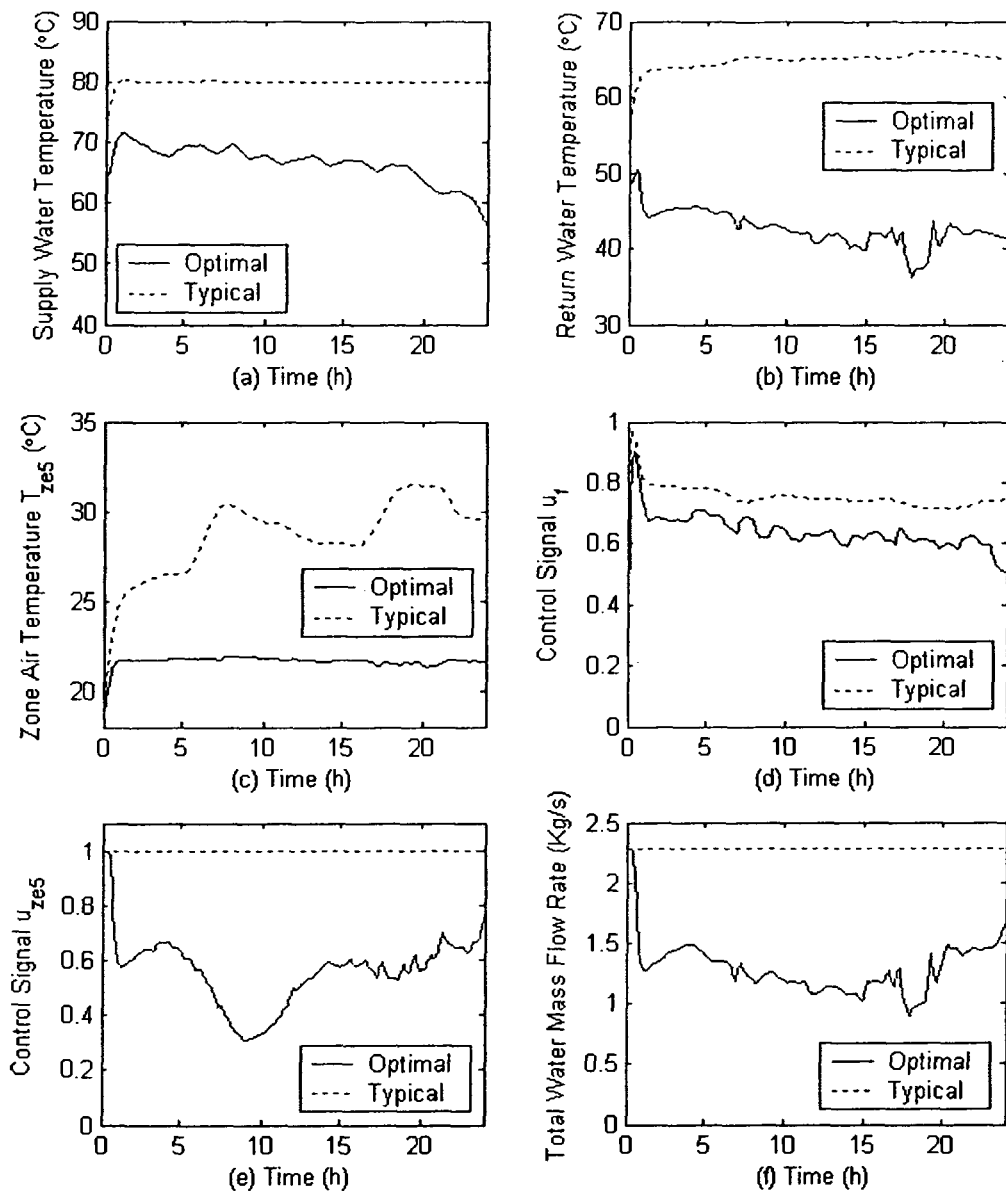


Figure 5.33 Comparison of dynamic responses between optimal and typical control

The energy consumed in the optimal and the typical control systems is compared and given in Table 5.5. From this table, it shows that the fuel consumption and pumping energy are decreased by 18.22% and 77.14% respectively in the optimal control system.

Table 5.5 Energy consumptions over one day

System control	Electricity		Fuel	
	KWH	%	GJ	%
Typical	13.91	100	14.71	100
Optimal	3.18	22.86	12.03	81.78

# **Chapter 6 Model-Based Fault Detection Diagnosis and Fault Tolerant Control of HWH Systems**

## **6.1 Introduction**

Due to more and more complexity and larger and larger scale of modern control systems in HVAC applications, safety, reliability and energy efficiency are paid greater attention. The reason behind this is that if a fault takes place in the systems, it will result in uneconomic operation, create safety problems and result in poor indoor environment. In order to decrease the risks caused by faults, fault detection and diagnosis and fault tolerant control techniques have been used to improve both the system reliability and optimal operation under faulty situations. As an important support of FTC systems, FDD techniques have been developed much earlier than FTC techniques in the recent decades. In addition, in most applications for implementing the FTC strategies, faults should be detected and isolated in advance.

From the literature surveys HWH system failures could be categorized as design, installation and operation faults. From system operation point of view, the faults could be divided into measurement faults and process faults. In this study, the faults caused by abrupt and degradation in system operation are considered.

Because faults in HWH systems cannot always be avoided, there is growing interest in the development of FDD methodologies for HWH systems. Faults existing in HWH systems not only lower thermal comfort of occupants but also result in waste of energy and corrupt system performance. To detect and isolate faults, two methodologies have been developed such as by using experimental data and by obtaining information

from reference models. For model-based FDD systems, most FDD processes need information from the system dynamic performance with and without fault conditions. The information is compared and analyzed to identify what kinds of faults occurring in the systems.

After the faults are detected and identified, they should be taken care in order to improve system performance. This could be achieved by designing fault tolerant control strategies. The idea of the tolerant control is that the control system can still operate properly whatever faults may have occurred in the system. In order to maintain good control, additional redundant information is required. The additional redundancy can be supported by either hardware redundancy or software redundancy; the software redundancy is more often used in practice.

The FTC systems can be designed without or with FDD information. In the FTC systems without FDD information, the controllers are designed based on both fault and fault free situations. In the FTC systems with FDD information, the faults are isolated first, and then associated control strategies are reconfigured automatically to smoothly and quickly change to the correct control strategies.

The FTC systems are also classified as passive FTC and active FTC systems. In passive FTC systems, the controllers are designed with fixed control structure by considering fault conditions in system operation. On the other hand, active FTC systems are designed based on the degree of the faults to adjust the control system parameters and/or control structure in order to maintain good performance. Therefore, prior knowledge of any kinds of faults is required in designing active FTC systems. Both

passive and active FTC systems are necessary to maintain system stable and ensure proper operation under fault situations.

In this chapter, the methodologies of the FDD and FTC systems are developed in the following section. Three fault situations are investigated by taking into account measurement and process faults in the HWH system in the case study section. The FTC systems are designed, simulated and explained for each case.

## **6.2 Methodologies for the FDD and FTC strategies**

In this study, model-based FDD and model-based FTC systems are considered for the HWH system. In other words, there are two separate models in the FTC. One is the normal dynamic model, which is the fault free model (reference model). By using this model, correct information of the dynamic system responses are obtained based on the operation. The other is the actual dynamic system model with fault conditions. Note that in spite of the fault, the normal system model and the actual system are different. Parameter uncertainty is considered in the actual system. This is because system uncertainties always exist; as a result, a perfect dynamic model can never be developed identical to the actual dynamic system. The dynamic responses from the reference model and the actual system model will be employed to compare the FDD and FTC simulation results.

### **6.2.1 Fault detection and diagnosis of MFMZ HWH system**

The block diagram of the model-based FDD strategy is depicted in Figure 6.1. The strategy consists of separate systems: a fault free system model (Normal) and the actual system (Fault). Each system consists of 241 dynamic variables, and one FL-PI

controller and 37 FLAC controllers for the boiler and the zone air temperature regulation respectively. Note that both the systems have the same disturbances and set points.

Both systems have to be simulated, and the outputs from the two systems have to be compared. Then, the deviation is analyzed by fuzzy inference engines to detect and diagnose faults, and the degree of confidence of the faults is estimated. Note that the prior knowledge related to the faults should be available before initialing the FDD process. Consequently, it is required to determine the parameter(s) which significantly affects the system performance. This knowledge will be useful in using fuzzy logic inference systems. Although the relationship between the deviation and the fault level cannot be identified accurately, FISs have the flexible and adaptable ability to obtain the relationship based on the understanding of HWH systems. In addition, the system fault level can be recognized based on the deviation between the measurements from the two systems.

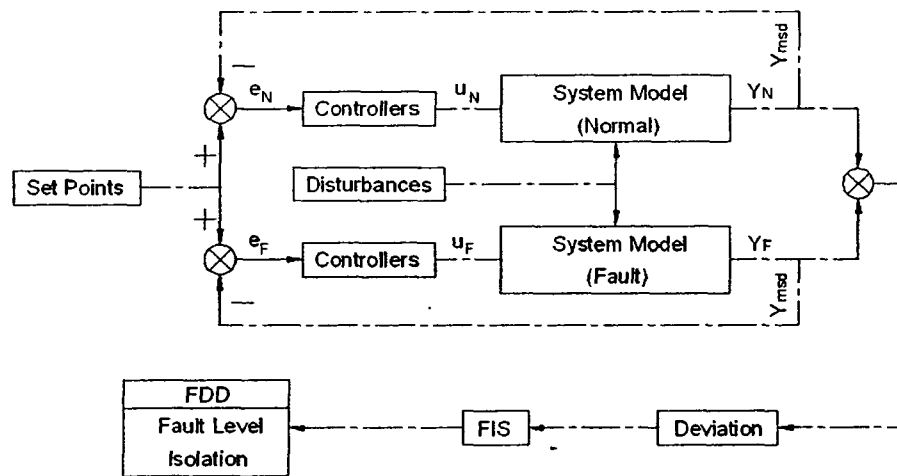


Figure 6.1 Model-based FDD configuration

The following FDD simulations are presented along with fault tolerant control results.

### 6.2.2 Fault tolerant control of MFMZ HWH system

When a fault is found and isolated in an actual (fault) system, to improve system operation, the FTC should be applied on the failed system. A block diagram of the model-based FTC is shown in Figure 6.2. The FTC system is composed of set points, controllers, measurement from the actual system and the error correcting function  $f(X, Y)$ .  $X$  and  $Y$  refer to the state variables and measurement variable respectively. From this figure it can be seen that the error between the reference points and the measurement ( $Y_{msd}$ ) of the actual system is corrected by the error correcting function  $\Delta Y$ . This correction is computed according to the function  $f(X, Y)$ , which is related to the state space variable “ $X$ ”, the measurement from the two systems and the FDD evaluation. After the adjustment of the error, the signal “ $e_F$ ” is sent to the controller in the FTC system. Note that the error correcting function could be different depending on what kind of fault and the degree of the fault.

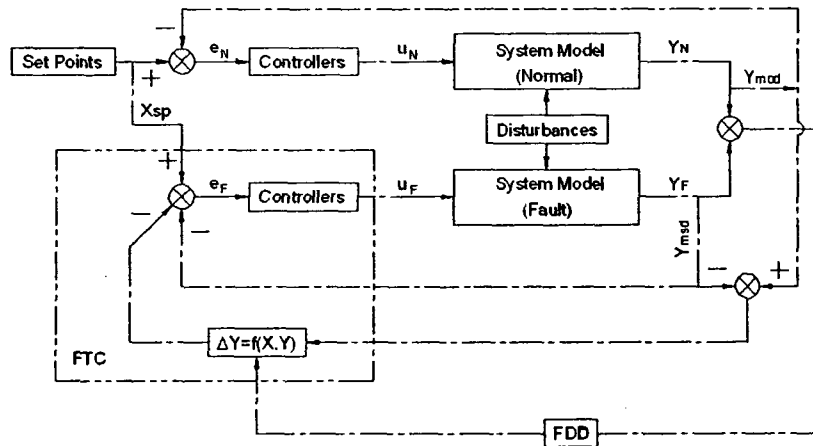


Figure 6.2 Model-based FTC configuration

The error correcting function  $\Delta Y$  can be expressed in Equation (6.1).

$$\Delta Y = f(X, Y) = \sum_{i=1}^n [\alpha_{Fi} (\beta_0 + \beta_1 \gamma_{FLi})] \quad (6.1)$$

where  $\alpha$ ,  $\beta$  and  $\gamma$  are fault factors:  $\alpha_{Fi}$  indicates fault isolation factor, and  $\beta$  refers to fault level estimation factor; while  $\gamma_{FL}$  refers to estimated value of fault level. Note that the factor  $\alpha_{Fi}$  takes binary value 0 or 1. If the faults are identified and the fault level  $\gamma_{FL}$  is greater than 0.2,  $\alpha_{Fi}=1$ ; otherwise,  $\alpha_{Fi}=0$ . The estimated fault level  $\gamma_{FL}$  is in the range of [0,1].  $i$  indicates the  $i^{\text{th}}$  fault that is isolated based on FDD in the control system. Generally, a fault level of 20% is considered adequate in HVAC applications.

In the PI controller, the error  $e_F$  is required to feed as input signal in order to calculate the output signal from the controller. The error  $e_F$  can be computed based on the set point, the measurement and the error correcting function shown in Equation (6.1). To this end, the error becomes

$$e_F = X_{sp} - Y_{msd} - \sum_{i=1}^n [\alpha_{Fi} (\beta_0 + \beta_1 \gamma_{FLi})], \quad Y_{lowbnd} \leq Y_{msd} \leq Y_{upbnd} \quad (6.2)$$

It is noted that the formulation of the error equation is distinguished based on what kinds of faults and the degree of faults occurred. Because all of the variables utilized to estimate the error in Equation (6.2) are bounded, the error  $e_F$  is also bounded depending on the type of fault and its fault level.

### 6.3 Case studies

In this section, two types of faults such as measurement and process faults are considered in the design of FTC system strategies. Measurement faults normally take place with cheaper instrument (sensors and transducers), erroneous installation, electrical and communication problems and improper maintenance. For instance, the supply water

temperature ( $T_s$ ) sensor fault is considered in the FTC system. The supply water temperature measurement fault will consume more energy as well as thermal comfort problems for the overall system. On the other hand, process faults such as degradation faults happen very often and are more difficult to identify and regulate. Abrupt faults such as blocked or broken pipes, blocked and leaky valves normally occur in large and old HWH systems; while degradation faults such as reduction in boiler efficiency, reduced heat transfer efficiency of baseboard heater and decrease in circulation pump efficiency can be found in many real system operations. In this study, the supply water temperature is considered as measurement fault; while the heater efficiency degradation and partially blocked control valve fault are considered as the process faults. The FTC systems are designed for the above mentioned faults, and simulation runs are made in the following sections.

In the simulation conducted, the following parameter uncertainties were assumed in the actual dynamic system: the overall heat transfer coefficient of the outside wall was increased by 20% of the design value, and the boiler efficiency is reduced by 5% of the design efficiency.

When a fault is identified, the degree of the fault was examined by a FIS depending on the deviation of state variables. As shown in Figure 6.1, the deviation of the outputs between the actual system ( $Y_F$ ) and the reference model ( $Y_N$ ) is employed to calculate the fault level. As an example for the supply water temperature, the membership functions of the linguistic variables used in the FIS, the deviation of the supply water temperature and the fault level, are presented in Figures 6.3(a) and (b). Four if-then rules were defined for each linguistic variable using the Mamdani type of fuzzy engine. The

same method could be used to estimate the fault level associated with different state variable deviations.

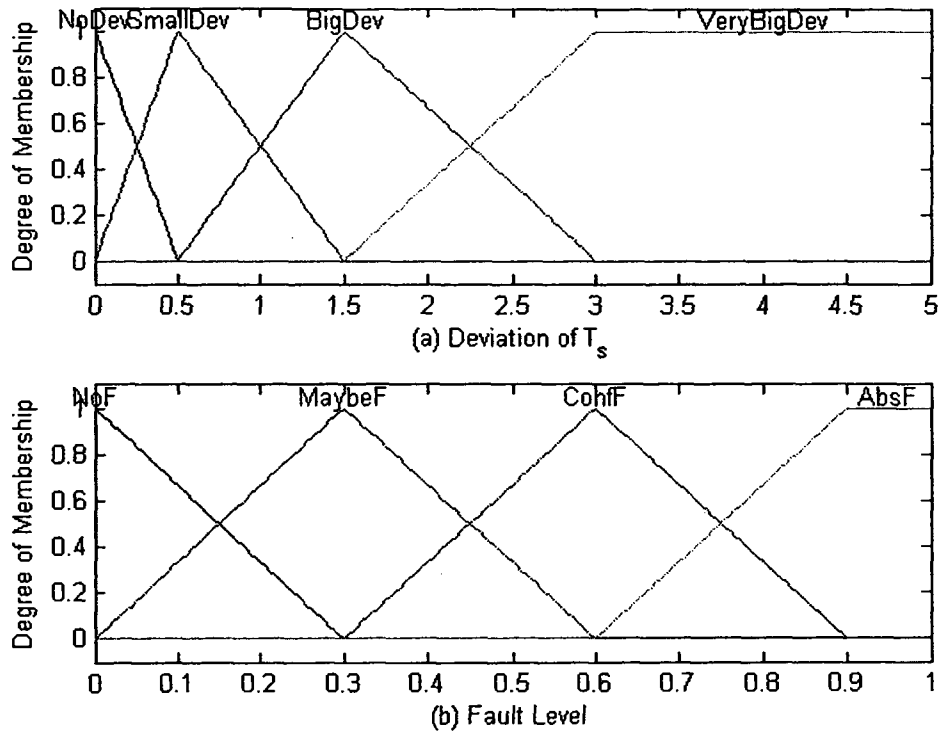


Figure 6.3 Membership functions of deviation of  $T_s$  and fault level

### 6.3.1 FTC system for measurement fault

In order to design the FTC system dealing with a measurement fault, the sensor fault of the supply water temperature from the boiler is assumed. The measured supply water temperature from the actual system is assumed to be  $3^\circ\text{C}$  higher than that of the fault free system in the first 8 hours; while it is assumed to be  $2^\circ\text{C}$  lower than that in the normal system in the last 8 hours. No measurement fault was deemed to have occurred in the other hours.

The simulation results are presented in Figure 6.4 and compared with the dynamic responses of the normal fault free system and the actual system with the fault. The

dynamic responses such as the supply and return water temperatures, the fuel control signal and the zone air temperature are depicted in Figures 6.4(a)~(d) respectively. From Figure 6.4(a) it can be seen that the supply water temperatures offset about 3 and 2°C between the fault and fault free systems in the first and the last 8 hours respectively. However, the responses of the return water temperature to the boiler shown in Figure 6.4(b) displays opposite trend. The fuel control signal in the actual system given in Figure 6.4(c) implies more fuel is consumed in this situation because of the uncertainty in the fault system and the fault. The zone air temperature ( $T_{ze5}$ ) fluctuation in the actual system (Figure 6.4(d)) is 0.5°C greater than that in the normal system. By comparing the magnitude of the deviation of these outputs, it is apparent that the supply water temperature deviation should be used to detect the fault. To this end, by using the FIS, the  $T_s$  sensor fault is estimated, and its fault level is presented in Figure 6.4(f). It is obvious that the fault level displays higher value in the first and the last 8 hours; therefore, the  $T_s$  measurement fault is implied in those periods.

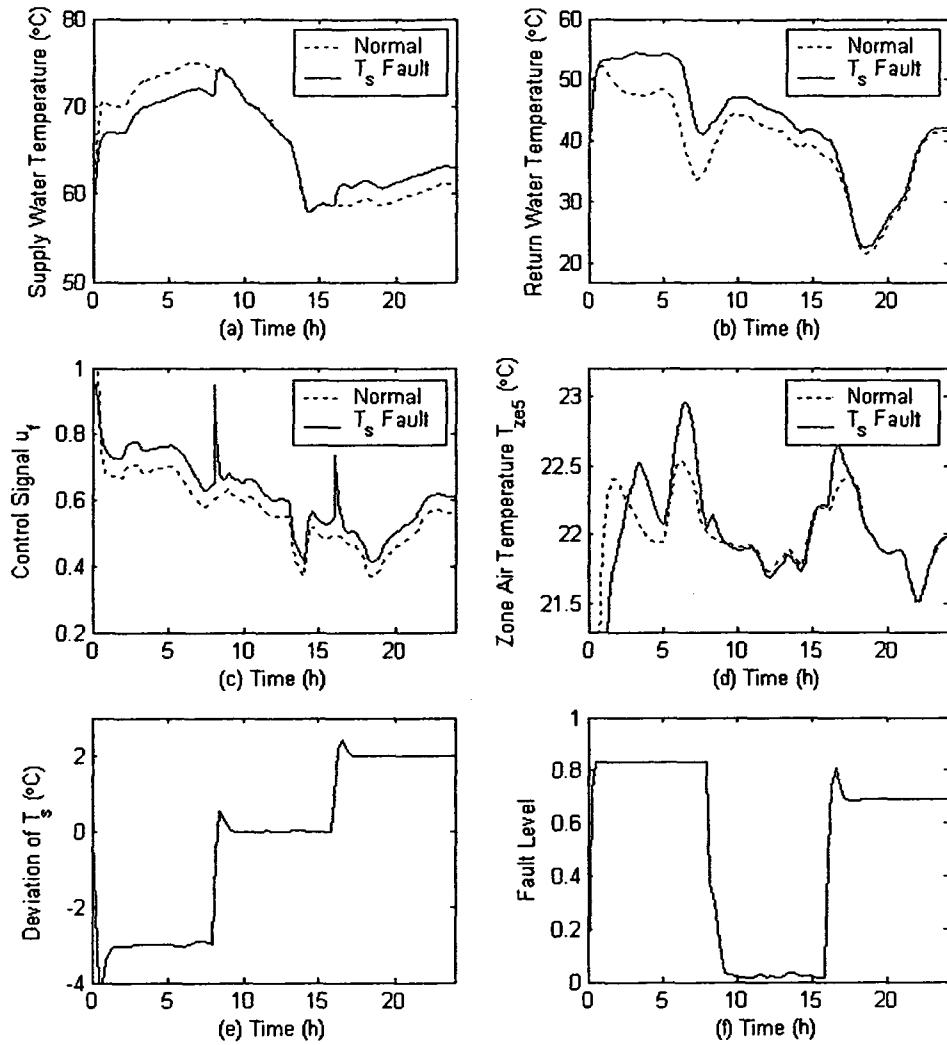


Figure 6.4 FDD for the  $T_s$  sensor fault

After isolating the  $T_s$  sensor fault, its impact on other system outputs can be minimized by designing a FTC system. The configuration of the FTC system for the  $T_s$  fault is presented in Figure 6.2. The major objective of the FTC system is to utilize the FDD information and the deviation between the measurement from the normal system and the actual system to correct the error signal  $e_F$ . The corrected error signal is then sent to the PI controller to regulate the fuel firing rate.

The dynamic responses of the FTC system is tested and depicted in Figure 6.5. In this figure the responses from three systems are compared: the normal system, the actual system with the fault and the system with the FTC strategy. As shown in Figure 6.5(a), the responses of the supply water temperatures from the normal system and the FTC system are very similar to each other. It means that the FTC system is able to completely deal with the measurement fault and give good tracking close to the fault free condition. The offset in the return water temperature and the fuel control signal in the system with the FTC presented in Figures 6.5(b) and (c) are due to the increased heating load. As shown in Figure 6.5(d), the zone air temperature fluctuation in the control system with the FTC is  $0.3^{\circ}\text{C}$  less than that in the actual fault system. By observing the deviation and the fault level of  $T_s$  given in Figures 6.5(e) and (f), it can be seen that large improvement can be achieved in dealing with the measurement fault using the FTC strategy.

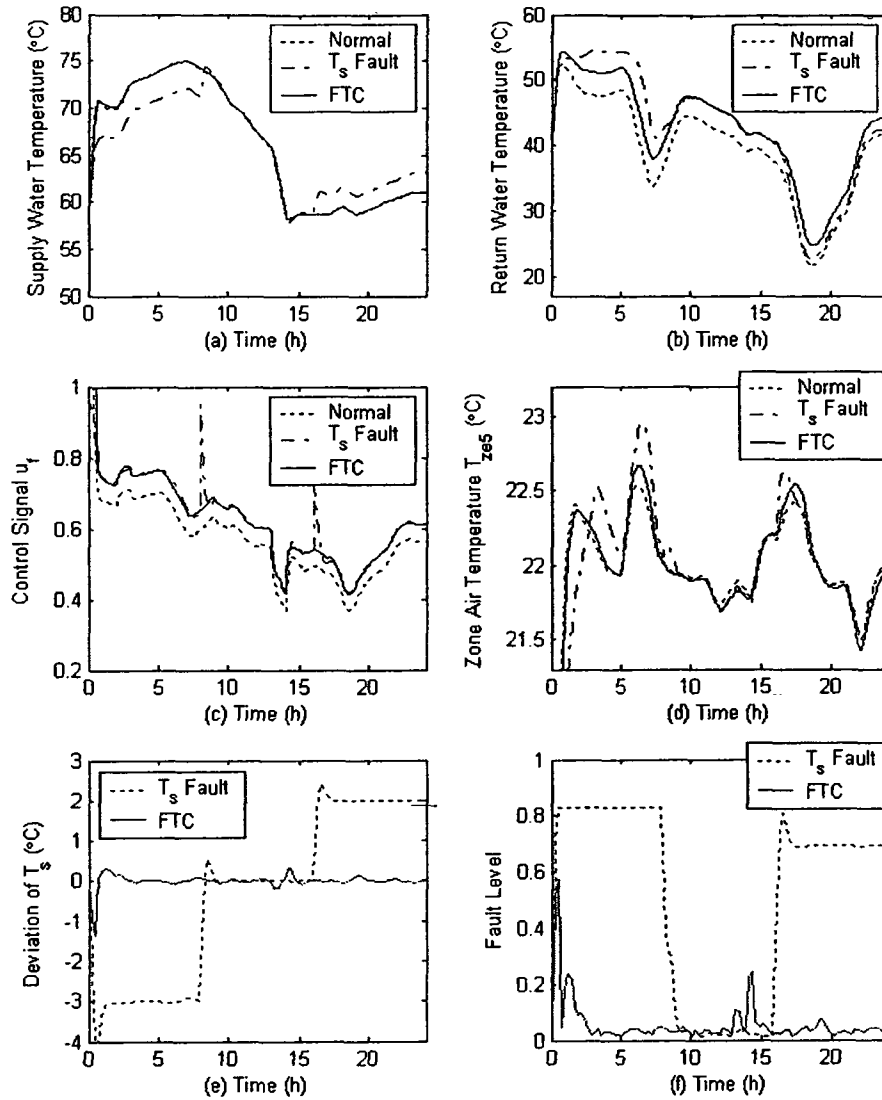


Figure 6.5 Responses of the FTC system for the  $T_s$  measurement fault

### 6.3.2 FTC system for process fault

In this section, the process fault problem such as a single fault: baseboard heater efficiency degradation and a multi-fault: baseboard heater efficiency degradation combined with a partially blocked control valve is considered. The baseboard heater efficiency reduction could be considered as a sluggish fault because normally fouling in

the air and water-side of the baseboard heater is a slow process; while the blocked control valve could be simulated as an abrupt fault.

#### *FTC for the baseboard heater fault*

With the increase of time, dusts accumulate on the air-side surface; while solid materials foul on the water-side surface in the finned-tube baseboard heaters. This phenomenon happens in HWH systems commonly. It can be simulated as the baseboard heater efficiency degradation fault. As a result, heat transfer from the water-side to the air-side in the finned-tube decreases. Hence, the return water temperature will increase compared with that in fault free condition, and the heating control system asks for more water mass flow rate and/or higher supply water temperature from the boiler to reach the zone air temperature set point. A simple way to estimate the baseboard heater efficiency is defined in Equation (6.3) based on its return water temperature.

$$H_e = \frac{100(T_s - T_r)}{T_s - T_{rN}} \% \quad (6.3)$$

where  $T_r$  and  $T_{rN}$  indicate the return water temperatures in the actual system or the FTC system, and the normal fault free model respectively.

To simulate the heater fault, the baseboard heater in the east zone on the 5<sup>th</sup> floor was considered. A 25% increase in thermal resistance on the water-side was assumed to induce the fault.

The simulation results of the system outputs and the control signals are depicted in Figure 6.6. It can be seen from the dynamic responses given in Figures 6.6(a)~(d) that the zone air temperature has significant fluctuation caused by the heater fault. Thus, the zone air temperature is employed to identify the fault and the fault level of the heater fault and presented in Figure 6.6(f). The fault level indicates higher value due to

degradation of the heat transfer process in the heater. The resulting dynamic variation of the heater efficiency is plotted in Figure 6.6(e).

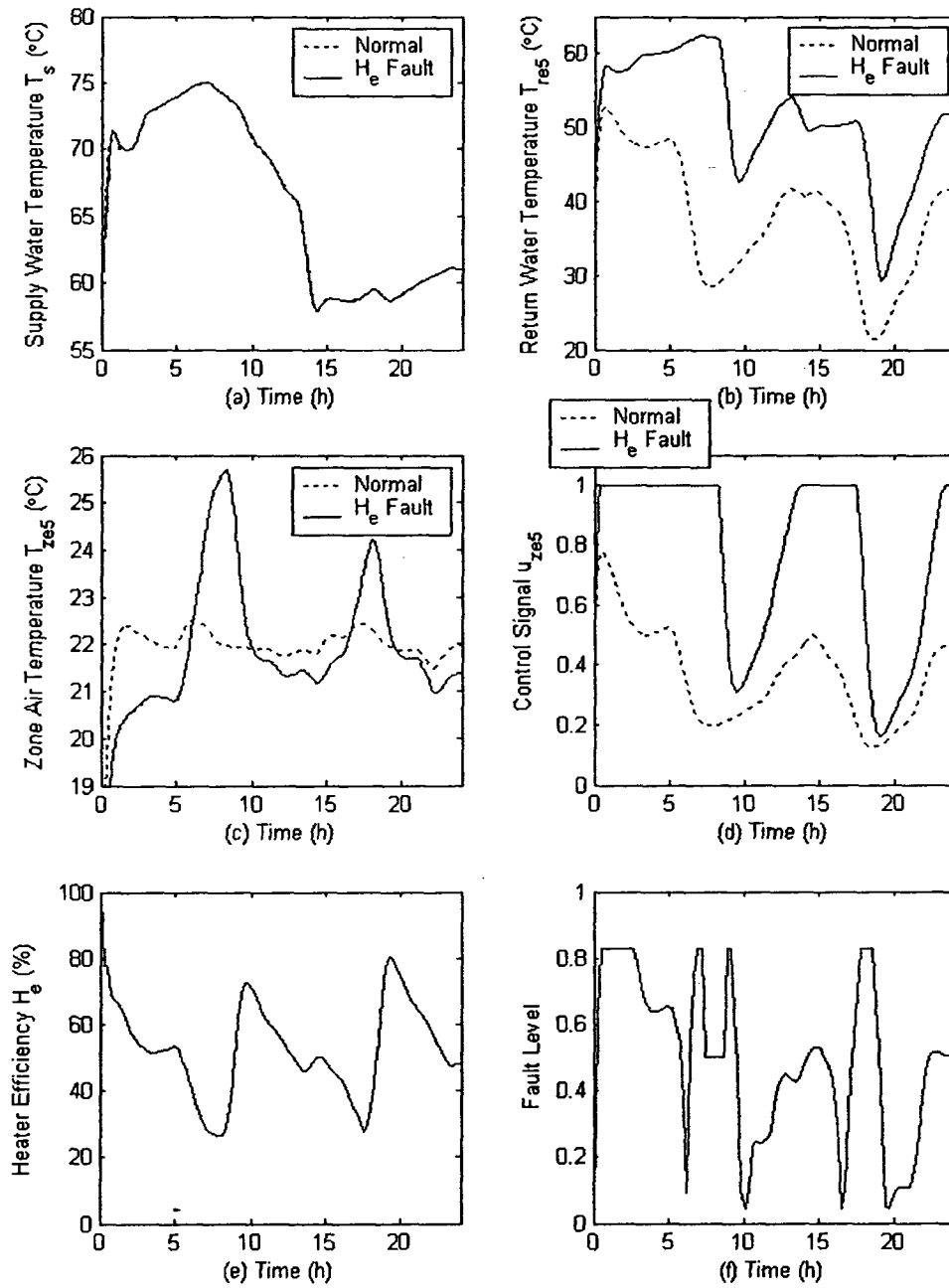


Figure 6.6 FDD for the baseboard heater efficiency ( $H_e$ ) fault

One way to compensate for the decrease in heater output is to increase the water mass flow rate. Nevertheless, the compensation of the heat output only based on increasing the water mass flow rate sometimes is not sufficient because the maximum water mass flow rate is limited by the hydraulic system configuration, system operation and the size of the control valve. Hence, the regulation of the supply water temperature from the boiler is essential in order to compensate the heat output from the heater under the fault situation. This strategy was implemented by designing on the FTC system shown in Figure 6.7. The key behind this FTC strategy is to correct the error input to the fuel firing rate controller according to the error correcting function. The error  $e_F$  is corrected based on the normal supply water temperature set point, the deviation between  $T_{sN}$  and  $T_{sF}$  and the fault level estimation from the FDD. The equation for computing the error is given in Equation (6.2). After the error correction, the error signal is fed to the controller  $C_{fF}$ , and then the output signal from the controller is used in the FTC system.

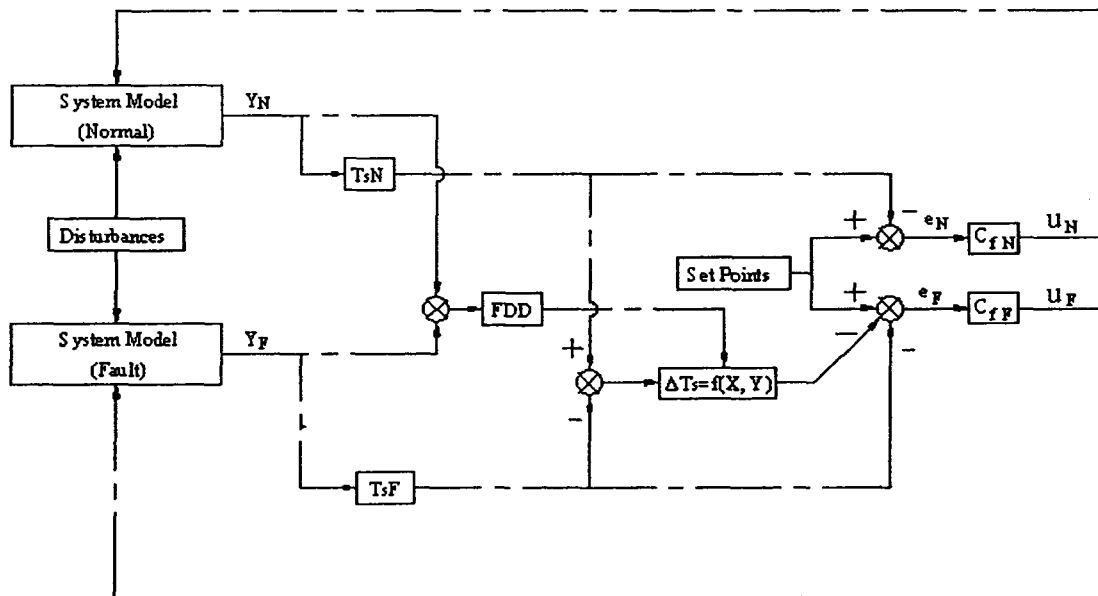


Figure 6.7 Configuration of the FTC system for the heater fault

The simulation runs were made with this FTC system and the results are displayed in Figure 6.8. Note that the dynamic responses of the three control systems are plotted in this figure for comparison. From Figure 6.8(a) it can be seen that the supply water temperature  $T_s$  in the FTC system is increased compared with those in the other systems. This is because more heat output is required in order to balance the heat requirement between the heat output from the heater and the heating load of the zone. The supply water temperatures in the normal and the actual systems remained almost identical due to the same set points of the supply water temperature. The responses of the return water temperature in the systems given in Figure 6.8(b) are associated with the changes of the water mass flow rate control signals presented in Figure 6.8(d). The water mass flow rate in the FTC system is decreased compared with that in the fault system because of the increased supply water temperature. The zone air temperature fluctuations shown in Figure 6.8(c) are 0.93, 5.17 and 1.26°C for the normal system, the fault system and the system with the FTC strategy respectively except for the influence of the initial conditions. Thus, greater improvement in the system performance is realized by using the FTC strategy. In addition, the heater efficiency depicted in Figure 6.8(e) in the FTC system is enhanced up to 72% compared with that of 44% in the fault system. The main reason is that the difference between the supply water and the return water temperature in the FTC system is higher than that in the fault system. As observed from Figure 6.8(f), the degradation of the heater efficiency could be well compensated by the FTC strategy. In other words, the appropriate operating periods could be extended even though the heater fault exists in the heating system.

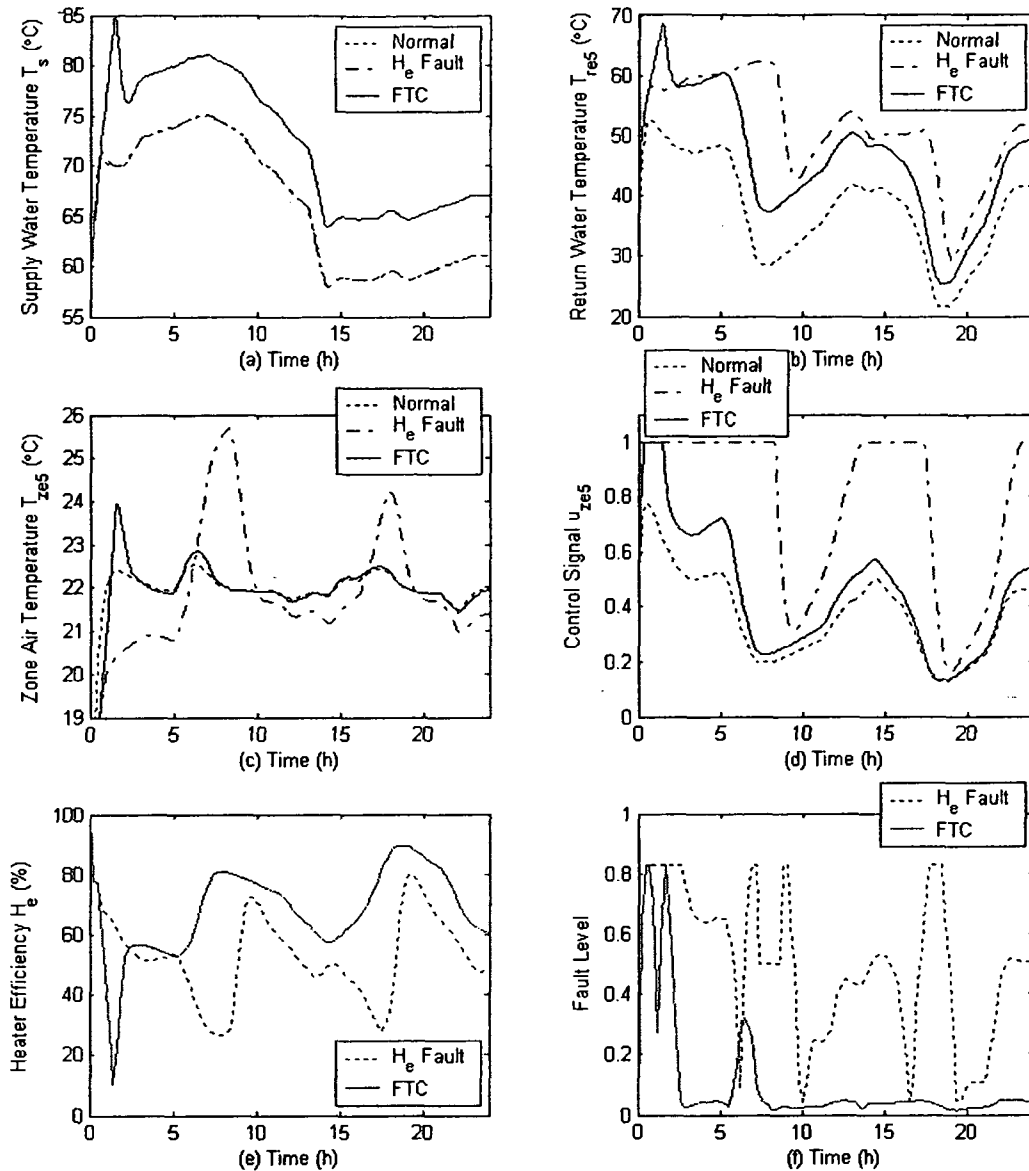


Figure 6.8 Dynamic responses of the FTC system for the heater fault

***FTC for a multi-fault: heater fault combined with control valve fault***

In this case, a multi-fault such as the heater efficiency degradation and a partially blocked control valve fault is taken together to account for both FDD and FTC systems. To begin with, the FDD for the multi-fault should be identified in advance. Therefore, the

multi-fault is addressed in order to identify the important parameters for the FDD analysis.

The fault situations are assumed as follows: the heater efficiency degradation is the same as in Section 6.3.2(b); the control valve is blocked 60% of its full water mass flow rate after 8 hours. Note that the opening of the valve is not the same as 60% of its fully opening because of the nonlinear property of the control valve. The multi-fault is considered taking place in the east zone on the 5<sup>th</sup> floor HWH system.

As stated previously, the heater efficiency degradation fault can be isolated based on the zone air temperature response mentioned in Section 6.3.2(b). On the other hand, the control valve fault could be identified by two state variables:  $T_{ze5}$  and  $T_{re5}$ . The FIS is designed with two antecedents given in Figure 6.9 and utilized to identify the control valve fault.

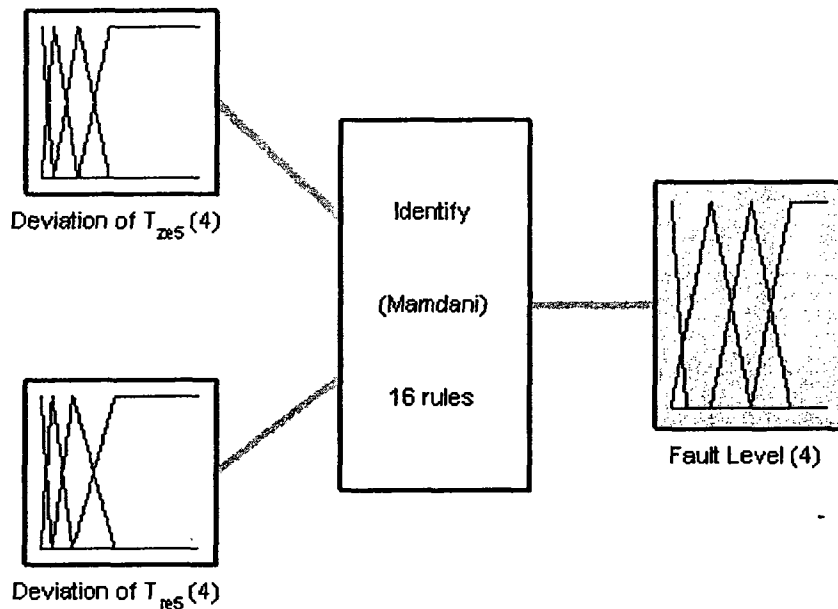


Figure 6.9 The FIS used to isolate the control valve fault

According to the analysis and simulation results from the multi-fault, the state variables such as the zone air temperature and the return water temperature were identified as state variables most suitable to detect and isolate the multi-fault. The structure of the FIS used in the FDD is identical for both state variables as shown in Figure 6.9 except for the difference in the membership functions.

The FDD test results for the multi-fault are depicted Figure 6.10. From Figure 6.10(a), it can be seen that the supply water temperature responses are almost the same as in the normal system and the multi-fault system because of the identical set points of the supply water temperature. As shown in Figures 6.10(b) and (d), the higher return water temperature in the multi-fault system compared with that in the normal system is as a result of both the control valve fault and the heater efficiency fault. The zone air temperature dynamic responses are shown in Figure 6.10(c) for the two systems. The swings in  $T_{ze5}$  in the normal system and the multi-fault system are 0.93 and 6.45°C respectively. Hence, the fluctuation of the zone air temperature should be controlled properly and compensated in order to improve thermal comfort of the occupants. The multi-fault is detected based on the deviations of the zone air and the return water temperatures illustrated in Figure 6.10(e). The fault level estimation for the multi-fault is presented in Figure 6.10(f). As shown in this figure, it is apparent that the system has fault(s) but the type of fault cannot be isolated by using single FIS.

To discriminate the multi-fault existing in the system, two FISs were employed to separate the faults individually. As a result, one FIS is used for the heater fault diagnosis according to the zone air temperature deviation, and the other is utilized for the control valve fault isolation based on both the deviations of the zone air and the return water

temperature. The FDD results are depicted in Figures 6.10(g) and (h). It can be seen that the multi-fault could be isolated with adequate confidence by using different FIS for each fault.

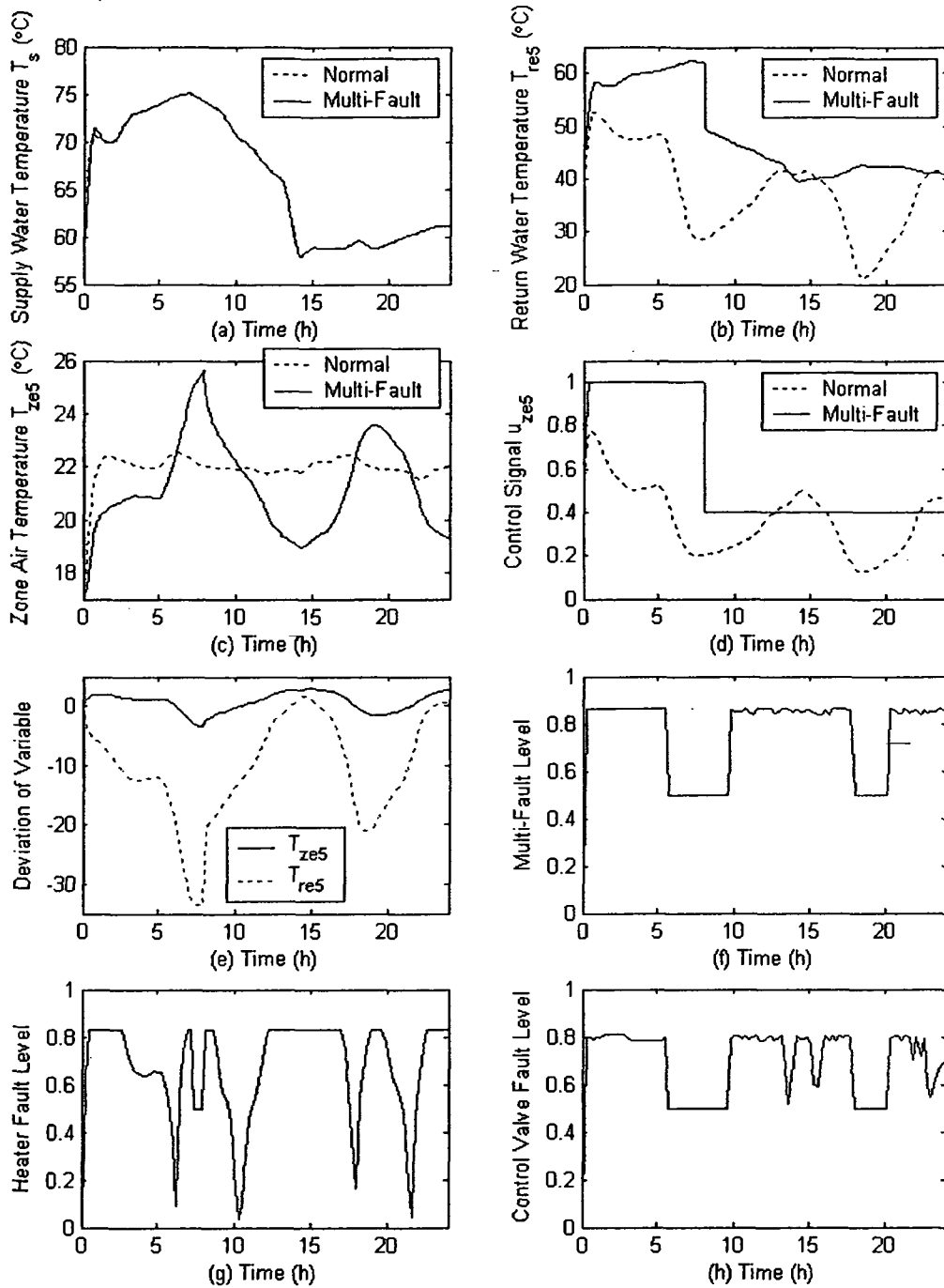


Figure 6.10 FDD for the multi-fault

In order to regulate the heat output from the baseboard heater, not only the water mass flow rate into the heater should be changed, but also the supply water temperature from the boiler has to be varied if the heater output is not adequate to meet the heating load requirement. A FTC system was developed for this type of multi-fault system, and its configuration is the same as given in Figure 6.7 with the exception of the error signal  $e_F$ .

The simulation runs for the three control systems are depicted in Figure 6.11. As seen from Figure 6.11(a) in the FTC system, the supply water temperature is greater than that in Figure 6.8(a) especially after 14 hours. This is due to the limited heat output from the baseboard heater caused by the multi-fault. Because of the increase in the supply water temperature, the response of the return water temperature in the FTC system shown in Figure 6.11(b) is more close to the normal system response. As illustrated in Figure 6.11(c), it can be seen that the biggest zone air temperature fluctuation takes place in the multi-fault system; while the smallest zone air temperature swing happens in the normal system. The zone air temperature response in the FTC system is similar to the temperature in the normal system. As seen from Figure 6.11(d), the control ability (observed by  $u_{ze5}$ ) of the control valve in the FTC system is improved in the FTC system compared with the control signal  $u_{ze5}$  in the multi-fault system. The reason behind this is that the increased supply water temperature brings additional heater output from the heater. In addition, from the zone air temperature responses showing the deviation in  $T_{ze5}$  without FTC (Figure 6.11(e)), and with FTC (Figure 6.11(f)), it can be stated that, greater thermal comfort improvement could be achieved by using the FTC system. The deviation of the zone air temperature in the FTC system ranges from  $-0.25$  to  $0.25^\circ\text{C}$  most of time;

while the deviation in  $T_{ze5}$  in the fault system without FTC range between  $-2.9$  to  $3.5^{\circ}\text{C}$ . From the simulation runs, it realizes that the multi-fault could be handled using the proposed FTC approach to diminish the undesired zone air temperature fluctuation and saving pumping energy.

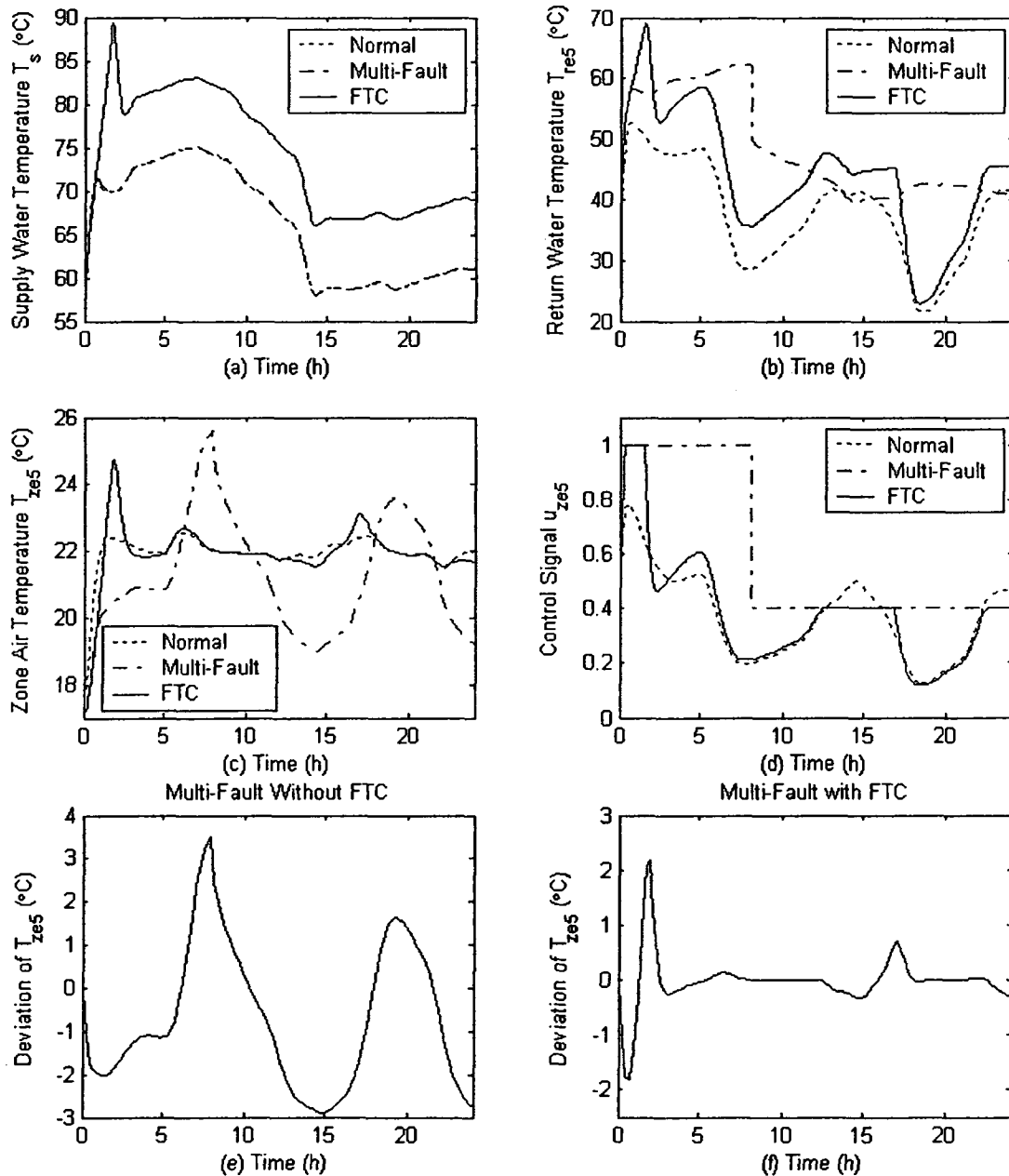


Figure 6.11 Dynamic responses of the FTC system for the multi-fault

# **Chapter 7 Conclusions, Contributions and Recommendations for Future Research**

## **7.1 Conclusions and contributions**

The development of the comprehensive dynamic model, the design and simulations of the advanced control strategies and the model-based FDD and FTC systems for the high-rise building HWH system have been presented in this thesis. The conclusions and contributions are stated in the following three sections: dynamic modeling of the overall HWH system, design of intelligent control strategies and model-based fault tolerant control strategies.

### **7.1.1 Dynamic modeling of the overall HWH system**

An overall dynamic HWH system model is needed not only for designing and simulating control strategies, FDD and fault tolerant control systems, but also for evaluating energy consumption, thermal comfort and fault level. The overall HWH system model was developed by the following steps. First of all, the single room dynamic model was developed based on first principles such as mass, momentum and energy balances. Then, the component (heater) model order was decreased by using a reduction technique. After that, the one room reduced-order model was extended to the single floor multi-zone (SFMZ) HWH system. By applying an aggregation technique for temperature dynamics of the SFMZ system, the SFMZ model was extended to the multi-floor multi-zone (MFMZ) model consisting of 241 dynamic equations. The overall system dynamic model can be used to design control strategies, compute electrical and fuel consumptions,

examine thermal comfort level, isolate faults and design model-based fault tolerant control systems.

Specific conclusions from the dynamic model simulations are summarized below:

(1) From one room model simulation results, it was noted that the system dynamic responses consist of fast-natural-convection driven air flow responses and slow zone air temperature response. The ratio of time scale between these responses ranged from 6 to 12.

(2) The density driven air flow rate in the vertical channel of the heater ranged between 0.007 to 0.019Kg/s with the corresponding water temperature ranging between 30 to 85°C.

(3) The ratio of heat output from the bare pipe to the finned-tube baseboard heater ranged between 0.082~0.125 depending on the zone air temperature and the water temperature in the tube.

(4) In order to achieve design zone air temperature with the design water mass flow rate, the supply water temperature into the heater should be less than its design value; this was due to the safety consideration such as additional heat transfer area in the design process. A relationship between outside air temperature and supply water temperature was developed for the HWH system.

(5) The supply water temperature has significant impact on the heat output from the baseboard heater. In other words, it is reasonable to regulate the water temperature to match the heating load in the system.

(6) Compared with one room model dynamic responses the full order model, the full order with zonal model and the reduced-order model had accuracies comparable to

the model complexity. It was found that the reduced-order model had enough accuracy and as such it was used to develop multi-zone models.

(7) The pressure drops in the control valves ranged from 40 to 60% of the total available pressure difference, and this corresponds to the normal range for good control.

(8) As expected on different floors, the pressure difference between the supply and return water has different values depending on the location and the configuration of each floor heating system.

(9) From the zonal model simulations, it could be seen that the distribution of the zone air temperature and air mass flow rate in the room varied according to the natural convection property. The air temperature decreased as the air flow rises up; while the air mass flow rate increased as the height of the plume goes up. A correction equation between the measured air temperature and the well-mixed one node room air temperature was formulated. The air temperature entering from the bottom of the heater was less than the assumed well-mixed one node air temperature.

The major contributions of the dynamic model development can be summarized as follows:

(1) An overall dynamic model for a high-rise building HWH system was developed by applying the first principles, model order reduction and aggregation techniques. Temperature and fluid flow dynamics were the focus of the modeling.

(2) A detailed full order finned-tube baseboard heater model was developed using control volume approach. Air flow dynamics were investigated using the developed model.

(3) The overall dynamic model was used to study system properties, control strategy, fault isolation, fault tolerant control, thermal comfort and set point accuracy and energy estimation.

### **7.1.2 Design of intelligent control strategies**

There are several reasons for requiring control in HWH systems. Firstly, the disturbances such as outside air temperature, solar radiation and internal heat gains need to be compensated to match the heating load. Secondly, process and measurement noises influence HWH system operation, and should be estimated to improve system operation. Finally, optimal control strategy could be employed to increase system efficiency and improve thermal comfort for occupants. To this end, four control strategies, namely boiler fuel firing rate control, fuzzy logic adaptive PI control (FLAC), hybrid control strategy with the EKF and supervisory control, were designed in this thesis to deal with different situations. Simulation results were presented after each control strategy design.

The following specific conclusions are drawn from the control strategy simulations presented in the thesis:

(1) In the multi-zone building, the use of only boiler fuel firing rate control caused greater zone air temperature fluctuations in different zones ranging from 7.95 to 10.35°C. In order to improve the performance the control system should be designed properly to quickly compensate heating load changes. This was achieved by considering supply water temperature and water mass flow rate regulation together.

(2) Simulation results of the fuzzy logic adaptive PI control (FLAC) strategy showed that, the zone air temperature swings were less than 0.5°C of the design zone air temperature set point. The greater improvement was not only resulted from the inferred

fuzzy logic augmented supply water temperature set points, but also contributed by the adaptive PI controllers rather than the fixed gain PI controllers.

(3) By comparing the hybrid control strategy with and without the EKF, it was noted that the impact of the noises on system outputs was reduced in the control strategy with the EKF. The supply water and the zone air temperature responses were smooth due to the EKF estimation. In addition, the tested results show that the process noise has more impact compared to measurement noise. The robustness of the control system was improved by compensating for the degradation of operation resulting from the noises.

(4) From the point of view of the energy consumption and daily comfort level, it can be concluded that the best control system design was the fuzzy logic adaptive PI control. One day savings in the pumping energy and fuel consumption were about 88% and 16% respectively (compared with controlling fuel firing rate of the boiler); while the daily comfort level reached about 84% confidence level. Also, larger process and measurement noises resulted in greater energy consumption and lower thermal comfort.

(5) Design of supervisory control strategy is very important for large HWH control systems. System optimal operation can be achieved by tracking optimal set points by local controllers. In the designed supervisory control strategy, optimal set points of the supply water and zone air temperatures were computed based on solving a multi-objective function. Simulation results showed that, although the optimization was not able to obtain the feasible solution all of the time, the thermal comfort was improved and the energy consumption was decreased most of the time. By evaluating the optimal operation with a typical HWH system operation, the supply water temperature in the

optimal system was reduced about 15°C, and the pumping energy and fuel consumption were decreased by 77% and 18% respectively.

The major contributions regarding the design of the intelligent control strategies are summarized below:

(1) A fuzzy logic adaptive PI control (FLAC) strategy was designed to achieve better system performance, improve thermal comfort and attain higher energy efficiency.

(2) To compensate for process and measurement noises, an EKF technique was designed and applied in the hybrid control system to reduce the influence of the noises and improve system efficiency.

(3) The multi-objective optimization problem was formulated and solved to design a supervisory control strategy. Optimal set points were obtained and employed in the local control loops.

### **7.1.3 Model-based fault tolerant control strategies**

There is a need to design fault tolerant control strategies because faults in HWH systems cannot always be avoided. Faults can result in uneconomic operation, create safety problems and cause poor indoor environment. In this thesis, model-based fault detection and diagnosis was employed to isolate component and system failures, and then, fault tolerant control strategies were designed to improve the MFMZ heating system performance and thermal comfort and save energy. In the FTC systems, the error input to the controller was calculated based on the set point, measurement and the error correction function using FDD information.

Specific conclusions on the model-based fault diagnosis and fault tolerant control strategies are summarized as follows:

(1) The degree of the faults such as the sensor fault, the heater efficiency degradation fault and the control valve fault was estimated by using fuzzy inference systems based on the deviation of the state variables.

(2) From the dynamic responses of the normal system, the fault system with the supply water temperature sensor fault and the system with the FTC strategy, it was noted that the FTC system was able to correct the measurement fault and give good tracking close to the fault free condition. The estimated lower fault level implied that good control was achieved by the designed FTC strategy.

(3) To deal with the heater efficiency fault, two solutions, one by regulating supply water temperature and the other by water mass flow rate control were essential. This was because only water mass flow rate control could not satisfy all situations. For example, lower mass flow rate of water resulted in inadequate heat output from the heaters; therefore, the supply water temperature had to be increased to compensate the heating load. From simulation results it was noted that, the heater efficiency in the FTC system was enhanced by up to 72% compared with that in the fault system. This was due to the fact that appropriate operation period was extended even though the heater fault existed in the heating system.

(4) Through the FDD analysis, the multi-fault: the heater efficiency fault combined with partially blocked control valve fault was isolated by using two FISs individually because it was difficult to diagnose the multi-fault by using single FIS. In the design of the FTC strategy with the multi-fault, both the supply water temperature and the water mass flow rate were varied to meet the heating load requirement. Simulation results showed that the supply water temperature in the multi-fault FTC system was

greater than that in the single heater efficiency fault. This was mainly due to the lower water mass flow rate entering the heater when the control valve was partially blocked. Moreover, the control ability of the control valve was enhanced due to the increased supply water temperature. The deviation of the zone air temperature from the set point in the FTC system was much lower compared with that in the fault system; therefore, the proposed FTC approach was able to diminish the zone air temperature fluctuations. The simulations also showed the potential for energy savings.

The major contributions drawn from the FDD and FTC strategies are as follows:

(1) Model-based FDD systems were designed and analyzed for the measurement fault and process faults. FIS(s) was employed to evaluate the fault level based on the important parameters influenced by the fault(s).

(2) An error correction function was formulated for each of the FTC strategies to adjust the error signals of the control systems with the failure situations. This function combines the reference signal, the measured parameter and the FDD information.

(3) The designed FTC strategies were able to handle single and multiple faults normally occurring in HWH systems, and the advantages of the FTC systems were realized such as improving system performance, increasing thermal comfort level, saving energy and extending appropriate operation range of the system.

## **7.2 Recommendations for future research**

Investigation conducted in this thesis provides opportunities for future work in system optimal operation and energy management of HWH systems.

(a) The principles of the dynamic modeling could be extended to real-world large direct and indirect district HWH systems.

(b) The component models and the overall model need to be validated using data from real building operation.

(c) The developed dynamic model could be identified based on online identification technique and may be extended to online dynamic optimal applications.

(d) To detect and isolate more faults, a database related to component and system faults may be developed and employed.

(e) Further work is needed to develop advanced model-based fault tolerant control strategies, and to validate them in real-world HWH system operation.

## References

- Al-Haik M. S. and Haik Y. S. 1999. "System Identification of a Lumped Heat Exchanger Using the Extended Information Filter." *SPIE Conference Sensor Fusion and Decentralized Control in Robotic Systems II*, pp9-20.
- Altrock C.V, Arend H.O., Krause B., and Steffens C. 1994. "Customer-Adaptive Fuzzy Logic Control of Home Heating System." *Fuzzy System, IEEE World Congress on Computational Intelligence, Proceedings of the 3<sup>rd</sup> IEEE Conference*, 3: pp1713-1718.
- ASHRAE Handbook-Fundamentals. 2001. American Society of Heating, Refrigerating and Air-Conditioning Engineers Inc. Atlanta, GA.
- Astrom K.J and Wittenmark B. 1989. "Advanced Control." Addison-Wesley Publication Company.
- Bendapudi S. and Braun J.E. 2002. "A Review of Literature on Dynamic Models for Vapor Compression Equipment." *HL 2002-9, Report #4036-5*. Ray Herrick Laboratories, Purdue University.
- Benjamin C.K. 1991. "Automatic Control Systems, 6th Edition." Prentice Hall, Englewood Cliffs, New Jersey.
- Benonysson A., BØhm B., and Ravn H.F. 1995. "Operational Optimization in a District Heating System." *Energy Conservation and Management*, 36(5): pp297-314.
- Bin C., and James E.B. 2001. "Simple Rule-Based Methods for Fault Detection and Diagnostic Applied to Packaged Air Conditioners." *ASHRAE Transactions*, 107 (1): pp847-857.
- Biyikoğlu A., Akcayol M.A., Özdemir V., and Sivrioğlu M. 2005. "Temperature Prediction in a Coal Fired Boiler with a Fixed Bed by Fuzzy Logic based on Numerical Solution." *Energy Conversion and Management*, 46: pp151-166.
- BLAST. 1979. "Blast 3.0: Building Loads Analysis and System Thermodynamics Program, User Manual." Support Office, Department of Mechanical and Industrial Engineering, University of Illinois, Urbana-Champaign.
- Borresen B.A. 1987. "Thermal Room Models for Control Analysis." *ASHRAE Transactions*, 93 (2): pp251-261.
- Brain J.M. and Fisher D.S. 2003. "Pump Differential Pressure Setpoint Reset Based on Chilled Water Valve Position." *ASHRAE Transactions*, 109(1): pp373-379.
- Brayton R.K., Director S.W., Hachtel G.D. and Vidigal L. 1979. "A New Algorithm for Statistical Circuit Design Based on Quasi-Newton Methods and Function Splitting." *IEEE Trans. of Circuits and Systems*, 26: pp.784-794.
- Breuker M.S. and Braun J.F. 1998. "Evaluating the Performance of a Fault Detection and Diagnostic system for Vapor Compression Equipment." *International Journal of HVAC&R Research*, 4(4): pp401-425.
- Burd A.L. 1997. "Deferred Heat Supply for Space Heating Using a Capacity Limiting Device-A Beneficial Approach for District Heating." *ASHRAE Transactions*, 103 (2): pp23-31.
- Buswell R.A. and Wright J.A. 2004. "Uncertainty in Model-Based Condition Monitoring." *Building Services Engineering Research & Technology*, 25(1): pp65-75.

- Cho S.H., Yang H.C., Zaheeruddin M. and Ahn B.C. 2005a. "Transient Pattern Analysis for Fault Detection and Diagnosis of HVAC Systems." *Energy Conversion and Management*, 46: pp3103-3116.
- Cho S.H., Hong Y.J., Kim W.T., and Zaheeruddin M. 2005b. "Multi-Fault Detection and Diagnosis of HVAC systems: an Experimental Study." *International Journal of Energy Research*, 29: pp471-483.
- Chuah Y.K. and Chen C.T. 2004. "Natural Convection Heat Transfer for Fin-Tube Heat Exchangers." *ASHRAE Transactions*, 110 (2): pp354-360.
- "Commercial Fin-Tube Radiation Selection Guide." 2004. Slant/Fin Corp. Greenvale, NY.
- Comstock M.C., Braun J.E., and Groll E.A. 2001. "The Sensitivity of Chiller Performance to Common Faults." *International Journal of HVAC&R Research*, 7(3): pp263-279.
- Dalichieux P. and Bouia H. 1991. "Présentation d'une Modélisation Simplifiée des Mouvements d'air à l'intérieur d'une Pièce D'habitation (Presentation of a Simplified Model of Air Movement Inside a Room)." *Electricité de France Report HE 12 W 3265*.
- David Z., Marta B., Mario J. and Alejandro C. 2007. "Robust Adaptive Predictive Fault-Tolerant Control Integrated to a Fault-Detection System Applied to a Nonlinear Chemical Process." *Centro Internacional Franco Argentino de Ciencias de Informacion y Sistemas*, Argentina.
- Delnero C.C., Dreisigmeyer D., Hittle D.C., Young P.M., Anderson C.W., and Anderson M.L. 2004. "Exact Solution to the Governing PDE of a Hot Water-to-Air Finned Tube Cross-Flow Heat Exchanger." *International Journal of HVAC&R Research*, 10(1): pp21-31.
- DOE-2. 1981. "DOE-2: Building Energy User Analysis Program, Engineering Manual Version 2.1A." Lawrence Berkeley Laboratory.
- Engdahl F. and Johannsson D. 2004. "Optimal Supply Air Temperature with Respect to Energy Use in a Variable Air Volume System." *Energy and Buildings*, 36: pp205-218.
- Gouda M.M., Danaher S., Underwood C.P. 2001. "Thermal Comfort Based Fuzzy Logic Controller." *Building Services and Engineering Research & Technology*, 22(4): pp237-253.
- Gouda M.M., Underwood C.P., and Danaher S. 2003. "Modeling the Robustness Properties of HVAC Plant under Feedback Control." *Building Services Engineering Research & Technology*, 24(4): pp271-280.
- Grace A.C.W. 1989. "Computer-Aided Control System Design Using Optimization Techniques." *Ph.D Thesis*, University of Wales, Bangor, Gwynedd, UK.
- Greitzer F.L. and Pawlowski R.A. 2002. "Embedded prognostics health monitoring. Presented at the Instrumentation Symposium Embedded Health Monitoring Workshop." *PNNL Report Number PNNL-SA-35920*. Pacific Northwest National Laboratory, Richland, Washington.
- Grelat A. 1987. "Approche des Phénomènes de Circulation et de Stratification de l'air dans les Locaux Chauffés par le Programme de Simulation Thermique BILGA (Approach Used by the Multizone Thermal Simulation Program BILGA to

- Calculate Air Circulation and Stratification Phenomena in Heated Rooms)." *CEBTP-EDF Contract Final Report*.
- Haissig C. 1999. "Adaptive Fuzzy Temperature Control for Hydronic Heating Systems." *Proceedings of the International Conference on Control Applications*, (1): pp582-588.
- Han S.P. 1977. "A Globally Convergent Method for Nonlinear Programming." *Journal of Optimization Theory and Applications*, 22(3), pp.297-309.
- Haorong L. and James E.B. 2003. "An Improved Method for Fault Detection and Diagnosis Applied to Packaged Air Conditioners." *ASHRAE Transactions*, 109(2): pp683-692.
- Hill C.R. 1985. "Simulation of a Multizone Air Handler." *ASHRAE Transactions*, 91(1B): pp752-764.
- Holman J.P. 1981. "Heat Transfer, 5th Edition." McGraw-Hill Book Company.
- Homme T.P. and Gillet D. 2001. "Advanced Control Strategy of a Solar Domestic Hot Water System with a Segmented Auxiliary Heater." *Energy and Buildings*, 33: pp463-475.
- Hongyu H. and Haghghat F. 2005. "An Integrated Zone Model for Predicting Indoor Airflow Temperature and VOC Distributions." *ASHRAE Transactions*, 111(1): pp601-611.
- Howarth A.T. 1985. "The Prediction of Air Temperature Variations in Naturally Ventilated Radiator and a Room with a Convective Heating." *Building Services Engineering Research Technology*, 6(4): pp169-175.
- Huang H.Y., Haghghat F. and Wurtz E. 2003. "An Integrated Zonal Model for Predicting Transient VOC Distribution in a Ventilated Room." *Canadian conference on building energy simulation*, Montreal, Canada.
- Inard C. 1988. "Contribution à l'étude du Couplage Thermique Entre une Source de Chaleur et un Local (Contribution to the Study of Thermal Coupling between a Heat Source and a Room)." *PhD Thesis*, INSA de Lyon, France.
- Inard C., Meslem A. and Depecker P. 1998. "Energy Consumption and Thermal Comfort in Dwelling-cells: A Zonal Model Approach." *Building and Environment*, 33(5): pp279-291.
- Itzhak M. and Reddy T.A. 2003. "Literature Review of Artificial Intelligence and Knowledge-Based Expert systems in Building and HVAC System Design." *ASHRAE Transactions*, 109(1): pp12-26.
- Jaćimovic B., Živković B., Genić S. and Zekonja P. 1998. "Supply Water Temperature Regulation Problems in District Heating Network with both Direct and Indirect Connection." *Energy and Buildings*, 28: pp317-322.
- James B.R. 2003. "Control of Variable Speed Pumps for HVAC Water Systems." *ASHRAE Transactions*, 109(1): pp380-389.
- Jili Z., Jinping O. and Dexing S. 2003a. "Study on Fuzzy Control for HVAC Systems-Part One: FFSI and Development of Single-Chip Fuzzy Controller." *ASHRAE Transactions*, 109a(1): pp27-35.
- Jili Z., Jinping O. and Dexing S. 2003b. "Study on Fuzzy Control for HVAC Systems-Part Two: Experiments of FFSI in Testing Room Dynamic Thermal System." *ASHRAE Transactions*, 109b(1): pp36-43.

- John E.S. 2007. "Using Intelligent Data Analysis to Detect Abnormal Energy Consumption in Buildings." *Energy and Buildings*, 39: pp52-58.
- John M.H., Hossein V.N., and Michael W. 2001. "An Expert Rule Set for Fault Detection in Air-Handling Units." *ASHRAE Transactions*, 107 (1): pp858-871.
- John N.W and Ray C. 1983. "The Application of Kalman Filtering Estimation Control Systems." *IEEE Transactions, Automat. Contr.*, 28: pp416-427.
- Jonsson G. and Palsson O. P. 1994. "An Application of Extended Kalman Filtering to Heat Exchanger Models." *ASME Journal of Dynamic System, Measurement and Control*, 116: pp257-264.
- Kalman R. E. 1960. "A New Approach to Linear Filtering and Prediction Problems." *Journal of Basic Engineering, Transaction of the ASME*, pp35-45.
- Kamimura K., Hashimoto Y., Yamazaki T., and Kurosu S. 2002. "A Comparison of controller Tuning Methods from a Design Viewpoint of the Potential for Energy Savings." *ASHRAE Transactions*, 108(2): pp155-164.
- Kanarachos A. and Geramanis K. 1998. "Multivariable Control of Single Zone Hydronic Heating Systems with Neural Networks." *Energy Conversion and Management*, 39(13): pp1317-1336.
- Karsten S., Dorte R. and Harald S. 2002. "Observer-Based Estimation of the Water-Mass-Flow through a Central Heating Boiler." *Proceedings of the American Control Conference*, pp.5054-5059.
- Kasahara M., Huzuu Y., Matsuba T., Hashimoto Y., Kamimura K. and Kurosu S. 2000. "Physical model of an Air-Conditioned Space for Control Analysis." *ASHRAE Transactions*, 106(2): pp304-317.
- Kasahara M., Matsuba T., Kuzuu Y., and Yamazaki T. 1999. "Design and Tuning of Robust PID Controller for HVAC Systems." *ASHRAE Transactions*, 105(2): pp154-166.
- Katipamula S. and Brambley M.R. 2005a. "Method for Fault Detection, Diagnostics, and Prognostics for Building Systems-A Review, Part I." *International Journal of HVAC&R Research*, 11(1): pp3-25.
- Katipamula S. and Brambley M.R. 2005b. "Method for Fault Detection, Diagnostics, and Prognostics for Building Systems-A Review, Part II." *International Journal of HVAC&R Research*, 11(2): pp169-187.
- Kelso R.M., and Wright J.A. 2005. "Application of Fault Detection and Diagnosis Techniques to Automated Functional Testing." *ASHRAE Transactions*, 111(2): pp964-970.
- Kitamori T. 1979. "A Design Method for Control System Based upon Partial Knowledge about Controlled Processes." *Transactions of the Society of Instrument and Control Engineers*, 15(4): pp549-555.
- Kitamori T. 1980. "Design Theory, Instrumentation and Control for PID Control Systems." *Journal of the Society of Instrument and Control Engineers*, 19(4): pp382-391.
- Klein S.A. et al. 1983. "TRANSYS, A Transient Simulation Program." *Report 38-12, Version 12.1*. Engineering Experimentation Station, University of Wisconsin-Madison.

- Kolokotsa D. 2003. "Comparison of the Performance of Fuzzy Controllers for the Management of the Indoor Environment." *Building and Environment*, 38: pp1439-1450.
- Kulkarni M.R. and Feng H. 2004. "Energy Optimal Control of a Residential Space-Conditioning System based on Sensible Heat Transfer Modeling." *Building and Environment*, 39: pp31-38.
- Lianzhong L. 2003. "Dynamic Modeling and Optimal Operation of District Heating Systems." *Master Thesis*, Concordia University.
- Lianzhong L. and Zaheeruddin M. 2005. "Dynamic Modeling and Simulation of a Room with Hot Water Baseboard Heater." *International Journal of Energy Research*, 30(6): pp427-445.
- Lianzhong L. and Zaheeruddin M. 2004. "A Control Strategy for Energy Optimal Operation of a Direct District Heating System." *International Journal of Energy Research*, 28: pp597-612.
- Lianzhong L. and Zaheeruddin M. 2007. "Hybrid fuzzy logic control strategies for hot water district heating systems." *Building Service Engineering*, 28: pp35-53.
- Liao Z. and Dexter A.L. 2003. "An Inferential Control Scheme for Optimizing the Operation of Boilers in Multi-Zone Heating Systems." *Building Services Engineering Research & Technology*, 24(4): pp245-256.
- Liao Z. and Dexter A.L. 2004. "A Simplified Physical Model for Estimating the Average Air Temperature in Multi-Zone Heating Systems." *Building and Environment*, 39: pp1013-1022.
- Liao Z. and Dexter A.L. 2005. "An Experimental Study on an Inferential Control Scheme for Optimizing the Control of Boilers in Multi-Zone Heating System." *Energy and Buildings*, 37: pp55-63.
- Linas L. and Elena T. 2004. "Refinement of Fault Tolerant Control System in B." *Turku Centre for Computer Science. TUCS Technical Report No. 603*.
- Madsen H. and Holst J. 1995. "Estimation of Continuous-Time Models for the Heat Dynamics of a Building." *Energy and Buildings*, 22: pp67-79.
- Madsen K. and Schjaer-Jacobsen H. 1979. "Algorithms for Worst Case Tolerance Optimization." *IEEE Trans. of Circuits and Systems*, 26: pp775-783.
- Masakazu K., Yuji Y., and Takanori Y. 2005. "A Tuning Method for PID Controller that Considers Changes in System Characteristics." *ASHRAE Transactions*, 111(2): pp13-22.
- McKellar M.G. 1987. "Failure Diagnosis for a Household Refrigerator." *Master's Thesis*. School of Mechanical Engineering, Purdue University, West Lafayette, Indiana.
- McQuiston F.C. and Parker J.D. 2005. "Heating, Ventilating, and Air Conditioning Analysis and Design, 6th Edition." John Wiley & Sons, Inc.
- Mei L. and Levermore G.J. 2002. "Simulation and Validation of a VAV System with an ANN Fan Model and a Non-Linear VAV Box Model." *Building and Environment*, 37: pp277-284.
- Mesbah S. and Pang P. 1999. "Fuzzy-Neural Control with Application to a Heating System." *Proceedings of the International Symposium on Computer Aided Control System Design, IEEE*. Hawai'i, US, pp533-538.

- Michael A., Michael B., Peter Y., Douglas H., Charles A., Jilin T. and David H. 2007. "An Experimental System for Advanced Heating, Ventilating and Air Conditioning (HVAC) Control." *Energy and Buildings*, 39: pp136-147.
- Musy M., Wurtz E. and Gagneau S. 1997. "Génération Automatisée d'une Simulation Thermique et Aéraulique dans le Bâtiment (Automatic Generation of a Thermal and Air-flow Simulation in a Building)." *Journée "Innovations et perspectives de recherche"*. Société Francaise, des Thermiciens.
- Nagib G., Gharieb W., and Binder Z. 1992. "Application of Fuzzy Control to a Nonlinear Thermal Process." *Proceedings of the 31st Conference on Decision and Control*. Tucson, Arizona.
- Nielsen H.A. and Madsen H. 2006. "Modeling the Heat Consumption in District Heating Systems Using a Grey-Box Approach." *Energy and Buildings*, 38: pp63-71.
- Niu Z. and Wong K.F.V. 1998. "Adaptive Simulation of Boiler Unit Performance." *Energy Conversion and Management*, 39(13): pp1383-1394.
- Noda Y., Yamazaki T. and Matsuba T. 2003. "Comparison in control performance Between PID and  $H_{\infty}$  Controllers for HVAC Control." *ASHRAE Transactions*, 109(1): pp3-11.
- Norford L.K., Wright J.A., Buswell R.A., Luo W., Klaassen C.J. and Suby A. 2002. "Demonstration of Fault Detection and Diagnosis Methods for Air-Handling Units (ASHRAE 1020-RP)." *International Journal of HVAC&R Research*, 8(1): pp41-71.
- Ozawa K., Noda Y. and Yamazaki T. 2003. "A Tuning Method for PID Controller Using Optimization Subject to Constrains on Control Input." *ASHRAE Transactions*, 109(2): pp79-88.
- Park C. Clark D.R. and Kelly G.E. 1985. "An Overview of HVACSIM+: a Dynamic Building/HVAC/Control System Simulation Program." *Building Energy Simulation Conference*, Seattle, pp.175-185.
- Peng X., Philip H., and Moosung K. 2005. "Model-Based Automated Functional Testing-Methodology and Application to Air-Handling Units." *ASHRAE Transactions*, 111(1): pp979-989.
- Powell M.J.D. 1978. "A Fast Algorithm for Nonlinearly Constrained Optimization Calculations." *Numerical Analysis*, Ed. G.A.Watson, *Lecture Notes in Mathematics*, 630, Springer Verlag.
- Prakash J., Patwardhan S.C. and Narasimhan. 2002. "A Supervisory Approach to Fault Tolerant Control of Linear Multivariable Systems." *Ind. Eng. Chem. Res.* 41(9): pp1181-2270.
- Prashant M., Adiwinata G., Nael H.E., Charles M., Panagiotis D.C. and James F.D. 2006. "Integrated Fault-Detection and Fault-Tolerant Control of Process Systems." *AIChE Journal*, 52: pp2129-2148.
- Reddy T.A., and Andersen K.K. 2002. "An Evaluation of Classical Steady-State Off-line Linear Parameter Estimation Methods Applied to Chiller Performance Data." *International Journal of HVAC&R Research*, 8(1): pp101-124.
- Reddy T.A., Niebur D., Andersen K.K., Pericolo P.P., and Cabrera G. 2003. "Evaluation of the Suitability of Different Chiller Performance Models for On-line Training Applied to Automated Fault Detection and Diagnosis." *International Journal of HVAC&R Research*, 9(4): pp385-414.

- Richard A.H. 1998. "Application of Control Valves and Balancing Valves in a Variable-Flow Hydronic System." *ASHRAE Transactions*, 104(1B): pp1615-1620.
- Richard M.K. and Jonathan A.W. 2005a. "Application of Fault Detection and Diagnosis Techniques to Automated Functional Testing." *ASHRAE Transactions*, 111a (1): pp964-970.
- Richard M.K. and Jonathan A.W. 2005b. "Developing Component Models for Automated Functional Testing." *ASHRAE Transactions*, 111b (1): pp971-978.
- Riederer P., Marchio D., Visier J.C., Husaunndee A. and Lahrech R. 2002. "Room Thermal Modeling Adapted to the Test of HVAC Control Systems." *Building and Environment*, 37: pp777-790.
- Roshenow W.M. and Choi H.Y. 1965. "Heat, Mass, and Momentum Transfer.", 193.
- Roy C.E.A. 1998. "Selection of Hydronic Balancing Valves." *ASHRAE Transactions*, 104(1B): pp1630-1635.
- Sebric, Jelena, Chen Q., Clicksman L.R. 2000. "A Coupled Airflow and Energy Simulation Program for Indoor Thermal Environment Studies." *ASHRAE Transactions*, 106(1): pp465-476.
- Silva P.M., Becerra V.M., Khoo I. and Calado J.M.F. 2006. "Multiple-Model Fault Tolerant Control of Terminal Units of HVAC Systems." *IEEE ISIE*. Montreal, pp2896-2901.
- Simon D. 2001. "Kalman Filtering. Embedded Systems Programming." pp72-79.
- Singh G., Zaheeruddin M., and Patel R.V. 2000. "Adaptive Control of Multivariable Thermal Processes in HVAC systems." *Energy Conversion & Management*, 41: pp1671-1685.
- Spreitzer K., Ruckbrodt D., and Straky H. 2002. "Observer-Based Estimation of the Water-Mass-Flow through a Central Heating Boiler." *Proceedings of the American Control Conference*, 6: pp5054-5059.
- Takagi T and Sugeno M. 1985. "Fuzzy identification of systems and its applications to modeling and control." *IEEE Trans. Syst., Man, Cybern.*, SMC-15(1): pp116-132.
- Tatsuo N. 2002. "Optimization Method for Minimizing Annual Energy, Peak Energy Demand, and Annual Cost Trough Use of Building Thermal Storage." *ASHRAE Transactions*, 108(1): pp43-53.
- Tudoroiu N. and Zaheeruddin M. 2005. "Fault Detection and Diagnosis of Valve Actuators in HVAC Systems." *Proceedings of the IEEE Conference on Control Applications*, Toronto, Canada, pp1281-1286.
- Venkatasubramanian V., Rengaswamy R., Yin K., and Kavuri S.N. 2003a. "A Review of Process Fault Detection and Diagnosis, Part I: Quantitative Model-Based Methods." *Computers in Chemical Engineering*, 27: pp293-311.
- Venkatasubramanian V., Rengaswamy R., Yin K., and Kavuri S.N. 2003b. "A Review of Process Fault Detection and Diagnosis, Part II: Qualitative Models and Search Strategies." *Computers in Chemical Engineering*, 27: pp313-326.
- Venkatasubramanian V., Rengaswamy R., Yin K., and Kavuri S.N. 2003c. "A Review of Process Fault Detection and Diagnosis, Part III: Process History Based Methods." *Computers in Chemical Engineering*, 27: pp327-346.

- Wang S.W. and Xinqiao J. 2000. "Model-Based Optimal Control of VAV Air-Conditioning System Using Genetic Algorithm." *Building and Environment*, 35: pp471-487.
- Welch G. and Bishop G. 2004. "An Introduction to the Kalman Filter." *TR95-041*, Department of Computer Science, University of North Carolina, Chapel Hill, NC.
- Wurtz E., Nataf J.M. and Winkelmann F. 1999. "Two-and Three-Dimensional Natural and Mixed Convection Simulation Using Modular Zonal Models." *International Journal of Heat and Mass Transfer*, 42: pp923-940.
- Xiaoming L., Vaezi-Nejad H., and Visier J.C. 1996a. "Development of Fault Diagnosis Method for Heating System Using Neural Networks." *ASHRAE Transactions*, 102(1): pp607-614.
- Xiaoming L., Vaezi-Nejad H., and Visier J.C. 1996b. "A Connectionist Approach to the Development of a Fault Detection and Diagnosis Method for Hydraulic Heating Systems." *Systems, Man, and Cybernetics, IEEE international Conference*, 4: pp2493-2497.
- Xiaoming L., Visier J.C. and Vaezi-Nejad H. 1997. "A Neural Network Prototype for Fault Detection and Diagnosis of Heating Systems." *ASHRAE Transactions*, 103(1): pp634-644.
- Xiongfu L. and Arthur D. 1999. "Fuzzy Model-Based Fault-Tolerant Control of Air-Conditioning Systems." *Proceedings of the 6th International IBPSA Conference*.
- Xuzhong Q., Yi J., and Yingxin Z. 2001. "Optimization of Hydraulic Conditions in District Heating Networks." *ASHRAE Transactions*, 107(1): pp270-274.
- Yi J., Jisheng L., and Xudong Y. 1995. "Fault Direction Space Method for On-Line Fault Detection." *ASHRAE Transactions*, 101(2): pp219-228.
- Yi J. and Xuzhong Q. 2000. "Hydraulic Process Fault Diagnosis and Parameter Identification in District heating Networks." *ASHRAE Transactions*, 106(2): pp284-291.
- Ying H. 2000. "TITO Mamdani Fuzzy P/PI/DP Controllers as Nonlinear, Variable Gain P/PI/DP Controllers." *International Journal of Fuzzy System*, 2(3): pp192-197.
- Youmin Z. and Jin J. 2003. "Bibliographical Review on Reconfigurable Fault-Tolerant Control Systems." *The University of Western Ontario, Canada*.
- Yu B., Jong W.D and Paassen A.H.C.V. 2003. "Modeling Analysis on Fin-Tube Heating Coil of Air Handling Unit." *Building Services Engineering Research & Technology, Technical Note*, 24(4): pp301-307.
- Zadeh L.A. 1965. "Fuzzy sets." *Information and Control*, 8: pp338-353.
- Zaheeruddin M and Monastiriakos P. 1998. "Hydronic Heating Systems: Transient Modeling, Validation and Load Matching Control." *International Journal of Energy Research*, 22: pp33-46.
- Zaheeruddin M. and Zheng G.R. 1994. "A VAV System Model for Simulation of Energy Management Control Functions: Off Normal Operation and Duty Cycling." *Energy Conversation Management*, 35(11): pp917-931.
- Zhang X.M. and Ren Z.P. 1979. "Heat Transfer, 2th Edition." China Construction Industry Press.
- Zheng G.R. 1997. "Dynamic Modeling and Global Optimal Operation of Multizone Variable Air Volume HVAC System." *PhD Thesis*, Concordia University, Montreal, Canada.

- Zhijian H., Zhiwei L., Ye Y. and Xinjian Y. 2006. "Data Mining Based Sensor Fault Diagnosis and Validation for Building Air Conditioning System." *Energy Conversion and Management*, 47: pp2479-2490.
- Zhimin D. and Xinqiao J. 2007. "Detection and Diagnosis for Sensor Fault in HVAC Systems." *Energy Conversion and Management*, 48: pp693-702.
- Zoltan M., and Robert P. 2002. "Energy Saving of District Heated Flats from the Recommendation of the Heating System in Hungary." *ASHRAE Transactions*, 108(2): pp575-579.

## **Appendices**

### **Appendix A Zonal model with the full order baseboard heater model**

#### **A.1 Zonal model**

The same room with the hot water baseboard heating system described for the one room heating is modeled using the zonal model technique. Seven cells were considered for this room as shown in Figure A.1. There are three types of cells: boundary cells such as Cell 1, Cell 6 and Cell 7, heater cell such as Cell 2 and plume cells such as Cell 3, Cell 4 and Cell 5. Note that the heater cell is a special cell that is similar to the full order dynamic model described in Chapter 3. Plume cells are a region of rising warm air produced by natural convection of the baseboard heater close to the outside wall. From this figure it can be seen that, the warm air in the plume cells rises from the heater cell and transfers mass and heat with the surrounding environment (outside, Cell 2, Cell 6 and Cell 7).

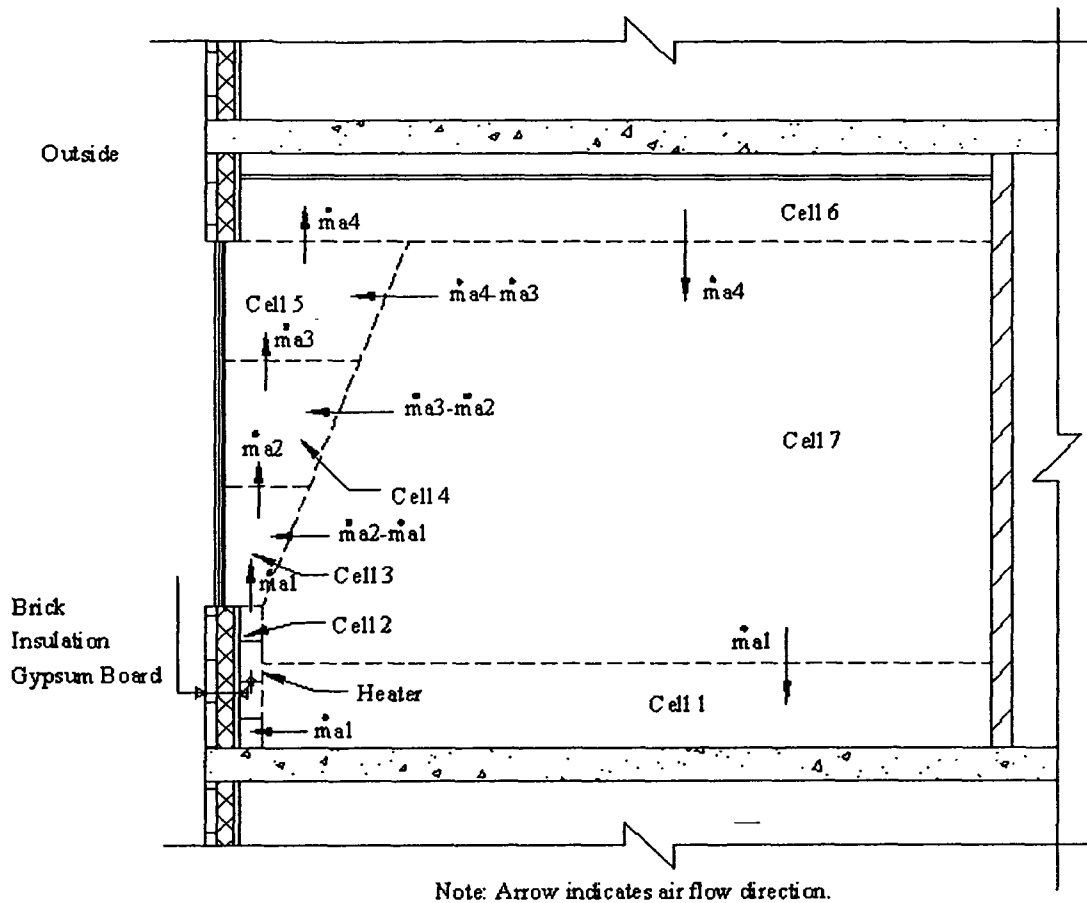


Figure A.1 Cells in the room with the hot water baseboard heater

By applying air mass balance for each cell except for Cell 2, the general equation can be written as

$$\frac{dG_{ai}}{dt} = \sum_{j=1}^6 \dot{m}_{aj} + \dot{m}_{asource} + \dot{m}_{asink} \quad (A.1)$$

Here, the steady state condition is considered for the air mass flow, the derivative of the air mass flow rate  $\frac{d(G_{ai})}{dt} = 0$ , and because of the natural convection of the baseboard heater, the air mass flow rates  $\dot{m}_{asource}$  and  $\dot{m}_{asink}$  are also set to zero.

By applying energy conservation law to the outside wall and the cells, a set of temperature dynamic equations were formulated as follows.

### Outside wall

The dynamic equations of the outside wall remain the same as in Equation (3.42) and (3.43).

### Cells

$$C_{ce1} \frac{dT_{ce1}}{dt} = c_a \dot{m}_{a1} T_{ce7} - c_a \dot{m}_{a1} T_{ce1} + h_{low} L_{fr} W_{fr} (T_{fr} - T_{ce1}) + h_{int i} H_{ce1} W_{fr} (T_{wl int} - T_{ce1}) + (q_{sol} + q_{int}) \frac{V_{ce1}}{V_{rm} - V_{ce2}} \quad (A.2)$$

$$C_{ce3} \frac{dT_{ce3}}{dt} = q_{hr} - U_{win} A_{win3} (T_{ce3} - T_o) - c_a \dot{m}_{a2} T_{ce3} - c_a (\dot{m}_{a1} - \dot{m}_{a2}) T_{ce7} + (q_{sol} + q_{int}) \frac{V_{ce3}}{V_{rm} - V_{ce2}} \quad (A.3)$$

$$C_{ce4} \frac{dT_{ce4}}{dt} = c_a \dot{m}_{a2} T_{ce3} - U_{win} A_{win4} (T_{ce4} - T_o) - c_a \dot{m}_{a3} T_{ce4} - c_a (\dot{m}_{a2} - \dot{m}_{a3}) T_{ce7} + (q_{sol} + q_{int}) \frac{V_{ce4}}{V_{rm} - V_{ce2}} \quad (A.4)$$

$$C_{ce5} \frac{dT_{ce5}}{dt} = c_a \dot{m}_{a3} T_{ce4} - U_{win} A_{win5} (T_{ce5} - T_o) - c_a \dot{m}_{a4} T_{ce5} - c_a (\dot{m}_{a3} - \dot{m}_{a4}) T_{ce7} + (q_{sol} + q_{int}) \frac{V_{ce5}}{V_{rm} - V_{ce2}} \quad (A.5)$$

$$C_{ce6} \frac{dT_{ce6}}{dt} = c_a \dot{m}_{a4} T_{ce5} - h_{wi} A_{wl6} (T_{ce6} - T_{wlsfi6}) - c_a \dot{m}_{a4} T_{ce6} - h_{int i} A_{wl6} (T_{ce6} - T_{wl int}) + h_{up} L_{hr} W_{hr} (T_{ce6} - T_{ce6}) + (q_{sol} + q_{int}) \frac{V_{ce6}}{V_{rm} - V_{ce2}} \quad (A.6)$$

$$C_{ce7} \frac{dT_{ce7}}{dt} = c_a \dot{m}_{a4} T_{ce6} + c_a (\dot{m}_{a3} - \dot{m}_{a4}) T_{ce7} + c_a (\dot{m}_{a2} - \dot{m}_{a3}) T_{ce7} + c_a (\dot{m}_{a1} - \dot{m}_{a2}) T_{ce7} - c_a \dot{m}_{a1} T_{ce7} + h_{int} W_{flr} H_{ce7} (T_{wint} - T_{ce7}) + q_{covce2} + (q_{sol} + q_{int}) \frac{V_{ce7}}{V_{rm} - V_{ce2}} \quad (A.7)$$

where  $T_{wlsfi1}$ ,  $T_{wlsfi2}$  and  $T_{wlsfi6}$  refer to the interior surface temperatures of the outside wall; while  $T_{flr}$ ,  $T_{ceil}$  and  $T_{wlint}$  indicate the temperatures of the floor, the ceiling and the interior wall.

In Equations (A.2)~(A.7), the net heat stored in each cell is equal to the heat transfer from the heat source and/or the air mass flow entering to the cell minus the heat from air mass flow leaving the cell and/or heat transferred between the cell and the interior surface of the enclosure and the outside environment. Note that the air mass flow rate  $\dot{m}_i$  is the summation of all air mass flow rate from the finned-tube and the bare pipe segments. Other air mass flow rates for the cells are computed based on Equation (A.8) (Riederer et al 2002):

$$\dot{m}_a(z) = \alpha_{plume} [q(z)_{conv}]^{(1/3)} (z - z_o)^{n_{plume}} \quad (A.8)$$

where,  $z$  and  $z_o$  express the height and the height of the fictive plume origin.

#### ***Baseboard heater model***

The baseboard heater model with the finned-tube and the bare pipe remains the same in Equations (3.1)~(3.40) except for Equation (3.13) is replaced by Equation (A.9).

$$T_{ain} = T_{cel} \quad (A.9)$$

In summary, the zonal model consists of 140 dynamic equations, which include equations for the baseboard heater, the bare pipe, the outside wall and the cells.

## A.2 Simulation results

To observe the dynamic responses of the cells and the distribution of the air temperature and the air mass flow rate in the room, open loop tests were made based on the developed zonal model.

Dynamic responses of the air temperature and the air mass flow rate for several cells of the room are simulated and depicted in Figures A.2(a) and (b) when  $T_s=84.2^\circ\text{C}$ ,  $\dot{m}_w=0.0358\text{Kg/s}$  and  $T_o=-21.8^\circ\text{C}$ . The temperatures of the floor, the ceiling and the interior wall are set to be  $22^\circ\text{C}$ . It can be seen from Figure A.2(a) that, Cell 2 has the highest temperature due to the fact that it is a heat source in the room. Note that the air temperature in Cell 2 is the average value for all leaving air temperature from the finned-tube and the bare pipe segments. Also, the temperature of the plume cells decreases from the bottom to the top because of the heat and mass transferred to the surrounding environment. Usually, the zone air temperature is measured in the area of Cell 7, and its temperature response is presented in Figure A.2(a). In addition, the mass flow rates have very fast dynamic responses illustrated in Figure A.2(b).

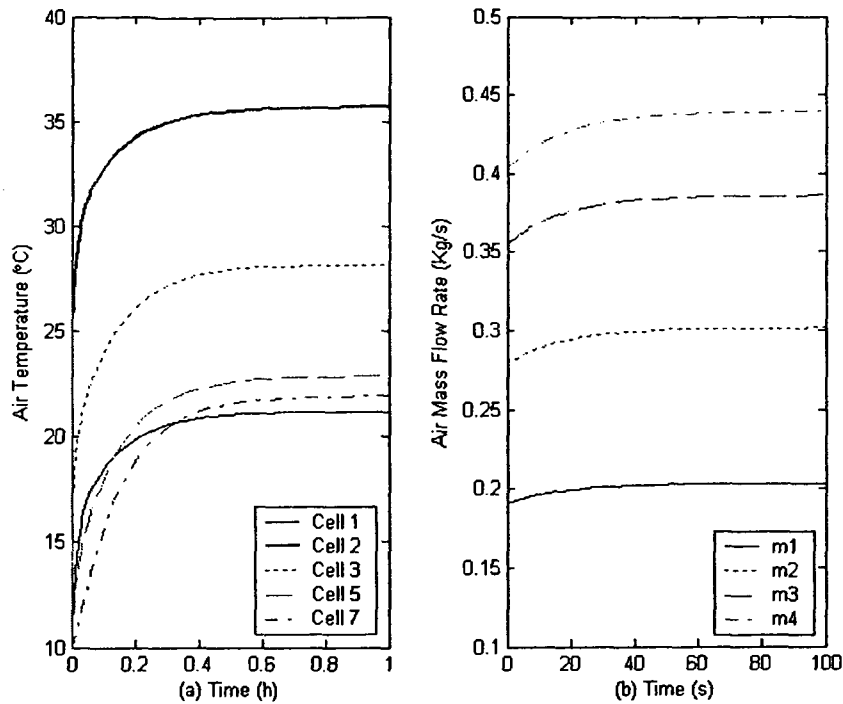


Figure A.2 Dynamic responses of cell temperature and air mass flow rate

The steady state values of all cells are reached after two hours and depicted in Figures A.3(a) and (b). The air temperature in the cells is differed each other. For instance, the temperature difference between Cell 7 and Cell 1 reaches  $0.74^{\circ}\text{C}$ . Meanwhile, the air mass flow distribution is shown in Figure A.3(b). The mass flow rates of  $\dot{m}_1$ ,  $\dot{m}_2$ ,  $\dot{m}_3$ , and  $\dot{m}_4$  increase as the height of the plume goes up.

From these results it can be noted that the assumption that inlet air temperature is less than well-mixed air temperature in the room (Equation 3.13) is indeed valid. The only question remains on the magnitude of the correction. In the above simulations the inlet air temperature to the heater is about  $0.74^{\circ}\text{C}$  less than the room temperature measured in the vicinity of Cell 7.

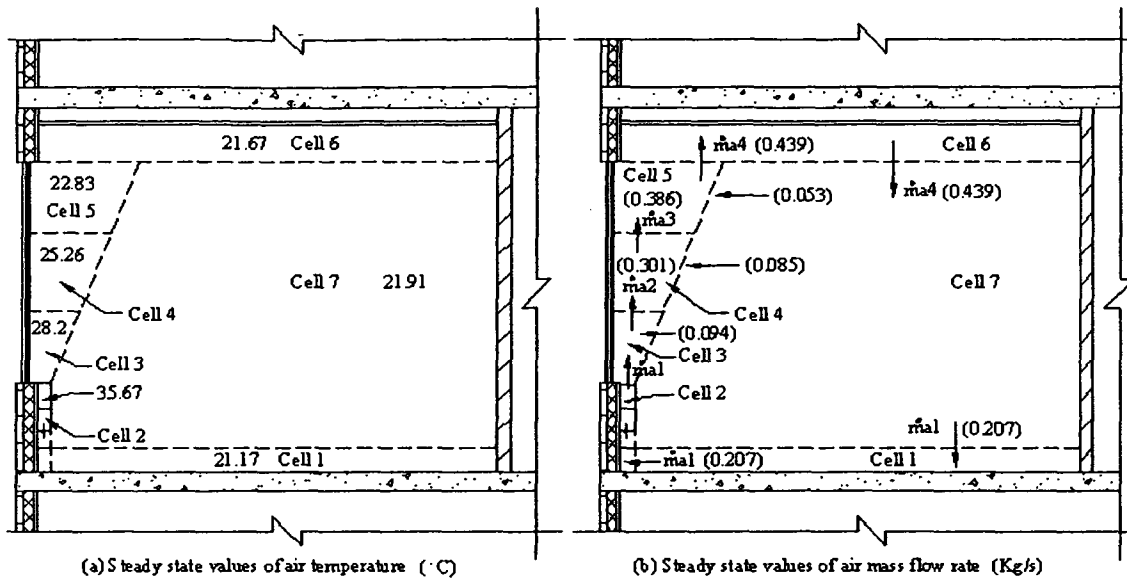


Figure A.3 Air temperature and air mass flow rate distribution

Generally, the real measurement for air temperature in a room is done in the region of Cell 7. By simulating the zonal model, a corrected equation between the measured air temperature ( $T_{zmsd}$ ) and the well-mixed one node room air temperature ( $T_z$ ) was formulated as given in Equation (A.10). This equation describes the normal measured zone air temperature which can be calculated by a quadratic function related to the supply water temperature and one node room air temperature. The correction factors  $\beta_2 \sim \beta_4$  were obtained by curve fitting technique.

$$T_{zmsd} = f(T_s, T_z) = \beta_2 T_s^2 + \beta_3 T_s T_z + \beta_4 T_z^2 \quad (\text{A.10})$$

## Appendix B Pressure drops from pipe segments, fittings and equipment

Momentum balance principle can be used to a micro control volume of a pipe segment. A pipe segment MN is assumed as shown in Figure B.1. The length is  $L$ , and the pressure entering and leaving the pipe segment is  $P_{in}$  and  $P_{out}$ . The control volume has the pressure drop  $\partial P$  over  $\partial x$ . The cross section area of the pipe is  $A$ . The mass flow rate of water, the density and the velocity of water are expressed as  $\dot{m}_w$ ,  $\rho_w$  and  $V_w$  respectively.

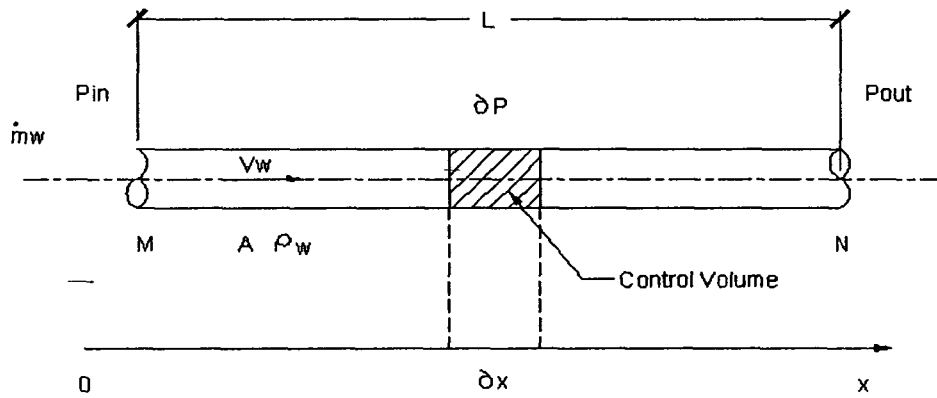


Figure B.1 Momentum balance in a pipe segment

Because water density changes based on water temperature are not significant in HWH systems, the water mass flow systems dynamics can be decoupled from the thermal system dynamics. Also, assuming incompressible flow the momentum balance for the control volume in the pipe segment can be written as

$$\frac{\partial \dot{m}}{\partial t} + \frac{\partial(\dot{m}^2 / m)}{\partial y} = -\frac{\partial(P\bar{A})}{\partial y} - \frac{C_f}{2mA} A_d \dot{m}^2 \quad (\text{B.1})$$

In this equation, the force balance on the control volume where the acceleration term is equal to the static pressure and the frictional forces acting on the control volume.

$C_f$  can be determined using Reynolds Number and geometry as described in the reference (McQuiston and Parker, 2005). Assuming the water mass flow rate and  $C_f$  values are constant along the pipe segment, by integrating from 0 to L, Equation (B.1) becomes

$$\frac{L}{A} \frac{d\dot{m}_w}{dt} = P_{in} - P_{out} - \sum f_{MN} \quad (\text{B.2})$$

Equation (B.2) represents that the changing momentum in the pipe segment is equal to the pressure force minus the frictional forces.

Frictional forces for pipe segments, fittings and equipment are described in the following equations.

For pipe segments:

$$f_{pipe} = 6.25 * 10^{-8} \frac{\lambda (3600 \dot{m}_w)^2}{\rho_w D_{pipe}^5} L_{pipe} \quad (\text{B.3})$$

where  $\lambda$  is the friction factor depending on the water mass flow rate. Note that the pressure drop for the baseboard heater is considered like a pipe segment.

For fittings:

$$f_{fit} = \xi \frac{\rho_w V_w^2}{2} \quad (\text{B.4})$$

where  $\xi$  is a frictional coefficient related to type of fittings.

For a boiler:

$$\Delta P_b = P_{bd} \left( \frac{\dot{m}_{wb}}{\dot{m}_{wbd}} \right)^2 \quad (\text{B.5})$$

For a nonlinear control valve, the pressure loss across the valve can be obtained from

$$\Delta P_{val} = (\beta_5 u_z^{\beta_6}) \frac{\dot{m}_w^2}{2 \rho_w A^2} \quad (\text{B.6})$$

In the equation, the factors  $\beta_5$  and  $\beta_6$  are obtained according to control valve type and from the manufacture's data. Note that  $u_z$  is the valve control signal used to control water mass flow rate entering the zone.

## Appendix C Aggregation model of a basement HWH system

The mass, energy and momentum balances are applied to the basement HWH system of the high-rise building in order to obtain the temperature and the water mass flow rate dynamics. Additionally, according to the property of the heating load acting on the basement, it is not necessary to distinguish the rooms with different zones. Thus, the basement is designed as one zone, and the dynamic equations are written based on an aggregation method for the zone. The designed layout of the basement heating system is given in Figure C.1, and the schematic diagram of the heating system with nodes is shown in Figure C.2. Note that surrounding soil temperature is assumed to be constant.

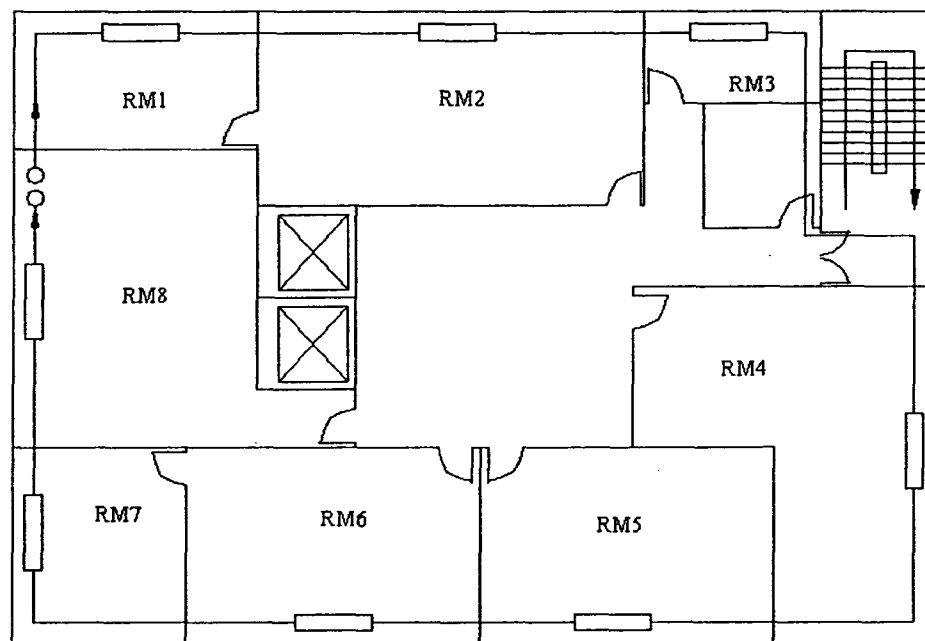


Figure C.1 Layout of the basement heating system

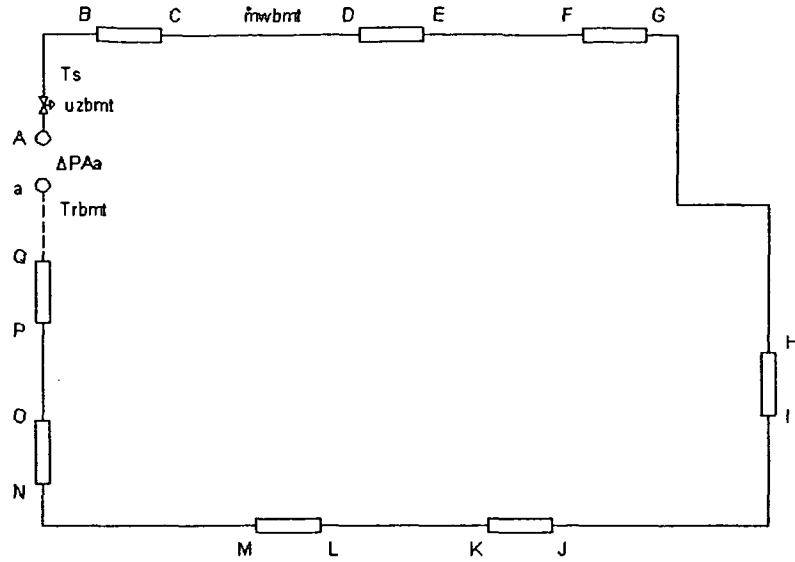


Figure C.2 Schematic diagram of the basement heating system with nodes

The dynamic equations of the basement HWH system can be expressed based on the aggregation technique for the zone air, the return water temperature, the outside wall and the water mass flow rate in the hydraulic circuit.

For the zone air:

$$C_{zbrmt} \frac{dT_{zbrmt}}{dt} = c_w \dot{m}_{wbmt} (T_s - T_{rbmt}) + Q_{int} A_{bmt} + U_{wlbmt} A_{wlbmt} (T_o - T_{zbrmt}) \quad (C.1)$$

For the return water temperature:

$$C_{hrbmt} \frac{dT_{rbmt}}{dt} = c_w \dot{m}_{wbmt} (T_s - T_{rbmt}) - f_w L_{hrbmt} \Omega_{hr} \left( \frac{T_s + T_{rbmt}}{2} - T_{zbrmt} \right)^{(1+n)} \quad (C.2)$$

For the outside wall:

$$C_{wlbmt} \frac{dT_{wlbmt}}{dt} = U_{wlbmt} A_{wlbmt} (T_{soil} - T_{wlbmt}) + U_{wlbmt} A_{wlbmt} (T_{zbrmt} - T_{wlbmt}) \quad (C.3)$$

For the mass flow of water:

$$\left[ \sum \left(\frac{L}{A}\right)_{hr} + \sum \left(\frac{L}{A}\right)_{pipe} \right]_{bmt} \frac{dn_{wbmt}}{dt} = \Delta P_{Aa} - \sum f_{Aa} \quad (C.4)$$

where

$$\sum f_{Aa} = f_{valbmt} + f_{hrbmt} + f_{pipebmt} \quad (C.5)$$

In Equation (C.5), the frictional loss from the control valve is a non-linear function related to the control signal  $u_{zbmt}$  and the water mass flow rate.

In general, the dynamic equations can be rewritten in state space matrix formulation as in Equation (C.6).

$$[C_1, C_2, \dots, C_{k1}] \begin{bmatrix} X_1' \\ X_2' \\ \vdots \\ X_{ks}' \end{bmatrix} = \begin{bmatrix} f_1(X_1, X_2, \dots, X_{ks}, u_1, u_2, \dots, u_{kc}) \\ f_2(X_1, X_2, \dots, X_{ks}, u_1, u_2, \dots, u_{kc}) \\ \dots \\ f_{k1}(X_1, X_2, \dots, X_{ks}, u_1, u_2, \dots, u_{kc}) \end{bmatrix} \quad (C.6)$$

In this equation, C, X and u refer to thermal capacity or  $\left(\frac{L}{A}\right)$  in mass dynamic equation, state space variables and control variables respectively; while subscript ks and kc express the number of state space variables and control variables.

The open loop test for the basement heating system was simulated with  $T_o = 21.8^\circ\text{C}$ ,  $\Delta P_{Aa} = 20\text{KPa}$  and the control valve fully open. In order to maintain the design zone air temperature, the supply water temperature was adjusted to  $86.1^\circ\text{C}$  after 12 hours; while it was set to  $90^\circ\text{C}$  before that time. The simulation results with the zone air temperature and the water mass flow rate are depicted in Figure C.3.

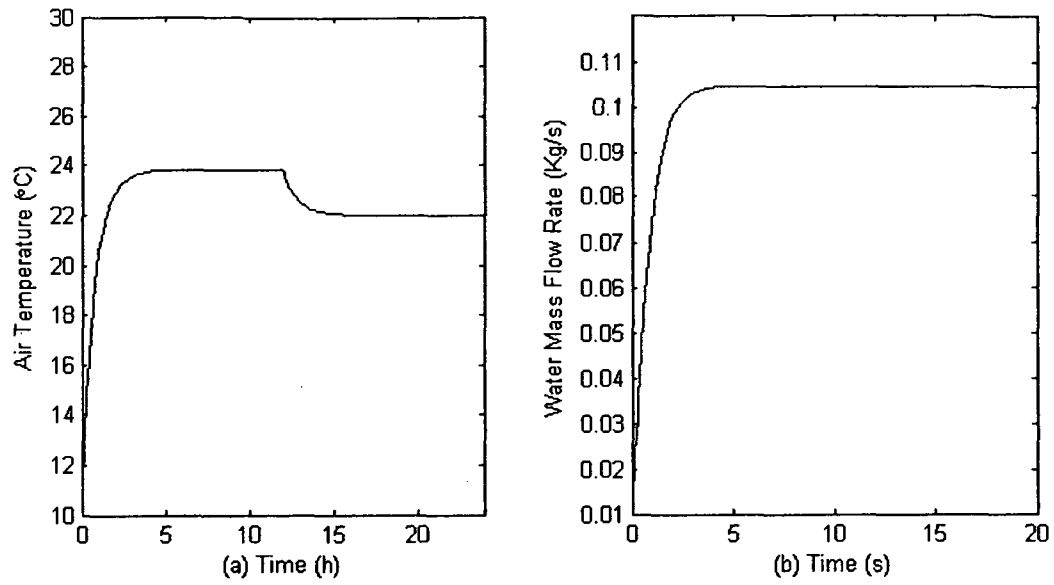


Figure C.3 Dynamic responses of air temperature and water mass flow rate

From Figure C.3(a) it is noted that the zone air temperature reaches  $23.82^{\circ}\text{C}$  at 12 hours, and finally reaches  $22^{\circ}\text{C}$  at 24 hours. The water mass flow rate remains at its steady state value of  $0.1046\text{Kg/s}$  shown in Figure C.3(b).